Rewiring cell fate: illuminating the mechanisms of developmental impairment by the oncoproteins H3 K27M and EZHIP

Ву

Samuel D. Krabbenhoft

A dissertation submitted in partial fulfillment of the requirements for the degree of

Doctor of Philosophy

(Cell and Molecular Biology)

at the

UNIVERSITY OF WISCONSIN-MADISON

2023

Date of final oral examination: 05/11/2023

The dissertation is approved by the following members of the Final Oral Committee:

Melissa Harrison, Professor, Biomolecular Chemistry

Anna Huttenlocher, Professor, Medical Microbiology and Immunology, Pediatrics

Phil Newmark, Professor, Integrative Biology

Peter Lewis, Associate Professor, Biomolecular Chemistry

Catherine Fox, Professor, Biomolecular Chemistry

David Wassarman, Professor, Medical Genetics

Acknowledgements

There are many people I need to thank for getting to this point. To Melissa Harrison, I am indebted to your mentorship. You are as dedicated to the success of your trainees as anybody I have known in science, medicine, or elsewhere. When we met to discuss my rotating in your Lab, I didn't have enough research experience to be starting a PhD. I needed more mentorship than many Pls would have been willing to provide. You are intellectually rigorous, creative, and you get the best out of people. Thank you for holding me to high standards for four years. I am better for it now. I feel lucky to have found the Harrison Lab.

To Peter Lewis, I am deeply thankful for your mentorship. When I started graduate school, the Harrison and Lewis Labs needed somebody dedicated to work full time on their collaboration. That collaboration became my thesis work, and you became my co-mentor. How fortunate I am that you did. From writing grants to developing research plans with a strong intellectual foundation, I benefitted from your guidance many times.

I would like the other members of the Harrison Lab to know how thankful I am to have worked them over these four years. Most of the faces that made up the lab when I joined are gone now. Turnover is hard, but I learned from every one of you over my time in graduate school. I will miss all of you. I would like to specially acknowledge Liz Larson and Tyler Gibson for spending so much time to help me learn bioinformatics. You were approachable always and I am a better scientist because of it. I would also like to thank the undergraduate students that I met and worked with over the years, especially Tyler

Masuda and Steven Huang. Graduate school is stressful, but it was gratifying to see so much growth from you two in the time that I knew you. I hope you will surpass me in everything.

To Anna Huttenlocher, Mark Burkard, and David Wassarman, thank you for the opportunity to join the MSTP and CMB programs. You changed my life. In 2018, I was a third-year medical student. I was having the success I envisioned for myself without the happiness that was supposed to come with it. I was losing the drive to be an academic, which had always been my dream. Joining the MSTP renewed my love for science and medicine. I will carry that with me for the rest of my career.

To my friends, I love you all. Most of you likely do not know how much you helped me get through these years. Really, I want to thank you for caring about me without caring much about the research I have done. You are some of the most important people in my life. To Max Frenkel and Tyler Reich specifically, you know how jarring it is trying to grow as a scientist, while the medical knowledge you acquired over three years slips away. I needed you both to vent my frustrations during low points. I consider you both lifelong friends. The time we spent in graduate school together is a big part of that.

To my family, an acknowledgement would never suffice. As the son of two parents with PhDs, I could have grown up with immense pressure follow your paths. Instead, you let me succeed or fail on my own terms. I would not love science and medicine without knowing that I came to them on my own, with love and support from you the entire time.

I hope I have made you both proud. To my sister Joanie and brother-in-law Brandon, thank you for constantly making me smile. You are my family, but you are also my dear friends. I love you both and am thankful for the support you have constantly shown towards me. Now, I am one step closer to paying for the drinks and meals that we share.

Finally, Rachel. You make my clock tick. You give my life direction. Without you, my moments of sorrow and celebration would mean so much less. I have shared every success and failure with you over seven years. Our lives became one during that time. I cannot wait to take the life we started in Madison to Chicago and beyond. Together. I love you.

To all of you, I dedicate my thesis work.

Abstract

Unique transcriptional programs define every cell type in multicellular animals. Gene expression patterns must be stable enough to maintain cellular identity over long periods of time, and nimble enough to undergo cell-fate transitions during development. Establishment and maintenance of cell-type specific gene-expression patterns rely on transcription factors and regulation of chromatin, through post-translational modifications on histones and DNA. By promoting or silencing gene expression, transcription factors and chromatin-modifying proteins define cellular identity. Impairments in these regulatory proteins alter gene-expression programs, giving rise to disease states like cancer. Polycomb repressive complex 2 (PRC2) maintains transcriptional repression through the deposition of histone H3 lysine 27 trimethylation (H3K27me3). Two pediatric brainstem gliomas, known as diffuse midline glioma (DMG) and posterior fossa ependymoma type A (PFA), are almost entirely devoid of H3K27me3. A missense mutation in histone H3 (H3 K27M) and expression EZHIP drive the loss of H3K27me3 through inhibition of PRC2. The loss of H3K27me3 corresponds with gains in activating histone modifications and aberrant gene activation. This repressive mark is retained at sites of PRC2 recruitment, which maintain gene silencing. We show here that H3K27me3 is lost from broad genomic regions, but spared at PRC2 recruitment sites in mammalian and Drosophila cell lines expressing EZHIP. These data support a model in which H3 K27M and EZHIP preferentially inhibit the spreading form of PRC2. Evidence from tissue-culture models of DMG suggests that additional chromatin modifiers mediate disease pathogenesis. However, the contributions of these chromatin modifiers are difficult to assess with the limited phenotypic range of cell culture. It is critical to study these oncoproteins in a model

organism that recapitulates the complexity of developing tissues. Here, we comprehensively test the contributions of chromatin modifiers to oncoprotein phenotypes in *Drosophila*, where most chromatin-regulatory proteins are conserved. We find that knockdown of transcriptional activators suppresses H3 K27M phenotypes. Suppressors are robust across multiple tissues and rescue severe EZHIP tissue phenotypes. These suppressors rescue normal development by reversing the transcriptional changes that underlie oncoprotein phenotypes. Together, this work deepens our understanding of the ways in which EZHIP and H3 K27M impair healthy development, and provides novel mechanisms by which their deleterious effects can be neutralized.

Table of Contents

Acknowledgements	i
Abstract	iv
List of Tables and Figures	ix
Chapter 1. A shifting paradigm: chromatin-regulatory proteins in cancer	1
Summary	2
The chromatinized genome controls gene expression	5
Polycomb and Trithorax group proteins reinforce early cell fate decisions	9
Polycomb protein structure and function across metazoan evolution	14
H3K27me3 as a true epigenetic mark	17
Chromatin-regulatory proteins in cancer	19
Diffuse midline glioma and posterior fossa ependymoma, type A: disease	s of
chromatin dysregulation	20
PRC2 activity is restricted by H3 K27M and EZHIP	23
Efforts to model H3 K27M in developing organisms	28
Drosophila melanogaster as a tool to identify disease-related pathways	31
Figures	33
References	45
Chapter 2: H3 K27M and EZHIP impede H3K27-methylation spreading by inhib	oiting
allosterically stimulated PRC2	83
Abstract	84
Introduction	85
Results	87

Discussion	96
Materials and Methods	97
Data Availability	107
Acknowledgements	107
Figures	109
Supplementary Figures	117
References	130
Chapter 3. Leveraging <i>Drosophila melanogaster</i> to identify conserved modi	fiers of PRC2-
mediated pediatric glioma	138
Abstract	138
Introduction	139
Results	142
Discussion	151
Materials and Methods	156
Acknowledgements	164
Figures	165
Supplementary Figures	173
Supplementary Tables	187
References	195
Conclusions and Future Directions	212
Summary	213
Conserved chromatin modifiers are essential components of	f oncoprotein
developmental defects	214

A fine balance: determining the mechanisms of H3 K27M suppression	216
Last lines of defense: determining mechanisms of oncoprotein enhancement.	218
H3 K27M enhancers and suppressors in mammalian tissue culture	220
References	222

List of Figures and Tables

Figure 1.1: Gene expression patterns underlie cell-fate specification
Figure 1.2: Chromatin is partitioned into active and repressed domains35
Figure 1.3: Body segment identity is established and maintained by regulated expression
of Hox genes
Figure 1.4: Polycomb repressive complex composition is highly conserved across
evolution39
Figure 1.5: Broad deposition of H3K27me3 requires PRC2 allosteric activation41
Figure 1.6: H3 K27M and EZHIP preferentially inhibit allosterically active PRC243
Figure 2.1: EZHIP Preferentially Interacts with Allosterically Stimulated PRC2 In Vitro and
In Vivo
Figure 2.2: EZHIP Reduces PRC2 Spreading by Stalling It at CpG Islands111
Figure 2.3: H3 K27M Reduces H3K27me3 in <i>Trans</i> by Stalling PRC2 at CpG Islands113
Figure 2.4: Human EZHIP Reduces H3K27me3 in Drosophila through a Conserved
Mechanism115
Supplemental Figure 2.1: EZHIP colocalizes with PRC2 and residual H3K27me3 in vivo
117
Supplemental Figure 2.2: Characterization of H3K27me3-PRC2-EZHIP interaction
interface in vivo
Supplemental Figure 2.3: EZHIP sequesters PRC2 at CpG islands containing residual
H3K27me3 and prevents PRC2 spreading121
Supplemental Figure 2.4: H3K27M interacts with PRC2 in vivo and stalls it at CpG islands
containing residual H3K27me3

Supplemental Figure 2.5: H3 K27M sequesters PRC2 at CpG islands containing residual
H3K27me3 in Diffuse Midline Gliomas
Supplemental Figure 2.6: Chromatin deposition of H3 K27M oncohistones is not
necessary for reduction of H3K27me3 in vivo
Figure 3.1: H3 K27M and EZHIP disrupt Drosophila development through inhibition of
PRC2-mediated H3K27me3165
Figure 3.2: Conserved chromatin modifiers enhance or suppress phenotypes caused by
H3 K27M in the wing
Figure 3.3: Similar chromatin modifiers and transcriptional changes underlie oncoprotein
phenotypes in multiple tissues
Figure 3.4: Suppressors counteract H3 K27M-mediated transcriptional changes171
Supplemental Figure 3.1: H3 K27M promotes expression of germline-related genes 173
Supplemental Figure 3.2: H3 K27M expression results I a near-complete loss of
H3K27me3175
Supplemental Figure 3.3: Knockdown of conserved chromatin modifiers identifies
enhancers and suppressors of H3 K27M phenotypes177
Supplemental Figure 3.4: H3 K27M and EZHIP phenotypes are suppressed in multiple
tissues independent of PRC2 inhibition
Supplemental Figure 3.5: H3 K27M induces similar transcriptional changes in developing
wings and eyes181
Supplemental Figure 3.6: Suppressor RNAi lines alter thousands of genes independently
of H3 K27M183
Supplemental Figure 3.7: Nup153 is a potential mediator of oncoprotein suppression 185

Supplemental Table 3.1: List of all H3 K27M enhancers and suppressors187
Supplemental Figure 3.2: Enhancers and suppressors do not exhibit nonspecific
interactions with overexpressed histone transgenes190
Supplemental Figure 3.3: EZHIP and H3 K27M are suppressed by similar chromatin-
related proteins193

Chapter 1. A shifting paradigm: chromatin-regulatory proteins in cancer

Summary

Tight spatiotemporal control of gene networks is a fundamentally conserved feature of multicellular life. The information encoded by a single genome must be accurately and differentially deployed to give rise to all of the specialized cell types that form each species. These feats of cellular specialization are accomplished by transcription factors, which regulate gene expression by binding DNA and recruiting transcriptional machinery to regions of accessible chromatin. Double-stranded DNA associates with histone octamers to form nucleosomes, the fundamental unit of chromatin. Chromatin is divided into regions that are accessible or inaccessible as a consequence of the histone proteins that compose individual nucleosomes, the position of DNA within or between those nucleosomes, and deposition of posttranslational modifications on histones and DNA. The writers and readers of these chromatin modifications thus create a regulatory language that upholds gene expression patterns established by transcription factors during the earliest stages of development. 3.4

The many cellular processes that occur during development disrupt chromatin stability. Chromatin states therefore exist in a state of dynamic equilibrium: capable of withstanding these disruptions and stabilizing gene expression programs, while allowing for changes in cellular state in response to signaling pathways.⁵ Numerous regulatory systems have evolved to stabilize these expression patterns, including the Polycomb and Trithorax protein families.^{6–8} Polycomb and Trithorax proteins are fundamental regulators of gene expression that act by forming stable regions of repressed or active chromatin, respectively. Polycomb proteins were discovered for their role in maintaining the

expression patterns of Hox transcription factors, whose ectopic expression in flies caused misspecification of various body segments in flies.^{9,10} The read-write functions of PRC1 and PRC2 are critical in defining regions of heterochromatin.¹¹ Polycomb proteins perform dual acts that are seemingly at odds with one another: they propagate cell-type specific gene expression patterns in a fashion that is agnostic to the cell type in which they are expressed. This paradox can be resolved by the "responsive" behaviors observed by Polycomb proteins.¹² They recognize and maintain the "off" state of genes established by transcription factors at earlier time points.^{7,13,14} The repressive function of Polycomb proteins cannot therefore be said to promote specific cellular state, but rather to reinforce those that exist.¹⁵

The fundamental roles that Polycomb and other chromatin-related proteins have in regulating cell identity also explains their contributions to cancer. ^{16,17} Chromatin-related proteins do not behave like traditional oncogenes and tumor suppressors, by positively or negatively growth and differentiation independent of cell context. Instead, the actions of these proteins changes based on the cell types in which they are found. ^{18,19} LOF and GOF mutations "hijack" chromatin regulation to promote oncogenic gene expression programs. Polycomb proteins are no exception to this. More recently, DMG and PFA were found to have near-total loss of H3K27me3, the classical mark of epigenetic silencing deposited by PRC2. ^{20–25} Somatic mutations in PRC2 subunits have not been found in these tumors. Instead, H3 K27M and EZHIP drive these cancers by inhibiting the catalytic activity of PRC2. ^{21,26,27}

DMG and PFA tumors are diseases of development featuring complex but similar changes in their chromatin environments. Combined analysis of gene expression, cell of origin, and developmental window in DMG and PFA tumors suggests that a complete understanding of these diseases will only be achieved by studying them in the context of development. EZHIP and H3 K27M have been examined in an array of model systems, but a detailed examination of the mechanisms by which these proteins disrupt development is still lacking. Systematic dissection of the chromatin environment imposed by these oncoproteins may reveal key, additional chromatin-related contributors to their deadly phenotypes. The information in this summary is discussed in detail below.

The chromatinized genome controls gene expression

Every species is defined by the information encoded in its genome. The DNA sequence of multicellular organisms encodes for the transformation of a single, totipotent zygote into a complex multicellular organism over the course of development. Hundreds of unique cell types compose some animals, despite every cell having the same DNA.³⁴ Animals achieve these extraordinary differences in cell morphology and function by differentially interpreting a single genome across developmental time and space.^{35,36} These changes in cellular state are driven and maintained by the unique gene expression patterns that define each cell type (Figure 1.1).

DNA is packaged with histone octamers to form nucleosomes, the physiologic unit of chromatin. Two copies of histones H2A, H2B, H3, and H4 compose each histone octamer. Two copies of histones H2A, H2B, H3, and H4 compose each histone octamer. This pattern occurs each nucleosome. H1 is the only histone that is not part of the nuclueosome core. This histone binds linker DNA as it enters or exits nucleosomes. This pattern occurs repetitively across the entire genome, a pattern that has been likened to beads on a string. Histones have extensive covalent post-translational modifications (PTMs), with the majority of these modifications being on the unstructured N-terminal tails that extend away from the nucleosome core.

Some histone PTMs alter chromatin in *cis* by changing the chemical properties of nucleosomes. For example, lysine acetylation neutralizes the positive charge of histones, directly loosening their interactions with DNA.⁴⁰ Loosening histone-DNA interactions increases the accessibility of DNA to transcriptional machinery, which facilitates gene

expression.^{40,41} Other modifications do not alter the inherent properties of chromatin but are recognized by "reader" proteins that alter chromatin structure (in *trans* chromatin regulation).⁴² The importance of these modifications led to the "histone code hypothesis," which states that collectively, chromatin modifications create a language allowing for differential interpretation of information encoded by DNA.⁴³

Information imparted by the histone code regulates myriad biological processes. Chief among these is transcription. Chromatin modifications partition the genome into regions that are accessible and inaccessible to transcriptional machinery. DNA-binding proteins known as transcription factors (TFs) bind enhancers and promoters to regulate transcription. These proteins establish cell-type specific gene expression patterns, though most TFs only bind regions of accessible chromatin. Lach cell type has a unique pattern of chromatin accessibility, which narrows the possible genes that can be expressed in each cell type. By regulating the access of transcription factors to their binding sites, chromatin modifications help to determine the gene expression patterns that give rise to all the cell types observed within a species.

Histone modifications are positively or negatively correlated with transcription of associated genes.^{3,4} Through deposition at characteristic sites across the genome, they define regions of euchromatin (accessible and transcriptionally active) and heterochromatin (inaccessible and transcriptionally quiescent). Histone acetylation is broadly found in euchromatin. Examples include H3K27ac, H3K9ac, and H4K16ac. Beyond histone acetylation, canonically active histone methyl marks include mono-, di-,

and trimethylation of key histone H3 lysine residues: H3K4me1/me2/me3, H3K36me2/me3, and H3K79me1/me2/me3 (Figure 1.2A). H3K4me1 methylation state of individual residues is highly site-specific. For example, H3K4me1 marks enhancers near active genes, while H3K4me3 overlaps active gene promoters. Rather than altering the physical properties of chromatin, these and other histone methyl marks regulate chromatin structure in *trans*. Trans-acting proteins ("readers") recognize histone PTMs and regulate chromatin structure. These proteins perform many functions, including shifting nucleosomes along the linear genome, directly opening and closing chromatin, and recruiting additional proteins to coordinate downstream actions. In doing so, histone readers translate complex patterns of histone modifications into sophisticated cellular responses.

Conversely, a host of modifications promote silenced heterochromatin. Heterochromatin can be divided into constitutive and facultative subtypes. Constitutive heterochromatin is primarily found at gene-poor regions, including centromeres and telomeres.⁵¹ It plays a critical role in silencing transposons and repetitive elements whose activities may trigger genomic instability.⁵² H4K20me3 and H3K9me2/me3 are the hallmark PTMs at these stably compacted sites.³ The reader protein heterochromatin protein 1 (HP1) α participates in a feed-forward loop to tightly compact these regions.⁵³ Specifically, HP1α recognizes H3K9me2/me3 and recruits H3K9 methyltransferases, promoting local deposition of this mark. HP1α polymerizes when bound to consecutive nucleosomes, thereby stably compacting these regions. Because the genetic elements flanked by constitutive heterochromatin do not play a role in regular cellular homeostasis, they are

targeted for repression in nearly all cell types.⁵² Facultative heterochromatin is also tightly compacted and transcriptionally silent. H3K27me3 and H2AK119 ubiquitination (H2AK119ub) define facultative heterochromatin (Figure 1.2B).^{3,48} Unlike constitutive heterochromatin, these regions are enriched for protein-coding genes and tend to vary between cell types. H3K27me3, H2AK119ub, and the enzymes that write and read these marks will be discussed in greater length later in this chapter.

In addition to chromatin posttranslational modifications, the constituent histone proteins within nucleosomes vary. Differentially composed nucleosomes add an additional layer of regulatory information. Most histones are synthesized during DNA replication and increase commensurately with newly synthesized DNA.⁵⁴ Eukaryotes have many copies of these so-called "canonical", or replication-dependent, histone genes to achieve appropriately high levels of transcription (e.g., canonical H3 proteins H3.1 and H3.2). Canonical histones are incorporated evenly throughout the genome.⁵⁵ Noncanonical or variant histones are transcribed throughout the cell cycle and have specific sites of incorporation. Variant histones, including the H3 variant H3.3, impact gene expression. H3.3 differs from H3.1 and H3.2 at five and four residues, including serine 31, a site of phosphorylation (H3.3S31ph).⁵⁵ The chaperone complex HIRA directs H3.3 to active enhancers and promoters where it is specifically phosphorylated. 56 H3.3S31ph promotes acetylation of multiple histone residues and H3K36me3 to activate gene expression. 57,58 H3.3 is incorporated in constitutive heterochromatin as well, though the importance of H3.3 in these regions is not well understood. 59,60

The constituent parts of nucleosomes, their spacing along the linear genome, and covalent modifications thereon partition the genome into accessible and inaccessible domains. This sequence-independent information thereby determines cell-type specific gene expression programs. Such intricate regulation must be robust against processes thar perturb the chromatin environment, including shifting metabolic demands, DNA replication, cell division, and differentiation. These chromatin perturbations may spuriously activate or repress critical genes if not properly "buffered." Metazoans have evolved regulatory systems that manage the steady state of chromatin across many cell types rather than relying on separate machinery for each biological context. The broad conservation of such systems reflects their fundamental importance in animal development.

Polycomb and Trithorax group proteins reinforce early cell fate decisions

Gene expression forms the bedrock of cell identity throughout animal life. Specific expression patterns are established with exquisite spatiotemporal precision but exist in a state of dynamic equilibrium. On the one hand, chromatin structure preserves the gene-expression programs underlying cellular identity. On the other, gene expression is rewired throughout development to install new cell fates. *Drosophila melanogaster* has been an exceptional model for understanding the mechanisms by which gene expression is stabilized or overturned during the transformation from a zygote to an adult fly.

Among the first cell-fate decisions during *Drosophila* development is the establishment of an anteroposterior (AP) body axis. In flies, gap and pair-rule transcription factors specify

this axis by activating different genes patterns along the length of the developing animal (Figure 1.3A).⁶¹ Gap and pair-rule genes are only expressed during early development, necessitating additional mechanisms to continually specify the anterior/posterior body plan. Later in development, unique combinations of Hox transcription factors are expressed in each body segment and maintain segment identity.⁶² Polycomb and Trithorax group proteins are highly conserved proteins that reinforce identity later in development to reinforce the gene expression pattern established in the early embryo.^{6,13,14}

These insights were made in spectacular fashion by Pam and Ed Lewis, who were studying *Drosophila* sex combs. Sex combs are normally present on the forelegs of adult male flies but were found on more posterior legs in these early studies. Several decades of work led to the realization that ectopic Hox gene expression caused sex comb mislocalization and other homeotic phenotypes. Given the original phenotype, this class of genes came to be known as Polycomb group proteins (PcG). The earliest identified Polycomb proteins included Polycomb (Pc), Polycomblike (PcI), Additional sex combs (Asx), Posterior sex combs (Psc), and Sex combs on midleg (Scm). Later work identified these proteins as members of three highly conserved protein complexes: Polycomb repressive complexes 1 and 2 (PRC1 and PRC2), and the polycomb repressive deubiquitinase complex (PR-DUB). All three complexes repress target genes by depositing or removing histone PTMs (H3K27me3 and H2A119Kub (H2AK118ub in flies)). Set

Additional Polycomb proteins were discovered in connection with non-homeotic phenotypes, including the *zeste* phenotype. Zeste is a DNA-binding protein whose gain-of-function z^1 allele decreases pigmentation in the *Drosophila* eye by repressing the *white* gene. Genetic screens with this phenotype identified *enhancer of zeste* (E(z)) and *suppressor of zeste 12* (Su(z)12), which encode two core subunits of PRC2. ^{65,66} A gain-of-function mutation in E(z) further repressed *white* (causing white eyes), and a loss-of-function Su(z)12 allele derepressed *white* (causing red eyes). Together these studies uncovered the role of Polycomb proteins in safeguarding cellular identity.

Concurrently with the identification of the repressive function of Polycomb Group proteins, it was proposed that other proteins might antagonize this function and promote Hox gene expression in the appropriate body segments. This group of proteins, now known as Trithorax group proteins (TrxG), was also identified by homeotic phenotypes and established the existence of protein families with antagonistic activities on Hox gene expression (Figure 1.3B). ^{67–69} The notion that Trithorax and Polycomb proteins opposed one another at Hox genes was more firmly cemented after discovering that heterozygous mutations in TrxG genes suppress Polycomb phenotypes. ⁷⁰ The first described TrxG genes were *female sterile* (1) homeotic (Fs(1)h), trithorax (Trx), and absent, small, or homeotic discs 1 and 2 (ash1 and ash2). Molecular characterization of TrxG proteins revealed them to be "writers" (depositors) and readers of histone modifications. Trx, Ash1, and Ash2 catalyze active chromatin modifications (H3K4me2, H3K36me2, and H3K4me3, respectively), while Fs(1)h binds acetylated histones and promotes gene activation by recruiting transcription factors. ⁶

Given the mutual antagonism of PcG and TrxG proteins, it is perhaps no surprise that they regulate a shared set of genes. Genome-wide binding patterns of these proteins in Drosophila and the histone marks they catalyze revealed that they target DNA elements known as Polycomb Response Elements (PREs). Despite targeting by both protein groups, individual PREs adopt either silent or active chromatin states, which correlate with the transcriptional state of nearby genes. The active or silent state of each PRE tends to be stable over time (a bistable system), even across numerous cellular divisions.⁷ Positive feedback mechanisms reinforce Polycomb and Trithorax protein activity at their target genes.⁶ These mechanisms extend beyond the chromatin modifications they deposit. PcG and TrxG proteins modulate the catalytic activity of opposing enzymes and remove antagonistic chromatin marks. 71,72 For example, PRC2 senses the methylation state of H3K36. H3K36me3 reduces PRC2 catalytic activity, thereby contributing to the near-mutual exclusivity of H3K27me3 and H3K36me3 on nucleosomes.⁷² Further, H3K36me2/me3 recruit DNA- and H3K4-methyltransferases (including Trx) that exclude H3K27me3 deposition in cis.71 Trx antagonizes PRC2 in multiple ways. Trx deposits the active H3K4me2, recruits histone acetyltransferases, as well as the H3K27 demethylase enzyme UTX.73

Polycomb proteins act reciprocally, by reinforcing Polylcomb-repressed regions and antagonizing TrxG activity at these sites. PR-DUB dually reinforces Polycomb and Trithorax activity. The complex removes excess H2AK119ub, which concentrates PRC1 and PRC2 at target genes (discussed below). In addition, PR-DUB recruits H3K4

methyltransferases to sites of H2AK119ub removal, solidifying the euchromatic state at regions depleted of Polycomb activity.⁷⁴ Finally, PRC1 member KDM2B demethylates H3K36 to promote deposition of H2AK119ub and H3K27me3 at target sites.^{75–77}

It is useful to think of chromatin as either silenced (heterochromatic) or active (euchromatic). However, heterochromatin and euchromatin are extensively regulated by both Polycomb and Trithorax group proteins. At some genes, this dual regulation leads to simultaneous enrichment of silent and active histone modifications. These genes, dually marked by H3K27me3 and H3K4me3, are said to have "bivalent" chromatin states.⁷⁸ Bivalent genes are transcriptionally repressed, reflecting their enrichment with H3K27me3. However, H3K4me3 "poises" them for activation in response to developmental signals. This so-called bivalent state challenges a strictly bistable model of gene regulation by PcG and TrxG proteins and argues for a more nuanced understanding of gene regulation.7 Continued "competition" by PcG and TrxG genes would maintain low transcriptional output under basal conditions, while a sufficiently strong stimulus (e.g., increased transcription factor levels) could override the predominant Polycomb repression to facilitate cell-fate transitions. Bivalent genes are the most obviously enriched by both silent and active regulatory proteins, though many apparently active PREs have detectable silent histone modifications, and vice versa. The complete loss of competition between PcG and TrxG proteins for "control" of PREs might therefore be an exception, rather than the rule.

Polycomb protein structure and function across metazoan evolution

The roles of TrxG and PcG proteins in regulating gene expression are conserved across metazoa. Comparative analysis of *Drosophila* and mammalian Polycomb proteins has illuminated their essential roles in developmental and disease contexts. Mammalian Polycomb complexes will be reviewed below.

Three Polycomb protein complexes are evolutionarily conserved: PRC1, PRC2, and PR-DUB. PRC1 forms two separate complex, described as canonical (cPRC1) and noncanonical (ncPRC1) (Figure 1.4).^{79,80} Both of these complexes are essential to formation of repressive domains. Noncanonical PRC1 catalyzes most of the H2AK119ub found genome-wide, while canonical PRC1 (cPRC1) directly compacts chromatin to which it is bound.^{81,82}

PRC2 is the only complex that methylates H3K27. The complex deposits H3K27me1, me2, and me3.¹¹ Of these, H3K27me3 is the only one with an obvious role in transcriptional repression. Four subunits compose the core of PRC2: one catalytically active subunit (EZH1 or 2)), EED, SUZ12, and RBAP46 or 48.⁸³ Accessory proteins associate with core PRC2 to form two mutually exclusive subcomplexes, known as PRC2.1 and PRC2.2 (Figure 1.4).⁸³ Though the core complex is sufficient to maintain global levels of H3K27me3, PRC2.1 and PRC2.2 assembly is required for accurate localization and maximum catalytic efficiency.^{80,84–88}

PRC1 and PRC2 generally follow a cascade of catalytic and noncatalytic events to repress target genes. Following recruitment, ncPRC1 deposits H2AK119ub. There is mixed evidence whether catalytic function of ncPRC1 is required for formation of broadly repressed regions. ^{89,90} PRC2 binds H2AK119ub, which promotes H3K27 methylation. ^{91,92} H3K27 is methylated in a step-wise fashion with only H3K27me3 contributing to stable silencing. ¹¹ Finally, canonical PRC1 (cPRC1) directly compacts chromatin by recognizing H3K27me3 and polymerizing through homotypic interactions. ^{93–95} This compaction by non-catalytic function of cPRC1 is essential for gene silencing, as loss of cPRC1 derepresses Polycomb target genes and causes homeotic phenotypes despite normal levels of H3K27me3 and H2AK119ub. ⁹⁶

Counterintuitively, PR-DUB promotes Polycomb-mediated repression by removing the normally repressive H2AK119ub. Without this complex, H2AK119ub accumulates massively at intergenic regions where the mark is not usually found. Intergenic H2AK119ub accumulation compromises PRC1 and PRC2 repression by redistributing them away from their targets. These complexes must be present above a critical concentration for repressive activity, and their recruitment away from target sites leads to chromatin decompaction. 97–99 By constraining the promiscuous activity of PRC1, PR-DUB maintains repressive concentrations of PRC1 and PRC2 at their target sites.

Key to Polycomb-mediated silencing is conversion of H3K27me1/me2 to H3K27me3. While this process occurs inefficiently under non-stimulating conditions, multiple positive-feedback mechanisms increase the efficiency of H3K27me3 deposition. The core PRC2

subunit EED binds H3K27me3 through its aromatic cage, whereupon EED and EZH2 undergo a conformational shift resulting in allosteric activation. Allosteric activation dramatically increases PRC2 catalytic activity and allows for broad deposition of H3K27me3 (Figure 1.5A). The dual "read-write" activities of PRC2 are essential to its repressive function. In addition to methylating H3K27me3, PRC2 methylates its own core and accessory subunits to regulate catalytic activity. Unmethylated EZH2 residues K510 and K514 exert autoinhibitory activity. K510 and K514 methylation by EZH2 relieves their inhibitory effects, and this is essential to reach wild-type levels of H3K27me3. The accessory subunits JARID2 and PALI1 are also targets of EZH2 methylation. Once methylated, these proteins allosterically activate PRC2 by interacting with the EED aromatic cage in a way that mirrors H3K27me3 (Figure 1.5B).

Efficient targeting of PRC1 and PRC2 is essential to their repressive functions, but it remains unclear how this is achieved. Despite the structural and functional conservation of PRC1, PRC2, and PR-DUB across species, their target sites show little sequence similarity between *Drosophila* and humans.⁸⁰ In *Drosophila*, sequence-specific binding factors recruit PRC2 to PREs.¹⁰⁸ Individual knockout of these recruitment factors does not broadly affect global PRC2 recruitment, suggesting that they recruit PRC2 combinatorially rather than being individually required.^{109,110} Pleiohomeotic (Pho) and Pho-like (Phol) are the only PRE-binding proteins whose mutations cause homeotic transformations. Pho or Phol associate with Sfmbt to form the Pho recruitment complex (PhoRC), the only Polycomb protein complex that is not conserved between flies and

humans.^{6,111} The unique importance of instructive PRC2 recruitment by sequence-specific transcription factors may explain the lack of PhoRC conservation.

While mammalian PRC2 targets similar genes in mammals and flies, PRC2 recruitment sites in mammals do not share sequence similarity with *Drosophila* PREs. Mammalian PRC2 binds CpG islands, which overlap most mammalian promoters and are enriched with hypomethylated CpG dinucleotides. 112 CpG islands are not enriched for sequences that explain mammalian PRC2 recruitment. This observation argues against an instructive mode of PRC2 recruitment in mammals. Instead, PRC2 must recognize CpG islands in a sequence-agnostic fashion. A "responsive" model better explains recruitment to CpG islands. 12 This model posits that PRC2 samples the transcriptional status of CpG islands genome wide. The absence of active chromatin modifications is sufficient for productive targeting and compaction by Polycomb proteins. 113–115 By responding to the transcriptional states of genes, PRC2 is positioned to reinforce transcriptional programs established at earlier developmental time points, regardless of cellular context.

H3K27me3 as a true epigenetic mark

In the long history of epigenetics, a consensus definition for the term has been lacking. One of the early conceptual frameworks for epigenetics came from C.H. Waddington in 1957, depicting the "landscape" of possible cellular states as a ball rolling downhill. Within this landscape stem cells pass through various stages of differentiation. Transitions across the cellular landscape are governed by transcription factors. These cell-fate transitions are reinforced by regulation of chromatin structure. Most histone modifications

are dynamically deposited and removed and therefore do not maintain gene expression patterns in the face of disruptions to the chromatin environment.¹¹⁷ Other, longer-lived chromatin features preserve cell identity by "remembering" transcriptional programs that existed prior to such disruptions.^{118–120}

DNA replication causes major changes to structure. During DNA replication, passage of replication machinery displaces nucleosomes from their native positions. Modified histones from the parental DNA strand and newly synthesized histones are equally distributed on parental and daughter strands after S phase, reducing the effective concentration of histone PTMs by half. 121,122 This poses a challenge to the stability of key transcriptional programs. Most active histone modifications do not maintain positional integrity after S phase and therefore may not confer "memory" of a previously active transcriptional state. 117 Repressive chromatin signatures, such as H3K27me3, are more robust in this context due to the dual read-write function of PRC2. PRC2 reader activity recognizes the H3K27me3 on each DNA strand, while its writer activity reestablishes previous levels of H3K27me3 to reestablish repressed domains. 100,123 H3K27me3 is thus a bona fide epigenetic mark that stabilizes the chromatin landscape across developmental time.

The stability of H3K27me3 is a conserved feature across evolution. However, mammalian and fly PRC2 have distinct requirements to reestablish H3K27me3 levels after cell division. This difference lies in their recruitment mechanisms. In humans, the presence of H3K27me3 on parental and daughter strands suffices to restore full levels of the mark on

each strand after DNA replication.¹²⁴ By contrast, *Drosophila* PRC2 requires continued recruitment by PREs to maintain silencing. Upon loss of a PRE, each cellular division reduces preexisting H3K27me3 levels by half, eventually falling below the required enrichment for gene repression.^{125,126} In native contexts, both mammalian and fly PRC2 establish repressive regions that endure against the disruptions that occur over the life of a cell. As we have seen, PRC2 was discovered decades ago for its role in maintaining *Drosophila* body segment identity. Since this initial characterization, PRC2 impairments have come to be recognized in a host of human diseases, including cancer.

Chromatin-regulatory proteins in cancer

Failures in proper cell-fate specification can lead to developmental diseases as well as cancer. Classical cancer paradigms posit that gain-of-function (GOF) mutations in progrowth pathways (e.g., the RAS/Raf/MEK pathway), or loss-of-function (LOF) mutations in pathways inhibiting control of cell growth or promoting apoptosis (p53) cause unchecked accumulation of poorly differentiated cells, which become tumors. Chromatin-regulatory proteins have also been classified as tumor suppressors and oncogenes, though most of these proteins do not possess intrinsic pro- or anti-growth properties.¹⁹ Unlike their traditional counterparts, the mechanisms of chromatin-related tumor suppressors and oncogenes promote disease states based on their cell-type specific behaviors.

PRC2 safeguards cell identity by maintaining the "off" state of developmentally important genes. As such, it is not surprising that somatic mutations in PRC2 complex members are

found in many cancers.¹²⁷ These mutations can be either GOF or LOF, implicating the complex as an oncogene and a tumor suppressor. For example, EZH2 Y641N/F mutations commonly occur in diffuse large B-cell lymphoma (DLBCL). EZH2 Y641N/F results in a constitutively allosterically active PRC2 enzyme and drives cancer by depositing excess H3K27me3 at tumor suppressor genes not normally targeted by PRC2.^{128,129} By contrast, multiple SUZ12 and EZH2 LOF mutations are found in T-cell acute lymphoblastic leukemia. These mutations mimic Notch-pathway activation, despite Notch itself remaining unaltered.¹³⁰ More generally, cancer-associated PRC2 mutations alter H3K27me3 according to their effects on basal catalysis or allosteric activation. Thus, gain- and loss-of-function mutations in PRC2 rewire cellular identity by inappropriately silencing or derepressing cell-fate determining genes.¹⁵ Nonetheless, their oncogenicity cannot be fully understood outside of the disease contexts in which they are found.

Diffuse midline glioma and posterior fossa ependymoma, type A: diseases of chromatin dysregulation

Central nervous system (CNS) tumors are the leading cause of cancer and cancer deaths before 14 years of age. ¹³¹ Approximately 75% of brainstem tumors in this age range are classified as diffuse midline glioma, or DMG. These tumors largely occur in the pons, though they may appear in the thalamus and spinal cord. DMG is a devastating disease with an average time between diagnosis and death of 11 months. Only 10% of children with DMG are alive two years after diagnosis. ¹³²

DMG tumors were classically defined by anatomic location and radiologic appearance. The last decade has seen a revolution in our understanding of DMG after the identification of novel lysine-to-methionine mutations in histone H3 (H3 K27M), present in around 80% of these tumors. ^{20,22,23} These mutations are the initiating molecular event for DMG tumors in which they are found. ^{32,133,134} Most of these mutations occur in the *H3F3A* gene, which encodes for the replication-independent histone H3.3 (H3.3 K27M). All other H3 K27M mutations occur in *HIST1H3B*, which encodes one copy of the canonical H3.1 histone (H3.1 K27M). ^{23,134–136} H3.1 and H3.3 K27M DMG occur in slightly different cell types, though the resultant disease phenotypes are nearly indistinguishable. ³¹

DMG infiltrates healthy brainstem tissues, making them inoperable in nearly every case. Radiation therapy is the current standard of care. Survival rates have not improved in many years, though the discovery of the H3 K27M oncohistone provides optimism that targeted therapies will emerge. Recent Phase 1 clinical trials targeted chromatin-related pathways, among them histone deacetylase (HDAC) and Polycomb inhibitors. An ongoing trial of chimeric antigen receptor T-cell immunotherapy (CAR T) may prove fruitful as well. However, most trials over the last few decades have failed during early stages. These disappointing results highlight the need to gain a better understanding of the molecular mechanisms underlying DMG.

Conspicuous parallels are found between DMG and posterior fossa ependymoma, type A (PFA), including anatomic location in or near the hindbrain. Ependymomas constitute 10% of pediatric CNS tumors.¹⁴² Nine molecularly distinct subgroups define pediatric

ependymoma based on DNA methylation and gene expression patterns.²⁴ PFA is responsible for about half of all pediatric ependymomas and, like DMG, has a poor prognosis (five-year overall survival around 50%).¹⁴² These tumors are diagnosed at a median age of three years old. Despite surgical, chemotherapeutic and radiation-based advances in many brain tumors, PFA outcomes have remained static.¹⁴³ Consistent with the young age of patients at the time of diagnosis, when identified PFAs have accrued very few somatic mutations, though they often harbor chromosome 1q gains.¹⁴⁴ The lack of additional mutations supports an epigenetic rather than a genetic cause of PFA.

Similar to the identification of recurrent H3 K27M mutations in DMG, 2018 saw a breakthrough in our understanding of PFA. It was found that nearly all of cases of PFA have aberrant expression of a gene known as *enhancer of zeste homolog inhibitory protein* (*EZHIP*).^{24,25} Very little was known about EZHIP until recently. Its aberrant expression is now understood to be the initiating event in PFA tumorigenesis.^{27,28} EZHIP is a largely unstructured protein conserved only in placental mammals. It is expressed in a limited range of human tissues, where its importance remains unresolved.¹⁴⁵ Similar to DMG, an increased understanding of the molecular features driving PFA may facilitate new treatment strategies.

Unlike nearly all solid tumors, histopathologic grade does not correlate with prognosis in DMG or PFA. Instead, outcomes are most accurately predicted by the presence of H3 K27M or EZHIP.^{24,146} DMG and PFA have distinct cells of origin and largely

nonoverlapping molecular drivers.^{28,32,147} However, these tumors have similar gene expression profiles, and a striking loss of H3K27me3.

The mechanisms by which H3 K27M drives DMG have been intensely studied since the identification of the link between the mutation and cancer in 2012. H3 K27M is a strong inhibitor of PRC2, suggesting that loss of PRC2 function may be driving DMG.²¹ However, mutations in PRC2 subunits have not been identified in DMG. Thus, it is unlikely that H3 K27M is equivalent to PRC2 loss-of-function. Reciprocally, H3 K27M is almost never found in other tumors. (Only 4% of PFA tumors have H3 K27M. 25,148) This argues that H3 K27M is uniquely oncogenic in the developing hindbrain. H3.1 or H3.3 K27M oncohistones are associated with different secondary mutations. H3.3 K27M mutations co-occur with mutations in TP53 and ATRX, as well as amplifications of PDGFRa. H3.1 K27M mutations co-occur with mutations in ACVR1 and PI3K. 20,136,149 The cell types in which these oncohistone mutations occur may be predisposed to these distinct secondary mutations.³¹ Nevertheless, H3.3 K27M and H3.1 K27M tumors have highly similar gene expression profiles and H3K27me3 landscapes. The restricted cancers in which H3 K27M and EZHIP are found implies that they are seemingly oncogenic in specific cellular contexts. By studying the mechanisms by which these oncoproteins disrupt PRC2 and the chromatin environment more broadly, the mechanisms by which they drive tumorigenesis have come into clearer focus.

PRC2 activity is restricted by H3 K27M and EZHIP

Much effort has gone into understanding the mechanisms by which H3 K27M inhibits PRC2, in hopes that this understanding will shed light on key features of DMG. Biochemically, the mutant methionine residue greatly enhances binding to the active site of EZH2 compared to wild-type H3. ^{150,151} This increased affinity compared to wild-type H3 led to speculation that H3 K27M sequesters PRC2 on chromatin and prevents its localization to normal targets. ¹⁵² If this were the case, PRC2 and H3K27me3 would be expected to colocalize with H3 K27M deposition. However, H3 K27M and H3K27me3 do not correlate. ¹⁵³ Since only one copy of H3 is mutated in DMG, the oncohistone comprises a small percentage of the total H3 pool (around 10%). ¹⁵¹ Thus, inability of PRC2 to methylate this mutant methionine residue does not explain the near-total loss of H3K27me3 genome-wide. H3 K27M is a gain-of-function mutation that functions as a dominant negative, competitive inhibitor of PRC2 (Figure 1.6A). ²¹ Recently, it was found that H3 K27M also inhibits EZH2 K514 automethylation, thereby inhibiting PRC2 at multiple levels. ¹⁰⁶

Chromatin immunoprecipitation followed by high-throughput sequencing (ChIP-seq) assays showed in greater detail where H3K27me3 was lost in the presence of H3 K27M. The mark is primarily lost at sites of PRC2 spreading but remains narrowly enriched at many CpG islands that recruit PRC2. Sa noted earlier, initial deposition of H3K27me3 relies on PRC2 basal catalytic activity, while efficient spreading requires allosteric activation of the complex. In These findings support a model in which H3 K27M preferentially inhibits allosterically active PRC2. *In vitro* studies confirmed that H3 K27M binds preferentially to allosterically active PRC2. Sa Thus, upon expression of H3

K27M PRC2 recruitment is largely unperturbed but spreading outside of CpG islands is substantially reduced (Figure 1.6B). 153 The patterns of H3K27me3 loss at spreading sites and retention at recruitment sites explains the characteristic gene expression changes found in DMG. Loss of PRC2 spreading corresponds to derepression of these genes, while residual H3K27me3 at CpG islands maintains repressive activity. 153,155 DMG oncogenesis relies on this residual H3K27me3, as pharmacologic inhibition of PRC2 is lethal to DMG cells in culture. 156 Reciprocally, knockout of the H3K27 demethylase UTX increases global H3K27me3 and kills DMG cells in culture. 157 This is clear evidence that the mechanisms by which H3 K27M results in disease differ substantively from those caused by loss of PRC2 function. Current evidence argues that a "goldilocks" amount of H3K27me3 is required for H3 K27M-mediated tumorigenesis.

Given its specific role in driving DMG, much scrutiny has gone towards understanding the specific pathogenicity of H3 K27M in the developing CNS. The human brainstem reaches its maximal proliferative rate around 5-6 years of age and may be particularly susceptible to impairments of growth and differentiation during this time. 147,158 This age overlaps with the peak incidence of DMG. In the developing CNS, PRC2-mediated repression of self-renewal genes promotes cellular differentiation. 159 H3 K27M upregulates self-renewal genes, which may introduce a differentiation block. The transcriptional profile of DMG closely resembles oligodendrocyte precursor cells (OPC). Considered together, H3 K27M may drive DMG by hindering pro-differentiation transcriptional programs in OPCs, which are especially susceptible to malignant transformation during the period of naturally increased brainstem proliferation.

Most transcriptional changes in DMG are associated with gene upregulation upon loss of PRC2-mediated repression. However, some genes are silenced *de novo* in an H3K27me3-dependent fashion. One of these genes is the tumor suppressor *CDKN2A*. *CDKN2A* encodes for the cell-cycle regulator p16, which negatively regulates the G1-S transition. p16 repression by H3 K27M promotes cell proliferation in DMG.^{29,160,161} Underscoring the importance of this locus to tumorigenesis, knockout of p16 in wild-type H3.3 mouse models of DMG eliminated survival differences when compared to H3.3 K27M tumors.¹⁵⁶ H3K27me3-dependent silencing of *CDKN2A* is also identified in PFA tumors, suggesting that this effect is not specific to H3 K27M.²⁶ More generally, the epigenetic and transcriptional overlaps between DMG and PFA are evidence that H3 K27M and EZHIP disrupt chromatin regulation by similar means.

Much is unknown about the role of EZHIP in normal human development, though its germline-restricted expression pattern suggests a role in gametogenesis or germ line homeostasis. Somatic mutations in EZHIP are rare, though mutations are found in up to 9% of PFA tumors. These mutations have no effect on PRC2 activity and are not associated with clinical outcome. EZHIP is poorly conserved outside of a 12-reside peptide near its C-terminus. This peptide strongly resembles the sequence surrounding H3 K27M and is named the K27M-like peptide (KLP). As its full name suggests (enhancer of zeste homolog inhibitory protein), EZHIP preferentially binds allosterically active PRC2. Direct in vitro comparison revealed that EZHIP is a more potent competitive inhibitor than H3 K27M. Though the KLP is necessary and sufficient to inhibit

PRC2, its full-length counterpart inhibits PRC2 at a lower IC₅₀.²⁶ Thus, the N-terminus contributes to PRC2 inhibition in an as-yet undefined way.

Given the highly similar means by which H3 K27M and EZHIP inhibit PRC2, it is no surprise that they disrupt the chromatin environment in similar ways. Profiling of H3K27me3 in EZHIP-driven PFA shows a global reduction of H3K27me3 and retained PRC2 activity at recruitment sites. ^{24,26,27,163} It is unknown whether mechanistic differences between these proteins cause their specific enrichment in distinct cancer types. Further characterization of the chromatin and transcriptional changes in DMG and PFA may clarify this, as it is known that chromatin structure is altered beyond the loss of H3K27me3.

In PFA and DMG tumors, loss of H3K27me3 is accompanied by changes in active histone PTMs. One well-described change is an increase in H3K36me2, a mark known to antagonize PRC2 activity. Tissue culture models also observe gains in H3K27ac, H3K9ac, and H3K4me3. The increase in H3K27ac may reflect increased H3K27 acetyltransferase activity following PRC2 inhibition, or increased substrate availability upon loss of H3K27me3. (H3K27me3 and H3K27ac are mutually exclusive on nucleosomes.) Active histone PTMs may promote gene derepression in the setting of H3K27me3 loss, even if their overall levels do not increase. For example, genes with bivalent chromatin are preferentially upregulated in DMG. The loss of PRC2 activity at these sites may increase access for transcriptional activators and result in increased deposition of H3K4me3. Alternatively, H3K4me3 levels at bivalent promoters may remain constant but become the dominant histone modifications upon loss of H3K27me3,

thereby favoring transcriptional activation. Though these changes are well-documented, it is unclear whether they have a role in disease pathogenesis.

Efforts to model H3 K27M in developing organisms

DMG and PFA are fundamentally developmental diseases. In fact, there is evidence that they originate as early as *in utero*. To better understand the origins of these diseases, it is important to model them in biologically relevant tissue-culture and animal models that recapitulate the environment in which they arise. Such models have been leveraged to address questions about the cell-type specificity, requisite developmental windows, and other chromatin-related factors that mediate H3 K27M phenotypes.

Tissue-culture models of DMG have explored the importance of cell type in DMG pathogenesis. In an early study, H3 K27M was expressed in cell lines that varied in their type and degree of differentiation.²⁹ Only neural precursor cells (NPCs) gained a proliferative advantage. NPCs were the most similar cell type to DMG among tested cell lines, supporting a the notion of cell-type specific H3 K27M oncogenicity. Disrupting additional pathways that are mutated in DMG (p53 and PDGFRα) compounded this growth advantage. In addition to increased proliferation, H3 K27M-expressing NPCs formed colonies, consistent with tumor-like and malignant transformation.²⁹

Numerous chemical and genetic screens have been performed with H3 K27M tissueculture models. These studies illuminated the dependencies of DMG cell lines on chromatin-related pathways that extend beyond PRC2 function. For example, chemical

and genetic inhibition of the PRC1 component BMI1 triggered senescence. 166 The senescent phenotype either promoted tumor recurrence or cell death, depending on whether this newly acquired cell state was targeted by additional therapies. Another chemical screen produced DMG growth defects by chemically inhibiting STAT3 kinase. 167 Treatment of mouse xenografts with STAT3 inhibitors similarly decreased tumor growth after eight weeks. A targeted screen of H3K36 writer and reader proteins produced growth defects in DMG cell culture upon knockdown of the NSD1/2 writers and LEDGF/HDGF2 readers. 168 Elsewhere, a dual HDAC-LSD1 histone demethylase inhibitor decreased DMG cell viability and induced transcriptional changes consistent with relief of the differentiation block caused by H3 K27M.¹⁶⁹ Finally, two recent screens identified a novel DMG dependence on the BAF chromatin remodeling complex member SMARCA4. 170,171 Knockdown of this protein caused severe growth defects in cell culture and mouse xenografts. Together, these screens revealed several exciting therapeutic avenues to explore and suggest that DMG tumorigenesis is driven by extensive changes to the epigenome.

The first animal model of H3 K27M was established in *Drosophila*.¹⁷² These animals exhibited morphologic defects, consistent with H3 K27M disruption of normal tissue development. H3 K27M expression in the developing fly wing (wing imaginal discs) reduced H3K27me3 and derepressed Hox genes, classical targets of Polycomb silencing. H3K27ac levels also increased, revealing altered active histone PTMs as a conserved consequence of H3 K27M.¹⁷² Others have built upon the initial *Drosophila* model to screen for chromatin-related factors to that mediate detrimental H3 K27M phenotypes.

One group screened for enhancement or suppression of lethality during development, upon expression of H3 K27M ubiquitously or in glia.¹⁷³ They found 8 genes that shifted death to a later timepoint (suppressors), and 41 genes that shifted it earlier (enhancers). Two suppressors partially reversed H3K27me3 loss. This finding implied that other chromatin-related factors contribute to H3 K27M-mediated loss of H3K27me3, and that the detrimental effects of the oncohistone can be suppressed by partial reversal of PRC2 inhibition. A second study examined the phenotypic effects of knocking down Polycomb proteins and H3K36 methyltransferases in an H3 K27M-mutant eye.¹⁷⁴ ash1, an H3K36 dimethyltransferase, was the only H3 K27M suppressor. Polycomb proteins broadly enhanced the phenotype, in agreement with tissue culture models of H3 K27M wherein pharmacologic inhibition of Polycomb proteins is lethal.¹⁵⁶

One of the outstanding questions in DMG is the developmental window during which H3 K27M is oncogenic. Animal models have clarified this by recapitulating DMG formation in mouse brain. Expression of H3 K27M in post-natal NPCs failed to induce tumorigenesis, even when combined with loss of p53. In contrast, H3 K27M expression and p53 knockout in fetal NPCs produced tumors with 100% penetrance. The authors also knocked down ATRX and overexpressed PDGFR-a to recapitulate other changes found in DMG, which produced tumors with shorter latency. Finally, the tumors were screened against 430 small-molecule inhibitors, showing a number of previously undescribed therapeutic vulnerabilities. This mouse DMG model underscored the oncogenicity of H3 K27M during specific developmental windows and established a platform to test drug efficacy in a biologically relevant context.

The more recent discovery of EZHIP in PFA has resulted in fewer animal models. Though the mechanisms of EZHIP and H3 K27M are similar, nobody has systematically tested whether they have similar genetic dependencies for tumorigenesis. Subtle differences in their modes of oncogenesis may underlie the distinct cells of origin in DMG and PFA and different secondary mutations found in each cancer. Breakthroughs in identification of novel PFA vulnerabilities are likely to require independent modeling of EZHIP.

Drosophila melanogaster as a tool to identify disease-related pathways

Many genes with indispensable roles in human development and disease were first discovered in *Drosophila melanogaster*. In fact, over 70% of genes associated with human disease are conserved in flies. The rapid generation time and wealth of genetic tools in *Drosophila* make them ideal organisms to identify and characterize novel genes. Many genes with indispensable roles in human development and disease were first discovered in *Drosophila melanogaster*.

The identification of many disease-related genes came from loss-of-function experiments in *Drosophila*, which differ from humans in their lack of genetic redundancy. Since the divergence of humans and *Drosophila*, at least two whole-genome duplications occurred in human ancestral species. For this reason, flies typically have a single ortholog of human genes, where humans often have multiple, functionally redundant gene paralogs (e.g., E(z) in flies vs. EZH1/2 in humans). Compensation by functionally related paralogs

often obfuscates characterization of human genes. In *Drosophila*, the lack of redundancy makes conserved genes simpler to study.

Our earliest understandings of tumorigenesis linked cancer to abnormal cell proliferation and apoptosis. Genetic screens in *Drosophila* tissues led to the discovery of many of the pathways that regulate these processes. These studies identified some of the most highly mutated pathways in cancer. For example, the first tumor suppressor (*lethal (2) giant larvae*) was identified in flies.¹⁷⁹ Additional examples include Hippo, Wnt, Notch, and Ras/Raf/MAPK, which are fundamental in both normal development and oncogenesis.^{180–184} The importance of chromatin-related proteins like Polycomb and Trithorax group proteins was not as immediately recognized in cancer. However, their fundamental conservation across evolution makes flies a powerful model to understand their function in diverse biological contexts.

Figure 1.1

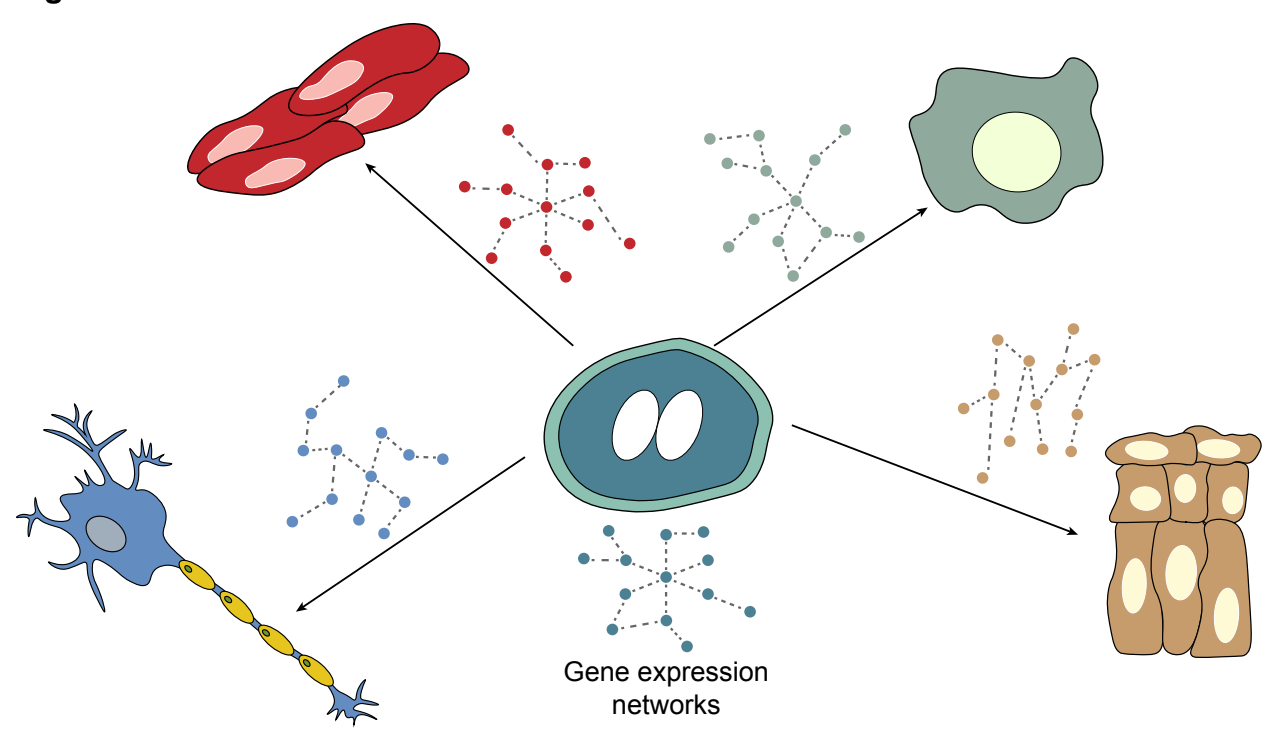
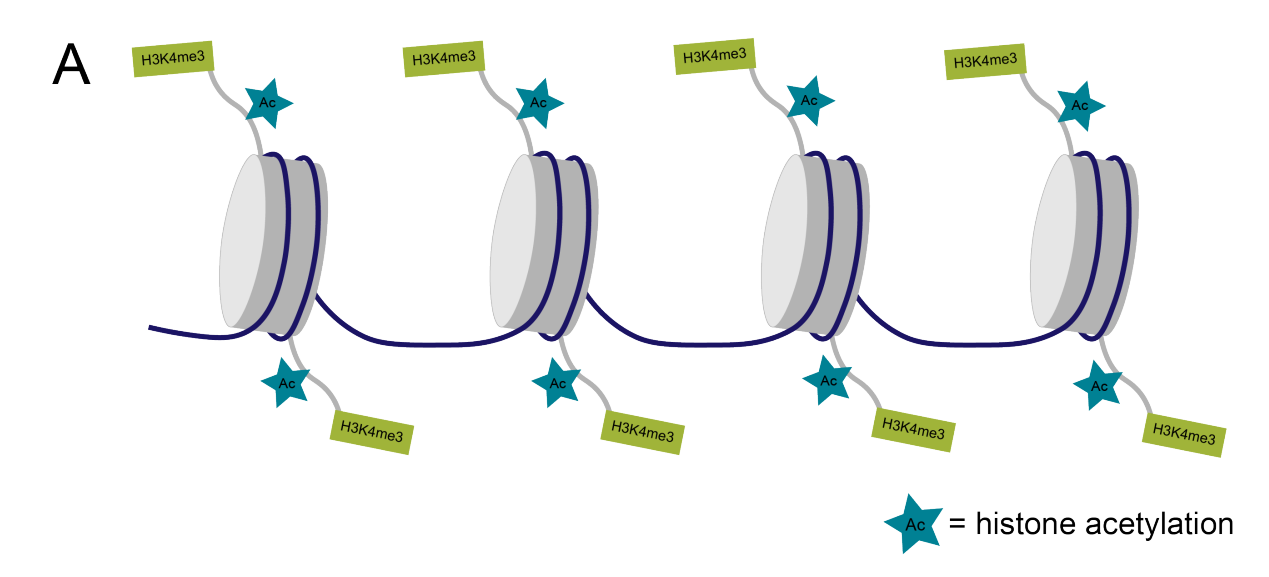


Figure 1.1: Gene expression patterns underlie cell-fate specification. During development, a totipotent zygote (middle) differentiates into all of the cell types that compose a multicellular organism. These differentiated cell types have essentially identical genomes and are therefore differentially interpreted at the level of gene expression. Each cell type contains a unique combination of gene activation and repression, including (clockwise, from bottom left): neurons, myocytes, partially differentiated/precursor cell types, or epithelial cells.

Figure 1.2



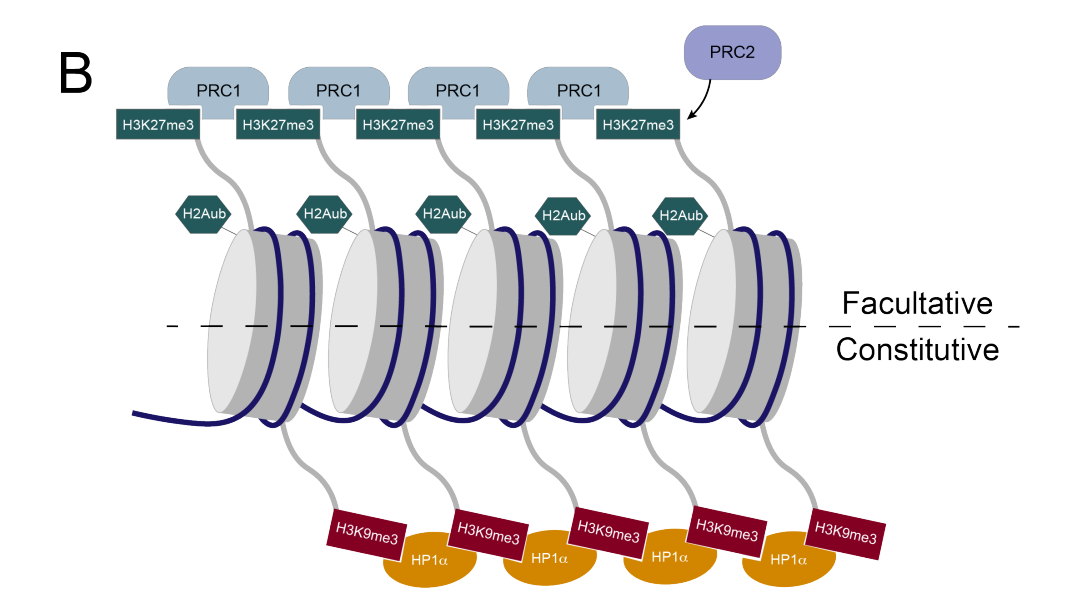


Figure 1.2. Chromatin is partitioned into active and repressed domains.

A. Euchromatin is defined by specific chromatin modifications, like histone acetylation and histone 3, lysine 4 trimethylation (H3K4me3). These marks positively correlate with accessibility to transcriptional machinery and expression of underlying or nearby genes. **B.** Heterochromatin is divided into facultative and constitutive subtypes. Facultative

heterochromatin is marked by H3K27me3 and H2AK119ub (H2AK118ub in flies). These marks are found in gene-rich regions but promote a compact and transcriptionally silent state. Constitutive heterochromatin is enriched near transposons and repetitive DNA elements. H3K9me2/me3, a canonical mark of constitutive chromatin, is bound by HP1α which forms clusters that stably silence these regions in nearly all cell types.

Figure 1.3

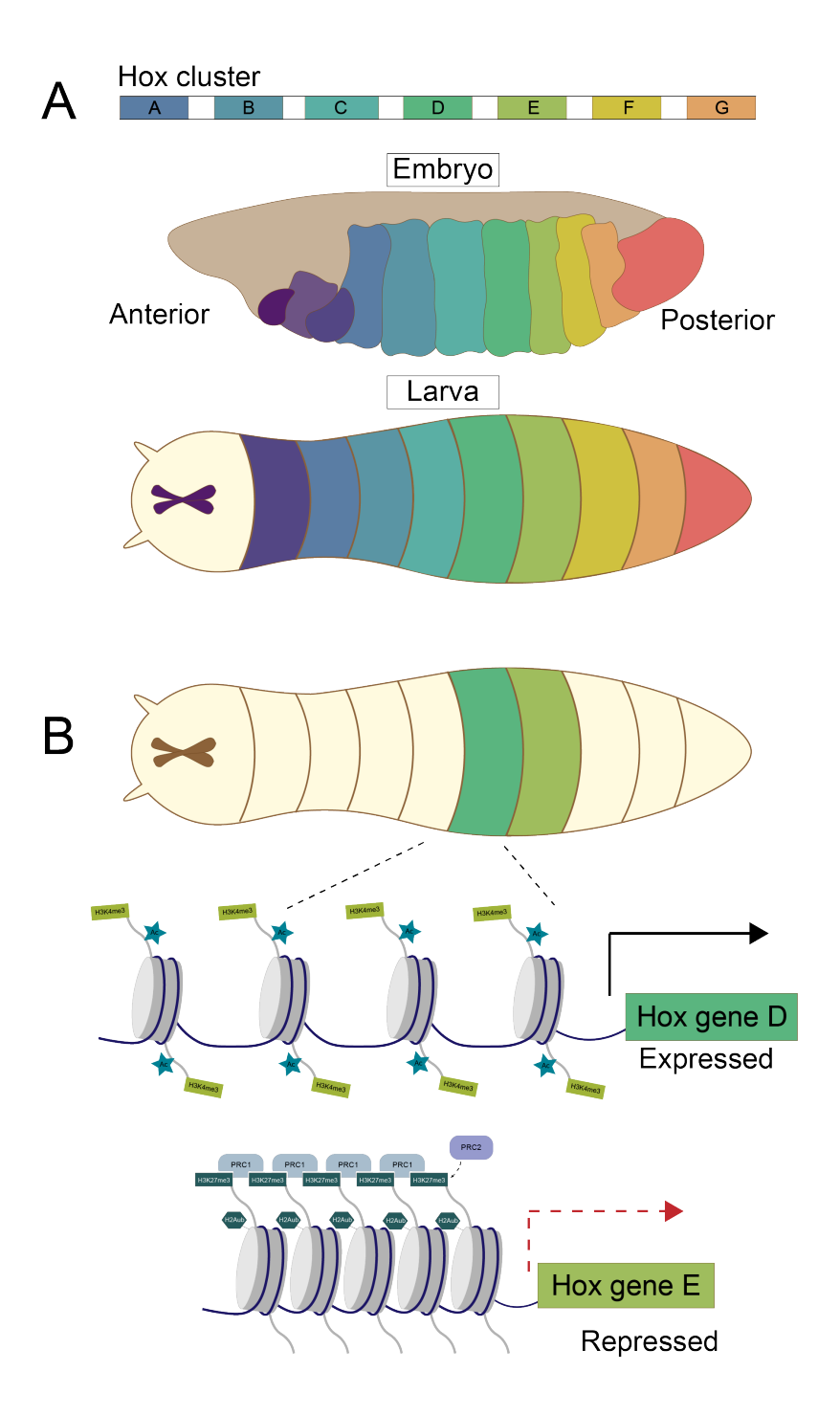


Figure 1.3. Body segment identity is established and maintained by regulated expression of Hox genes. A. Gap and pair-rule transcription factors activate gene expression programs in the early embryo that are maintained across multiple developmental stages. Proper spatiotemporal expression of these genes (including Hox transcription factors) is essential to establish each body segment identity during development. B. Successful cellular differentiation within each body segment requires maintenance of transcriptional programs established earlier in development. Hox genes that coordinate differentiation have euchromatic signatures, while Polycomb proteins propagate the "off" state of other Hox genes.

Figure 1.4

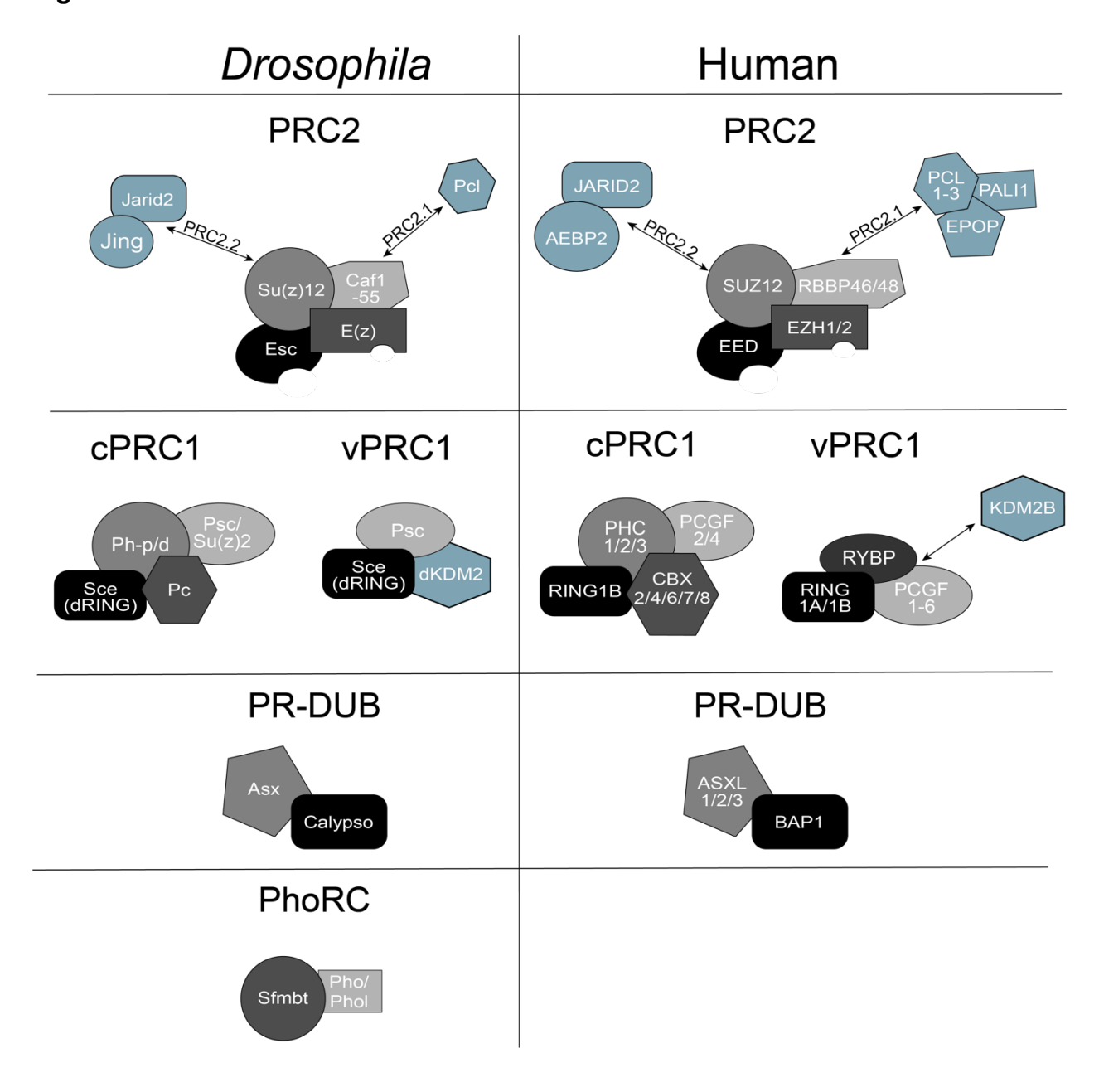


Figure 1.4. Polycomb repressive complex composition is highly conserved across evolution. The three major Polycomb protein complexes (PRC1, PRC2, and PR-DUB) are structurally and functionally conserved between *Drosophila* and humans. Conservation of individual complex members between species is indicated by color and shape. Pleiohomeotic recruitment complex (PhoRC) is the only Polycomb complex that is unique to *Drosophila* and facilitates recruitment to Polycomb response elements in flies (PREs).

Figure 1.5

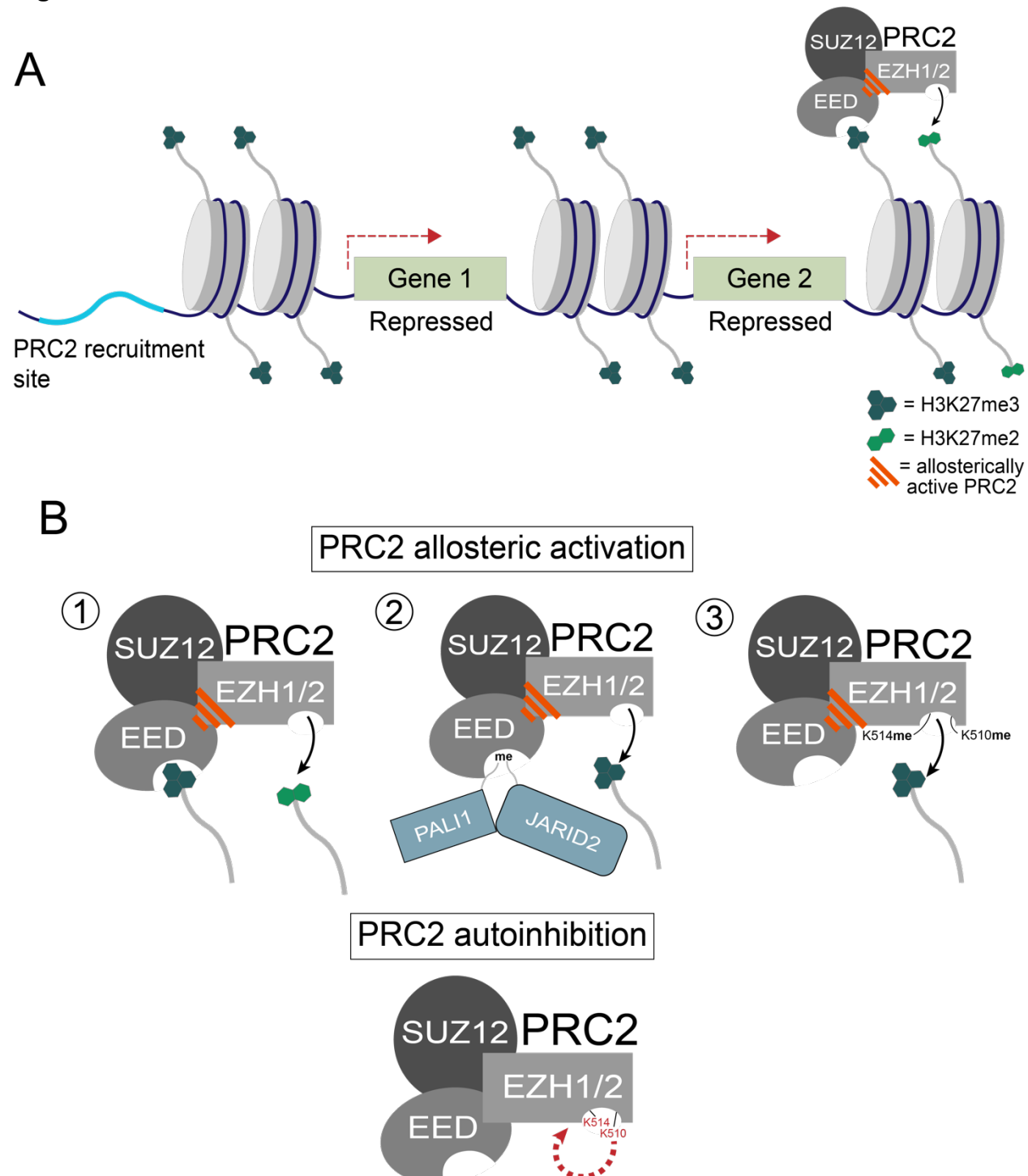


Figure 1.5. Broad deposition of H3K27me3 requires PRC2 allosteric activation.

A. The basal state of PRC2 inefficiently catalyzes H3K27me3 compared to H3K27me1/me2. EED binds H3K27me3, causing a conformational shift in EED and EZH2 within core PRC2 (allosteric activation). This shift increases PRC2 catalytic efficiency and allows the complex to establish broadly repressive domains. **B.** Multiple forms of allostery enhance or inhibit PRC2 activity. Top: Allosteric activation of PRC2 occurs through EED binding to H3K27me3 (1) or the methylated forms of PALI1 or JARID2 (accessory subunits in PRC2.1 and PRC2.2, respectively) (2). Methylation of EZH2 residues K510 and K514 allow for allosteric activation, as well. Bottom: K514 and K510 exist in an unmethylated state at baseline and exert an inhibitory effect on PRC2 activity. Automethylation of these residues by EZH2 alters their localization within active site and allows full catalytic efficiency to be achieved.

Figure 1.6

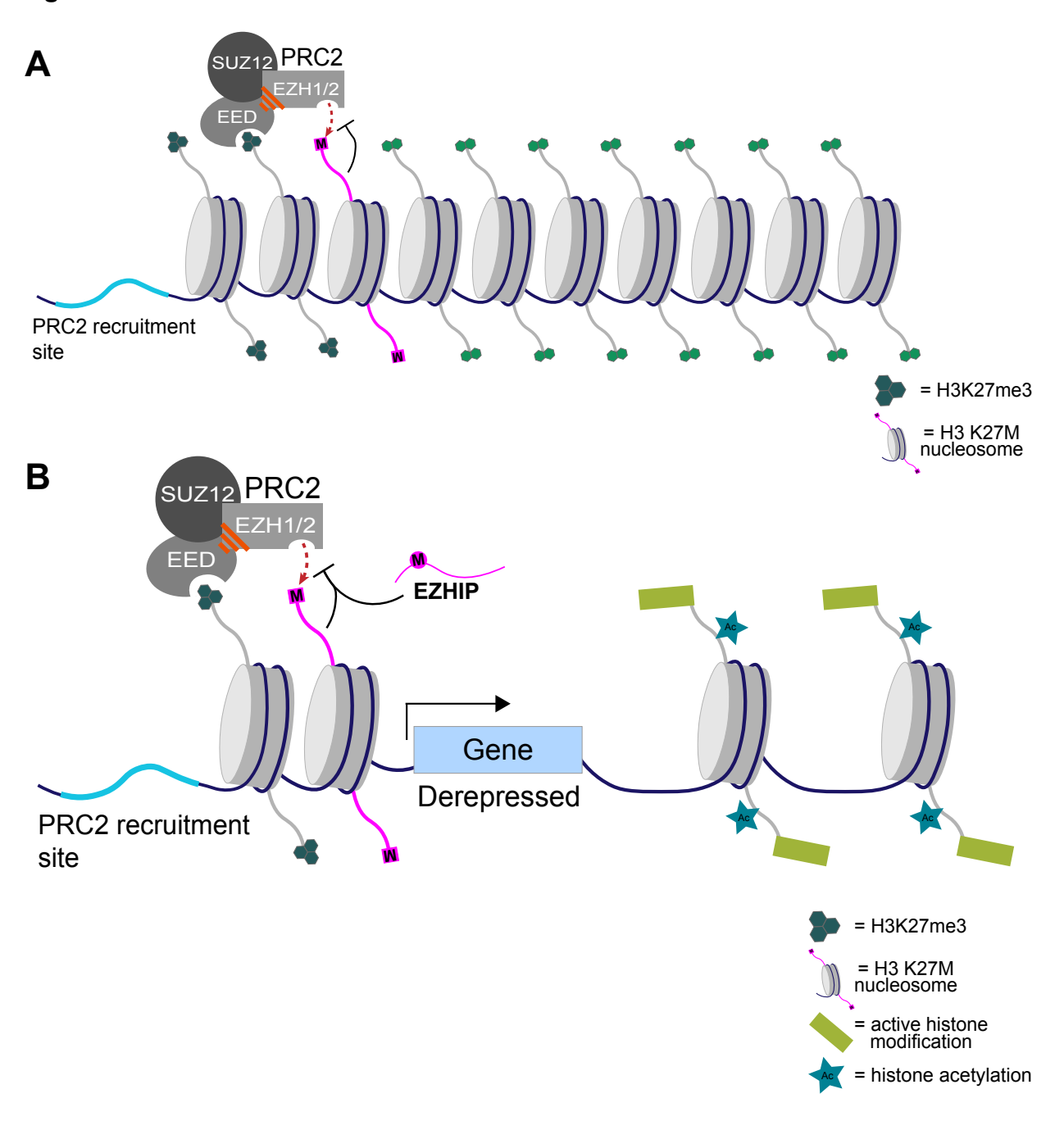


Figure 1.6. H3 K27M and EZHIP preferentially inhibit allosterically active PRC2.

A. H3 K27M is a dominant negative gain-of-function mutation. H3 K27M-positive DMG tumors have a single mutant copy of H3, comprising a small proportion of the total histone pool. H3 K27M tightly binds allosterically active PRC2 and prevents its spread across broad domains, exerting genome-wide effects on H3K27me3 levels. **B.** EZHIP and H3 K27M inhibit allosterically active PRC2 in highly similar fashions. At sites where H3K27me3 is lost, there are increased levels of active histone modifications. These modifications may play an important role in the transcriptional changes that underly DMG and PFA pathogenesis.

References

- (1) Moris, N.; Pina, C.; Arias, A. M. Transition States and Cell Fate Decisions in Epigenetic Landscapes. *Nat Rev Genet* 2016, 17 (11), 693–703. https://doi.org/10.1038/nrg.2016.98.
- (2) Kouzarides, T. Chromatin Modifications and Their Function. Cell 2007, 128 (4), 693–705. https://doi.org/10.1016/j.cell.2007.02.005.
- (3) Kharchenko, P. V.; Alekseyenko, A. A.; Schwartz, Y. B.; Minoda, A.; Riddle, N. C.; Ernst, J.; Sabo, P. J.; Larschan, E.; Gorchakov, A. A.; Gu, T.; Linder-Basso, D.; Plachetka, A.; Shanower, G.; Tolstorukov, M. Y.; Luquette, L. J.; Xi, R.; Jung, Y. L.; Park, R. W.; Bishop, E. P.; Canfield, T. K.; Sandstrom, R.; Thurman, R. E.; MacAlpine, D. M.; Stamatoyannopoulos, J. A.; Kellis, M.; Elgin, S. C. R.; Kuroda, M. I.; Pirrotta, V.; Karpen, G. H.; Park, P. J. Comprehensive Analysis of the Chromatin Landscape in Drosophila Melanogaster. *Nature* 2011, 471 (7339), 480–485. https://doi.org/10.1038/nature09725.
- (4) Mikkelsen, T. S.; Ku, M.; Jaffe, D. B.; Issac, B.; Lieberman, E.; Giannoukos, G.; Alvarez, P.; Brockman, W.; Kim, T.-K.; Koche, R. P.; Lee, W.; Mendenhall, E.; O'Donovan, A.; Presser, A.; Russ, C.; Xie, X.; Meissner, A.; Wernig, M.; Jaenisch, R.; Nusbaum, C.; Lander, E. S.; Bernstein, B. E. Genome-Wide Maps of Chromatin State in Pluripotent and Lineage-Committed Cells. *Nature* 2007, 448 (7153), 553–560. https://doi.org/10.1038/nature06008.
- (5) Ho, L.; Crabtree, G. R. Chromatin Remodelling during Development. *Nature* 2010, 463 (7280), 474–484. https://doi.org/10.1038/nature08911.

- (6) Kassis, J. A.; Kennison, J. A.; Tamkun, J. W. Polycomb and Trithorax Group Genes in Drosophila. Genetics 2017, 206 (4), 1699–1725. https://doi.org/10.1534/genetics.115.185116.
- (7) Kuroda, M. I.; Kang, H.; De, S.; Kassis, J. A. Dynamic Competition of Polycomb and Trithorax in Transcriptional Programming. *Annual Review of Biochemistry* 2020, 89 (1), 235–253. https://doi.org/10.1146/annurev-biochem-120219-103641.
- (8) Piunti, A.; Shilatifard, A. Epigenetic Balance of Gene Expression by Polycomb and COMPASS Families. *Science* 2016, 352 (6290), aad9780. https://doi.org/10.1126/science.aad9780.
- (9) Lewis, E. B. A Gene Complex Controlling Segmentation in Drosophila. *Nature* 1978, 276 (5688), 565–570. https://doi.org/10.1038/276565a0.
- (10) Krumlauf, R. Hox Genes in Vertebrate Development. *Cell* **1994**, 78 (2), 191–201. https://doi.org/10.1016/0092-8674(94)90290-9.
- (11) Yu, J.-R.; Lee, C.-H.; Oksuz, O.; Stafford, J. M.; Reinberg, D. PRC2 Is High Maintenance. *Genes Dev.* 2019, 33 (15–16), 903–935.
 https://doi.org/10.1101/gad.325050.119.
- (12) Klose, R. J.; Cooper, S.; Farcas, A. M.; Blackledge, N. P.; Brockdorff, N. Chromatin Sampling—An Emerging Perspective on Targeting Polycomb Repressor Proteins. *PLoS Genet* 2013, 9 (8). https://doi.org/10.1371/journal.pgen.1003717.
- (13) Beuchle, D.; Struhl, G.; Müller, J. Polycomb Group Proteins and Heritable Silencing of Drosophila Hox Genes. *Development* 2001, 128 (6), 993–1004. https://doi.org/10.1242/dev.128.6.993.

- (14) Pelegri, F.; Lehmann, R. A Role of Polycomb Group Genes in the Regulation of Gap Gene Expression in Drosophila. *Genetics* **1994**, *136* (4), 1341–1353. https://doi.org/10.1093/genetics/136.4.1341.
- (15) Riising, E. M.; Comet, I.; Leblanc, B.; Wu, X.; Johansen, J. V.; Helin, K. Gene Silencing Triggers Polycomb Repressive Complex 2 Recruitment to CpG Islands Genome Wide. *Molecular Cell* 2014, 55 (3), 347–360. https://doi.org/10.1016/j.molcel.2014.06.005.
- (16) Garraway, L. A.; Lander, E. S. Lessons from the Cancer Genome. *Cell* 2013, *153*(1), 17–37. https://doi.org/10.1016/j.cell.2013.03.002.
- (17) Shen, H.; Laird, P. W. Interplay between the Cancer Genome and Epigenome. *Cell* 2013, 153 (1), 38–55. https://doi.org/10.1016/j.cell.2013.03.008.
- (18) Morgan, M. A.; Shilatifard, A. Chromatin Signatures of Cancer. *Genes Dev.* 2015, 29 (3), 238–249. https://doi.org/10.1101/gad.255182.114.
- (19) Valencia, A. M.; Kadoch, C. Chromatin Regulatory Mechanisms and Therapeutic Opportunities in Cancer. *Nat Cell Biol* 2019, 21 (2), 152–161. https://doi.org/10.1038/s41556-018-0258-1.
- (20) Khuong-Quang, D.-A.; Buczkowicz, P.; Rakopoulos, P.; Liu, X.-Y.; Fontebasso, A. M.; Bouffet, E.; Bartels, U.; Albrecht, S.; Schwartzentruber, J.; Letourneau, L.; Bourgey, M.; Bourque, G.; Montpetit, A.; Bourret, G.; Lepage, P.; Fleming, A.; Lichter, P.; Kool, M.; von Deimling, A.; Sturm, D.; Korshunov, A.; Faury, D.; Jones, D. T.; Majewski, J.; Pfister, S. M.; Jabado, N.; Hawkins, C. K27M Mutation in Histone H3.3 Defines Clinically and Biologically Distinct Subgroups of Pediatric

- Diffuse Intrinsic Pontine Gliomas. *Acta Neuropathol* **2012**, *124* (3), 439–447. https://doi.org/10.1007/s00401-012-0998-0.
- (21) Lewis, P. W.; Müller, M. M.; Koletsky, M. S.; Cordero, F.; Lin, S.; Banaszynski, L. A.; Garcia, B. A.; Muir, T. W.; Becher, O. J.; Allis, C. D. Inhibition of PRC2 Activity by a Gain-of-Function H3 Mutation Found in Pediatric Glioblastoma. *Science* **2013**, *340* (6134), 857–861. https://doi.org/10.1126/science.1232245.
- (22) Schwartzentruber, J.; Korshunov, A.; Liu, X.-Y.; Jones, D. T. W.; Pfaff, E.; Jacob, K.; Sturm, D.; Fontebasso, A. M.; Quang, D.-A. K.; Tönjes, M.; Hovestadt, V.; Albrecht, S.; Kool, M.; Nantel, A.; Konermann, C.; Lindroth, A.; Jäger, N.; Rausch, T.; Ryzhova, M.; Korbel, J. O.; Hielscher, T.; Hauser, P.; Garami, M.; Klekner, A.; Bognar, L.; Ebinger, M.; Schuhmann, M. U.; Scheurlen, W.; Pekrun, A.; Frühwald, M. C.; Roggendorf, W.; Kramm, C.; Dürken, M.; Atkinson, J.; Lepage, P.; Montpetit, A.; Zakrzewska, M.; Zakrzewski, K.; Liberski, P. P.; Dong, Z.; Siegel, P.; Kulozik, A. E.; Zapatka, M.; Guha, A.; Malkin, D.; Felsberg, J.; Reifenberger, G.; von Deimling, A.; Ichimura, K.; Collins, V. P.; Witt, H.; Milde, T.; Witt, O.; Zhang, C.; Castelo-Branco, P.; Lichter, P.; Faury, D.; Tabori, U.; Plass, C.; Majewski, J.; Pfister, S. M.; Jabado, N. Driver Mutations in Histone H3.3 and Chromatin Remodelling Genes in Paediatric Glioblastoma. *Nature* 2012, *482* (7384), 226–231. https://doi.org/10.1038/nature10833.
- (23) Wu, G.; Broniscer, A.; McEachron, T. A.; Lu, C.; Paugh, B. S.; Becksfort, J.; Qu, C.; Ding, L.; Huether, R.; Parker, M.; Zhang, J.; Gajjar, A.; Dyer, M. A.; Mullighan, C. G.; Gilbertson, R. J.; Mardis, E. R.; Wilson, R. K.; Downing, J. R.; Ellison, D. W.; Zhang, J.; Baker, S. J.; St. Jude Children's Research Hospital–Washington

- University Pediatric Cancer Genome Project. Somatic Histone H3 Alterations in Pediatric Diffuse Intrinsic Pontine Gliomas and Non-Brainstem Glioblastomas. *Nat Genet* **2012**, *44* (3), 251–253. https://doi.org/10.1038/ng.1102.
- (24) Pajtler, K. W.; Wen, J.; Sill, M.; Lin, T.; Orisme, W.; Tang, B.; Hübner, J.-M.;
 Ramaswamy, V.; Jia, S.; Dalton, J. D.; Haupfear, K.; Rogers, H. A.; Punchihewa,
 C.; Lee, R.; Easton, J.; Wu, G.; Ritzmann, T. A.; Chapman, R.; Chavez, L.; Boop, F.
 A.; Klimo, P.; Sabin, N. D.; Ogg, R.; Mack, S. C.; Freibaum, B. D.; Kim, H. J.; Witt,
 H.; Jones, D. T. W.; Vo, B.; Gajjar, A.; Pounds, S.; Onar-Thomas, A.; Roussel, M. F.;
 Zhang, J.; Taylor, J. P.; Merchant, T. E.; Grundy, R.; Tatevossian, R. G.; Taylor, M.
 D.; Pfister, S. M.; Korshunov, A.; Kool, M.; Ellison, D. W. Molecular Heterogeneity
 and CXorf67 Alterations in Posterior Fossa Group A (PFA) Ependymomas. *Acta Neuropathol* 2018, *136* (2), 211–226. https://doi.org/10.1007/s00401-018-1877-0.
- (25) Pajtler, K. W.; Witt, H.; Sill, M.; Jones, D. T. W.; Hovestadt, V.; Kratochwil, F.; Wani, K.; Tatevossian, R.; Punchihewa, C.; Johann, P.; Reimand, J.; Warnatz, H.-J.; Ryzhova, M.; Mack, S.; Ramaswamy, V.; Capper, D.; Schweizer, L.; Sieber, L.; Wittmann, A.; Huang, Z.; van Sluis, P.; Volckmann, R.; Koster, J.; Versteeg, R.; Fults, D.; Toledano, H.; Avigad, S.; Hoffman, L. M.; Donson, A. M.; Foreman, N.; Hewer, E.; Zitterbart, K.; Gilbert, M.; Armstrong, T. S.; Gupta, N.; Allen, J. C.; Karajannis, M. A.; Zagzag, D.; Hasselblatt, M.; Kulozik, A. E.; Witt, O.; Collins, V. P.; von Hoff, K.; Rutkowski, S.; Pietsch, T.; Bader, G.; Yaspo, M.-L.; von Deimling, A.; Lichter, P.; Taylor, M. D.; Gilbertson, R.; Ellison, D. W.; Aldape, K.; Korshunov, A.; Kool, M.; Pfister, S. M. Molecular Classification of Ependymal Tumors across All

- CNS Compartments, Histopathological Grades, and Age Groups. *Cancer Cell* **2015**, 27 (5), 728–743. https://doi.org/10.1016/j.ccell.2015.04.002.
- (26) Jain, S. U.; Do, T. J.; Lund, P. J.; Rashoff, A. Q.; Diehl, K. L.; Cieslik, M.; Bajic, A.; Juretic, N.; Deshmukh, S.; Venneti, S.; Muir, T. W.; Garcia, B. A.; Jabado, N.; Lewis, P. W. PFA Ependymoma-Associated Protein EZHIP Inhibits PRC2 Activity through a H3 K27M-like Mechanism. *Nature Communications* 2019, 10 (1), 2146. https://doi.org/10.1038/s41467-019-09981-6.
- (27) Hübner, J.-M.; Müller, T.; Papageorgiou, D. N.; Mauermann, M.; Krijgsveld, J.; Russell, R. B.; Ellison, D. W.; Pfister, S. M.; Pajtler, K. W.; Kool, M. EZHIP/CXorf67 Mimics K27M Mutated Oncohistones and Functions as an Intrinsic Inhibitor of PRC2 Function in Aggressive Posterior Fossa Ependymoma. *Neuro Oncol* 2019, 21 (7), 878–889. https://doi.org/10.1093/neuonc/noz058.
- (28) Bayliss, J.; Mukherjee, P.; Lu, C.; Jain, S. U.; Chung, C.; Martinez, D.; Sabari, B.; Margol, A. S.; Panwalkar, P.; Parolia, A.; Pekmezci, M.; McEachin, R. C.; Cieslik, M.; Tamrazi, B.; Garcia, B. A.; Rocca, G. L.; Santi, M.; Lewis, P. W.; Hawkins, C.; Melnick, A.; Allis, C. D.; Thompson, C. B.; Chinnaiyan, A. M.; Judkins, A. R.; Venneti, S. Lowered H3K27me3 and DNA Hypomethylation Define Poorly Prognostic Pediatric Posterior Fossa Ependymomas. *Science Translational Medicine* 2016, 8 (366), 366ra161-366ra161.
 https://doi.org/10.1126/scitranslmed.aah6904.
- (29) Funato, K.; Major, T.; Lewis, P. W.; Allis, C. D.; Tabar, V. Use of Human Embryonic Stem Cells to Model Pediatric Gliomas with H3.3K27M Histone Mutation. *Science* **2014**, *346* (6216), 1529–1533. https://doi.org/10.1126/science.1253799.

- (30) Pathania, M.; De Jay, N.; Maestro, N.; Harutyunyan, A. S.; Nitarska, J.; Pahlavan, P.; Henderson, S.; Mikael, L. G.; Richard-Londt, A.; Zhang, Y.; Costa, J. R.; Hébert, S.; Khazaei, S.; Ibrahim, N. S.; Herrero, J.; Riccio, A.; Albrecht, S.; Ketteler, R.; Brandner, S.; Kleinman, C. L.; Jabado, N.; Salomoni, P. H3.3K27M Cooperates with Trp53 Loss and PDGFRA Gain in Mouse Embryonic Neural Progenitor Cells to Induce Invasive High-Grade Gliomas. *Cancer Cell* 2017, 32 (5), 684-700.e9. https://doi.org/10.1016/j.ccell.2017.09.014.
- (31) Jessa, S.; Mohammadnia, A.; Harutyunyan, A. S.; Hulswit, M.; Varadharajan, S.; Lakkis, H.; Kabir, N.; Bashardanesh, Z.; Hébert, S.; Faury, D.; Vladoiu, M. C.; Worme, S.; Coutelier, M.; Krug, B.; Faria Andrade, A.; Pathania, M.; Bajic, A.; Weil, A. G.; Ellezam, B.; Atkinson, J.; Dudley, R. W. R.; Farmer, J.-P.; Perreault, S.; Garcia, B. A.; Larouche, V.; Blanchette, M.; Garzia, L.; Bhaduri, A.; Ligon, K. L.; Bandopadhayay, P.; Taylor, M. D.; Mack, S. C.; Jabado, N.; Kleinman, C. L. K27M in Canonical and Noncanonical H3 Variants Occurs in Distinct Oligodendroglial Cell Lineages in Brain Midline Gliomas. *Nat Genet* 2022, *54* (12), 1865–1880. https://doi.org/10.1038/s41588-022-01205-w.
- (32) Filbin, M. G.; Tirosh, I.; Hovestadt, V.; Shaw, M. L.; Escalante, L. E.; Mathewson, N. D.; Neftel, C.; Frank, N.; Pelton, K.; Hebert, C. M.; Haberler, C.; Yizhak, K.; Gojo, J.; Egervari, K.; Mount, C.; Galen, P. van; Bonal, D. M.; Nguyen, Q.-D.; Beck, A.; Sinai, C.; Czech, T.; Dorfer, C.; Goumnerova, L.; Lavarino, C.; Carcaboso, A. M.; Mora, J.; Mylvaganam, R.; Luo, C. C.; Peyrl, A.; Popović, M.; Azizi, A.; Batchelor, T. T.; Frosch, M. P.; Martinez-Lage, M.; Kieran, M. W.; Bandopadhayay, P.; Beroukhim, R.; Fritsch, G.; Getz, G.; Rozenblatt-Rosen, O.; Wucherpfennig, K. W.;

- Louis, D. N.; Monje, M.; Slavc, I.; Ligon, K. L.; Golub, T. R.; Regev, A.; Bernstein, B. E.; Suvà, M. L. Developmental and Oncogenic Programs in H3K27M Gliomas

 Dissected by Single-Cell RNA-Seq. *Science* **2018**, *360* (6386), 331–335.

 https://doi.org/10.1126/science.aao4750.
- (33) Lange, C.; Huttner, W. B.; Calegari, F. Cdk4/CyclinD1 Overexpression in Neural Stem Cells Shortens G1, Delays Neurogenesis, and Promotes the Generation and Expansion of Basal Progenitors. *Cell Stem Cell* **2009**, *5* (3), 320–331. https://doi.org/10.1016/j.stem.2009.05.026.
- (34) Aebersold, R.; Agar, J. N.; Amster, I. J.; Baker, M. S.; Bertozzi, C. R.; Boja, E. S.; Costello, C. E.; Cravatt, B. F.; Fenselau, C.; Garcia, B. A.; Ge, Y.; Gunawardena, J.; Hendrickson, R. C.; Hergenrother, P. J.; Huber, C. G.; Ivanov, A. R.; Jensen, O. N.; Jewett, M. C.; Kelleher, N. L.; Kiessling, L. L.; Krogan, N. J.; Larsen, M. R.; Loo, J. A.; Ogorzalek Loo, R. R.; Lundberg, E.; MacCoss, M. J.; Mallick, P.; Mootha, V. K.; Mrksich, M.; Muir, T. W.; Patrie, S. M.; Pesavento, J. J.; Pitteri, S. J.; Rodriguez, H.; Saghatelian, A.; Sandoval, W.; Schlüter, H.; Sechi, S.; Slavoff, S. A.; Smith, L. M.; Snyder, M. P.; Thomas, P. M.; Uhlén, M.; Van Eyk, J. E.; Vidal, M.; Walt, D. R.; White, F. M.; Williams, E. R.; Wohlschlager, T.; Wysocki, V. H.; Yates, N. A.; Young, N. L.; Zhang, B. How Many Human Proteoforms Are There? *Nat Chem Biol* 2018, 14 (3), 206–214. https://doi.org/10.1038/nchembio.2576.
- (35) Voss, T. C.; Hager, G. L. Dynamic Regulation of Transcriptional States by Chromatin and Transcription Factors. *Nat Rev Genet* **2014**, *15* (2), 69–81. https://doi.org/10.1038/nrg3623.

- (36) Spitz, F.; Furlong, E. E. M. Transcription Factors: From Enhancer Binding to Developmental Control. *Nat Rev Genet* 2012, 13 (9), 613–626. https://doi.org/10.1038/nrg3207.
- (37) Cutter, A. R.; Hayes, J. J. A Brief Review of Nucleosome Structure. FEBS Letters 2015, 589 (20, Part A), 2914–2922. https://doi.org/10.1016/j.febslet.2015.05.016.
- (38) Teves, S. S.; Weber, C. M.; Henikoff, S. Transcribing through the Nucleosome.

 *Trends in Biochemical Sciences 2014, 39 (12), 577–586.

 https://doi.org/10.1016/j.tibs.2014.10.004.
- (39) Woodcock, C. L.; Skoultchi, A. I.; Fan, Y. Role of Linker Histone in Chromatin Structure and Function: H1 Stoichiometry and Nucleosome Repeat Length.

 Chromosome Res 2006, 14 (1), 17–25. https://doi.org/10.1007/s10577-005-1024-3.
- (40) Shogren-Knaak, M.; Ishii, H.; Sun, J.-M.; Pazin, M. J.; Davie, J. R.; Peterson, C. L. Histone H4-K16 Acetylation Controls Chromatin Structure and Protein Interactions. Science 2006, 311 (5762), 844–847. https://doi.org/10.1126/science.1124000.
- (41) Sheikh, B. N.; Akhtar, A. The Many Lives of KATs Detectors, Integrators and Modulators of the Cellular Environment. *Nat Rev Genet* 2019, 20 (1), 7–23. https://doi.org/10.1038/s41576-018-0072-4.
- (42) Fujisawa, T.; Filippakopoulos, P. Functions of Bromodomain-Containing Proteins and Their Roles in Homeostasis and Cancer. *Nat Rev Mol Cell Biol* **2017**, *18* (4), 246–262. https://doi.org/10.1038/nrm.2016.143.
- (43) Strahl, B. D.; Allis, C. D. The Language of Covalent Histone Modifications. *Nature* **2000**, *403* (6765), 41–45. https://doi.org/10.1038/47412.

- (44) Klemm, S. L.; Shipony, Z.; Greenleaf, W. J. Chromatin Accessibility and the Regulatory Epigenome. *Nat Rev Genet* 2019, 20 (4), 207–220. https://doi.org/10.1038/s41576-018-0089-8.
- (45) Tsompana, M.; Buck, M. J. Chromatin Accessibility: A Window into the Genome. *Epigenetics & Chromatin* **2014**, *7* (1), 33. https://doi.org/10.1186/1756-8935-7-33.
- (46) Liu, T.; Rechtsteiner, A.; Egelhofer, T. A.; Vielle, A.; Latorre, I.; Cheung, M.-S.;
 Ercan, S.; Ikegami, K.; Jensen, M.; Kolasinska-Zwierz, P.; Rosenbaum, H.; Shin,
 H.; Taing, S.; Takasaki, T.; Iniguez, A. L.; Desai, A.; Dernburg, A. F.; Kimura, H.;
 Lieb, J. D.; Ahringer, J.; Strome, S.; Liu, X. S. Broad Chromosomal Domains of
 Histone Modification Patterns in C. Elegans. *Genome Res.* 2011, 21 (2), 227–236.
 https://doi.org/10.1101/gr.115519.110.
- (47) Filion, G. J.; van Bemmel, J. G.; Braunschweig, U.; Talhout, W.; Kind, J.; Ward, L. D.; Brugman, W.; de Castro, I. J.; Kerkhoven, R. M.; Bussemaker, H. J.; van Steensel, B. Systematic Protein Location Mapping Reveals Five Principal Chromatin Types in Drosophila Cells. *Cell* 2010, 143 (2), 212–224. https://doi.org/10.1016/j.cell.2010.09.009.
- (48) Barski, A.; Cuddapah, S.; Cui, K.; Roh, T.-Y.; Schones, D. E.; Wang, Z.; Wei, G.; Chepelev, I.; Zhao, K. High-Resolution Profiling of Histone Methylations in the Human Genome. *Cell* 2007, 129 (4), 823–837.
 https://doi.org/10.1016/j.cell.2007.05.009.
- (49) Santos-Rosa, H.; Schneider, R.; Bannister, A. J.; Sherriff, J.; Bernstein, B. E.; Emre, N. C. T.; Schreiber, S. L.; Mellor, J.; Kouzarides, T. Active Genes Are Tri-

- Methylated at K4 of Histone H3. *Nature* **2002**, *419* (6905), 407–411. https://doi.org/10.1038/nature01080.
- (50) Musselman, C. A.; Lalonde, M.-E.; Côté, J.; Kutateladze, T. G. Perceiving the Epigenetic Landscape through Histone Readers. *Nat Struct Mol Biol* 2012, 19 (12), 1218–1227. https://doi.org/10.1038/nsmb.2436.
- (51) Saksouk, N.; Simboeck, E.; Déjardin, J. Constitutive Heterochromatin Formation and Transcription in Mammals. *Epigenetics & Chromatin* **2015**, *8* (1), 3. https://doi.org/10.1186/1756-8935-8-3.
- (52) Peng, J. C.; Karpen, G. H. Heterochromatic Genome Stability Requires Regulators of Histone H3 K9 Methylation. *PLOS Genetics* **2009**, *5* (3), e1000435. https://doi.org/10.1371/journal.pgen.1000435.
- (53) Lachner, M.; O'Carroll, D.; Rea, S.; Mechtler, K.; Jenuwein, T. Methylation of Histone H3 Lysine 9 Creates a Binding Site for HP1 Proteins. *Nature* 2001, 410 (6824), 116–120. https://doi.org/10.1038/35065132.
- (54) Peterson, C. L.; Laniel, M.-A. Histones and Histone Modifications. *Current Biology* **2004**, *14* (14), R546–R551. https://doi.org/10.1016/j.cub.2004.07.007.
- (55) Tagami, H.; Ray-Gallet, D.; Almouzni, G.; Nakatani, Y. Histone H3.1 and H3.3 Complexes Mediate Nucleosome Assembly Pathways Dependent or Independent of DNA Synthesis. *Cell* **2004**, *116* (1), 51–61. https://doi.org/10.1016/S0092-8674(03)01064-X.
- (56) Ray-Gallet, D.; Woolfe, A.; Vassias, I.; Pellentz, C.; Lacoste, N.; Puri, A.; Schultz,D. C.; Pchelintsev, N. A.; Adams, P. D.; Jansen, L. E. T.; Almouzni, G. Dynamics ofHistone H3 Deposition In Vivo Reveal a Nucleosome Gap-Filling Mechanism for

- H3.3 to Maintain Chromatin Integrity. *Molecular Cell* **2011**, *44* (6), 928–941. https://doi.org/10.1016/j.molcel.2011.12.006.
- (57) Sitbon, D.; Boyarchuk, E.; Dingli, F.; Loew, D.; Almouzni, G. Histone Variant H3.3 Residue S31 Is Essential for Xenopus Gastrulation Regardless of the Deposition Pathway. *Nat Commun* 2020, *11* (1), 1256. https://doi.org/10.1038/s41467-020-15084-4.
- (58) Martire, S.; Gogate, A. A.; Whitmill, A.; Tafessu, A.; Nguyen, J.; Teng, Y.-C.; Tastemel, M.; Banaszynski, L. A. Phosphorylation of Histone H3.3 at Serine 31 Promotes P300 Activity and Enhancer Acetylation. *Nat Genet* 2019, *51* (6), 941–946. https://doi.org/10.1038/s41588-019-0428-5.
- (59) Michod, D.; Bartesaghi, S.; Khelifi, A.; Bellodi, C.; Berliocchi, L.; Nicotera, P.; Salomoni, P. Calcium-Dependent Dephosphorylation of the Histone Chaperone DAXX Regulates H3.3 Loading and Transcription upon Neuronal Activation. Neuron 2012, 74 (1), 122–135. https://doi.org/10.1016/j.neuron.2012.02.021.
- (60) Lewis, P. W.; Elsaesser, S. J.; Noh, K.-M.; Stadler, S. C.; Allis, C. D. Daxx Is an H3.3-Specific Histone Chaperone and Cooperates with ATRX in Replication-Independent Chromatin Assembly at Telomeres. *Proceedings of the National Academy of Sciences* 2010, 107 (32), 14075–14080. https://doi.org/10.1073/pnas.1008850107.
- (61) Nüsslein-Volhard, C.; Wieschaus, E. Mutations Affecting Segment Number and Polarity in Drosophila. *Nature* **1980**, 287 (5785), 795–801. https://doi.org/10.1038/287795a0.

- (62) Lawrence, P. A.; Morata, G. Homeobox Genes: Their Function in Drosophila Segmentation and Pattern Formation. *Cell* **1994**, 78 (2), 181–189. https://doi.org/10.1016/0092-8674(94)90289-5.
- (63) Jürgens, G. A Group of Genes Controlling the Spatial Expression of the Bithorax Complex in Drosophila. *Nature* 1985, 316 (6024), 153–155. https://doi.org/10.1038/316153a0.
- (64) Aranda, S.; Mas, G.; Di Croce, L. Regulation of Gene Transcription by Polycomb Proteins. Science Advances 2015, 1 (11), e1500737. https://doi.org/10.1126/sciadv.1500737.
- (65) Kalisch, W.-E.; Rasmuson, B. Changes of Zeste Phenotype Induced by Autosomal Mutations in Drosophila Melanogaster. *Hereditas* 1974, 78 (1), 97–103. https://doi.org/10.1111/j.1601-5223.1974.tb01432.x.
- (66) Birve, A.; Sengupta, A. K.; Beuchle, D.; Larsson, J.; Kennison, J. A.; Rasmuson-Lestander, Å.; Müller, J. Su(z)12, a Novel Drosophila Polycomb Group Gene That Is Conserved in Vertebrates and Plants. *Development* 2001, 128 (17), 3371–3379. https://doi.org/10.1242/dev.128.17.3371.
- (67) Ingham, P. W. Differential Expression of Bithorax Complex Genes in the Absence of the Extra Sex Combs and Trithorax Genes. *Nature* **1983**, *306* (5943), 591–593. https://doi.org/10.1038/306591a0.
- (68) Tripoulas, N. A.; Hersperger, E.; La Jeunesse, D.; Shearn, A. Molecular Genetic Analysis of the Drosophila Melanogaster Gene Absent, Small or Homeotic Discs1 (Ash1). Genetics 1994, 137 (4), 1027–1038. https://doi.org/10.1093/genetics/137.4.1027.

- (69) Klymenko, T.; Müller, J. The Histone Methyltransferases Trithorax and Ash1

 Prevent Transcriptional Silencing by Polycomb Group Proteins. *EMBO reports* **2004**, *5* (4), 373–377. https://doi.org/10.1038/sj.embor.7400111.
- (70) Fauvarque, M.-O.; Laurenti, P.; Boivin, A.; Bloyer, S.; Griffin-Shea, R.; Bourbon, H.-M.; Dura, J.-M. Dominant Modifiers of the Polyhomeotic Extra-Sex-Combs Phenotype Induced by Marked P Element Insertional Mutagenesis in Drosophila. *Genetics Research* 2001, 78 (2), 137–148. https://doi.org/10.1017/S0016672301005274.
- (71) Schmitges, F. W.; Prusty, A. B.; Faty, M.; Stützer, A.; Lingaraju, G. M.; Aiwazian, J.; Sack, R.; Hess, D.; Li, L.; Zhou, S.; Bunker, R. D.; Wirth, U.; Bouwmeester, T.; Bauer, A.; Ly-Hartig, N.; Zhao, K.; Chan, H.; Gu, J.; Gut, H.; Fischle, W.; Müller, J.; Thomä, N. H. Histone Methylation by PRC2 Is Inhibited by Active Chromatin Marks. *Molecular Cell* 2011, 42 (3), 330–341. https://doi.org/10.1016/j.molcel.2011.03.025.
- (72) Jani, K. S.; Jain, S. U.; Ge, E. J.; Diehl, K. L.; Lundgren, S. M.; Müller, M. M.; Lewis, P. W.; Muir, T. W. Histone H3 Tail Binds a Unique Sensing Pocket in EZH2 to Activate the PRC2 Methyltransferase. *PNAS* 2019, *116* (17), 8295–8300. https://doi.org/10.1073/pnas.1819029116.
- (73) Herz, H.-M.; Mohan, M.; Garruss, A. S.; Liang, K.; Takahashi, Y.; Mickey, K.; Voets, O.; Verrijzer, C. P.; Shilatifard, A. Enhancer-Associated H3K4 Monomethylation by Trithorax-Related, the Drosophila Homolog of Mammalian Mll3/Mll4. *Genes Dev.* 2012, 26 (23), 2604–2620. https://doi.org/10.1101/gad.201327.112.
- (74) Wang, L.; Zhao, Z.; Ozark, P. A.; Fantini, D.; Marshall, S. A.; Rendleman, E. J.; Cozzolino, K. A.; Louis, N.; He, X.; Morgan, M. A.; Takahashi, Y.; Collings, C. K.;

- Smith, E. R.; Ntziachristos, P.; Savas, J. N.; Zou, L.; Hashizume, R.; Meeks, J. J.; Shilatifard, A. Resetting the Epigenetic Balance of Polycomb and COMPASS Function at Enhancers for Cancer Therapy. *Nat Med* **2018**, *24* (6), 758–769. https://doi.org/10.1038/s41591-018-0034-6.
- (75) Farcas, A. M.; Blackledge, N. P.; Sudbery, I.; Long, H. K.; McGouran, J. F.; Rose, N. R.; Lee, S.; Sims, D.; Cerase, A.; Sheahan, T. W.; Koseki, H.; Brockdorff, N.; Ponting, C. P.; Kessler, B. M.; Klose, R. J. KDM2B Links the Polycomb Repressive Complex 1 (PRC1) to Recognition of CpG Islands. *eLife* 2012, 1, e00205. https://doi.org/10.7554/eLife.00205.
- (76) Gao, Z.; Zhang, J.; Bonasio, R.; Strino, F.; Sawai, A.; Parisi, F.; Kluger, Y.; Reinberg, D. PCGF Homologs, CBX Proteins, and RYBP Define Functionally Distinct PRC1 Family Complexes. *Molecular Cell* 2012, 45 (3), 344–356. https://doi.org/10.1016/j.molcel.2012.01.002.
- (77) Lagarou, A.; Mohd-Sarip, A.; Moshkin, Y. M.; Chalkley, G. E.; Bezstarosti, K.; Demmers, J. A. A.; Verrijzer, C. P. DKDM2 Couples Histone H2A Ubiquitylation to Histone H3 Demethylation during Polycomb Group Silencing. *Genes Dev.* 2008, 22 (20), 2799–2810. https://doi.org/10.1101/gad.484208.
- (78) Bernstein, B. E.; Mikkelsen, T. S.; Xie, X.; Kamal, M.; Huebert, D. J.; Cuff, J.; Fry, B.; Meissner, A.; Wernig, M.; Plath, K.; Jaenisch, R.; Wagschal, A.; Feil, R.; Schreiber, S. L.; Lander, E. S. A Bivalent Chromatin Structure Marks Key Developmental Genes in Embryonic Stem Cells. Cell 2006, 125 (2), 315–326. https://doi.org/10.1016/j.cell.2006.02.041.

- (79) Connelly, K. E.; Dykhuizen, E. C. Compositional and Functional Diversity of Canonical PRC1 Complexes in Mammals. *Biochimica et Biophysica Acta (BBA) -Gene Regulatory Mechanisms* 2017, 1860 (2), 233–245. https://doi.org/10.1016/j.bbagrm.2016.12.006.
- (80) Bauer, M.; Trupke, J.; Ringrose, L. The Quest for Mammalian Polycomb Response Elements: Are We There Yet? *Chromosoma* **2016**, *125* (3), 471–496. https://doi.org/10.1007/s00412-015-0539-4.
- (81) Fursova, N. A.; Blackledge, N. P.; Nakayama, M.; Ito, S.; Koseki, Y.; Farcas, A. M.; King, H. W.; Koseki, H.; Klose, R. J. Synergy between Variant PRC1 Complexes Defines Polycomb-Mediated Gene Repression. *Molecular Cell* 2019, 74 (5), 1020-1036.e8. https://doi.org/10.1016/j.molcel.2019.03.024.
- (82) Moussa, H. F.; Bsteh, D.; Yelagandula, R.; Pribitzer, C.; Stecher, K.; Bartalska, K.; Michetti, L.; Wang, J.; Zepeda-Martinez, J. A.; Elling, U.; Stuckey, J. I.; James, L. I.; Frye, S. V.; Bell, O. Canonical PRC1 Controls Sequence-Independent Propagation of Polycomb-Mediated Gene Silencing. *Nat Commun* 2019, 10 (1), 1931. https://doi.org/10.1038/s41467-019-09628-6.
- (83) Healy, E.; Mucha, M.; Glancy, E.; Fitzpatrick, D. J.; Conway, E.; Neikes, H. K.; Monger, C.; Van Mierlo, G.; Baltissen, M. P.; Koseki, Y.; Vermeulen, M.; Koseki, H.; Bracken, A. P. PRC2.1 and PRC2.2 Synergize to Coordinate H3K27 Trimethylation. *Molecular Cell* 2019, 76 (3), 437-452.e6. https://doi.org/10.1016/j.molcel.2019.08.012.
- (84) Landeira, D.; Sauer, S.; Poot, R.; Dvorkina, M.; Mazzarella, L.; Jørgensen, H. F.; Pereira, C. F.; Leleu, M.; Piccolo, F. M.; Spivakov, M.; Brookes, E.; Pombo, A.;

- Fisher, C.; Skarnes, W. C.; Snoek, T.; Bezstarosti, K.; Demmers, J.; Klose, R. J.; Casanova, M.; Tavares, L.; Brockdorff, N.; Merkenschlager, M.; Fisher, A. G. Jarid2 Is a PRC2 Component in Embryonic Stem Cells Required for Multi-Lineage Differentiation and Recruitment of PRC1 and RNA Polymerase II to Developmental Regulators. *Nat Cell Biol* **2010**, *12* (6), 618–624. https://doi.org/10.1038/ncb2065.
- (85) Shen, X.; Liu, Y.; Hsu, Y.-J.; Fujiwara, Y.; Kim, J.; Mao, X.; Yuan, G.-C.; Orkin, S. H. EZH1 Mediates Methylation on Histone H3 Lysine 27 and Complements EZH2 in Maintaining Stem Cell Identity and Executing Pluripotency. *Molecular Cell* 2008, 32 (4), 491–502. https://doi.org/10.1016/j.molcel.2008.10.016.
- (86) Shen, X.; Kim, W.; Fujiwara, Y.; Simon, M. D.; Liu, Y.; Mysliwiec, M. R.; Yuan, G.-C.; Lee, Y.; Orkin, S. H. Jumonji Modulates Polycomb Activity and Self-Renewal versus Differentiation of Stem Cells. *Cell* 2009, *139* (7), 1303–1314. https://doi.org/10.1016/j.cell.2009.12.003.
- (87) Li, G.; Margueron, R.; Ku, M.; Chambon, P.; Bernstein, B. E.; Reinberg, D. Jarid2 and PRC2, Partners in Regulating Gene Expression. *Genes Dev.* **2010**, *24* (4), 368–380. https://doi.org/10.1101/gad.1886410.
- (88) Li, H.; Liefke, R.; Jiang, J.; Kurland, J. V.; Tian, W.; Deng, P.; Zhang, W.; He, Q.; Patel, D. J.; Bulyk, M. L.; Shi, Y.; Wang, Z. Polycomb-like Proteins Link the PRC2 Complex to CpG Islands. *Nature* 2017, 549 (7671), 287–291. https://doi.org/10.1038/nature23881.
- (89) Blackledge, N. P.; Fursova, N. A.; Kelley, J. R.; Huseyin, M. K.; Feldmann, A.; Klose, R. J. PRC1 Catalytic Activity Is Central to Polycomb System Function.

- Molecular Cell **2020**, 77 (4), 857-874.e9. https://doi.org/10.1016/j.molcel.2019.12.001.
- (90) Pengelly, A. R.; Kalb, R.; Finkl, K.; Müller, J. Transcriptional Repression by PRC1 in the Absence of H2A Monoubiquitylation. *Genes Dev.* 2015, 29 (14), 1487–1492. https://doi.org/10.1101/gad.265439.115.
- (91) Blackledge, N. P.; Farcas, A. M.; Kondo, T.; King, H. W.; McGouran, J. F.; Hanssen, L. L. P.; Ito, S.; Cooper, S.; Kondo, K.; Koseki, Y.; Ishikura, T.; Long, H. K.; Sheahan, T. W.; Brockdorff, N.; Kessler, B. M.; Koseki, H.; Klose, R. J. Variant PRC1 Complex-Dependent H2A Ubiquitylation Drives PRC2 Recruitment and Polycomb Domain Formation. *Cell* 2014, 157 (6), 1445–1459. https://doi.org/10.1016/j.cell.2014.05.004.
- (92) Kalb, R.; Latwiel, S.; Baymaz, H. I.; Jansen, P. W. T. C.; Müller, C. W.; Vermeulen, M.; Müller, J. Histone H2A Monoubiquitination Promotes Histone H3 Methylation in Polycomb Repression. *Nat Struct Mol Biol* 2014, 21 (6), 569–571. https://doi.org/10.1038/nsmb.2833.
- (93) Cao, R.; Wang, L.; Wang, H.; Xia, L.; Erdjument-Bromage, H.; Tempst, P.; Jones, R. S.; Zhang, Y. Role of Histone H3 Lysine 27 Methylation in Polycomb-Group Silencing. *Science* 2002, 298 (5595), 1039–1043.
 https://doi.org/10.1126/science.1076997.
- (94) Czermin, B.; Melfi, R.; McCabe, D.; Seitz, V.; Imhof, A.; Pirrotta, V. Drosophila Enhancer of Zeste/ESC Complexes Have a Histone H3 Methyltransferase Activity That Marks Chromosomal Polycomb Sites. *Cell* 2002, 111 (2), 185–196. https://doi.org/10.1016/S0092-8674(02)00975-3.

- (95) Kim, C. A.; Gingery, M.; Pilpa, R. M.; Bowie, J. U. The SAM Domain of Polyhomeotic Forms a Helical Polymer. *Nat Struct Mol Biol* 2002, 9 (6), 453–457. https://doi.org/10.1038/nsb802.
- (96) Gambetta, M. C.; Müller, J. O-GlcNAcylation Prevents Aggregation of the Polycomb Group Repressor Polyhomeotic. *Developmental Cell* 2014, 31 (5), 629–639. https://doi.org/10.1016/j.devcel.2014.10.020.
- (97) Bonnet, J.; Boichenko, I.; Kalb, R.; Jeune, M. L.; Maltseva, S.; Pieropan, M.; Finkl, K.; Fierz, B.; Müller, J. PR-DUB Preserves Polycomb Repression by Preventing Excessive Accumulation of H2Aub1, an Antagonist of Chromatin Compaction.
 Genes Dev. 2022, 36 (19–20), 1046–1061. https://doi.org/10.1101/gad.350014.122.
- (98) Fursova, N. A.; Turberfield, A. H.; Blackledge, N. P.; Findlater, E. L.; Lastuvkova, A.; Huseyin, M. K.; Dobrinić, P.; Klose, R. J. BAP1 Constrains Pervasive H2AK119ub1 to Control the Transcriptional Potential of the Genome. *Genes Dev.* 2021, 35 (9–10), 749–770. https://doi.org/10.1101/gad.347005.120.
- (99) Conway, E.; Rossi, F.; Fernandez-Perez, D.; Ponzo, E.; Ferrari, K. J.; Zanotti, M.; Manganaro, D.; Rodighiero, S.; Tamburri, S.; Pasini, D. BAP1 Enhances Polycomb Repression by Counteracting Widespread H2AK119ub1 Deposition and Chromatin Condensation. *Molecular Cell* 2021, 81 (17), 3526-3541.e8. https://doi.org/10.1016/j.molcel.2021.06.020.
- (100) Margueron, R.; Justin, N.; Ohno, K.; Sharpe, M. L.; Son, J.; Drury Iii, W. J.; Voigt, P.; Martin, S. R.; Taylor, W. R.; De Marco, V.; Pirrotta, V.; Reinberg, D.; Gamblin, S. J. Role of the Polycomb Protein EED in the Propagation of Repressive Histone Marks. *Nature* 2009, *461* (7265), 762–767. https://doi.org/10.1038/nature08398.

- (101) Hansen, K. H.; Bracken, A. P.; Pasini, D.; Dietrich, N.; Gehani, S. S.; Monrad, A.; Rappsilber, J.; Lerdrup, M.; Helin, K. A Model for Transmission of the H3K27me3 Epigenetic Mark. *Nature Cell Biology* 2008, *10* (11), 1291–1300. https://doi.org/10.1038/ncb1787.
- (102) Jiao, L.; Liu, X. Structural Basis of Histone H3K27 Trimethylation by an Active Polycomb Repressive Complex 2. Science 2015, 350 (6258), aac4383. https://doi.org/10.1126/science.aac4383.
- (103) Müller, J.; Hart, C. M.; Francis, N. J.; Vargas, M. L.; Sengupta, A.; Wild, B.; Miller, E. L.; O'Connor, M. B.; Kingston, R. E.; Simon, J. A. Histone Methyltransferase Activity of a Drosophila Polycomb Group Repressor Complex. *Cell* 2002, 111 (2), 197–208. https://doi.org/10.1016/S0092-8674(02)00976-5.
- (104) Wang, X.; Long, Y.; Paucek, R. D.; Gooding, A. R.; Lee, T.; Burdorf, R. M.; Cech, T. R. Regulation of Histone Methylation by Automethylation of PRC2. *Genes Dev.*2019, 33 (19–20), 1416–1427. https://doi.org/10.1101/gad.328849.119.
- (105) Wang, X.; Paucek, R. D.; Gooding, A. R.; Brown, Z. Z.; Ge, E. J.; Muir, T. W.; Cech, T. R. Molecular Analysis of PRC2 Recruitment to DNA in Chromatin and Its Inhibition by RNA. *Nat Struct Mol Biol* 2017, 24 (12), 1028–1038. https://doi.org/10.1038/nsmb.3487.
- (106) Lee, C.-H.; Yu, J.-R.; Granat, J.; Saldaña-Meyer, R.; Andrade, J.; LeRoy, G.; Jin, Y.; Lund, P.; Stafford, J. M.; Garcia, B. A.; Ueberheide, B.; Reinberg, D. Automethylation of PRC2 Promotes H3K27 Methylation and Is Impaired in H3K27M Pediatric Glioma. *Genes Dev.* 2019, 33 (19–20), 1428–1440. https://doi.org/10.1101/gad.328773.119.

- (107) Zhang, Q.; Agius, S. C.; Flanigan, S. F.; Uckelmann, M.; Levina, V.; Owen, B. M.; Davidovich, C. PALI1 Facilitates DNA and Nucleosome Binding by PRC2 and Triggers an Allosteric Activation of Catalysis. *Nat Commun* **2021**, *12* (1), 4592. https://doi.org/10.1038/s41467-021-24866-3.
- (108) Chan, C. s.; Rastelli, L.; Pirrotta, V. A Polycomb Response Element in the Ubx Gene That Determines an Epigenetically Inherited State of Repression. *The EMBO Journal* 1994, 13 (11), 2553–2564. https://doi.org/10.1002/j.1460-2075.1994.tb06545.x.
- (109) De, S.; Cheng, Y.; Sun, M.; Gehred, N. D.; Kassis, J. A. Structure and Function of an Ectopic Polycomb Chromatin Domain. *Science Advances* **2019**, *5* (1), eaau9739. https://doi.org/10.1126/sciadv.aau9739.
- (110) De, S.; Mitra, A.; Cheng, Y.; Pfeifer, K.; Kassis, J. A. Formation of a Polycomb-Domain in the Absence of Strong Polycomb Response Elements. *PLoS Genet.*2016, 12 (7), e1006200. https://doi.org/10.1371/journal.pgen.1006200.
- (111) Frey, F.; Sheahan, T.; Finkl, K.; Stoehr, G.; Mann, M.; Benda, C.; Müller, J.
 Molecular Basis of PRC1 Targeting to Polycomb Response Elements by PhoRC.
 Genes Dev. 2016, 30 (9), 1116–1127. https://doi.org/10.1101/gad.279141.116.
- (112) Deaton, A. M.; Bird, A. CpG Islands and the Regulation of Transcription. Genes Dev. 2011, 25 (10), 1010–1022. https://doi.org/10.1101/gad.2037511.
- (113) Reddington, J. P.; Perricone, S. M.; Nestor, C. E.; Reichmann, J.; Youngson, N. A.; Suzuki, M.; Reinhardt, D.; Dunican, D. S.; Prendergast, J. G.; Mjoseng, H.; Ramsahoye, B. H.; Whitelaw, E.; Greally, J. M.; Adams, I. R.; Bickmore, W. A.; Meehan, R. R. Redistribution of H3K27me3 upon DNA Hypomethylation Results in

- De-Repression of Polycomb Target Genes. *Genome Biology* **2013**, *14* (3), R25. https://doi.org/10.1186/gb-2013-14-3-r25.
- (114) Mendenhall, E. M.; Koche, R. P.; Truong, T.; Zhou, V. W.; Issac, B.; Chi, A. S.; Ku, M.; Bernstein, B. E. GC-Rich Sequence Elements Recruit PRC2 in Mammalian ES Cells. *PLOS Genetics* 2010, 6 (12), e1001244.
 https://doi.org/10.1371/journal.pgen.1001244.
- (115) Jermann, P.; Hoerner, L.; Burger, L.; Schübeler, D. Short Sequences Can Efficiently Recruit Histone H3 Lysine 27 Trimethylation in the Absence of Enhancer Activity and DNA Methylation. PNAS 2014, 111 (33), E3415–E3421. https://doi.org/10.1073/pnas.1400672111.
- (116) Waddington, C. H. *The Strategy of the Genes*; Routledge, 2014.
- (117) Escobar, T. M.; Oksuz, O.; Saldaña-Meyer, R.; Descostes, N.; Bonasio, R.; Reinberg, D. Active and Repressed Chromatin Domains Exhibit Distinct Nucleosome Segregation during DNA Replication. *Cell* **2019**, *179* (4), 953-963.e11. https://doi.org/10.1016/j.cell.2019.10.009.
- (118) Allshire, R. C.; Madhani, H. D. Ten Principles of Heterochromatin Formation and Function. *Nat Rev Mol Cell Biol* **2018**, *19* (4), 229–244. https://doi.org/10.1038/nrm.2017.119.
- (119) Allis, C. D.; Jenuwein, T. The Molecular Hallmarks of Epigenetic Control. *Nat Rev Genet* **2016**, *17* (8), 487–500. https://doi.org/10.1038/nrg.2016.59.
- (120) Trojer, P.; Reinberg, D. Facultative Heterochromatin: Is There a Distinctive Molecular Signature? *Molecular Cell* 2007, 28 (1), 1–13. https://doi.org/10.1016/j.molcel.2007.09.011.

- (121) Petryk, N.; Dalby, M.; Wenger, A.; Stromme, C. B.; Strandsby, A.; Andersson, R.; Groth, A. MCM2 Promotes Symmetric Inheritance of Modified Histones during DNA Replication. *Science* **2018**, *361* (6409), 1389–1392. https://doi.org/10.1126/science.aau0294.
- (122) Yu, C.; Gan, H.; Serra-Cardona, A.; Zhang, L.; Gan, S.; Sharma, S.; Johansson, E.; Chabes, A.; Xu, R.-M.; Zhang, Z. A Mechanism for Preventing Asymmetric Histone Segregation onto Replicating DNA Strands. *Science* 2018, *361* (6409), 1386–1389. https://doi.org/10.1126/science.aat8849.
- (123) Reinberg, D.; Vales, L. D. Chromatin Domains Rich in Inheritance. *Science* **2018**, 361 (6397), 33–34. https://doi.org/10.1126/science.aat7871.
- (124) Simon, J. A.; Kingston, R. E. Occupying Chromatin: Polycomb Mechanisms for Getting to Genomic Targets, Stopping Transcriptional Traffic, and Staying Put. *Molecular Cell* 2013, 49 (5), 808–824. https://doi.org/10.1016/j.molcel.2013.02.013.
- (125) Coleman, R. T.; Struhl, G. Causal Role for Inheritance of H3K27me3 in Maintaining the OFF State of a Drosophila HOX Gene. Science 2017, 356 (6333). https://doi.org/10.1126/science.aai8236.
- (126) Laprell, F.; Finkl, K.; Müller, J. Propagation of Polycomb-Repressed Chromatin
 Requires Sequence-Specific Recruitment to DNA. *Science* 2017, 356 (6333), 85–88. https://doi.org/10.1126/science.aai8266.
- (127) Comet, I.; Riising, E. M.; Leblanc, B.; Helin, K. Maintaining Cell Identity: PRC2-Mediated Regulation of Transcription and Cancer. *Nat Rev Cancer* 2016, *16* (12), 803–810. https://doi.org/10.1038/nrc.2016.83.

- Morin, R. D.; Johnson, N. A.; Severson, T. M.; Mungall, A. J.; An, J.; Goya, R.;
 Paul, J. E.; Boyle, M.; Woolcock, B. W.; Kuchenbauer, F.; Yap, D.; Humphries, R.
 K.; Griffith, O. L.; Shah, S.; Zhu, H.; Kimbara, M.; Shashkin, P.; Charlot, J. F.;
 Tcherpakov, M.; Corbett, R.; Tam, A.; Varhol, R.; Smailus, D.; Moksa, M.; Zhao, Y.;
 Delaney, A.; Qian, H.; Birol, I.; Schein, J.; Moore, R.; Holt, R.; Horsman, D. E.;
 Connors, J. M.; Jones, S.; Aparicio, S.; Hirst, M.; Gascoyne, R. D.; Marra, M. A.
 Somatic Mutations Altering EZH2 (Tyr641) in Follicular and Diffuse Large B-Cell
 Lymphomas of Germinal-Center Origin. *Nature Genetics* 2010, *42* (2), 181–185.
 https://doi.org/10.1038/ng.518.
- (129) McCabe, M. T.; Ott, H. M.; Ganji, G.; Korenchuk, S.; Thompson, C.; Van Aller, G. S.; Liu, Y.; Graves, A. P.; Iii, A. D. P.; Diaz, E.; LaFrance, L. V.; Mellinger, M.; Duquenne, C.; Tian, X.; Kruger, R. G.; McHugh, C. F.; Brandt, M.; Miller, W. H.; Dhanak, D.; Verma, S. K.; Tummino, P. J.; Creasy, C. L. EZH2 Inhibition as a Therapeutic Strategy for Lymphoma with EZH2-Activating Mutations. *Nature* 2012, 492 (7427), 108–112. https://doi.org/10.1038/nature11606.
- (130) Ntziachristos, P.; Tsirigos, A.; Vlierberghe, P. V.; Nedjic, J.; Trimarchi, T.; Flaherty, M. S.; Ferres-Marco, D.; da Ros, V.; Tang, Z.; Siegle, J.; Asp, P.; Hadler, M.; Rigo, I.; Keersmaecker, K. D.; Patel, J.; Huynh, T.; Utro, F.; Poglio, S.; Samon, J. B.; Paietta, E.; Racevskis, J.; Rowe, J. M.; Rabadan, R.; Levine, R. L.; Brown, S.; Pflumio, F.; Dominguez, M.; Ferrando, A.; Aifantis, I. Genetic Inactivation of the Polycomb Repressive Complex 2 in T Cell Acute Lymphoblastic Leukemia. *Nature Medicine* 2012, *18* (2), 298–302. https://doi.org/10.1038/nm.2651.

- (131) Ostrom, Q. T.; Cioffi, G.; Gittleman, H.; Patil, N.; Waite, K.; Kruchko, C.; Barnholtz-Sloan, J. S. CBTRUS Statistical Report: Primary Brain and Other Central Nervous System Tumors Diagnosed in the United States in 2012-2016. *Neuro* Oncol 2019, 21 (Suppl 5), v1–v100. https://doi.org/10.1093/neuonc/noz150.
- (132) Cooney, T. M.; Lubanszky, E.; Prasad, R.; Hawkins, C.; Mueller, S. Diffuse Midline Glioma: Review of Epigenetics. *J Neurooncol* **2020**, *150* (1), 27–34. https://doi.org/10.1007/s11060-020-03553-1.
- (133) Vinci, M.; Burford, A.; Molinari, V.; Kessler, K.; Popov, S.; Clarke, M.; Taylor, K.
 R.; Pemberton, H. N.; Lord, C. J.; Gutteridge, A.; Forshew, T.; Carvalho, D.;
 Marshall, L. V.; Qin, E. Y.; Ingram, W. J.; Moore, A. S.; Ng, H.-K.; Trabelsi, S.;
 H'mida-Ben Brahim, D.; Entz-Werle, N.; Zacharoulis, S.; Vaidya, S.; Mandeville, H.
 C.; Bridges, L. R.; Martin, A. J.; Al-Sarraj, S.; Chandler, C.; Sunol, M.; Mora, J.; de
 Torres, C.; Cruz, O.; Carcaboso, A. M.; Monje, M.; Mackay, A.; Jones, C. Functional
 Diversity and Cooperativity between Subclonal Populations of Pediatric
 Glioblastoma and Diffuse Intrinsic Pontine Glioma Cells. *Nat Med* 2018, 24 (8),
 1204–1215. https://doi.org/10.1038/s41591-018-0086-7.
- (134) Mackay, A.; Burford, A.; Carvalho, D.; Izquierdo, E.; Fazal-Salom, J.; Taylor, K. R.; Bjerke, L.; Clarke, M.; Vinci, M.; Nandhabalan, M.; Temelso, S.; Popov, S.; Molinari, V.; Raman, P.; Waanders, A. J.; Han, H. J.; Gupta, S.; Marshall, L.; Zacharoulis, S.; Vaidya, S.; Mandeville, H. C.; Bridges, L. R.; Martin, A. J.; Al-Sarraj, S.; Chandler, C.; Ng, H.-K.; Li, X.; Mu, K.; Trabelsi, S.; Brahim, D. H.-B.; Kisljakov, A. N.; Konovalov, D. M.; Moore, A. S.; Carcaboso, A. M.; Sunol, M.; de Torres, C.; Cruz, O.; Mora, J.; Shats, L. I.; Stavale, J. N.; Bidinotto, L. T.; Reis, R.

- M.; Entz-Werle, N.; Farrell, M.; Cryan, J.; Crimmins, D.; Caird, J.; Pears, J.; Monje, M.; Debily, M.-A.; Castel, D.; Grill, J.; Hawkins, C.; Nikbakht, H.; Jabado, N.; Baker, S. J.; Pfister, S. M.; Jones, D. T. W.; Fouladi, M.; von Bueren, A. O.; Baudis, M.; Resnick, A.; Jones, C. Integrated Molecular Meta-Analysis of 1,000 Pediatric High-Grade and Diffuse Intrinsic Pontine Glioma. *Cancer Cell* **2017**, *32* (4), 520-537.e5. https://doi.org/10.1016/j.ccell.2017.08.017.
- (135) Buczkowicz, P.; Hoeman, C.; Rakopoulos, P.; Pajovic, S.; Letourneau, L.;
 Dzamba, M.; Morrison, A.; Lewis, P.; Bouffet, E.; Bartels, U.; Zuccaro, J.; Agnihotri,
 S.; Ryall, S.; Barszczyk, M.; Chornenkyy, Y.; Bourgey, M.; Bourque, G.; Montpetit,
 A.; Cordero, F.; Castelo-Branco, P.; Mangerel, J.; Tabori, U.; Ho, K. C.; Huang, A.;
 Taylor, K. R.; Mackay, A.; Bendel, A. E.; Nazarian, J.; Fangusaro, J. R.; Karajannis,
 M. A.; Zagzag, D.; Foreman, N. K.; Donson, A.; Hegert, J. V.; Smith, A.; Chan, J.;
 Lafay-Cousin, L.; Dunn, S.; Hukin, J.; Dunham, C.; Scheinemann, K.; Michaud, J.;
 Zelcer, S.; Ramsay, D.; Cain, J.; Brennan, C.; Souweidane, M. M.; Jones, C.; Allis,
 C. D.; Brudno, M.; Becher, O.; Hawkins, C. Genomic Analysis of Diffuse Intrinsic
 Pontine Gliomas Identifies Three Molecular Subgroups and Recurrent Activating
 ACVR1 Mutations. *Nat. Genet.* 2014, 46 (5), 451–456.
 https://doi.org/10.1038/ng.2936.
- (136) Fontebasso, A. M.; Papillon-Cavanagh, S.; Schwartzentruber, J.; Nikbakht, H.; Gerges, N.; Fiset, P.-O.; Bechet, D.; Faury, D.; De Jay, N.; Ramkissoon, L. A.; Corcoran, A.; Jones, D. T. W.; Sturm, D.; Johann, P.; Tomita, T.; Goldman, S.; Nagib, M.; Bendel, A.; Goumnerova, L.; Bowers, D. C.; Leonard, J. R.; Rubin, J. B.; Alden, T.; Browd, S.; Geyer, J. R.; Leary, S.; Jallo, G.; Cohen, K.; Gupta, N.;

- Prados, M. D.; Carret, A.-S.; Ellezam, B.; Crevier, L.; Klekner, A.; Bognar, L.; Hauser, P.; Garami, M.; Myseros, J.; Dong, Z.; Siegel, P. M.; Malkin, H.; Ligon, A. H.; Albrecht, S.; Pfister, S. M.; Ligon, K. L.; Majewski, J.; Jabado, N.; Kieran, M. W. Recurrent Somatic Mutations in ACVR1 in Pediatric Midline High-Grade Astrocytoma. *Nat. Genet.* **2014**, *46* (5), 462–466. https://doi.org/10.1038/ng.2950.
- (137) Gallitto, M.; Lazarev, S.; Wasserman, I.; Stafford, J. M.; Wolden, S. L.; Terezakis, S. A.; Bindra, R. S.; Bakst, R. L. Role of Radiation Therapy in the Management of Diffuse Intrinsic Pontine Glioma: A Systematic Review. *Advances in Radiation Oncology* 2019, 4 (3), 520–531. https://doi.org/10.1016/j.adro.2019.03.009.
- (138) Vanan, M. I.; Eisenstat, D. D. DIPG in Children What Can We Learn from the Past? *Frontiers in Oncology* **2015**, *5*.
- (139) Cooney, T.; Onar-Thomas, A.; Huang, J.; Lulla, R.; Fangusaro, J.; Kramer, K.; Baxter, P.; Fouladi, M.; Dunkel, I. J.; Warren, K. E.; Monje, M. DIPG-22. A PHASE 1 TRIAL OF THE HISTONE DEACETYLASE INHIBITOR PANOBINOSTAT IN PEDIATRIC PATIENTS WITH RECURRENT OR REFRACTORY DIFFUSE INTRINSIC PONTINE GLIOMA: A PEDIATRIC BRAIN TUMOR CONSORTIUM (PBTC) STUDY. Neuro-Oncology 2018, 20 (suppl_2), i53. https://doi.org/10.1093/neuonc/noy059.115.
- (140) Mueller, S.; Jain, P.; Liang, W. S.; Kilburn, L.; Kline, C.; Gupta, N.; Panditharatna, E.; Magge, S. N.; Zhang, B.; Zhu, Y.; Crawford, J. R.; Banerjee, A.; Nazemi, K.; Packer, R. J.; Petritsch, C. K.; Truffaux, N.; Roos, A.; Nasser, S.; Phillips, J. J.; Solomon, D.; Molinaro, A.; Waanders, A. J.; Byron, S. A.; Berens, M. E.; Kuhn, J.; Nazarian, J.; Prados, M.; Resnick, A. C. A Pilot Precision Medicine Trial for

- Children with Diffuse Intrinsic Pontine Glioma-PNOC003: A Report from the Pacific Pediatric Neuro-Oncology Consortium. *Int J Cancer* **2019**, *145* (7), 1889–1901. https://doi.org/10.1002/ijc.32258.
- (141) Majzner, R. G.; Ramakrishna, S.; Yeom, K. W.; Patel, S.; Chinnasamy, H.;
 Schultz, L. M.; Richards, R. M.; Jiang, L.; Barsan, V.; Mancusi, R.; Geraghty, A. C.;
 Good, Z.; Mochizuki, A. Y.; Gillespie, S. M.; Toland, A. M. S.; Mahdi, J.; Reschke,
 A.; Nie, E. H.; Chau, I. J.; Rotiroti, M. C.; Mount, C. W.; Baggott, C.; Mavroukakis,
 S.; Egeler, E.; Moon, J.; Erickson, C.; Green, S.; Kunicki, M.; Fujimoto, M.;
 Ehlinger, Z.; Reynolds, W.; Kurra, S.; Warren, K. E.; Prabhu, S.; Vogel, H.;
 Rasmussen, L.; Cornell, T. T.; Partap, S.; Fisher, P. G.; Campen, C. J.; Filbin, M.
 G.; Grant, G.; Sahaf, B.; Davis, K. L.; Feldman, S. A.; Mackall, C. L.; Monje, M.
 GD2-CAR T Cell Therapy for H3K27M-Mutated Diffuse Midline Gliomas. *Nature*2022, 603 (7903), 934–941. https://doi.org/10.1038/s41586-022-04489-4.
- (142) Jenseit, A.; Camgöz, A.; Pfister, S. M.; Kool, M. EZHIP: A New Piece of the Puzzle towards Understanding Pediatric Posterior Fossa Ependymoma. *Acta Neuropathol* 2022, 143 (1), 1–13. https://doi.org/10.1007/s00401-021-02382-4.
- (143) Grundy, R. G.; Wilne, S. A.; Weston, C. L.; Robinson, K.; Lashford, L. S.;
 Ironside, J.; Cox, T.; Chong, W. K.; Campbell, R. H.; Bailey, C. C.; Gattamaneni, R.;
 Picton, S.; Thorpe, N.; Mallucci, C.; English, M. W.; Punt, J. A.; Walker, D. A.;
 Ellison, D. W.; Machin, D. Primary Postoperative Chemotherapy without
 Radiotherapy for Intracranial Ependymoma in Children: The UKCCSG/SIOP
 Prospective Study. *The Lancet Oncology* 2007, 8 (8), 696–705.
 https://doi.org/10.1016/S1470-2045(07)70208-5.

- (144) Parker, M.; Mohankumar, K. M.; Punchihewa, C.; Weinlich, R.; Dalton, J. D.; Li, Y.; Lee, R.; Tatevossian, R. G.; Phoenix, T. N.; Thiruvenkatam, R.; White, E.; Tang, B.; Orisme, W.; Gupta, K.; Rusch, M.; Chen, X.; Li, Y.; Nagahawhatte, P.; Hedlund, E.; Finkelstein, D.; Wu, G.; Shurtleff, S.; Easton, J.; Boggs, K.; Yergeau, D.; Vadodaria, B.; Mulder, H. L.; Becksfort, J.; Gupta, P.; Huether, R.; Ma, J.; Song, G.; Gajjar, A.; Merchant, T.; Boop, F.; Smith, A. A.; Ding, L.; Lu, C.; Ochoa, K.; Zhao, D.; Fulton, R. S.; Fulton, L. L.; Mardis, E. R.; Wilson, R. K.; Downing, J. R.; Green, D. R.; Zhang, J.; Ellison, D. W.; Gilbertson, R. J. C11orf95–RELA Fusions Drive Oncogenic NF-KB Signalling in Ependymoma. *Nature* 2014, *506* (7489), 451–455. https://doi.org/10.1038/nature13109.
- (145) Ragazzini, R.; Pérez-Palacios, R.; Baymaz, I. H.; Diop, S.; Ancelin, K.; Zielinski, D.; Michaud, A.; Givelet, M.; Borsos, M.; Aflaki, S.; Legoix, P.; Jansen, P. W. T. C.; Servant, N.; Torres-Padilla, M.-E.; Bourc'his, D.; Fouchet, P.; Vermeulen, M.; Margueron, R. EZHIP Constrains Polycomb Repressive Complex 2 Activity in Germ Cells. *Nature Communications* 2019, *10* (1), 3858. https://doi.org/10.1038/s41467-019-11800-x.
- (146) Mosaab, A.; El-Ayadi, M.; Khorshed, E. N.; Amer, N.; Refaat, A.; El-Beltagy, M.; Hassan, Z.; Soror, S. H.; Zaghloul, M. S.; El-Naggar, S. Histone H3K27M Mutation Overrides Histological Grading in Pediatric Gliomas. *Sci Rep* 2020, *10* (1), 8368. https://doi.org/10.1038/s41598-020-65272-x.
- (147) Mendez, F. M.; Núñez, F. J.; Garcia-Fabiani, M. B.; Haase, S.; Carney, S.; Gauss, J. C.; Becher, O. J.; Lowenstein, P. R.; Castro, M. G. Epigenetic Reprogramming and Chromatin Accessibility in Pediatric Diffuse Intrinsic Pontine Gliomas: A Neural

- Developmental Disease. *Neuro Oncol* **2020**, *22* (2), 195–206. https://doi.org/10.1093/neuonc/noz218.
- (148) Nambirajan, A.; Sharma, A.; Rajeshwari, M.; Boorgula, M. T.; Doddamani, R.; Garg, A.; Suri, V.; Sarkar, C.; Sharma, M. EZH2 Inhibitory Protein (EZHIP/Cxorf67) Expression Correlates Strongly with H3K27me3 Loss in Posterior Fossa Ependymomas and Is Mutually Exclusive with H3K27M Mutations. *Brain Tumor Pathol* 2020. https://doi.org/10.1007/s10014-020-00385-9.
- (149) Nikbakht, H.; Panditharatna, E.; Mikael, L. G.; Li, R.; Gayden, T.; Osmond, M.; Ho, C.-Y.; Kambhampati, M.; Hwang, E. I.; Faury, D.; Siu, A.; Papillon-Cavanagh, S.; Bechet, D.; Ligon, K. L.; Ellezam, B.; Ingram, W. J.; Stinson, C.; Moore, A. S.; Warren, K. E.; Karamchandani, J.; Packer, R. J.; Jabado, N.; Majewski, J.; Nazarian, J. Spatial and Temporal Homogeneity of Driver Mutations in Diffuse Intrinsic Pontine Glioma. *Nat Commun* 2016, 7 (1), 11185.
 https://doi.org/10.1038/ncomms11185.
- (150) Justin, N.; Zhang, Y.; Tarricone, C.; Martin, S. R.; Chen, S.; Underwood, E.; De Marco, V.; Haire, L. F.; Walker, P. A.; Reinberg, D.; Wilson, J. R.; Gamblin, S. J. Structural Basis of Oncogenic Histone H3K27M Inhibition of Human Polycomb Repressive Complex 2. *Nature Communications* 2016, 7 (1), 11316. https://doi.org/10.1038/ncomms11316.
- (151) Stafford, J. M.; Lee, C.-H.; Voigt, P.; Descostes, N.; Saldaña-Meyer, R.; Yu, J.-R.; Leroy, G.; Oksuz, O.; Chapman, J. R.; Suarez, F.; Modrek, A. S.; Bayin, N. S.; Placantonakis, D. G.; Karajannis, M. A.; Snuderl, M.; Ueberheide, B.; Reinberg, D. Multiple Modes of PRC2 Inhibition Elicit Global Chromatin Alterations in H3K27M

- Pediatric Glioma. *Science Advances* **2018**, *4* (10), eaau5935. https://doi.org/10.1126/sciadv.aau5935.
- (152) Fang, D.; Gan, H.; Cheng, L.; Lee, J.-H.; Zhou, H.; Sarkaria, J. N.; Daniels, D. J.; Zhang, Z. H3.3K27M Mutant Proteins Reprogram Epigenome by Sequestering the PRC2 Complex to Poised Enhancers. *eLife* 2018, 7, e36696.
 https://doi.org/10.7554/eLife.36696.
- (153) Harutyunyan, A. S.; Krug, B.; Chen, H.; Papillon-Cavanagh, S.; Zeinieh, M.; De Jay, N.; Deshmukh, S.; Chen, C. C. L.; Belle, J.; Mikael, L. G.; Marchione, D. M.; Li, R.; Nikbakht, H.; Hu, B.; Cagnone, G.; Cheung, W. A.; Mohammadnia, A.; Bechet, D.; Faury, D.; McConechy, M. K.; Pathania, M.; Jain, S. U.; Ellezam, B.; Weil, A. G.; Montpetit, A.; Salomoni, P.; Pastinen, T.; Lu, C.; Lewis, P. W.; Garcia, B. A.; Kleinman, C. L.; Jabado, N.; Majewski, J. H3K27M Induces Defective Chromatin Spread of PRC2-Mediated Repressive H3K27me2/Me3 and Is Essential for Glioma Tumorigenesis. *Nature Communications* 2019, *10* (1), 1262. https://doi.org/10.1038/s41467-019-09140-x.
- (154) Diehl, K. L.; Ge, E. J.; Weinberg, D. N.; Jani, K. S.; Allis, C. D.; Muir, T. W. PRC2 Engages a Bivalent H3K27M-H3K27me3 Dinucleosome Inhibitor. *Proceedings of the National Academy of Sciences* 2019, *116* (44), 22152–22157. https://doi.org/10.1073/pnas.1911775116.
- (155) Chan, K.-M.; Fang, D.; Gan, H.; Hashizume, R.; Yu, C.; Schroeder, M.; Gupta, N.; Mueller, S.; James, C. D.; Jenkins, R.; Sarkaria, J.; Zhang, Z. The Histone H3.3K27M Mutation in Pediatric Glioma Reprograms H3K27 Methylation and Gene

- Expression. *Genes Dev.* **2013**, 27 (9), 985–990. https://doi.org/10.1101/gad.217778.113.
- (156) Mohammad, F.; Weissmann, S.; Leblanc, B.; Pandey, D. P.; Højfeldt, J. W.; Comet, I.; Zheng, C.; Johansen, J. V.; Rapin, N.; Porse, B. T.; Tvardovskiy, A.; Jensen, O. N.; Olaciregui, N. G.; Lavarino, C.; Suñol, M.; de Torres, C.; Mora, J.; Carcaboso, A. M.; Helin, K. EZH2 Is a Potential Therapeutic Target for H3K27M-Mutant Pediatric Gliomas. *Nature Medicine* 2017, 23 (4), 483–492. https://doi.org/10.1038/nm.4293.
- (157) Hashizume, R.; Andor, N.; Ihara, Y.; Lerner, R.; Gan, H.; Chen, X.; Fang, D.; Huang, X.; Tom, M. W.; Ngo, V.; Solomon, D.; Mueller, S.; Paris, P. L.; Zhang, Z.; Petritsch, C.; Gupta, N.; Waldman, T. A.; James, C. D. Pharmacologic Inhibition of Histone Demethylation as a Therapy for Pediatric Brainstem Glioma. *Nat Med* 2014, 20 (12), 1394–1396. https://doi.org/10.1038/nm.3716.
- (158) Monje, M.; Mitra, S. S.; Freret, M. E.; Raveh, T. B.; Kim, J.; Masek, M.; Attema, J. L.; Li, G.; Haddix, T.; Edwards, M. S. B.; Fisher, P. G.; Weissman, I. L.; Rowitch, D. H.; Vogel, H.; Wong, A. J.; Beachy, P. A. Hedgehog-Responsive Candidate Cell of Origin for Diffuse Intrinsic Pontine Glioma. *Proceedings of the National Academy of Sciences* 2011, 108 (11), 4453–4458. https://doi.org/10.1073/pnas.1101657108.
- (159) Tsuboi, M.; Kishi, Y.; Yokozeki, W.; Koseki, H.; Hirabayashi, Y.; Gotoh, Y.
 Ubiquitination-Independent Repression of PRC1 Targets during Neuronal Fate
 Restriction in the Developing Mouse Neocortex. *Developmental Cell* 2018, 47 (6),
 758-772.e5. https://doi.org/10.1016/j.devcel.2018.11.018.

- (160) Cordero, F. J.; Huang, Z.; Grenier, C.; He, X.; Hu, G.; McLendon, R. E.; Murphy, S. K.; Hashizume, R.; Becher, O. J. Histone H3.3K27M Represses P16 to Accelerate Gliomagenesis in a Murine Model of DIPG. *Mol Cancer Res* 2017, 15 (9), 1243–1254. https://doi.org/10.1158/1541-7786.MCR-16-0389.
- (161) Larson, J. D.; Kasper, L. H.; Paugh, B. S.; Jin, H.; Wu, G.; Kwon, C.-H.; Fan, Y.; Shaw, T. I.; Silveira, A. B.; Qu, C.; Xu, R.; Zhu, X.; Zhang, J.; Russell, H. R.; Peters, J. L.; Finkelstein, D.; Xu, B.; Lin, T.; Tinkle, C. L.; Patay, Z.; Onar-Thomas, A.; Pounds, S. B.; McKinnon, P. J.; Ellison, D. W.; Zhang, J.; Baker, S. J. Histone H3.3 K27M Accelerates Spontaneous Brainstem Glioma and Drives Restricted Changes in Bivalent Gene Expression. *Cancer Cell* 2019, 35 (1), 140-155.e7. https://doi.org/10.1016/j.ccell.2018.11.015.
- (162) Piunti, A.; Smith, E. R.; Morgan, M. A. J.; Ugarenko, M.; Khaltyan, N.; Helmin, K. A.; Ryan, C. A.; Murray, D. C.; Rickels, R. A.; Yilmaz, B. D.; Rendleman, E. J.; Savas, J. N.; Singer, B. D.; Bulun, S. E.; Shilatifard, A. CATACOMB: An Endogenous Inducible Gene That Antagonizes H3K27 Methylation Activity of Polycomb Repressive Complex 2 via an H3K27M-like Mechanism. *Science Advances* 2019, *5* (7), eaax2887. https://doi.org/10.1126/sciadv.aax2887.
- (163) Jain, S. U.; Rashoff, A. Q.; Krabbenhoft, S. D.; Hoelper, D.; Do, T. J.; Gibson, T. J.; Lundgren, S. M.; Bondra, E. R.; Deshmukh, S.; Harutyunyan, A. S.; Juretic, N.; Jabado, N.; Harrison, M. M.; Lewis, P. W. H3 K27M and EZHIP Impede H3K27-Methylation Spreading by Inhibiting Allosterically Stimulated PRC2. *Molecular Cell* 2020, 80 (4), 726-735.e7. https://doi.org/10.1016/j.molcel.2020.09.028.

- (164) Brien, G. L.; Bressan, R. B.; Monger, C.; Gannon, D.; Lagan, E.; Doherty, A. M.; Healy, E.; Neikes, H.; Fitzpatrick, D. J.; Deevy, O. Simultaneous Disruption of PRC2 and Enhancer Function Underlies Histone H3. 3-K27M Oncogenic Activity in Human Hindbrain Neural Stem Cells. *Nature Genetics* 2021, 53 (8), 1221–1232.
- (165) Nagaraja, S.; Quezada, M. A.; Gillespie, S. M.; Arzt, M.; Lennon, J. J.; Woo, P. J.; Hovestadt, V.; Kambhampati, M.; Filbin, M. G.; Suva, M. L.; Nazarian, J.; Monje, M. Histone Variant and Cell Context Determine H3K27M Reprogramming of the Enhancer Landscape and Oncogenic State. *Molecular Cell* 2019, 76 (6), 965-980.e12. https://doi.org/10.1016/j.molcel.2019.08.030.
- (166) Kumar, S. S.; Sengupta, S.; Lee, K.; Hura, N.; Fuller, C.; DeWire, M.; Stevenson, C. B.; Fouladi, M.; Drissi, R. BMI-1 Is a Potential Therapeutic Target in Diffuse Intrinsic Pontine Glioma. *Oncotarget* 2017, 8 (38), 62962–62975.
 https://doi.org/10.18632/oncotarget.18002.
- (167) Zhang, L.; Nesvick, C. L.; Day, C. A.; Choi, J.; Lu, V. M.; Peterson, T.; Power, E. A.; Anderson, J. B.; Hamdan, F. H.; Decker, P. A.; Simons, R.; Welby, J. P.; Siada, R.; Ge, J.; Kaptzan, T.; Johnsen, S. A.; Hinchcliffe, E. H.; Daniels, D. J. STAT3 Is a Biologically Relevant Therapeutic Target in H3K27M-Mutant Diffuse Midline Glioma. *Neuro-Oncology* 2022, *24* (10), 1700–1711.
 https://doi.org/10.1093/neuonc/noac093.
- (168) Yu, J.-R.; LeRoy, G.; Bready, D.; Frenster, J. D.; Saldaña-Meyer, R.; Jin, Y.;
 Descostes, N.; Stafford, J. M.; Placantonakis, D. G.; Reinberg, D. The H3K36me2
 Writer-Reader Dependency in H3K27M-DIPG. Science Advances 2021, 7 (29),
 eabg7444. https://doi.org/10.1126/sciadv.abg7444.

- (169) Anastas, J. N.; Zee, B. M.; Kalin, J. H.; Kim, M.; Guo, R.; Alexandrescu, S.;
 Blanco, M. A.; Giera, S.; Gillespie, S. M.; Das, J.; Wu, M.; Nocco, S.; Bonal, D. M.;
 Nguyen, Q.-D.; Suva, M. L.; Bernstein, B. E.; Alani, R.; Golub, T. R.; Cole, P. A.;
 Filbin, M. G.; Shi, Y. Re-Programing Chromatin with a Bifunctional LSD1/HDAC
 Inhibitor Induces Therapeutic Differentiation in DIPG. Cancer Cell 2019, 36 (5),
 528-544.e10. https://doi.org/10.1016/j.ccell.2019.09.005.
- (170) Mo, Y.; Duan, S.; Zhang, X.; Hua, X.; Zhou, H.; Wei, H.-J.; Watanabe, J.;
 McQuillan, N.; Su, Z.; Gu, W.; Wu, C.-C.; Vakoc, C. R.; Hashizume, R.; Chang, K.;
 Zhang, Z. Epigenome Programming by H3.3K27M Mutation Creates a
 Dependence of Pediatric Glioma on SMARCA4. *Cancer Discovery* 2022, *12* (12),
 2906–2929. https://doi.org/10.1158/2159-8290.CD-21-1492.
- (171) Panditharatna, E.; Marques, J. G.; Wang, T.; Trissal, M. C.; Liu, I.; Jiang, L.;
 Beck, A.; Groves, A.; Dharia, N. V.; Li, D.; Hoffman, S. E.; Kugener, G.; Shaw, M.
 L.; Mire, H. M.; Hack, O. A.; Dempster, J. M.; Lareau, C.; Dai, L.; Sigua, L. H.;
 Quezada, M. A.; Stanton, A.-C. J.; Wyatt, M.; Kalani, Z.; Goodale, A.; Vazquez, F.;
 Piccioni, F.; Doench, J. G.; Root, D. E.; Anastas, J. N.; Jones, K. L.; Conway, A. S.;
 Stopka, S.; Regan, M. S.; Liang, Y.; Seo, H.-S.; Song, K.; Bashyal, P.; Jerome, W.
 P.; Mathewson, N. D.; Dhe-Paganon, S.; Suvà, M. L.; Carcaboso, A. M.; Lavarino,
 C.; Mora, J.; Nguyen, Q.-D.; Ligon, K. L.; Shi, Y.; Agnihotri, S.; Agar, N. Y. R.;
 Stegmaier, K.; Stiles, C. D.; Monje, M.; Golub, T. R.; Qi, J.; Filbin, M. G. BAF
 Complex Maintains Glioma Stem Cells in Pediatric H3K27M Glioma. *Cancer Discovery* 2022, *12* (12), 2880–2905. https://doi.org/10.1158/2159-8290.CD-21-1491.

- (172) Herz, H.-M.; Morgan, M.; Gao, X.; Jackson, J.; Rickels, R.; Swanson, S. K.; Florens, L.; Washburn, M. P.; Eissenberg, J. C.; Shilatifard, A. Histone H3 Lysine-to-Methionine Mutants as a Paradigm to Study Chromatin Signaling. *Science* 2014, 345 (6200), 1065–1070. https://doi.org/10.1126/science.1255104.
- (173) Berlandi, J.; Chaouch, A.; De Jay, N.; Tegeder, I.; Thiel, K.; Shirinian, M.;
 Kleinman, C. L.; Jeibmann, A.; Lasko, P.; Jabado, N.; Hasselblatt, M. Identification of Genes Functionally Involved in the Detrimental Effects of Mutant Histone H3.3-K27M in Drosophila Melanogaster. *Neuro Oncol* 2019, 21 (5), 628–639.
 https://doi.org/10.1093/neuonc/noz021.
- (174) Chaouch, A.; Berlandi, J.; Chen, C. C. L.; Frey, F.; Badini, S.; Harutyunyan, A. S.; Chen, X.; Krug, B.; Hébert, S.; Jeibmann, A.; Lu, C.; Kleinman, C. L.; Hasselblatt, M.; Lasko, P.; Shirinian, M.; Jabado, N. Histone H3.3 K27M and K36M Mutations de-Repress Transposable Elements through Perturbation of Antagonistic Chromatin Marks. *Molecular Cell* 2021, *81* (23), 4876-4890.e7. https://doi.org/10.1016/j.molcel.2021.10.008.
- (175) Reiter, L. T.; Potocki, L.; Chien, S.; Gribskov, M.; Bier, E. A Systematic Analysis of Human Disease-Associated Gene Sequences In Drosophila Melanogaster. Genome Res. 2001, 11 (6), 1114–1125. https://doi.org/10.1101/gr.169101.
- (176) Rubin, G. M.; Lewis, E. B. A Brief History of Drosophila's Contributions to Genome Research. *Science* 2000, 287 (5461), 2216–2218. https://doi.org/10.1126/science.287.5461.2216.
- (177) Wangler, M. F.; Yamamoto, S.; Bellen, H. J. Fruit Flies in Biomedical Research. *Genetics* **2015**, *199* (3), 639–653. https://doi.org/10.1534/genetics.114.171785.

- (178) McLysaght, A.; Makino, T.; Grayton, H. M.; Tropeano, M.; Mitchell, K. J.; Vassos, E.; Collier, D. A. Ohnologs Are Overrepresented in Pathogenic Copy Number Mutations. *Proceedings of the National Academy of Sciences* 2014, 111 (1), 361–366. https://doi.org/10.1073/pnas.1309324111.
- (179) Hadorn, E. An Accelerating Effect of Normal "Ring-Glands" on Puparium-Formation in Lethal Larvae of Drosophila Melanogaster. *Proceedings of the National Academy of Sciences* 1937, 23 (9), 478–484. https://doi.org/10.1073/pnas.23.9.478.
- (180) Huang, A. M.; Rubin, G. M. A Misexpression Screen Identifies Genes That Can Modulate RAS1 Pathway Signaling in Drosophila Melanogaster. *Genetics* 2000, 156 (3), 1219–1230. https://doi.org/10.1093/genetics/156.3.1219.
- (181) Irvine, K. D.; Rauskolb, C. Boundaries in Development: Formation and Function.
 Annual Review of Cell and Developmental Biology 2001, 17 (1), 189–214.
 https://doi.org/10.1146/annurev.cellbio.17.1.189.
- (182) Wassarman, D. A.; Therrien, M.; Rubin, G. M. The Ras Signaling Pathway in Drosophila. *Current Opinion in Genetics & Development* **1995**, *5* (1), 44–50. https://doi.org/10.1016/S0959-437X(95)90052-7.
- (183) Snigdha, K.; Gangwani, K. S.; Lapalikar, G. V.; Singh, A.; Kango-Singh, M. Hippo Signaling in Cancer: Lessons From Drosophila Models. *Frontiers in Cell and Developmental Biology* **2019**, 7.

(184) Hafen, E.; Dickson, B.; Raabe, T.; Brunner, D.; Oellers, N.; van der Straten, A. Genetic Analysis of the Sevenless Signal Transduction Pathway of Drosophila.
Development 1993, 119 (Supplement), 41–46.
https://doi.org/10.1242/dev.119.Supplement.41.

Chapter 2: H3 K27M and EZHIP impede H3K27-methylation spreading by inhibiting allosterically stimulated PRC2

The work presented in this chapter has been published:

Jain, S. U., Rashoff, A. Q.*, Krabbenhoft, S. D.*, Hoelper, D., Do, T. J., Gibson, T. J., ... & Lewis, P. W. (2020). H3 K27M and EZHIP impede H3K27-methylation spreading by inhibiting allosterically stimulated PRC2. *Molecular cell*, 80(4), 726-735.

doi: 10.1016/j.molcel.2020.09.028. Epub 2020 Oct 12.

Statement of contribution: S.U.J. and P.W.L. conceptualized the study and wrote the manuscript. S.U.J. and A.Q.R. performed most experiments in mammalian cells. I performed all *Drosophila*-related experiments, excluding the ChIP-seq analysis and ATAC-seq/ATAC analysis (performed by S.U.J. and T.J.G.). S.U.J analyzed ChIP and RNA sequencing data. D.H. performed analyses of H3.3L126A;I130 histones. T.J.D. performed PRC2 assays, and S.M.L. generated PRC2 complexes. S.D., A.S.H., and N. Juretic. helped with NGS samples. N. Jabado., M.M.H, and P.W.L. supervised the experiments. All authors read and edited the manuscript.

^{*} These authors contributed equally.

<u>Abstract</u>

Diffuse midline gliomas and posterior fossa type A ependymomas contain the recurrent histone H3 lysine 27 (H3 K27M) mutation and express the H3 K27M-mimic EZHIP (CXorf67), respectively. H3 K27M and EZHIP are competitive inhibitors of Polycomb Repressive Complex 2 (PRC2) lysine methyltransferase activity. *In vivo*, these proteins reduce overall H3 lysine 27 trimethylation (H3K27me3) levels; however, residual peaks of H3K27me3 remain at CpG islands (CGIs) through an unknown mechanism. Here, we report that EZHIP and H3 K27M preferentially interact with PRC2 that is allosterically activated by H3K27me3 at CGIs and impede its spreading. Moreover, H3 K27M oncohistones reduce H3K27me3 in trans, independent of their incorporation into the chromatin. Although EZHIP is not found outside placental mammals, expression of human EZHIP reduces H3K27me3 in *Drosophila* melanogaster through a conserved mechanism. Our results provide mechanistic insights for the retention of residual H3K27me3 in tumors driven by H3 K27M and EZHIP.

Introduction

Diffuse midline gliomas (DMGs) are highly aggressive pediatric tumors with poor prognoses. About 80% of DMGs contain the recurrent histone H3 lysine 27 (H3 K27M) mutation in genes encoding histone H3 proteins that are assembled into nucleosomes through replication-coupled (H3.1/2) and replication-independent mechanisms (H3.3).^{1,2} Despite representing a small fraction of total histone H3 (3%–17%), H3 K27M causes a global reduction in levels of H3 lysine 27 trimethylation (H3K27me3) in DMGs.³⁻⁶ Posterior fossa type A ependymomas (PFA ependymomas) display similar gene expression, DNA methylation, and low H3K27me3 profiles as DMGs.⁷ Instead of containing the recurrent H3 K27M mutations, PFA ependymomas aberrantly express a newly discovered gene, EZHIP (CXorf67).⁸ EZHIP-expressing ependymomas display a poorer prognosis than other posterior fossa ependymomas.

Polycomb Repressive Complex 2 (PRC2) catalyzes H3K27me3, which is involved in transcriptional silencing. The EZHIP and H3 K27M oncoproteins are competitive inhibitors of PRC2.9 A peptide within EZHIP mimics the H3 K27M sequence and is necessary and sufficient to inhibit PRC2 activity and reduce H3K27me3 levels in cells.9–12 However, hundreds of CpG islands (CGIs) that represent high-affinity PRC2-binding sites retain residual H3K27me3.9 Residual PRC2 activity is necessary for the survival of H3-K27M-containing gliomas, and it has been proposed that the retention of H3K27me3 at CGIs is necessary to silence tumor suppressor genes and maintain cell proliferation.13–15 Nonetheless, the molecular mechanism by which EZHIP and H3 K27M reduce

H3K27me3 specifically from intergenic regions but disproportionately retain H3K27me3 at CGIs remains elusive.

PRC2 interacts with unmethylated CGIs through its auxiliary subunits, Polycomb-like proteins (PCLs) or JARID2, where it catalyzes high levels of H3K27me3. ^{16–19} H3K27me3, initially catalyzed at CGIs, interacts with its EED subunit of PRC2 and allosterically stimulates its catalytic activity by ~8-fold. ²⁰ This "read-write" mechanism triggers PRC2 spread into the intergenic regions and formation of broad H3K27me3 domains. Remarkably, the inhibitory potential of H3 K27M and EZHIP oncoproteins is substantially enhanced by allosteric stimulation of PRC2 *in vitro*. ^{9,21–23} It is unclear if the preferential inhibition of allosterically stimulated PRC2 by EZHIP and H3 K27M plays a functional role *in vivo*.

Several studies demonstrated that H3 K27M directly contacts and inhibits PRC2 *in vitro*. ^{3,6,9,22–24} However, direct inhibition of PRC2 by H3 K27M oncohistones *in vivo* is still debated. ^{13,23,25} Instead, it has been proposed that H3 K27M reduces H3K27me3 in cis by altering histone post-translational modifications locally through the formation of heterotypic nucleosomes. ^{13,26} These heterotypic nucleosomes, in turn, reduce H3K27me3 in cis by evicting PRC2 from genomic regions where H3 K27M oncohistones are incorporated. Therefore, the molecular mechanism through which H3 K27M reduces H3K27me2/3 in cells remains controversial.

Here, we demonstrate that EZHIP preferentially interacts with allosterically stimulated PRC2. EZHIP impedes PRC2 spreading by stabilizing a high-affinity complex between H3K27me3-PRC2-EZHIP at CGIs containing residual H3K27me3. Using Tandem ChIP (reChIP) experiments, we demonstrate that H3 K27M proteins interact with and stall PRC2 at CGIs. Moreover, supporting the trans mechanism of action, incorporation of H3 K27M proteins into nucleosomes is not necessary for the reduction of H3K27me3 in cells. Finally, despite its absence outside placental mammals, we demonstrate that EZHIP reduces H3K27me3 in *Drosophila* melanogaster through a conserved molecular mechanism. In summary, we provide evidence that EZHIP and H3 K27M bind PRC2 *in vivo* and reduce H3K27me2/3 in trans by blocking PRC2 spreading.

Results

EZHIP Preferentially Interacts with Allosterically Stimulated PRC2 *In Vitro* and *In Vivo*

Expression of EZHIP in cells leads to an overall reduction of H3K27me3; however, residual H3K27me3 is retained at CGIs (Supplemental Figure 2.1A⁹). Using chromatin immunoprecipitation sequencing (ChIP-seq), we found that EZHIP and EZH2 colocalized with residual H3K27me3 at CGIs (Figures 2.1A, 2.1B, Supplemental Figures 2.1B, and 2.1C). Depletion of PRC2, through genetic ablation of Eed, abolished the EZHIP ChIP signal suggesting that EZHIP binds to chromatin indirectly through PRC2 (Figures 2.1A, 2.1B, Supplemental Figures 2.1D, and 2.1E). A K27M-like peptide (KLP) within the C-terminus of EZHIP interacts with the EZH2 active site residues (where M406 is equivalent to H3 K27M). Consequently, EZHIP M406E failed to inhibit PRC2 *in vitro* and did not

immunoprecipitate PRC2 subunits from nuclear extract (Figures 2.1C, 2.1D, and Supplemental Figure 2.2.D). Moreover, EZHIP M406E did not colocalize with PRC2 and H3K27me3 at CGIs *in vivo* (Figure 2.1E, Supplemental Figures 2.1F, and 2.1G). These data linked *in vitro* PRC2 inhibition to *in vivo* interaction between EZHIP and EZH2 at CGIs and reduction of H3K27me3.

Previously, we showed that the PRC2 inhibitory potential of EZHIP is significantly enhanced in the presence of the H3K27me3 peptide. The interaction between EED and H3K27me3 is proposed to induce a conformation of EZH2 that has increased affinity toward its substrates and competitive inhibitors, such as EZHIP (Figure 2.1F). Indeed, EZHIP KLP captured more PRC2 in the presence of H3K27me3 *in vitro* (Figure 2.1G). Similarly, EZHIP co-immunoprecipitated substantially lower amounts of PRC2 subunits and displayed lower PRC2 inhibitory potential in the presence of A-395, a small molecule that binds to EED and competes with H3K27me3 (Figures 2.H and 2.1I). These data suggest that EZHIP has an increased affinity for allosterically stimulated PRC2 and help explain the paradox that the inhibitor EZHIP interacts with PRC2 at sites containing H3K27me3 *in vivo*.

Our results indicated that EZHIP interacts with allosterically stimulated PRC2, which is bound to H3K27me3 through EED (Supplemental Figure 2.2A). Elimination of residual H3K27me3 using the S-adenosyl methionine analog tazemetostat led to a substantial reduction of EZH2 and, hence, EZHIP at CGIs (Supplemental Figures 2.2B and 2.2C). These results suggest that H3K27me3 helps to stabilize PRC2 on chromatin, likely

through an interaction with the EED subunit. To confirm that PRC2 interacts with H3K27me3 at CGIs through EED, we rescued EED-/- cells with EED Y365A, a mutant that does not bind H3K27me3 (Supplemental Figure 2.2D).²⁸ Indeed, PRC2 recruitment was reduced 4-fold by the Y365A mutation (Supplemental Figures 2.2E-G), suggesting that most PRC2 molecules at CGIs assume the allosterically stimulated conformation. Taken together, our experiments indicate that EZHIP forms a high-affinity complex with allosterically stimulated EZH2 at CGIs (Figure 2.1F).

EZHIP Reduces PRC2 Spreading by Stalling It at CGIs

We hypothesize that the formation of a catalytically inactive ternary complex, H3K27me3-PRC2-EZHIP, restrains PRC2 from spreading into the intergenic regions. If this is true, we would expect increased PRC2 residency at CGIs in cells expressing EZHIP (Figures 2.2A and Supplemental Figure 2.3A). Indeed, expression of wild-type EZHIP, but not the PRC2-binding-deficient M406E mutant, led to a substantial increase of EZH2 occupancy at residual H3K27me3 sites containing high CpG density (Figures 2.2B, 2.2C, and Supplemental Figures 2.3B–2.3F). Simultaneously, EZH2 enrichment was significantly reduced from CpG-poor domains of H3K27me3 (Supplemental Figures 2.3C and 2.3D). To test our model in human cancers, we used SUZ12 CUT&RUN data from U2OS cells that express endogenous EZHIP. Mirroring our results in MEFs expressing EZHIP, U2OS cells exhibited sharp SUZ12 peaks, which redistributed to broader intergenic domains upon the loss of EZHIP (Figures 2.2D, 2.2E, and Supplemental Figures 2.3G–I). These results indicate that EZHIP impedes PRC2 spreading.

To directly test the hypothesis that EZHIP promotes the formation of narrow peaks of H3K27me3 by impeding PRC2 spreading (Figures 2.2A and 2.2F), we sought a PRC2 mutant that is defective in allosteric activation and spreading but not in recruitment. Binding of H3K27me3 to EED induces a conformational change of the EZH2 SRM domain to stimulate EZH2 catalytic activity (Figure 2.2G). An EED mutation found in Weaver syndrome, R302S, maps to a residue that interacts with EZH2 H158 (Supplemental Figure 2.3J). PRC2 containing EEDR302S did not respond to H3K27me3 in activity assays but retained its ability to bind H3K27me3 at CGIs (Figures 2.2H, Supplemental Figure 2.2K, and 2.3L). Likewise, EZHIP displayed lower binding and inhibition potential for PRC2 containing EEDR302S, further confirming that EZHIP preferentially interacts with allosterically stimulated PRC2 (Supplemental Figures 2.3M-O). Altogether, EEDR302S provides a "spreading defective" PRC2 mutant to test our hypothesis *in vivo*.

Expression of EEDR302S in EED-/- cells failed to rescue overall levels of H3K27me3 (Figures 2.2I and 2.2J). Although EEDWT restored the global H3K27me3 profile, EEDR302S exhibited H3K27me3 only at CpG-rich PRC2 recruitment sites (Figures 2.2I and Supplemental Figure 2.3L). Importantly, cells rescued with the spreading defective EEDR302S mutant exhibited a remarkably similar H3K27me3 profile to that of cells expressing EZHIP, i.e., sharp H3K27me3 peaks at CGIs (Figures 2.2K and 2.2L). These data support the model that EZHIP blocks PRC2 spreading on chromatin and provide a mechanistic explanation for retention of narrow H3K27me3 in tumors expressing EZHIP. The global loss of H3K27me3 in cells expressing EZHIP from intergenic regions leads to widespread upregulation of genes (Jain et al., 2019). However, the retention of residual

H3K27me3 might safeguard some genes against aberrant upregulation, which cannot be achieved by a complete loss of PRC2. Genes containing residual H3K27me3 remained silenced in cells expressing EZHIP, whereas genetic depletion of EED led to their upregulation (Figure 2.2M). Altogether, we propose that EZHIP specifically blocks PRC2 spreading by stabilizing PRC2 at CGIs, which provides a mechanism for the retention of residual H3K27me3 at developmentally regulated genes.

H3 K27M Interacts with PRC2 In Vivo and Impedes Its Spreading

The H3 K27M-mimic EZHIP interacts with allosterically stimulated PRC2 to impede its spreading. However, whether H3 K27M directly interacts with PRC2 *in vivo* is controversial primarily because H3 K27M and PRC2 occupancies do not correlate positively in cells. ^{13,15,23} The amount of H3 K27M far exceeds that of PRC2 in the nucleus. ²³ H3 K27M, being histones, are incorporated into nucleosomes and are present throughout the genome. In contrast, PRC2 is detected in relatively narrow peaks at CGIs, which may explain the poor correlation between the enrichment of H3 K27M and PRC2. Previously, we and others showed that H3 K27M preferentially binds and inhibits PRC2 in the presence of H3K27me3, which is similar to EZHIP. ^{9,21–23} Therefore, we hypothesize that H3 K27M also stalls PRC2 at CGIs containing residual H3K27me3 by binding allosterically stimulated PRC2.

To directly map genomic regions where H3 K27M interacts with PRC2 *in vivo*, we used H3 K27M ChIP followed by EZH2 reChIP-seq (Figures 2.3A, Supplemental Figures 2.4A, and 2.4B). We selected reads with a fragment size smaller than 400 bp for our analyses

to selectively capture PRC2 bound to mono- or di-nucleosomes. As predicted, H3 K27M-bound EZH2 was enriched at CGIs containing residual H3K27me3 (Figures 2.3B–3E, Supplemental Figures 2.4C-E). We did not detect EZH2 reChIP enrichment in control cells that did not express a FLAG-tagged H3 K27M transgene, confirming our detection of only H3 K27M-bound EZH2 instead of a background signal (Supplemental 2.44C). These data demonstrate that H3.1 and H3.3 K27M directly interact with PRC2 *in vivo*.

Next, we examined changes in PRC2 distribution in cells expressing H3 K27M by mapping the EZH2 binding profile. Similar to EZHIP, expression of H3.1 or H3.3 K27M led to an increase in EZH2 occupancy at CGIs containing residual H3K27me3 (Figure 2.3F and Supplemental Figures 2.4F-K). To ascertain a causal relationship between H3 K27M expression and PRC2 redistribution, we used EZH2 ChIP-seq in 293T-Rex cells containing a doxycycline-inducible H3.3 K27M transgene.²³ We observed a time-dependent increase of EZH2 occupancy at recruitment sites after expression of H3 K27M, supporting our model that H3 K27M sequesters PRC2 at its recruitment sites (Figure 2.3G and Supplemental Figure 2.4L).

To corroborate our model in gliomas, we profiled the genomic distribution of SUZ12 in patient-derived DMG cell lines with wild-type H3 or H3 K27M mutations. DMG lines containing H3.3 K27M had significantly higher SUZ12 enrichment at CGIs containing residual H3K27me3 than H3 wild-type gliomas (Figure 2.3H and Supplemental Figures 2.5A-D). Importantly, Cas9-mediated genetic ablation of H3.3 K27M substantially reduced SUZ12 occupancy at these sites (Figure 2.3I and Supplemental Figures 2.5E-K). Taken

together, our results suggest that H3 K27M directly interacts with PRC2 *in vivo* and stalls it at CGIs containing residual H3K27me3.

H3 K27M Oncohistones Reduce H3K27me3 Independent of Their Incorporation into Chromatin

The direct interaction between H3 K27M and PRC2 *in vivo* suggests that the K27M mutant reduces global H3K27 methylation through inhibiting EZH1/2 activity. In favor of this trans mode of PRC2 inhibition, we did not identify any correlation between the genomic enrichment of H3 K27M oncohistones and loss of H3K27me3 (Supplemental Figures 2.6A-D). In an alternative model, H3 K27M histones have been proposed to reduce local H3K27me3 in cis by evicting PRC2 from genomic regions where these oncohistones are enriched. In this model, a critical step toward a reduction of H3K27me3 by H3 K27M oncohistones is their incorporation into chromatin and deposition of histone modification(s) in cis that are refractory for PRC2 binding. To directly distinguish between these trans versus cis mechanisms, we sought histone H3 mutations that would abrogate its incorporation into chromatin.

Previously, we and others reported that H3 residues L126 and I130 are necessary for H3-H3 dimerization for the formation of nucleosomes. Recombinant dimerization mutant H3.3 failed to generate H3.3-H4 tetramers *in vitro* (Supplemental Figures 2.6E and 2.6F). We confirmed that the H3.3 dimerization mutant was absent from chromatin and is only present in the soluble nuclear fraction (Supplemental Figures 2.6G and 2.6H). These experiments demonstrate that H3.3 L126A;I130A is not incorporated into chromatin. To

test whether chromatin incorporation of H3 K27M oncohistones is necessary for the reduction of H3K27me3, we expressed a H3.3 K27M;L126A;I130A triple-mutant transgene in mouse embryonic fibroblasts (MEFs). Because cells maintain low levels of unincorporated histone H3, we found extremely low levels of the mutant protein relative to H3.3 K27M alone (Figure 2.3J).³³

Interestingly, the H3.3 K27M;L126A;I130A mutant reduced global H3K27me2/3, despite its extremely low levels in cells (Figure 2.3J). H3.3 K27M;L126A;I130A, but not K27R, immunoprecipitated PRC2 subunits from cell lysates, linking the reduction of H3K27me3 to a direct interaction with PRC2 *in vivo* (Figure 2.3K). The "depositable" and "non-depositable" H3.3 K27M mutant displayed similar H3K27me3 profiles: reduction from intergenic regions and retention at CGIs (Figure 2.3L, Supplemental Figures 2.6I, and 2.6J). Altogether, we demonstrate that the H3 K27M oncohistones reduce H3K27 methylation in trans by directly inhibiting PRC2 *in vivo*, independent of their incorporation into chromatin.

Mammalian EZHIP Inhibits Drosophila PRC2 through a Conserved Mechanism

Our studies demonstrate striking similarities in the mechanism through which EZHIP and H3 K27M directly inhibit PRC2 at its recruitment sites. Although histone H3 is highly conserved among eukaryotes, EZHIP is only present in placental mammals. Previous studies found that the expression of H3 K27M in fruit flies largely phenocopies the loss of PRC2 activity. Because EZHIP mimics the molecular function of the H3 K27M oncohistone, we hypothesized that human EZHIP inhibits *Drosophila* PRC2 despite its

evolutionary absence in flies. Indeed, we found that the expression of human EZHIP or H3.3 K27M in imaginal wing discs led to a substantial reduction of H3K27me3, relative to EZHIP M406E or H3 K27R controls (Figure 2.4A). These data further highlight the similarity between the molecular functions of the two oncogenes.

The cis-regulatory elements involved in PRC2 recruitment that account for the global H3K27 methylation profile have not been identified in mammals. However, in *Drosophila* melanogaster, PRC2 is recruited to Polycomb Response Elements (PREs) by the DNA-binding protein Pho.^{34,35} Therefore, *Drosophila* presents an excellent model to study and validate PRC2 recruitment versus spreading defects mediated by EZHIP. Having validated the ability of EZHIP to inhibit H3K27me3 *in vivo*, we established a copper-inducible system to express EZHIP in *Drosophila* S2 cells and showed that the expression of EZHIP led to a dose-dependent reduction of H3K27me3, which is consistent with a competitive mode of inhibition (Figures 2.4B–D). Despite a global reduction of H3K27me3, most PREs retained residual H3K27me3 in cells expressing EZHIP (Figure 2.4E).

To distinguish between PRC2 recruitment versus spreading defects, we identified genomic regions that disproportionately retained H3K27me3 in cells expressing EZHIP (Figure 2.4F). Using Assay for Transposase-Accessible Chromatin (ATAC-seq), we identified accessible regions within residual H3K27me3 sites as potential polycomb-recruitment sites. Consistent with our model that EZHIP preferentially impedes PRC2 spreading, 178/326 (55%) of the regions that retained H3K27me3 contained previously

annotated PREs and displayed an enrichment of the polycomb protein Polyhomeotic (Ph) (Figures 2.4G and 2.4H). Moreover, an additional 111 (34%) sites also displayed Ph occupancy, designating ~90% of regions that retained H3K27me3 as polycomb-recruitment sites (Figures 2.4G and 2.4H). These results further support the model that EZHIP preferentially inhibits PRC2 spreading while sparing its activity at recruitment sites. Notably, the amplitude of Ph enrichment at the additional Ph binding sites was lower than that at annotated PREs (Figures 2.4I and 2.4J), which may represent cell-type-specific, weaker PREs.³⁶

Discussion

Since the discovery of H3 K27M mutations in DMGs, several studies showed that H3 K27M is a competitive inhibitor of PRC2 *in vitro*. However, it had remained challenging to assess the PRC2-H3 K27M interaction *in vivo* by using genomic approaches. Here, we show that the non-histone H3-K27M-mimic EZHIP occupies the same sites as PRC2 *in vivo*. Importantly, we successfully detected the interaction between H3 K27M and PRC2 *in vivo* by using a tandem ChIP strategy. Our demonstration that H3 K27M directly interacts with and inhibits PRC2 activity *in vivo* links the numerous studies that characterized the PRC2-K27M interactions *in vitro* to the in vivo loss of H3K27me3.

Recurrent H3 K27M mutations and aberrant EZHIP expression are preferentially found in distinct gliomas, namely, DMGs and PFA ependymomas, respectively. Remarkably, two recent studies discovered aberrant expression of EZHIP in a subset of DMGs lacking H3 K27M mutations.^{37,38} Similarly, a small fraction of PFA ependymomas contain H3 K27M

mutations that are mutually exclusively with EZHIP expression.⁸ Our finding that EZHIP and H3 K27M have similar underlying biochemical mechanisms explains the clinical observations that both oncoproteins can drive the same subtype of gliomas. Therefore, pharmacological interventions proposed for H3-K27M-positive gliomas might be promising candidates in gliomas expressing EZHIP.^{13,14,39–42}

We validated our findings that EZHIP disproportionately blocks PRC2 spreading while sparing residual H3K27me3 at recruitment sites using *Drosophila* melanogaster S2 cells. Using ectopic expression of EZHIP in S2 cells, we identified >100 new, weak polycomb-binding sites that likely represent tissue-specific PREs. Although previous studies used a combination of H3K27me3 ChIP- and ATAC-seq to identify PREs in *Drosophila* melanogaster, the expression of EZHIP may provide a tool to filter out most genomic regions containing H3K27me3 and a more sensitive method to detect tissue-specific PREs in future studies.

Materials and Methods

Fly stocks

All stocks were grown on molasses food at 22°C (room temperature). N-terminally FLAG-tagged EZHIP WT, EZHIP M406E, H3 K27M or H3 K27R were cloned into pUASt-attB (DGRC#1419) and integrated into ZH-86Fb on the third chromosome using PhiC31 integrase-mediated recombination into BDSC#24749 with fluorescence marker removed (Best Gene). *en-Gal4*, *UAS-RFP/CyO* (II) (BDSC#30557) was used to drive expression in the larval wing disc.

Transgenic cell lines and culture

Mouse embryonic fibroblasts (sex:F, derived from embryonic state E13.5) used in this study containing loxP sites flanking exon 3-6 of EED were described previously (Jain et al., 2019). MEFs were previously verified through their gene expression signature (RNA-Seq). Cells were cultured in DMEM supplemented with 10% FBS, 1x glutamax and 1x penicillin-streptomycin. S2 cells in this study were cultured at 25°C in Schneider's Media (Thermo Fisher) containing 10% FBS (Omega Scientific), and 1% antibiotic/antimycotic (Thermo Fisher).

Immunohistochemistry

Crawling third instar larvae were harvested and dissected in pre-chilled (4°C) 1X PBS. Wing imaginal discs were removed from larvae and placed into 1X PBS on ice and fixed in 4% formaldehyde for 30 min. Fixed wing imaginal discs were washed in 1X PBS + 0.1% Triton X-100, (PBST) and blocked in PBST + 1% BSA (PAT). After removal of PAT, wing discs were resuspended in PAT + anti-H3K27me3 (1:1600) (Cell Signaling Technology #9733S) and incubated overnight at 4°C, washed in PBST, incubated in PBST + 2% normal goat serum for 10 min, followed by incubation with PBST + 2% normal goat serum and goat anti-rabbit DyLight 488 conjugated secondary antibody (1:2000) (Fisher Scientific #35552). Larvae were imaged at 10X using a Nikon Ti2-E epifluorescent microscope.

Production of stable S2 cell lines

FLAG-tagged human EZHIP was cloned into the pMT-puro vector (Addgene #17923). Transfections were performed with 2 μ g plasmid DNA, using Effectene Transfection Reagent (QIAGEN), and cells were selected using 2 μ g/ml puromycin for approximately three weeks. For induction, 5 μ M or 10 μ M copper sulfate was added to cells at one million cells/ ml density. Cells were incubated for 72 h and harvested for immunoblot or ChIP.

Production of mammalian cell lines

Lentiviruses were produces by co-transfecting packaging vectors (psPAX2 and pMD2.G) and transfer vector (pCDH-EF1a-MCS-PuroR) in HEK293T cells (ATCC CRL-3216) using GenJet *in vitro* DNA transfection reagent (SignaGen Laboratories SL100488). Media containing lentiviruses were collected 48 and 72 h after transfection. MEFs were transduced with lentiviruses for 2 days and selected using 1.5 µg/µl puromycin for 4 days. Mouse and human EZHIP DNA sequences were used in mouse and human cell lines respectively; however, only human amino acid numbers were used in the figures to avoid confusion.

Peptide pulldown

25 μ l of high capacity streptavidin agarose beads (Thermo Scientific Pierce PI20359) saturated with biotinylated EZHIP peptides were incubated with 1 μ g recombinant PRC2 purified from SF9 cells for 2 hs at 4°C in the presence or absence of 20 μ M H3K27me3 stimulatory peptides in 500 μ L of binding buffer (20 mM Tris-HCl pH 8, 125 mM NaCl, 0.01% NP-40, 0.4 mM PMSF, 1 mM β -mercaptoethanol), and 100 nM of oligonucleosomes. Following binding, beads were washed four times in 1 mL of binding

buffer. Bound proteins were eluted with 2x SDS sample buffer (10% glycerol, 50 mM Tris-HCl pH 6.8, 4% SDS, 0.04% bromophenol blue, 143 mM β-mercaptoethanol) and analyzed by immunoblotting.

FLAG affinity purification

~80 million cells were homogenized in hypotonic lysis buffer (15 mM HEPES pH 7.9, 4 mM MgCl2, 10 mM KCl, 1 mM EDTA, 8 mM PMSF) to isolate nuclei. Nuclei were resuspended in Buffer-M (15 mM HEPES pH 7.9, 1 mM CaCl2, 30 mM KCl, 1X protease inhibitor cocktail, 8 mM PMSF, 1 mM beta-mercaptoethanol) and treated with 750 units of Micrococcal Nuclease, MNase (Worthington Biochemical Corporation, LS004798) for 20 min at 37°C. MNase digestion was quenched and nuclear extract was prepared by adding 10 mM EDTA, 5 mM EGTA, 270 mM KCl, 0.05% Triton X-100). Nuclear extract was incubated with 75 μl of M2 anti-FLAG affinity gel (Sigma A2220) for 2 h. Beads were washed 5-times with wash buffer (15 mM HEPES pH 7.9, 500 mM KCl, 1 mM EDTA, 0.05% Triton X-100, 8 mM PMSF) and captured proteins were eluted using 300 μg/ml of 3x FLAG peptides. For FLAG affinity purification in the presence of A-395, 1 μM A-395 (or DMSO control) was added to cultured cells for 6 h before cells were harvested and nuclear extract was prepared. 1 μM A-395 (or DMSO) was added to all buffers throughout the protocol.

Immunoprecipitation of pre-deposition complexes

Lysate from 40 × 106 HEK293T cells transduced with H3.3-FLAG-HA transgenes was prepared by resuspension in 3.0 mL lysis buffer [20 mM HEPES pH 7.9, 200 mM KCl, 0.5

mM EDTA, 2 mM MgCl2, 0.2% Triton X-100, 2 × Protease Inhibitor Cocktail (Roche), 2 mM 2-mercaptoethanol, 1 mM benzamidine, 0.4 mM PMSF, 300 μM S-adenosyl methionine), followed by douncing and separation of the insoluble fraction by centrifugation. Per sample, 30 μL of packed anti-FLAG M2 beads (Sigma) were added to the lysate and incubated rotating at 4°C for 2 h. Beads were transferred onto microspin columns (Enzymax) and washed three times with wash buffer (20 mM HEPES pH 7.9, 300 mM KCl, 1 mM EDTA, 0.12% Triton X-100, 0.4 mM PMSF, 1 mM benzamidine, 150 μM S-adenosyl methionine) for 5 min. Finally, samples were eluted with 2 × 25 μL elution buffer [wash buffer supplemented with 500 ng μl-1 3 × FLAG peptide (Tufts University Peptide Core Facility)] via incubation for 5 min on ice and centrifugation at 300 g.

100 × 106 HEK293T cells expressing H3.3-FLAG-HA transgenes were harvested via trypsinization and the trypsin reaction was quenched by addition of growth media. Cells were pelleted via centrifugation for 2 min at 1,000 g and cell pellets were resuspended in 20 mL of growth media. Paraformaldehyde (Electron Microscopy Sciences) was added at a final concentration of 0.5%, followed by incubation for 5 min at room temperature. The crosslinking reaction was quenched by the addition of glycine at 200 mM final and incubation for 5 min at room temperature. Cells were pelleted by centrifugation at 1,000 g for 2 min and pellets were resuspended in phosphate-buffered saline supplemented with 200 mM glycine. Cells were then pelleted again and washed with cold phosphate-buffered saline. For cells to be analyzed under native condition, all steps were performed equally with the omission of paraformaldehyde. For separation of soluble nuclear proteins from chromatin, 1/10th volume of saturated solution of ammonium sulfate was added to

nuclei resuspended in 15 mM HEPES pH 7.9, 1 mM EDTA, 0.4 mM PMSF, 4 mM MgCl2 . Chromatin was separated from nuclear extract by ultracentrifugation for 90 min at 85,000 g. Chromatin pellets were subsequently washed three times with 1 mL chromatin wash buffer (20 mM HEPES, 500 mM KCl, 1 mM EDTA, 0.01% Nonidet P-40, 5% glycerol, 0.4 mM PMSF, 2 mM 2-mercaptoethanol) and subjected to acid histone extraction. Briefly, chromatin pellets were dissolved in 0.4 N H2SO4 by overnight rotation at room temperature. After centrifugation, proteins from the collected supernatants were precipitated by addition of 1/3 volume 100% trichloroacetic acid with 0.1% sodium deoxycholate on ice, washed twice with ice cold acetone, and resuspended in distilled water.

Reconstitution of recombinant tetramers

Recombinant 6X-His-tagged H3.3 histones (C110A background; with or without L126A-I130A mutation) and H4 histones were expressed in E. coli Rosetta cells. For purification, inclusion bodies were solubilized in D500 buffer (6.3 M Guanidine-HCI, 500 mM NaCI, 50 mM Tris pH 8, and 10 mM 2-mercaptoethanol), followed by purification via Ni-NTA batch chromatography. For the removal of guanidine, eluates were desalted using PD10 columns into buffer containing 100 mM trimethylamine acetate pH5 and 5 mM 2-mercaptoethanol and subsequently lyophilized. For tetramer reconstitution, equimolar amounts of H3.3 and H4 histones were mixed und denaturing conditions and dialyzed against HDB Buffer (20 mM Tris pH 8, 1 mM EDTA, 5% (v/v) glycerol, 10mM 2-mercaptoethanol, 1mM PMSF) supplemented with different concentrations of 2M NaCI. Dialyzed samples were run on a Superdex 200 column in buffer containing 20 mM

HEPES, 1 mM EDTA, 0.01% NP40, 10% glycerol supplemented with KCl at the concentrations given in the figure legend. This gel filtration step was performed with 50 μ L injection volume, a flow rate of 50 μ L/min and 40 μ L fractions were collected for further analysis by SDS-PAGE.

Purification of native oligonucleosomes

Native oligonucleosomes were purified from EED-/- MEFs. Nuclei were prepared by resuspending 100 million cells in hypotonic lysis buffer and centrifugation at 2100 Å~g for 5 min Nuclei were resuspended in buffer-AP (15 mM HEPES pH 8, 15 mM NaCl, 60 mM KCl, 5% Sucrose, 0.5 mM Sperimine, 0.15 mM Spermidine, 0.4 mM PMSF, 1 mM β-mercaptoethanol) and treated with 0.2 units μl-1 MNase for 20 min at 37 oC. After quenching with 5 mM EDTA, nuclei were centrifuged at 2100 Å~g for 5 min. Nuclei were lysed by resuspension in 10 mM EDTA and 500 mM NaCl. Oligonucleosomes were purified over a sucrose gradient (5%–30% sucrose, 15 mM HEPES pH7.9, 1 mM EDTA, 500 mM NaCl, 0.5 mM PMSF). Oligonucleosomes in fractions 15–21 mL were concentrated and dialyzed against 15 mM Tris pH 8.0, 100 mM NaCl, 1 mM EDTA, 0.4 mM PMSF, 10% glycerol.

Histone methyltransferase assays

200 nM oligonucleosome arrays or 25 μ M H3 peptide (18-32) substrates were incubated with 20 nM recombinant PRC2 complex, 4 μ M S-adenosyl Methionine (1 μ M 3H-SAM; 3 μ M cold SAM) and 20 μ M H3K27me3 stimulatory peptide in 25 mM Tris pH 8.0, 2 mM MgSO4, 5 mM DTT, 0.4 mM PMSF for 90 min. Reaction was spotted on phosphocellulose

membrane (Whatman p81) and dried for 10 min. Filters were washed 3-times with 100 mM NaHCO3 for 5 min each, rinsed in acetone and dried for 10 min. Scintillation counting was performed using Tri-Carb 2910 TR liquid Scintillation analyzer (Perkin Elmer). For fluorography, reaction was resolved on 15% SDS-PAGE gel, stained with Coomassie, incubated in Amersham Amplify Fluorography reagent (GE healthcare) for 10 min and dried under vacuum. Films capturing fluorography signal were developed after 24–48 h. Experiment specific details are in figure legend.

Chromatin immunoprecipitation

~80 million S2 cells were crosslinked with 0.8% Paraformaldehyde (Electron Microscopy Sciences) for 8 min at room temperature and quenched with 0.2 M glycine. Cells were lysed by resuspending in lysis buffer (50 mM HEPES pH 7.9, 140 mL NaCl, 1 mM EDTA, 10% glycerol, 0.5% NP40, 0.25% Triton X-100, 0.8 mM PMSF). Nuclei were washed once and resuspended in digestion buffer (50 mM HEPES pH 7.9, 1 mM CaCl2, 20 mM NaCl, 1x protease inhibitor cocktail, and 0.8 mM PMSF), and treated with 200 units of MNase (Worthington Biochemical Corporation, LS004798) for 10 min. Reaction was quenched by adding 10 mM EDTA, 5 mM EGTA, 80 mM NaCl, 0.1% sodium deoxycholate, 0.5% N-lauroyl sarcosine. Mono-nucleosomes were solubilized by sonication using a Covaris S220 (160 peak incidental power, 5% duty factor, 200 cycles/burst, 45" ON-30" OFF) 3-times. 1% Triton X-100 was added to the chromatin and insoluble chromatin was removed using centrifugation. Chromatin was dialyzed against RIPA buffer (10 mM Tris pH 7.6, 1 mM EDTA, 0.1% SDS, 0.1% sodium deoxycholate, 1% Triton X-100) for 2 h. Chromatin concentration was measured using gubit and spike-in chromatin was added at 1:40 ratio.

Chromatin was incubated with primary antibodies overnight. Antibodies was captured using Dynabeads for 4 h and washed 3x using RIPA buffer, 2x using RIPA+300 mM NaCl and 2x with LiCl buffer. Chromatin was eluted in 10 mM Tris, 1 mM EDTA, and 1% SDS, incubated with proteinase K, and RNase A and DNA was purified using PCR purification columns. Sequencing libraries were prepared using NEB Next Ultra kit. ChIPs were performed in at least two independent replicates with similar results, at least one replicate was sequenced using NGS; p-values were determined by paired, non-parametric t-test.

ChIP-sequencing analysis

Reads that passed quality score were aligned to the *Drosophila* (dm6) genome using bowtie1 (parameters: -q -v 2 -m 2 -a -best -strata).⁴³ Sample normalization factor was determined as ChIP-Rx = 10⁶ / (total reads aligned to exogenous reference genome). Sam files were converted to bam files using samtools.⁴⁴ Bigwig files were generated using deeptools (-bs 50 -smoothLength 600).⁴⁵ Peaks were called using mosaics-HMM (typically using FDR = 0.01, maxgap = 2-10K, minsize = 1K).⁴⁶ Residual H3K27me3 sites in cells expressing EZHIP were determined as peaks found in two independent ChIP-Seq experiments. Heatmaps were generated using deeptools. -Rx normalization factor was used in boxplot quantification everywhere. Statistical analysis was performed using R.

For identification of potential PRC2 binding sites in S2 cells, regions containing disproportionate retention of H3K27me3 were determined as the difference in H3K27me3 RPKM enrichment in control and cells expressing EZHIP. Bins with change in H3K27me3 < 10 within 5KB were merged and regions with delH3K27me3 < 500 were removed.

Finally, ATAC-Seq peaks within these regions with residual H3K27me3 were defined as potential PRC2 recruitment sites. Annotations of PREs in dm6 genome were obtained from a recent report.⁴⁷ Ph ChIP-Seq data from S2 cells were downloaded from GEO (GSE60686).

ATAC-Sequencing

2 × 105 *Drosophila* S2 cells were washed once with 1X PBS and then resuspended in 100 μL ATAC lysis buffer (10mM Tris 7.5, 10mM NaCl, 3mM MgCl2, 0.1% NP-40). Cells were centrifuged at 600 × g for 10 min at 4°C. The resulting pellet was resuspended in 47.5 μL buffer TD (Illumina 15027866) before adding 2.5 μL Tn5 transposase (Tagment DNA Enzyme, Illumina 15027865) and incubating in 37°C water bath for 30 min. The tagmented DNA was immediately purified using MinElute Cleanup Kit (QIAGEN 28204) and eluted in 10 μL buffer EB. Tagmented DNA was amplified with 12 cycles of PCR using the NEBNext Hi-Fi 2X PCR Master Mix (NEB M0541) and unique dual index primers. Libraries were purified using a 1.2X ratio of Axygen magnetic beads. 150bp, paire-end sequencing was performed at the University of Wisconsin-Madison Biotechnology Center on the Illumina Nova Seq 6000 platform.

ATAC-Sequencing analysis

Raw reads were trimmed to remove adaptor sequences using NGmerge.⁴⁸ Trimmed reads were aligned to the *Drosophila* (dm6) genome using bowtie2 with the following parameters:-very-sensitive,-no-mixed,-no-discordant, -X 5000, -k 2. Only reads with a mapping quality score >30 that aligned to major chromosomes (2, 3, 4, X, Y) were

retained for downstream analysis. In order to enrich for fragments originating from nucleosome-free regions, only fragments < 100 bp were retained. Peak calling was performed on accessible fragments using MACS2 with the following parameters: -f BAMPE-keep-dup all -g 1.2e8-call-summits.

Quantification and Statistical Analysis

Statistical analysis for ChIP-Seq was performed using R. Wilcoxon rank sum test was used to calculate p values in boxplots. p value for bar chart representing ChIP-qPCR data were calculated using paired, parametric t test. n values are provided in the figures. n in boxplots represents total number of elements such as peaks or genes for which boxplot is generated. Outliers in the boxplot are not shown ("outline= F" in R). None of the data points in any analyses were excluded.

Data availability

The accession number for the Next-generation sequencing data generated and reported in this paper is GEO:. Original data have been deposited to Mendeley Data, https://doi.org/10.17632/xtp4xytd2c.1. Code used to analyze data are described in the STAR methods.

Acknowledgements

We thank Dr. Tom W. Muir and Sara K. Daley for key discussions. We thank MilliporeSigma for generating the EZHIP antibody. This research was supported by funding from National Institues of Health, P01CA196539 (to P.W.L. and N. Jabado.);

the Greater Milwaukee Foundation (to P.W.L.); the Sidney Kimmel Foundation (Kimmel Scholar Award to P.W.L.); the Childhood Brain Tumor Foundation (to P.W.L.); the Rally Foundation for Childhood Cancer Research (to P.W.L.); the Vallee Foundation (to M.M.H.); and a pilot grant from University of Wisconsin Carbone Cancer Center (to P.W.L. and M.M.H.). T.J.G. is supported by National Research Service Award T32 GM007215. P.W.L. is a Pew Scholar in the Biomedical Sciences. This work was performed within the context of the I-CHANGE consortium and supported by funding from Genome Canada, Genome Quebec, The Institute for Cancer Research of the Canadian Institutes for Health Research (CIHR), McGill University, and the Montreal Children's Hospital Foundation. N. Jabado. is a member of the Penny Cole lab and the recipient of a Chercheur Clinician Senior Award.

Figure 2.1

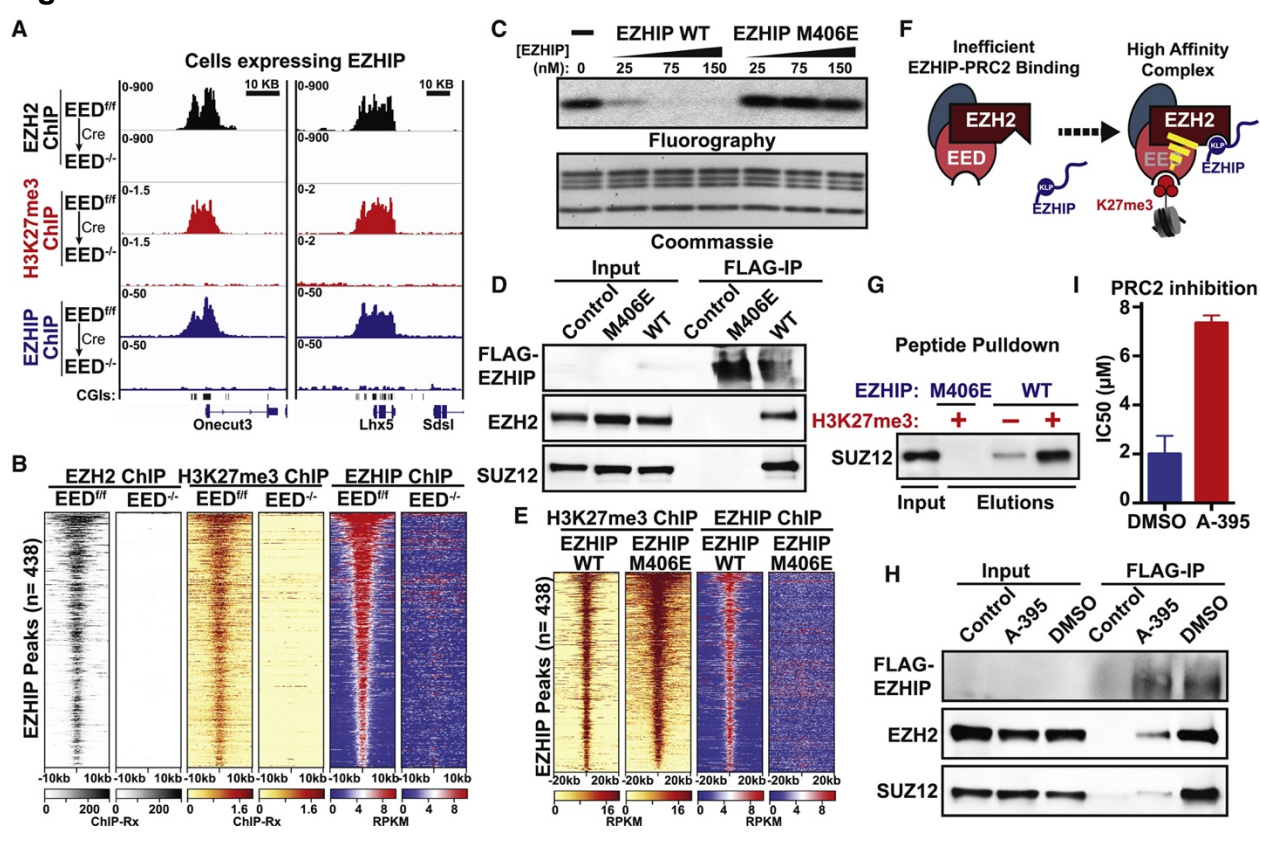


Figure 2.1. EZHIP Preferentially Interacts with Allosterically Stimulated PRC2 In Vitro and In Vivo. A and B. EZH2, H3K27me3, and EZHIP ChIP-seq enrichments in Eedf/f or Eed-/- MEFs expressing FLAG-tagged EZHIP. Heatmap displaying ChIP enrichments at all EZHIP peaks in shown in (B). C. PRC2 inhibition assays by EZHIP wild-type (WT) M406E using oligonucleosome substrates. FLAGor immunoprecipitation of FLAG-tagged EZHIP WT or M406E from MEFs. E. H3K27me3 and FLAG-EZHIP ChIP enrichment in MEFs expressing EZHIP WT or M406E. F. The H3K27me3-EED interaction stabilizes a PRC2 conformation that has an increased affinity for EZHIP. G. Peptide pull-downs of rPRC2 with EZHIP KLP peptide in the presence or absence of the H3K27me3 stimulatory peptide. H. FLAG-immunoprecipitation of FLAGtagged EZHIP from MEFs in the presence or absence of A-395. I. IC50 (Half Maximal Inhibitory Concentration) of PRC2 inhibition by the EZHIP KLP peptide with or without A-395 in the reactions. Error bars represent standard error.

Figure 2.2

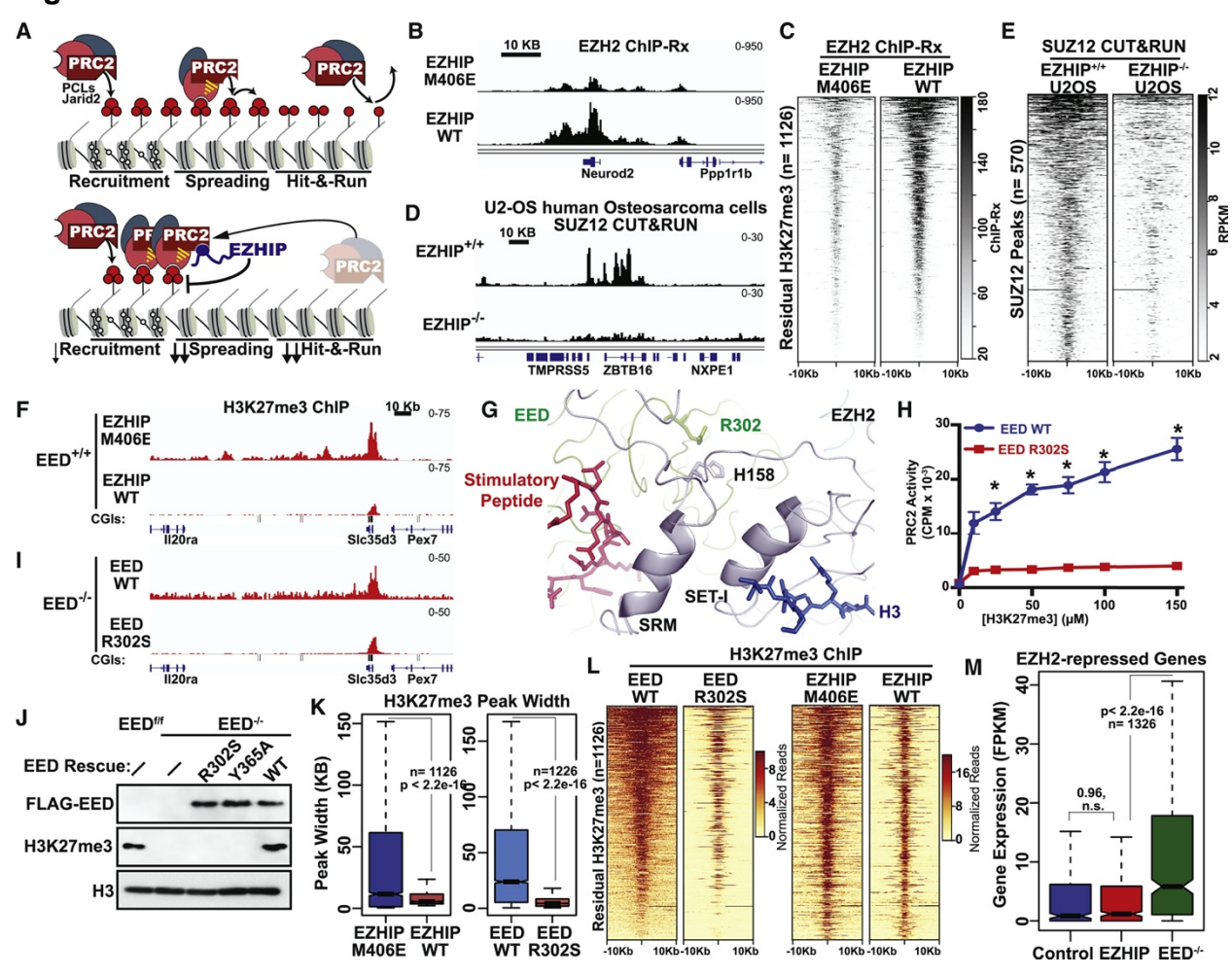


Figure 2.2. EZHIP Reduces PRC2 Spreading by Stalling It at CpG Islands. A. EZHIPmediated re-distribution of PRC2. See Supplemental Figure 3.3A for details. B. EZH2 ChIP-Rx profiles in MEFs expressing EZHIP WT or M406E. C. EZH2 ChIP-Rx enrichment at residual H3K27me3 peaks. D. SUZ12 occupancy (RPKM) in EZHIP+/+ or EZHIP-/-U2OS cells. E. SUZ12 enrichment (RPKM) at SUZ12 peaks in U2OS cells. F. H3K27me3 ChIP-seg profiles in MEFs expressing EZHIP WT or M406E. G. Binding of H3K27me3 or Jarid2 K116me3 (red) to EED leads to allosteric stimulation of EZH2 through an interaction between EED R302 and EZH2 H158. H. In vitro PRC2 assays using peptide substrates. The H3K27me3 stimulatory peptide (H3 18-37) was titrated into the reaction. The p value of the difference between EED WT and R302S at each concentration of H3K27me3 was determined using a parametric, paired t test (n = 3; *p < 0.05). I. H3K27me3 ChIP-seq profiles in Eed-/- MEFs rescued with EED WT or R302S. J. Immunoblots of cell extracts from Eed-/- cells overexpressing EED WT, R302S, or Y365A. K. Widths of H3K27me3 peaks in MEFs expressing EZHIP WT or M406E (left) or Eed-/- MEFs expressing EED WT or R302S (right). L. H3K27me3 RPKM enrichment in MEFs expressing EZHIP WT or M406E and Eed-/- MEFs expressing EED WT or R302S at H3K27me3 peaks found in EED R302S cells. M. Expression of silenced genes (FPKM < 20) with residual H3K27me3 at their promoters. The p values in boxplots were calculated using Wilcoxon's rank-sum test.

Figure 2.3

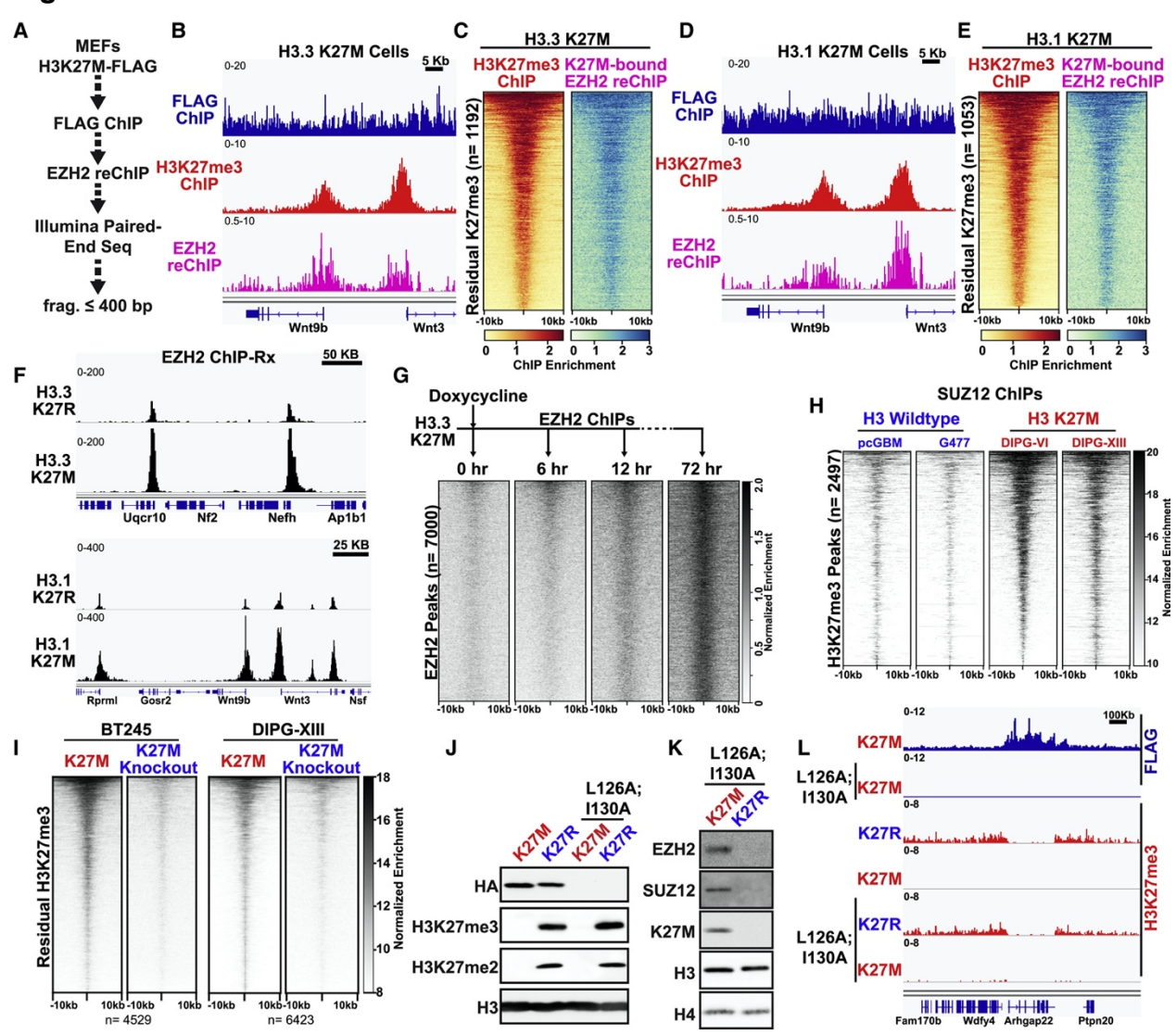


Figure 2.3. Figure 2.3. H3 K27M Reduces H3K27me3 in Trans by Stalling PRC2 at CpG Islands. A. Tandem ChIP-seq to identify genomic locations of H3 K27M-bound EZH2. B. H3 K27M-FLAG ChIP, H3K27me3 ChIP, and EZH2 reChIP in cells expressing FLAG-tagged H3.3 K27M. C. H3K27me3 and EZH2 reChIP profiles in cells expressing H3.3 K27M at residual H3K27me3 peaks. **D** and **E**. Same as (B) and (C) but for cells expressing FLAG-tagged H3.1 K27M. F. EZH2 ChIP-Rx in cells expressing H3.3 (top) or H3.1 (bottom) K27M or K27R. G. EZH2 enrichment in 293T-Rex cells expressing doxycycline-inducible H3.3 K27M at 0, 6, 12, and 72 h after treatment with doxycycline at steady state EZH2 peaks. H. SUZ12 enrichment in DMGs containing H3 K27M or H3 WT at common H3K27me3 peaks. I. Heatmap displaying SUZ12 enrichment in DMGs containing a H3 K27M mutation or corresponding H3 K27M knockout cells. J. extracts from MEFs expressing H3.3 K27M, K27R, Immunoblots cell K27M;I126A;L130A, or K27R;I126A;L130A. K. Immunoblots of eluates from FLAG affinity purification of H3.3 K27M or K27R with I126A;L130A mutations. L. H3.3-FLAG and H3K27me3 ChIP-Rx profiles in MEFs expressing H3.3 K27M, K27R, K27M;I126A;L130A, or K27R;I126A;L130A.

Figure 2.4

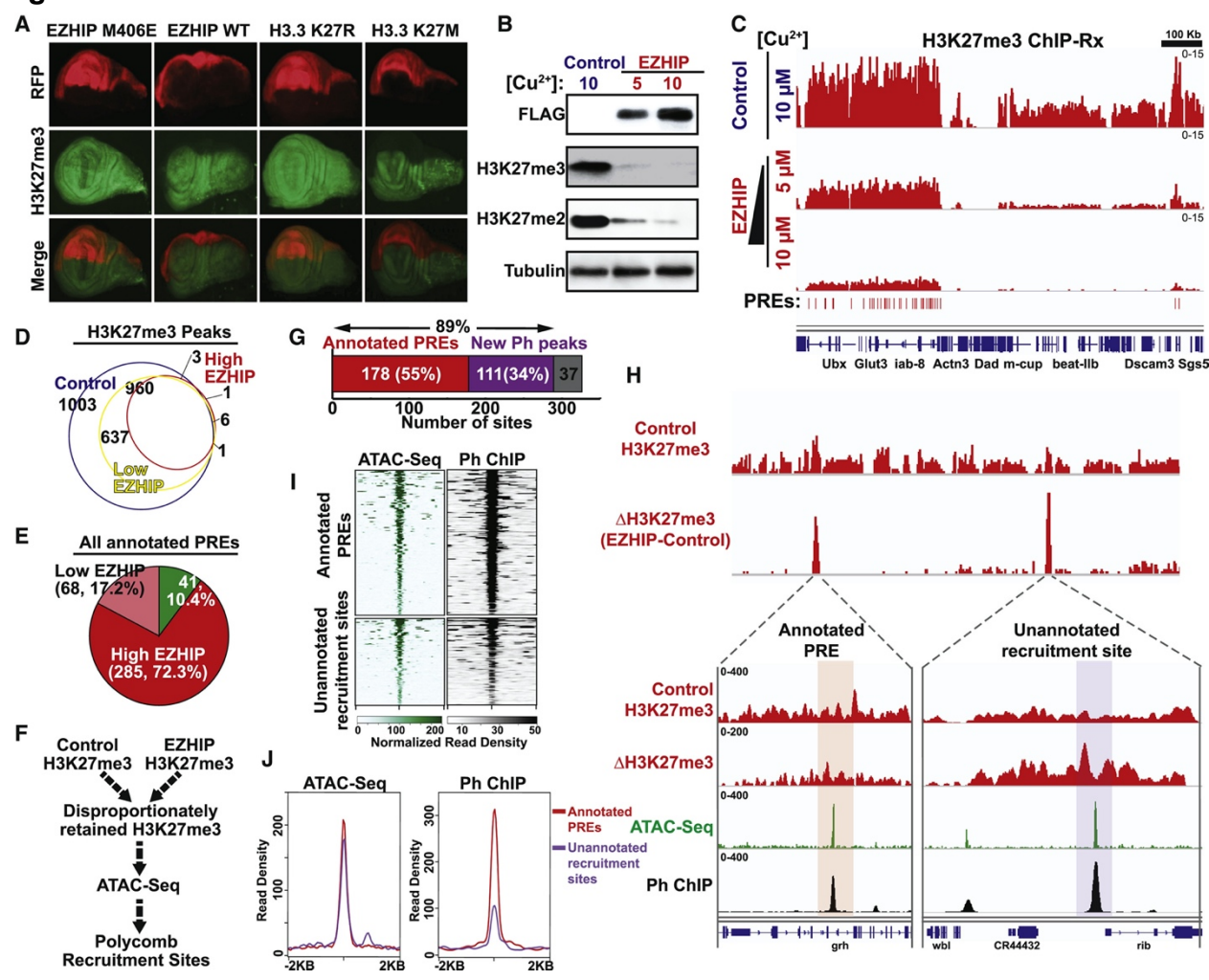
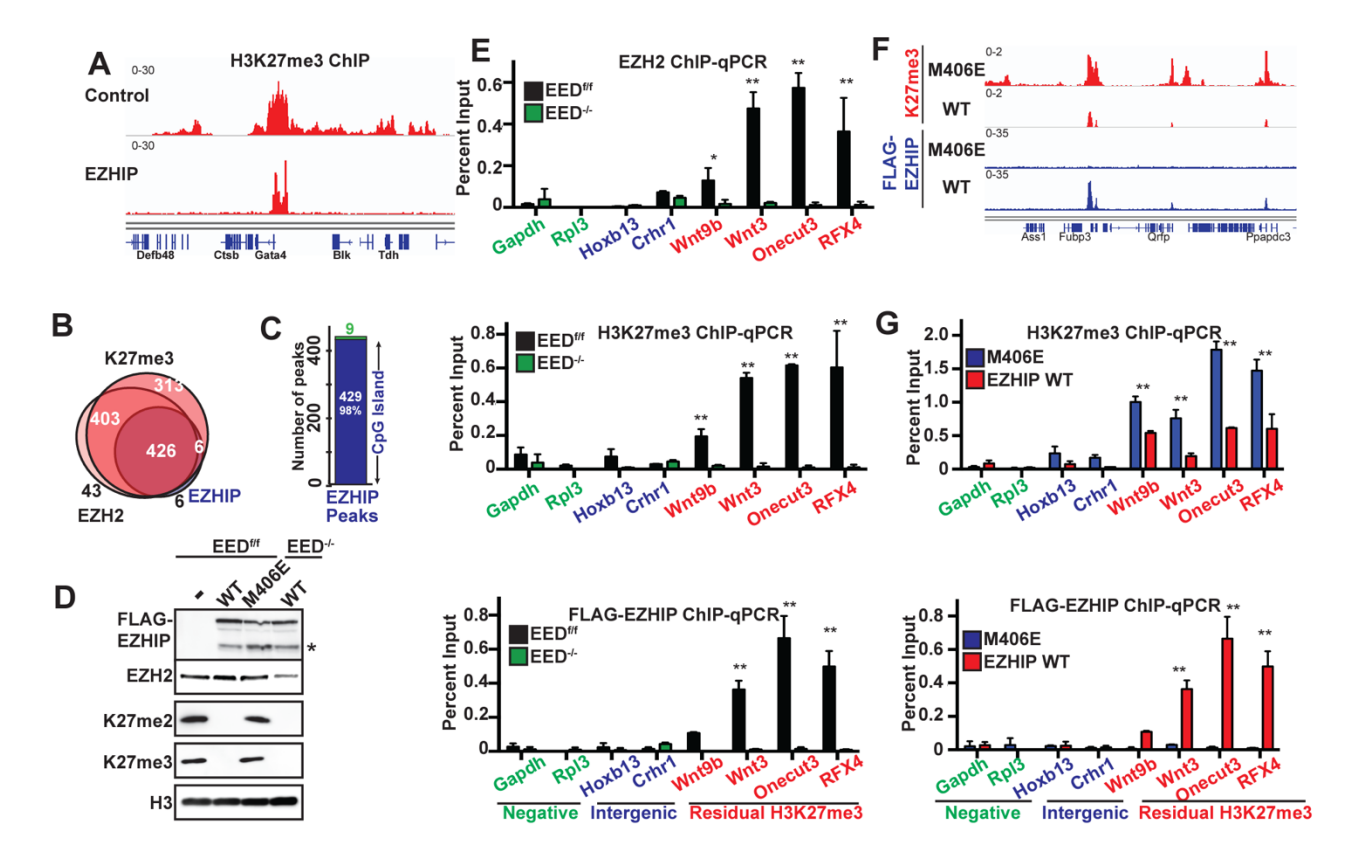


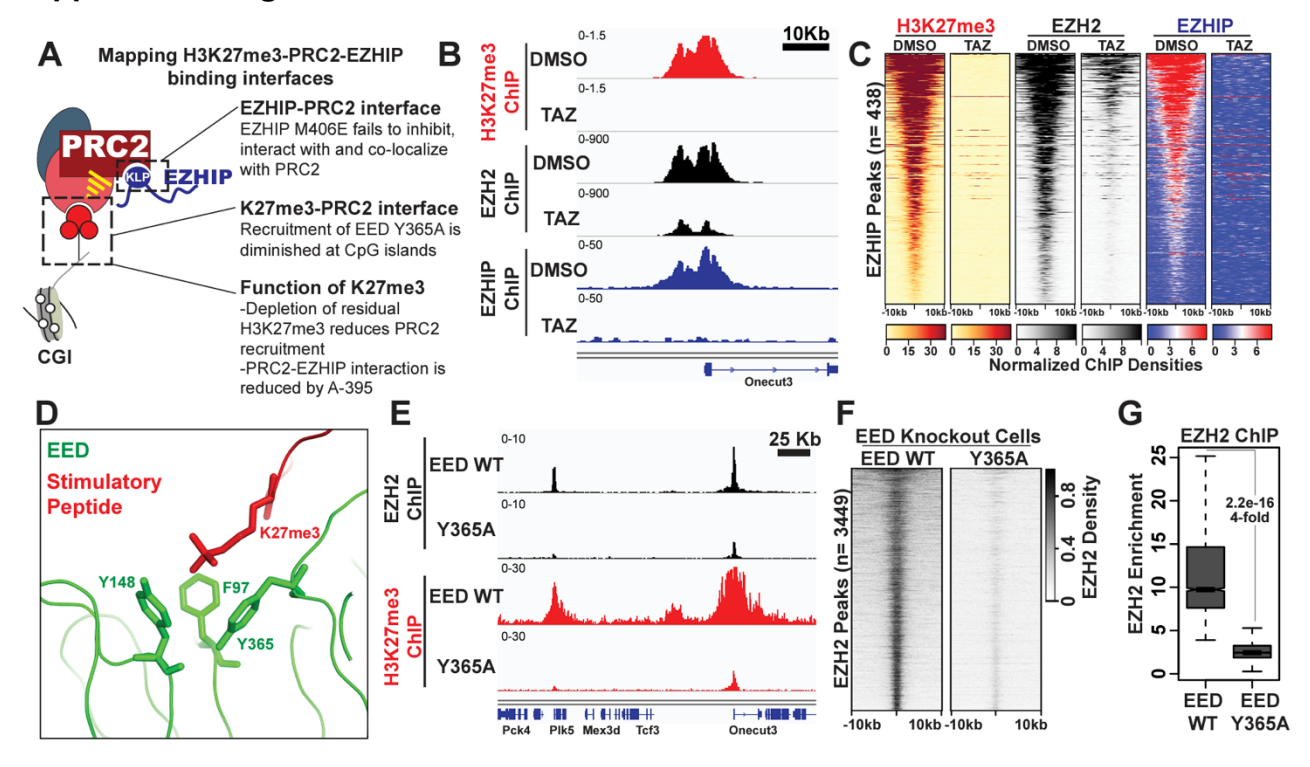
Figure 2.4. Human EZHIP Reduces H3K27me3 in *Drosophila* through a Conserved Mechanism. A. H3K27me3 staining (green) of wing imaginal discs from third instar larvae expressing either EZHIP WT, EZHIP M406E, H3 K27M, or H3 K27R driven by engrailed-GAL4. RFP (red) indicates the region of engrailed-GAL4 expression. B. Immunoblots of S2 cells expressing FLAG-tagged EZHIP induced with 5 µM or 10 µM copper or empty vector as control. C. H3K27me3 ChIP-Rx profile in S2 cells as described in (B). D. Overlap of H3K27me3 peaks in S2 cells expressing high (10 µM Cu2+) or low (10 µM Cu2+) levels of EZHIP. E. Fraction of annotated PREs that retained H3K27me3 in cells expressing EZHIP. F. Difference of internally normalized H3K27me3 (EZHIP-control) was used to identify loci that disproportionately retained H3K27me3 upon EZHIP expression. ATACseg peak within these loci represent putative PRC2 recruitment sites. G. Fraction of putative polycomb-recruitment sites that contain annotated PREs or unannotated Ph peaks. H. Baseline H3K27me3 ChIP, ΔH3K27me3 (EZHIP-Control), ATAC-seq, and Ph ChIP-seq profiles Red, previously annotated PREs; purple, unannotated recruitment sites. I and J. ATAC-seq and Ph ChIP-seq densities at putative PRC2 recruitment sites.

Supplemental Figure 2.1



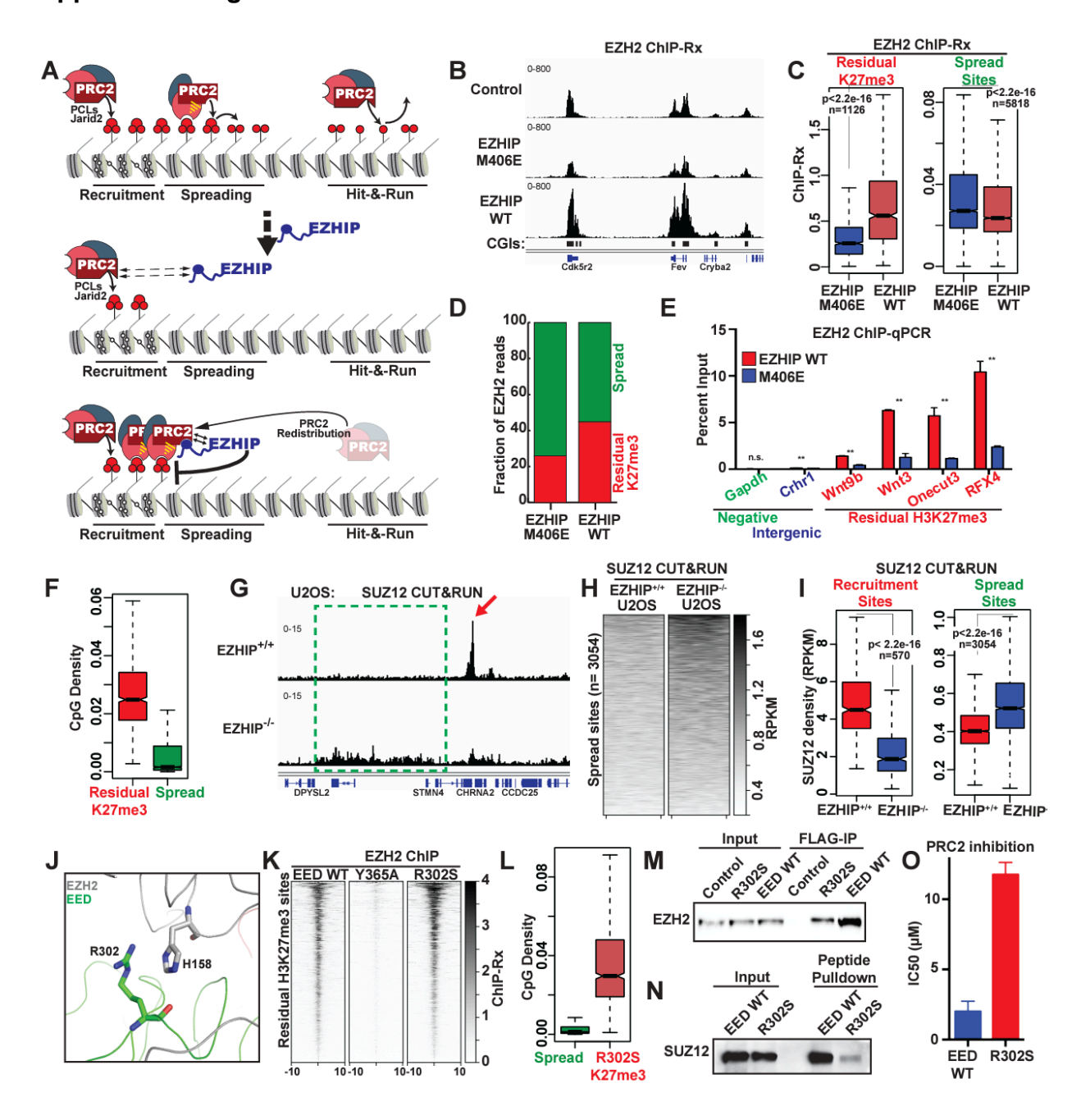
Supplemental Figure 2.1. EZHIP colocalizes with PRC2 and residual H3K27me3 in vivo. Related to Figure 2.1. A. Genome browser view of H3K27me3 in control MEFs or MEFs expressing EZHIP. B. Overlap between EZHIP, H3K27me3 and EZH2 peaks in MEFs expressing EZHIP. C. Fraction of EZHIP peaks that contain CpG islands (blue). D. Immunoblots of whole cell extracts from cells expressing EZHIP wild-type, EZHIP M406E, and EED knockout cells expressing EZHIP WT. (* degradation product). E. ChIP-qPCR of EZH2, H3K27me3 and EZHIP-FLAG ChIPs in cells expressing EZHIP before and after Cre-recombinase mediated EED knockout. F. Genomic profile of H3K27me3 and EZHIP-FLAG ChIPs in cells expressing EZHIP wildtype or M406E. G. ChIP-qPCR analyses of H3K27me3 and EZHIP-FLAG ChIPs in cells expressing EZHIP wildtype or M406E. **p<0.05. p-value in bar graphs were determined using parametric paired t-test.

Supplemental Figure 2.2



Supplemental Figure 2.2. Characterization of H3K27me3-PRC2-EZHIP interaction interface *in vivo*. Related to Figure 2.1. A. Schematic displaying the H3K27me3-PRC2-EZHIP interaction and the strategy used to analyze their interactions in cells. B and C. Genome browser view of H3K27me3, EZH2 and EZHIP ChIP-Seq profiles in cells expressing EZHIP treated with DMSO control or 10 µM Tazemetostat. Heatmap displaying the ChIP-Seq densities at EZHIP peaks in shown in C. D. Crystal structure of PRC2 bound to stimulatory peptide. H3K27me3 interacts with the aromatic amino acids within the WD40-repeat of EED. E. Genome browser view of EZH2 and H3K27me3 ChIP-Seq profiles in EED knockout cells expressing EED wildtype or EED Y365A mutant. F. Heatmap displaying EZH2 enrichment at all EZH2 peaks is shown in F. G. Boxplot displaying the reference-normalized (ChIP-Rx) EZH2 enrichment at all EZH2 peaks in cells expressing EED WT or Y365A mutant.

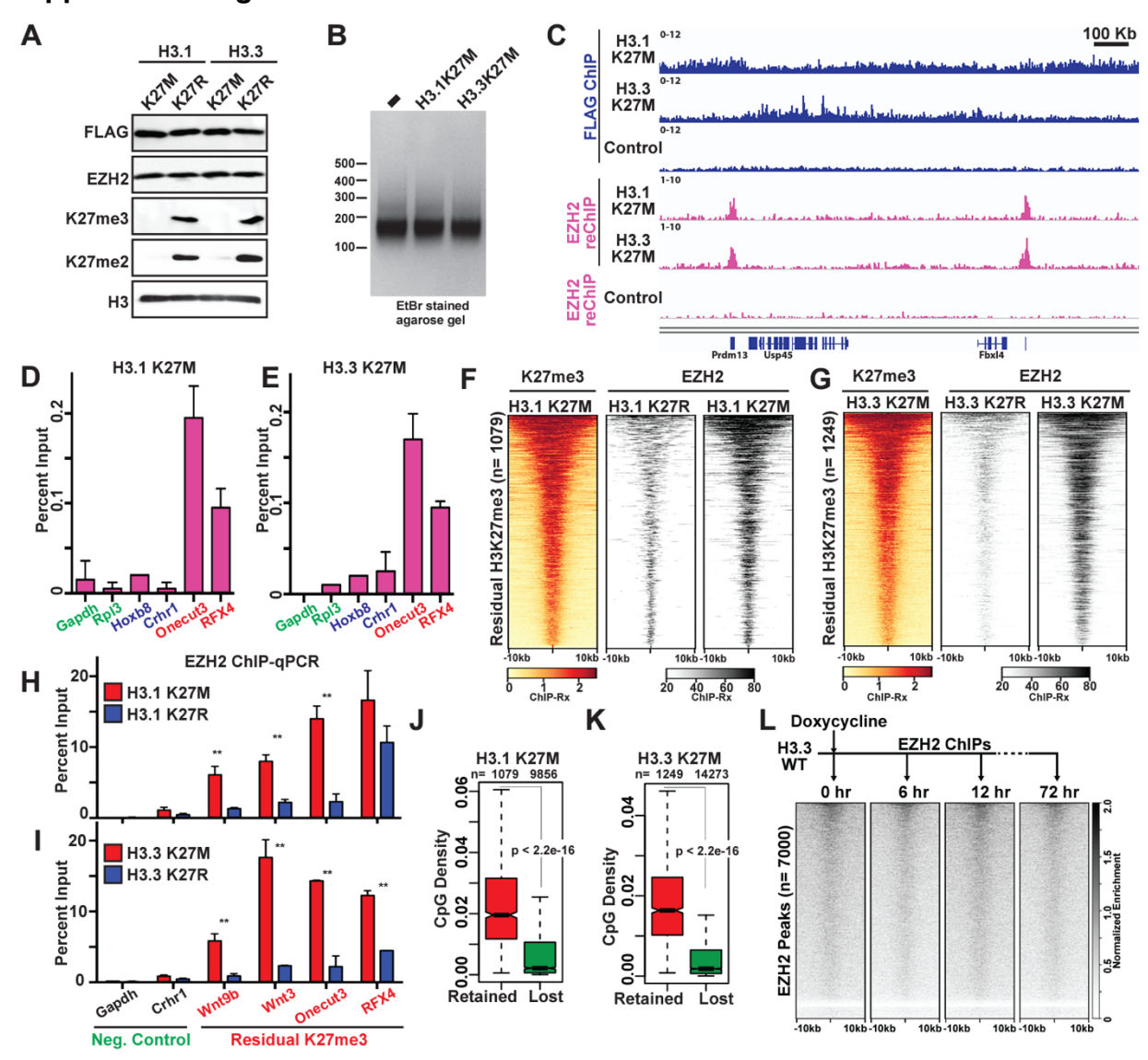
Supplemental Figure 2.3



Supplemental Figure 2.3. EZHIP sequesters PRC2 at CpG islands containing residual H3K27me3 and prevents PRC2 spreading. Related to figure 2. A. Schematic depicting the mechanism of EZHIP-mediated PRC2 redistribution. In normal cells, PRC2 is recruited to its high-affinity sites at CGIs through Polycomb-Like Proteins (PCLs) or JARID2, where it initiates H3K27me3. Binding of initial H3K27me3 to EED instigates allosteric-stimulation of EZH2 and PRC2 spreading in cis. Therefore, concentrations of PRC2 at CGIs and spreading sites reaches an equilibrium. In cells expressing EZHIP, PRC2 is able to catalyze initial H3K27me3 since EZHIP has poorer affinity for unstimulated PRC2. However, allosteric stimulation of PRC2 by initial H3K27me3 leads to the formation of a high-affinity EZHIP-PRC2 complex at CGIs. Therefore, PRC2 occupancy is shifted towards CGI away from spreading sites at equilibrium, which results in a disproportionate reduction of intergenic H3K27me3. B. Genome browser view of EZH2 ChIP-Rx in control cells (no EZHIP expression) and cells expressing EZHIP WT or M406E. EZHIP WT, but not M406E mutant, causes accumulation of PRC2 at CGIs. C. Boxplot displaying the reference-normalized EZH2 enrichment at recruitment and spreading sites in cells expressing EZHIP WT or M406E mutant. D. Barchart displaying the fraction of EZH2 read densities within the recruitment or spreading sites in cells expressing EZHIP WT or M406E. E. EZH2 ChIP enrichment in cells expressing EZHIP WT or M406E as measured by qPCR (p<0.05**). F. Boxplot displaying CpG densities (total number of CpGs/length of the region) at residual H3K27me3 (red) and spreading (green) sites. G. Genome browser view of SUZ12 CUT&RUN enrichemnt in EZHIP+/+ and EZHIP-/- U2OS cells. EZHIP expression leads to redistribution of PRC2 from broad PRC2 domains (red arrow) to recruitment sites (green box). H. Heatmap displaying

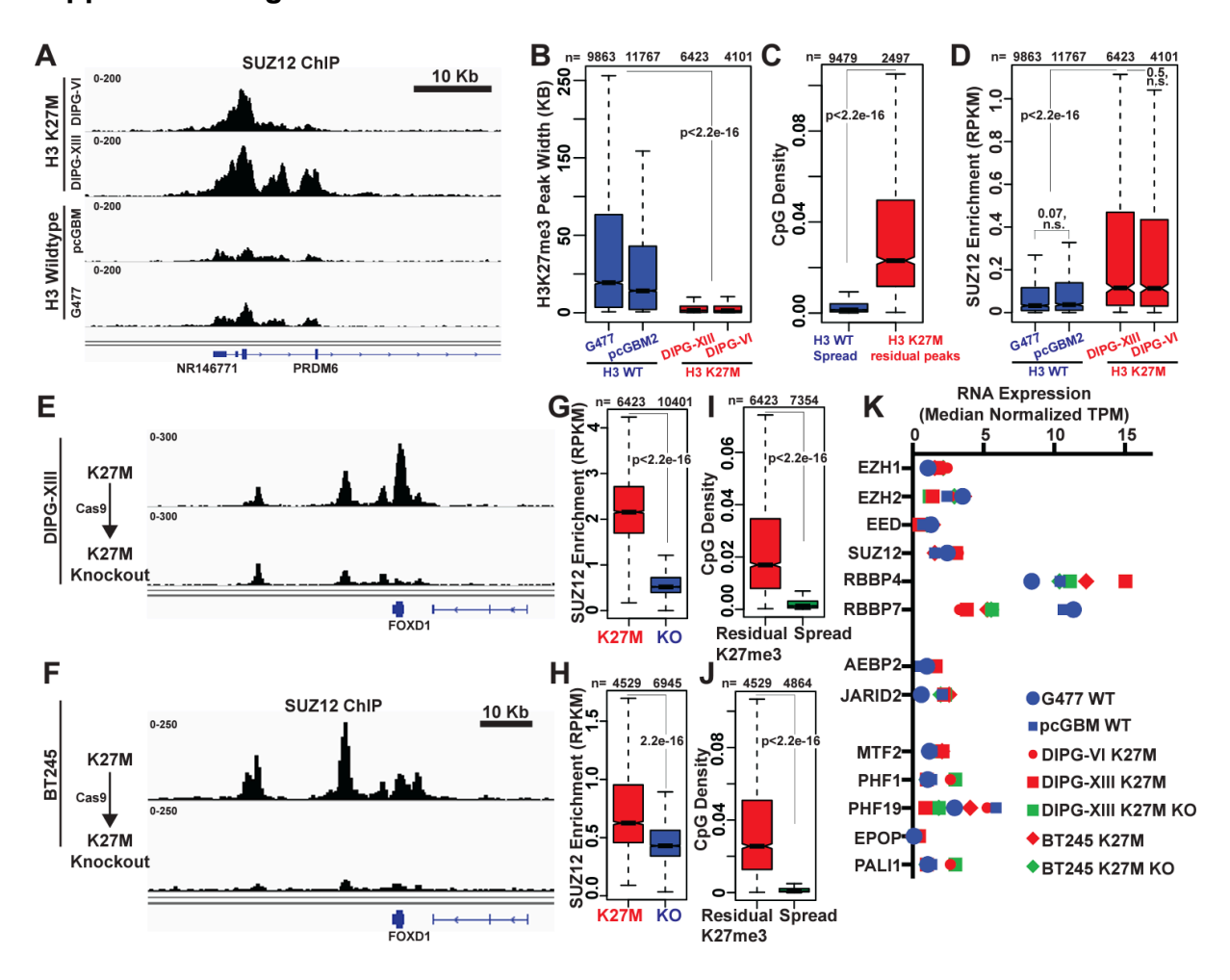
SUZ12 enrichment in EZHIP+/+ and EZHIP-/- U2OS cells at spread sites. I. Boxplots displaying SUZ12 enrichment at recruitment sites and spread sites in EZHIP+/+ and EZHIP-/- U2OS cells. Recruitment sites were defined as SUZ12 peaks in parental U2OS cells and spreading sites were identified as H3K27me3 domains in EZHIP-/- cells other than the recruitment sites. J. Interaction between EED R302 and EZH2 H158 which serves to stimulate EZH2 in response to H3K27me3 binding to EED. K. Heatmap displaying reference-normalized EZH2 enrichments at residual H3K27me3 peaks in EED-/- cells rescues with EED WT, Y365A or R302S. L. Boxplot displaying CpG density at residual H3K27me3 peaks in EED-/- cells rescued with EED R302S or spread sites. M. Immunoblots of inputs and elutions from FLAG-affinity purification of FLAG-tagged EZHIP from EED-/- MEFs rescued with HA-tagged EED WT or R302S. N. Peptide pulldowns of recombinant PRC2 containing EED WT or R302S using EZHIP KLP peptide. O. IC50 of in vitro PRC2 inhibition by EZHIP KLP peptide for PRC2 containing EED WT or R302S.

Supplemental Figure 2.4.



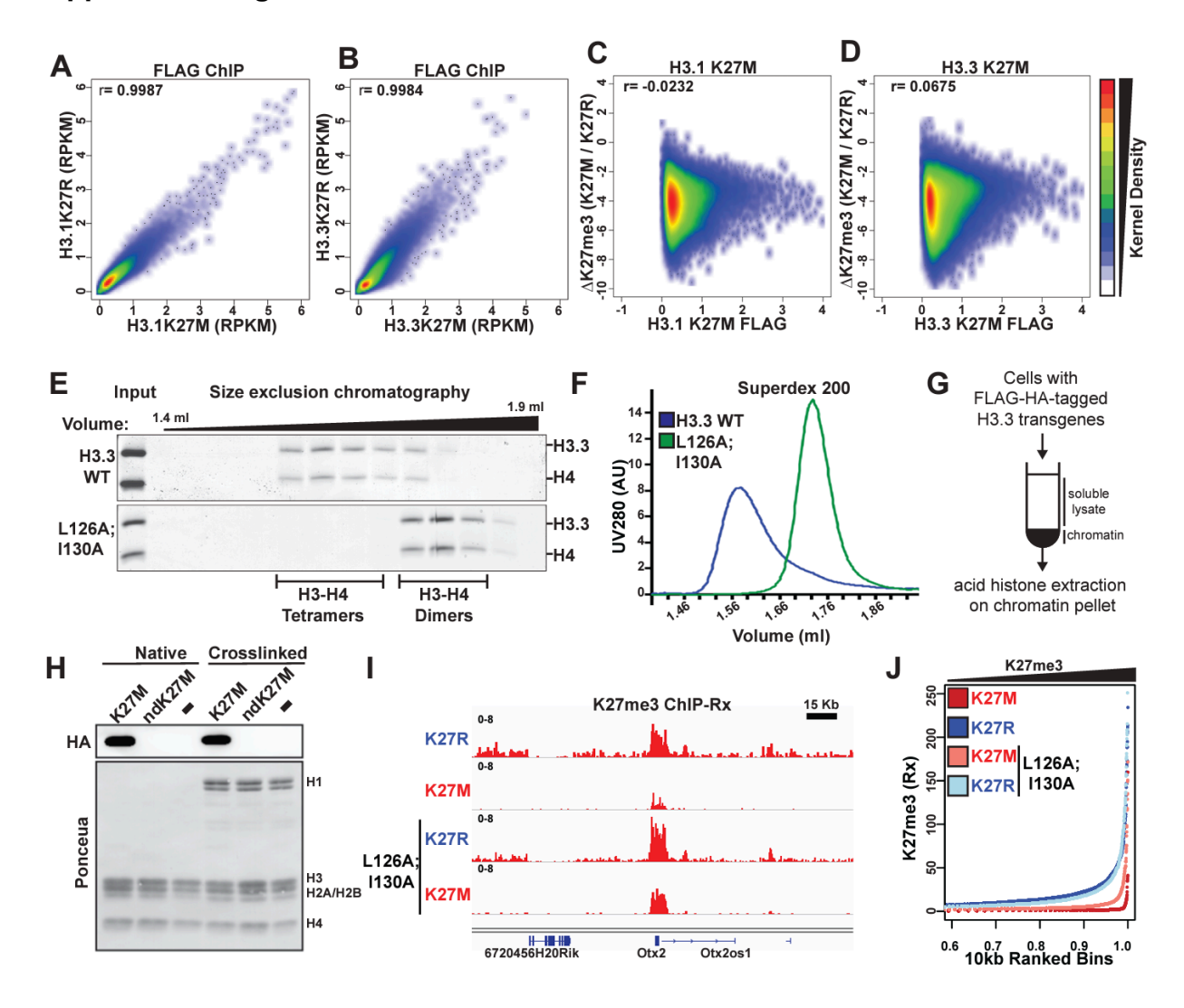
Supplemental Figure 2.4. H3K27M interacts with PRC2 in vivo and stalls it at CpG islands containing residual H3K27me3. Related to Figure 2.3. A. Immunoblots from whole cell extracts of MEFs expressing H3.1 or H3.3 K27M and K27R. B. Representative image of ethidium bromide stained agarose gel displaying the fragment size distribution of nucleosomes used in ChIP/reChIP experiments in this study. C. Genome browser view of FLAG-EZH2 ChIP-reChIP densities in cells expressing H3.1K27M or H3.3K27M. EZH2 reChIP enrichment was not found in control cells lacking FLAG-tagged H3 transgene. D and E. EZH2 reChIP enrichment at a subset of promoters in cells expressing H3.1K27M (D) or H3.3K27M (E) as measured by qPCR. F and G. Heatmap displaying EZH2 enrichment at residual H3K27me3 in cells expressing H3.1 K27M and K27R (F), or H3.3 K27M and K27R (G). H and I. EZH2 ChIP enrichment in cells expressing H3.1K27M (H) or H3.3 K27M (I) at a subset of target loci measured by qPCR (** p<0.05). J and K. Boxplot displaying CpG densities at residual H3K27me3 peaks and regions that displayed loss of H3K27me3. L. Heatmaps displaying EZH2 enrichment in 29T-Rex cells expressing doxycycline-inducible H3.3 WT at 0, 6, 12 and 72 hours after treatment with Doxycycline around EZH2 peaks at 72 hours after induction (related to Figure 2.3G).

Supplemental Figure 2.5



Supplemental Figure 2.5. H3 K27M sequesters PRC2 at CpG islands containing residual H3K27me3 in Diffuse Midline Gliomas. Related to Figure 2.3. A. Genome browser view of SUZ12 occupancies in DMG cell lines containing H3 K27M mutations (DIPG-XIII and DIPG-VI) or H3 WT (G477 and pcGMB2). B. Boxplots displaying the H3K27me3 peak width in DMG cell lines as describes in A. C. Boxplot displaying CpG densities within residual H3K27me3 peaks (red) or spreading sites that lost H3K27me3 (blue). D. Boxplots displaying RPKM normalized SUZ12 enrichment at residual H3K27me3 peaks. E and F. Genome browser view of SUZ12 occupancies in DIPG-XIII (E) or BT245 (F) cell line containing H3.3 K27M mutation or after cas9-mediated genetic depletion of H3.3 K27M. G and H. Boxplot displaying SUZ12 RPKM enrichment at residual H3K27me3 peaks in DIPG-XIII cells (G) or BT245 cells (H) containing H3.3 K27M or H3.3 K27M Knockout cells. I and J. Boxplot displaying CpG densities within residual H3K27me3 peaks or at spreading sites that gained H3K27me3 upon H3.3 K27M knockout in DIPG-XIII (I) or BT245 cells (J). K. Plot displaying the RNA expression of PRC2 subunits in DMGs containing H3 WT (blue) or H2 K27M mutations (red) or H3.3 K27M knockout cells (green). None of the PRC2 subunits were differentially expressed in H3 K27M mutant tumors or upon H3 K27M knockout.

Supplemental Figure 2.6.



Supplemental Figure 2.6. Chromatin deposition of H3 K27M oncohistones is not necessary for reduction of H3K27me3 in vivo. Related to Figure 2.3. A. Correlation between genomic enrichment of H3.1 K27M and H3.1 K27R oncohistones as measured by FLAG-ChIP enrichments. B. Correlation between genomic enrichment of H3.3K27M and H3.3K27R as measured by FLAG-ChIP. C and D. Correlation between changes in H3K27me3 enrichment (log2[K27M/K27R]) and H3 K27M oncohistone enrichment in cells expressing H3.1 K27M (C) or H3.3 K27M D. Each point in correlation plots represent a 10 KB genomic bin, p represents Spearman correlation coefficient, Color code for kernel densities for A-D is shown on right. E. In vitro reconstitution of H3-H4 histone complex assembly with H3.3 wildtype or L126A;1130A mutant using salt dialysis method. Coomassie stained SDS-PAGE gel of eluates from size-exclusion chromatography column displays the fraction of H3-H4 dimers and tetramers within each sample. F. Curve displaying the protein content (measure by UV A285) of eluates from superdex size exclusion chromatography column as described in E. G. Strategy used to fractionate 293T nuclei into chromatin and soluble nuclear fraction. Nuclei were also crosslinked in parallel to detect transiently chromatin-bound proteins. H. Immunoblots of chromatin fraction from cells expressing HA-tagged H3.3 K27M or K27M;L126A;I130A "non-depositable" triple mutant (ndK27M). I. Genome browser view H3K27me3 enrichment in cells expressing H3.3K27M or H3.3K27R with or without L126A;I130A non-depositable mutants. J. H3K27me3 reference-normalized (ChIP-Rx) enrichment at 10 Kb genomic bins is plotted against the rank of each bins in cells expressing H3.3K27M or H3.3K27R with or without L126A;I130A non-depositable mutants.

References

- Wu G, Broniscer A, McEachron TA, et al. Somatic histone H3 alterations in pediatric diffuse intrinsic pontine gliomas and non-brainstem glioblastomas. *Nat Genet*. 2012;44(3):251-253. doi:10.1038/ng.1102
- Schwartzentruber J, Korshunov A, Liu XY, et al. Driver mutations in histone H3.3 and chromatin remodelling genes in paediatric glioblastoma. *Nature*.
 2012;482(7384):226-231. doi:10.1038/nature10833
- Bender S, Tang Y, Lindroth AM, et al. Reduced H3K27me3 and DNA
 Hypomethylation Are Major Drivers of Gene Expression in K27M Mutant Pediatric
 High-Grade Gliomas. Cancer Cell. 2013;24(5):660-672.
 doi:10.1016/j.ccr.2013.10.006
- Larson JD, Kasper LH, Paugh BS, et al. Histone H3.3 K27M Accelerates
 Spontaneous Brainstem Glioma and Drives Restricted Changes in Bivalent Gene
 Expression. Cancer Cell. 2019;35(1):140-155.e7. doi:10.1016/j.ccell.2018.11.015
- Chan KM, Fang D, Gan H, et al. The histone H3.3K27M mutation in pediatric glioma reprograms H3K27 methylation and gene expression. *Genes Dev.* 2013;27(9):985-990. doi:10.1101/gad.217778.113
- Lewis PW, Müller MM, Koletsky MS, et al. Inhibition of PRC2 Activity by a Gain-of-Function H3 Mutation Found in Pediatric Glioblastoma. *Science*.
 2013;340(6134):857-861. doi:10.1126/science.1232245
- 7. Bayliss J, Mukherjee P, Lu C, et al. Lowered H3K27me3 and DNA hypomethylation define poorly prognostic pediatric posterior fossa ependymomas. *Science*

- *Translational Medicine*. 2016;8(366):366ra161-366ra161. doi:10.1126/scitranslmed.aah6904
- 8. Pajtler KW, Wen J, Sill M, et al. Molecular heterogeneity and CXorf67 alterations in posterior fossa group A (PFA) ependymomas. *Acta Neuropathol*. 2018;136(2):211-226. doi:10.1007/s00401-018-1877-0
- Jain SU, Do TJ, Lund PJ, et al. PFA ependymoma-associated protein EZHIP inhibits PRC2 activity through a H3 K27M-like mechanism. *Nature Communications*.
 2019;10(1):2146. doi:10.1038/s41467-019-09981-6
- 10. Hübner JM, Müller T, Papageorgiou DN, et al. EZHIP/CXorf67 mimics K27M mutated oncohistones and functions as an intrinsic inhibitor of PRC2 function in aggressive posterior fossa ependymoma. *Neuro Oncol.* 2019;21(7):878-889. doi:10.1093/neuonc/noz058
- 11. Piunti A, Smith ER, Morgan MAJ, et al. CATACOMB: An endogenous inducible gene that antagonizes H3K27 methylation activity of Polycomb repressive complex 2 via an H3K27M-like mechanism. *Science Advances*. 2019;5(7):eaax2887. doi:10.1126/sciadv.aax2887
- 12. Ragazzini R, Pérez-Palacios R, Baymaz IH, et al. EZHIP constrains Polycomb Repressive Complex 2 activity in germ cells. *Nature Communications*. 2019;10(1):3858. doi:10.1038/s41467-019-11800-x
- 13. Piunti A, Hashizume R, Morgan MA, et al. Therapeutic targeting of polycomb and BET bromodomain proteins in diffuse intrinsic pontine gliomas. *Nature Medicine*. 2017;23(4):493-500. doi:10.1038/nm.4296

- 14. Mohammad F, Weissmann S, Leblanc B, et al. EZH2 is a potential therapeutic target for H3K27M-mutant pediatric gliomas. *Nature Medicine*. 2017;23(4):483-492. doi:10.1038/nm.4293
- 15. Harutyunyan AS, Krug B, Chen H, et al. H3K27M induces defective chromatin spread of PRC2-mediated repressive H3K27me2/me3 and is essential for glioma tumorigenesis. *Nature Communications*. 2019;10(1):1262. doi:10.1038/s41467-019-09140-x
- 16. Healy E, Mucha M, Glancy E, et al. PRC2.1 and PRC2.2 Synergize to Coordinate H3K27 Trimethylation. *Molecular Cell*. 2019;76(3):437-452.e6. doi:10.1016/j.molcel.2019.08.012
- 17. Højfeldt JW, Hedehus L, Laugesen A, Tatar T, Wiehle L, Helin K. Non-core Subunits of the PRC2 Complex Are Collectively Required for Its Target-Site Specificity.

 *Molecular Cell. 2019;76(3):423-436.e3. doi:10.1016/j.molcel.2019.07.031
- 18. Pasini D, Cloos PAC, Walfridsson J, et al. JARID2 regulates binding of the Polycomb repressive complex 2 to target genes in ES cells. *Nature*. 2010;464(7286):306-310. doi:10.1038/nature08788
- 19. Li H, Liefke R, Jiang J, et al. Polycomb-like proteins link the PRC2 complex to CpG islands. *Nature*. 2017;549(7671):287-291. doi:10.1038/nature23881
- 20. Margueron R, Justin N, Ohno K, et al. Role of the polycomb protein EED in the propagation of repressive histone marks. *Nature*. 2009;461(7265):762-767. doi:10.1038/nature08398

- 21. Diehl KL, Ge EJ, Weinberg DN, Jani KS, Allis CD, Muir TW. PRC2 engages a bivalent H3K27M-H3K27me3 dinucleosome inhibitor. *Proceedings of the National Academy of Sciences*. 2019;116(44):22152-22157. doi:10.1073/pnas.1911775116
- 22. Justin N, Zhang Y, Tarricone C, et al. Structural basis of oncogenic histone H3K27M inhibition of human polycomb repressive complex 2. *Nature Communications*. 2016;7(1):11316. doi:10.1038/ncomms11316
- 23. Stafford JM, Lee CH, Voigt P, et al. Multiple modes of PRC2 inhibition elicit global chromatin alterations in H3K27M pediatric glioma. *Science Advances*.
 2018;4(10):eaau5935. doi:10.1126/sciadv.aau5935
- 24. Brown ZZ, Müller MM, Jain SU, Allis CD, Lewis PW, Muir TW. Strategy for "Detoxification" of a Cancer-Derived Histone Mutant Based on Mapping Its Interaction with the Methyltransferase PRC2. J Am Chem Soc. 2014;136(39):13498-13501. doi:10.1021/ja5060934
- 25. Delaney K, Strobino M, Wenda JM, Pankowski A, Steiner FA. H3.3K27M-induced chromatin changes drive ectopic replication through misregulation of the JNK pathway in C. elegans. *Nat Commun*. 2019;10(1):2529. doi:10.1038/s41467-019-10404-9
- 26. Herz HM, Morgan M, Gao X, et al. Histone H3 lysine-to-methionine mutants as a paradigm to study chromatin signaling. *Science*. 2014;345(6200):1065-1070. doi:10.1126/science.1255104
- 27. He Y, Selvaraju S, Curtin ML, et al. The EED protein–protein interaction inhibitor A-395 inactivates the PRC2 complex. *Nat Chem Biol*. 2017;13(4):389-395. doi:10.1038/nchembio.2306

- 28. Oksuz O, Narendra V, Lee CH, et al. Capturing the Onset of PRC2-Mediated Repressive Domain Formation. *Molecular Cell*. 2018;70(6):1149-1162.e5. doi:10.1016/j.molcel.2018.05.023
- 29. Cohen ASA, Yap DB, Lewis MES, et al. Weaver Syndrome-Associated EZH2 Protein Variants Show Impaired Histone Methyltransferase Function In Vitro. *Human Mutation*. 2016;37(3):301-307. doi:10.1002/humu.22946
- 30. Lee CH, Yu JR, Kumar S, et al. Allosteric Activation Dictates PRC2 Activity
 Independent of Its Recruitment to Chromatin. *Molecular Cell*. 2018;70(3):422-434.e6. doi:10.1016/j.molcel.2018.03.020
- 31. Ramachandran S, Vogel L, Strahl BD, Dokholyan NV. Thermodynamic Stability of Histone H3 Is a Necessary but not Sufficient Driving Force for its Evolutionary Conservation. *PLOS Computational Biology*. 2011;7(1):e1001042. doi:10.1371/journal.pcbi.1001042
- 32. Hoelper D, Huang H, Jain AY, Patel DJ, Lewis PW. Structural and mechanistic insights into ATRX-dependent and -independent functions of the histone chaperone DAXX. *Nat Commun*. 2017;8(1):1193. doi:10.1038/s41467-017-01206-y
- 33. Kimura H, Cook PR. Kinetics of Core Histones in Living Human Cells: Little Exchange of H3 and H4 and Some Rapid Exchange of H2b. *Journal of Cell Biology*. 2001;153(7):1341-1354. doi:10.1083/jcb.153.7.1341
- 34. Orsi GA, Kasinathan S, Hughes KT, Saminadin-Peter S, Henikoff S, Ahmad K. High-resolution mapping defines the cooperative architecture of Polycomb response elements. *Genome Res.* 2014;24(5):809-820. doi:10.1101/gr.163642.113

- 35. Müller J, Kassis JA. Polycomb response elements and targeting of Polycomb group proteins in Drosophila. *Current Opinion in Genetics & Development*.
 2006;16(5):476-484. doi:10.1016/j.gde.2006.08.005
- 36. De S, Mitra A, Cheng Y, Pfeifer K, Kassis JA. Formation of a Polycomb-Domain in the Absence of Strong Polycomb Response Elements. *PLoS Genet*. 2016;12(7):e1006200. doi:10.1371/journal.pgen.1006200
- 37. Castel D, Kergrohen T, Tauziède-Espariat A, et al. Histone H3 wild-type DIPG/DMG overexpressing EZHIP extend the spectrum diffuse midline gliomas with PRC2 inhibition beyond H3-K27M mutation. *Acta Neuropathol*. 2020;139(6):1109-1113. doi:10.1007/s00401-020-02142-w
- 38. Pratt D, Quezado M, Abdullaev Z, et al. Diffuse intrinsic pontine glioma-like tumor with EZHIP expression and molecular features of PFA ependymoma. Acta Neuropathologica Communications. 2020;8(1):37. doi:10.1186/s40478-020-00905-w
- 39. Anastas JN, Zee BM, Kalin JH, et al. Re-programing Chromatin with a Bifunctional LSD1/HDAC Inhibitor Induces Therapeutic Differentiation in DIPG. *Cancer Cell*. 2019;36(5):528-544.e10. doi:10.1016/j.ccell.2019.09.005
- 40. Grasso CS, Tang Y, Truffaux N, et al. Functionally defined therapeutic targets in diffuse intrinsic pontine glioma. *Nat Med*. 2015;21(6):555-559. doi:10.1038/nm.3855
- 41. Krug B, De Jay N, Harutyunyan AS, et al. Pervasive H3K27 Acetylation Leads to ERV Expression and a Therapeutic Vulnerability in H3K27M Gliomas. *Cancer Cell*. 2019;35(5):782-797.e8. doi:10.1016/j.ccell.2019.04.004

- 42. Nagaraja S, Quezada MA, Gillespie SM, et al. Histone Variant and Cell Context

 Determine H3K27M Reprogramming of the Enhancer Landscape and Oncogenic

 State. *Molecular Cell*. 2019;76(6):965-980.e12. doi:10.1016/j.molcel.2019.08.030
- 43. Langmead B, Trapnell C, Pop M, Salzberg SL. Ultrafast and memory-efficient alignment of short DNA sequences to the human genome. *Genome Biology*. 2009;10(3):R25. doi:10.1186/gb-2009-10-3-r25
- 44. Li H, Handsaker B, Wysoker A, et al. The Sequence Alignment/Map format and SAMtools. *Bioinformatics*. 2009;25(16):2078-2079.

 doi:10.1093/bioinformatics/btp352
- 45. Ramírez F, Ryan DP, Grüning B, et al. deepTools2: a next generation web server for deep-sequencing data analysis. *Nucleic Acids Research*. 2016;44(W1):W160-W165. doi:10.1093/nar/gkw257
- 46. Sun G, Chung D, Liang K, Keleş S. Statistical Analysis of ChIP-seq Data with MOSAiCS. In: Shomron N, ed. *Deep Sequencing Data Analysis*. Methods in Molecular Biology. Humana Press; 2013:193-212. doi:10.1007/978-1-62703-514-9_12
- 47. Alecki C, Chiwara V, Sanz LA, et al. RNA-DNA strand exchange by the Drosophila Polycomb complex PRC2. *Nature Communications*. 2020;11(1). doi:10.1038/s41467-020-15609-x
- 48. Gaspar JM. NGmerge: merging paired-end reads via novel empirically-derived models of sequencing errors. *BMC Bioinformatics*. 2018;19(1):536. doi:10.1186/s12859-018-2579-2

Chapter 3: Leveraging *Drosophila melanogaster* to identify conserved modifiers of PRC2-mediated pediatric glioma

The work in this chapter is in preparation for submission.

Krabbenhoft, S. D., Masuda, T.E., Do, T.J., Jain, S. U. Lewis, P. W., and Harrison, M. M.

Statement of contribution: I designed, wrote, and revised this article in collaboration with Drs. Melissa Harrison and Peter Lewis. I performed all experiments, excluding generation of *5x-UAS H3 K27M*, *5x-UAS H3 K27R*, and *5x-UAS EZHIP* plasmids for generation of transgenic fly lines (S.U.J. and T.J.D.). T.E.M and I independently scored all RNAi lines included in H3 K27M and EZHIP screens.

Abstract

Two key molecular events define nearly all cases of diffuse midline glioma (DMG) and posterior fossa ependymoma type A (PFA): a histone H3 lysine 27 mutation (H3 K27M) in DMG, or elevated expression of EZHIP in PFA. H3 K27M and EZHIP potently inhibit the H3K27 methyltransferase polycomb repressive complex 2 (PRC2), causing a nearcomplete loss of H3 lysine 27 trimethylation (H3K27me3). PRC2 recruitment sites retain H3K27me3, while aberrantly expressed genes feature reduced H3K27me3 and concomitantly increased active histone modifications. DMG and PFA may therefore stem from continued repression of some genes, and an imbalance between transcriptional activators and repressors at others. Here, we leverage Drosophila melanogaster to screen for conserved enhancers and suppressors of H3 K27M. Suppressors are robust across multiple tissues and rescue the severe impairments caused by EZHIP. We find that suppressors restore normal development despite the continued loss of H3K27me3, instead reversing the transcriptional changes imparted by H3 K27M. Our data suggest that PRC2 inhibition by H3 K27M and EZHIP dysregulates development by creating an imbalance between the repressive H3K27me3 and marks of active chromatin at generegulatory elements.

Introduction

Diffuse midline glioma (DMG) is an almost universally fatal form of pediatric brain cancer. Around 80% of DMG tumors harbor lysine-to-methionine mutations in one copy of histone H3 (H3 K27M).^{1,2} H3 K27M-positive DMG tumors exhibit a near-complete loss of histone H3 lysine 27 trimethylation (H3K27me3), a modification associated with transcriptional repression.^{3–5} H3K27me3 is also reduced in posterior fossa ependymoma type A (PFA) tumors.⁶ PFA and DMG tumors are diagnosed in young children, occur in anatomically related regions, and have similar transcriptional profiles.^{6–8} Nevertheless, H3 K27M mutations are rarely found in PFA.^{6,9} Instead, most cases of PFA have high expression levels of *EZHIP*, a gene about which little was known until its recent discovery in this cancer.⁸ The H3 K27M mutation and elevated EZHIP expression are now understood to be the initiating molecular events in DMG and PFA.^{10–12}

Polycomb repressive complex 2 (PRC2) is a highly conserved histone methyltransferase complex trimethylates H3K27. H3 K27M and EZHIP are competitive inhibitors of PRC2. 13 Within EZHIP, a 12-residue peptide resembles the sequence of histone H3 surrounding lysine 27, but includes a methionine making it more closely resemble H3K27M. 13–16 These methionine residues are essential for the ability of both EZHIP and H3K27M to bind the active site of PRC2 and, in so doing, inhibit its catalytic activity. 13,14 Despite these similar mechanisms, EZHIP is a more potent inhibitor of PRC2 than H3 K27M. 13 It is unknown whether the biochemical discrepancies between H3 K27M and EZHIP have phenotypic consequences.

Upon recruitment to the genome, PRC2 catalyzes H3K27me3 inefficiently. Binding to previously deposited H3K27me3 reorganizes the conformation of the complex, resulting in allosteric activation. Allosterically active PRC2 spreads H3K27me3 across broad genomic regions. H3 K27M and EZHIP preferentially inhibit allosterically active PRC2. Thus, their expression drives the loss of H3K27me3 at regions outside of initial PRC2-recruitment sites. Because PRC2 recruitment and initial H3K27me3 do not rely on allosterically active PRC2, these processes are largely unperturbed.

As predicted from DMG and PFA tumors, residual H3K27me3 is detected at PRC2 recruitment sites, consistent with the specific loss of allosterically active PRC2 activity. Gene expression changes in these tumors reflect the distribution of H3K27me3. Residual H3K27me3 retains repressive activity, while derepression occurs where the H3K27me3 is lost.^{4,23} H3 K27M and EZHIP therefore do not phenocopy a complete loss of PRC2 function. At derepressed genes, the reduction in H3K27me3 coincides with an increase in histone modifications associated with active transcription.^{24–26} The chromatin-modifying proteins that deposit these active histone marks may be required to establish oncogenic transcriptional programs.

H3 K27M or EZHIP have almost exclusively been linked to cancers in the developing hindbrain. The reasons for this tissue specificity are not fully understood. It is possible that intrinsic properties of H3 K27M and EZHIP make them uniquely oncogenic in the hindbrain. This is improbable, since PRC2 is important in many developing tissues. More likely, hindbrain transcriptional programs are uniquely susceptible to oncogenic

transformation by H3 K27M or EZHIP. Though these oncoproteins drive tumorigenesis in a small region, the chromatin modifiers that mediate their transcriptional changes are likely conserved. Modeling these oncoproteins in a developing organism may reveal the chromatin-related proteins that mediate impaired development in DMG and PFA.

Most chromatin-modifying proteins are conserved between humans and flies.^{27,28} *Drosophila* have been indispensable in identifying many chromatin-related proteins, including the discovery of Polycomb proteins.²⁹ Moreover, the lack of genetic redundancy in *Drosophila* simplifies functional characterization of conserved genes. *Drosophila* are therefore an appealing model with which to disentangle the contributions of various chromatin-related proteins to the phenotypes caused by H3 K27M and EZHIP.

We and others showed that H3 K27M and EZHIP impair *Drosophila* development. Here, we establish models of H3 K27M and EZHIP and compare their effects on development. We leverage these models to conduct a comprehensive, quantitative screen for enhancers and suppressors of oncoprotein phenotypes. Previous efforts to identify modifiers of H3 K27M in *Drosophila* were limited in scope or phenotypic sensitivity. He identify numerous suppressors of H3 K27M and EZHIP tissue phenotypes. Suppressors restore normal development without reversing the loss of H3K27me3. PRC2 inhibition is therefore insufficient to cause EZHIP and H3 K27M phenotypes. Though EZHIP more severely disrupts *Drosophila* development than H3 K27M, these oncoproteins share genetic dependencies. Finally, we show that H3 K27M phenotypes can be suppressed by reversing their underlying transcriptional changes.

Results

Expression of H3 K27M or EZHIP inhibits allosterically activated PRC2 in *Drosophila*

H3 K27M and EZHIP are strong competitive inhibitors of PRC2, and we previously showed that this inhibition is conserved in *Drosophila*.^{13,30} *In vitro*, EZHIP inhibits PRC2 more potently than H3 K27M, though the biological significance of this is not understood.¹³ To compare the developmental consequences of their expression, we engineered transgenic *Drosophila* that enabled us to express H3 K27M and EZHIP in various tissues. Ubiquitous expression of either H3 K27M or EZHIP was lethal: EZHIP-expressing animals died as third-instar larvae, while H3 K27M-expressing animals died after pupation (Figure 3.1A). This finding suggests that EZHIP is more detrimental to fly development than H3 K27M. Expression of the non-inhibitory controls H3 K27R and EZHIP M406E did not affect viability. PRC2 inhibition is therefore essential to H3 K27M- and EZHIP-mediated lethality.

To more directly compare their effects, we expressed H3 K27M and EZHIP in a tissue not necessary for viability. We used the wing-specific *nub-Gal4* driver, allowing us to circumvent the lethality of ubiquitous expression. At similar expression levels, H3 K27M caused wing wrinkling and vein-pattering defects, while EZHIP eliminated wing development (Figure 3.1B). Increasing transgene expression caused more severe wing phenotypes, consistent with the fact that both proteins competitively inhibit PRC2. We conclude that the key biochemical features of H3 K27M and EZHIP correspond to their developmental phenotypes.

To determine how oncoprotein expression disrupts wing development, we identified changes in gene expression and H3K27me3. Because expression of EZHIP drastically reduced wing size and likely changed the cellular composition, we focused on the effects of H3 K27M expression, which resulted in milder phenotypes. To avoid the need to sort the for H3 K27M-expressing cells, we developed a system to induce ubiquitous H3 K27M expression in a temperature-controlled manner (Supplemental Figure 3.1A).³³ Using this system, we expressed ubiquitously expressed H3 K27M and harvested wing discs after 72 h. We verified that 72 h of H3 K27M induction resulted in a robust suppression of H3K27me3 levels, demonstrating the suitability of the system to examine changes in gene expression caused by oncoprotein-mediated PRC2 inhibition (Figure 3.1C, Supplemental Figure 3.1B). Using RNA-seq, we identified 181 genes that were misregulated upon H3 K27M expression as compared to the H3 K27R controls. 148 of these genes were upregulated (82%), consistent with the role of H3 K27M in PRC2 inhibition (Figure 3.1D, Supplemental Figure 3.1B, C). Differentially expressed genes had at least a 1.5-fold expression change between H3 K27M and H3 K27R, and an adjusted p-value < 0.05. For each genotype, we sequenced three replicates, with ten wing discs per replicate. Gene ontology (GO) analysis revealed that upregulated genes were enriched for germline- and piRNA-related processes (Supplemental Figure 3.1D).

To more precisely link the gene expression changes to the inhibition of PRC2, we identified the genome-wide changes in H3K27me3 using Cleavage Under Targets and Release Under Nuclease (CUT&RUN). H3 K27M caused an overall loss of H3K27me3, including a drastic reduction at genes differentially expressed in H3 K27M wing discs

(Figure 3.1 E & F, Supplemental Figure 3.2A). Studies in mammalian systems demonstrated that H3 K27M inhibits the allosterically active form of PRC2, which is not required for recruitment of the complex to the genome but is required for spreading of H3K27me3 from these recruitment sites.^{20–22} This preferential inhibition of allosterically active PRC2 results in residual H3K27me3 at PRC2-recruitment sites but a loss at regions outside these sites. In H3 K27M wing discs, residual H3K27me3 overlapped with Polycomb Response elements (PREs), the recruitment sites of *Drosophila* PRC2 (Supplemental Figure 3.2B). By subtracting the H3K27me3 signal in H3 K27R wing discs from that in H3 K27M wing discs, it was evident that some PREs had increased signals for H3K27me3 upon H3 K27M expression. These data support the model that in *Drosophila*, as in mammals, H3 K27M primarily affects H3K27me3 spreading from recruitment sites and not the initial deposition of the mark (Supplemental Figure 3.2C). Together, our results show that EZHIP and H3 K27M disrupt development through highly conserved mechanisms of PRC2 inhibition.

Conserved chromatin-related proteins mediate the H3 K27M wing phenotype

While it is clear that loss of H3K27me3 induced by H3 K27M results in changes to the distribution other chromatin modifications, it is unknown how these changes contribute to the phenotypes observed upon H3 K27M expression. Having developed the *Drosophila* wing as a system to investigate H3 K27M-mediated phenotypes, we leveraged this system to identify how additional chromatin-related proteins modify the phenotype. We screened genes that met three main criteria: they had chromatin-related functions, were conserved between flies and humans, and were expressed in the developing fly wing

(Supplemental Figure 3.3A).³⁴ In total, we screened 438 genes with 630 fly lines (Supplemental Figure 3.3B). For each line, we generated two scores based on their phenotypes: an "RNAi score" based upon the phenotype caused by expression of the *RNAi* construct alone, and a "screen score" based upon co-expression of the *RNAi* construct with H3 K27M (Figure 3.2A). Scores ranged from 0 to 10 and resulted from a composition of scores for distinct wing characteristics such as vein patterning, size, and smoothness (Figure 3.2B). Using our scoring rubric, the wing vein defects and wrinkling observed in H3 K27M wings resulted in a score of 4 (Figure 3.2C). 20 genes reduced the severity of the H3 K27M phenotype and were termed strong suppressors. Of these, 5 strong suppressors restored development such that wings were indistinguishable from wild type (Figure 3.2D & E, Supplemental Figure 3.3C-E). Some lines exhibited mutual suppression, whereby the RNAi and H3 K27M phenotypes suppressed one another (Figure 3.2E). Collectively, the strong suppressors are associated with transcriptional activation.

Enhancers exhibited synergy between H3 K27M and RNAi lines. That is, the screen score exceeded the sum total of its RNAi and H3 K27M scores (Figure 3.2F). In total, we identified 51 enhancers (Supplemental Table 3.1). Enhancers were divided into strong and weak subtypes, where strong enhancers abolished wing development (Figure 3.2F-H, Supplemental Figure 3.3D). Polycomb proteins were the most strongly enriched group among enhancers, including multiple core PRC2 subunits (Supplemental Figure 3.3G). To control for nonspecific interactions between RNAi lines and histone overexpression, we co-expressed enhancers and suppressors with *H3 K27R* and assigned an "H3 K27R

score." H3 K27R and RNAi scores were identical, suggesting that the phenotypic modifications represent a true genetic interaction with H3 K27M (Supplemental Table 3.2).

PRC2 inhibition is insufficient to drive EZHIP and H3 K27M phenotypes

To address the mechanisms by which knockdown of chromatin modifiers could restore wild-type wing development in animals expressing H3 K27M, we first determined whether the H3 K27M transgene remained expressed in the rescued tissue. We immunostained wing discs for the FLAG epitope on H3 K27M either in discs dissected from animals expressing H3 K27M alone or in combination with strong suppressors. In all cases, we confirmed that suppression did not result from the loss of transgene expression (Figure 3.3A). In addition, suppression did not result from a restoration of PRC2 activity as H3K27me3 levels remained low in these tissues. Thus, the inhibition of PRC2-mediated H3K27me3 alone is insufficient to impair wing development. Rather, additional chromatin-related proteins facilitate H3 K27M phenotypes, at least some of which we identified in this screen.

As demonstrated above, EZHIP expression is more detrimental to *Drosophila* development than H3 K27M expression (Figure 3.3B, Supplemental Figure 3.4A). These phenotypic differences may be due to biochemical differences between the two proteins or disruption of additional, developmentally important pathways by EZHIP.¹³ To distinguish between these possibilities, we tested whether suppressors and enhancers of H3 K27M functioned similarly when combined with EZHIP expression. The extreme EZHIP phenotype prevented our ability to identify clear enhancers. We therefore focused on the

H3 K27M suppressors (Figure 3.3C). 6 of the 20 suppressors rescued wing development of EZHIP expressing flies, albeit not to a fully wild-type state (Figures 3.3D & E, Supplemental Table 3.3). Most of the RNAi lines that did not alter the EZHIP phenotype were classified as weak H3 K27M suppressors. The comparatively mild H3 K27M phenotype allowed to detect subtler forms of suppression. The severe EZHIP phenotype likely would have masked such subtle effects, even if a genetic interaction existed. Our ability to restore wing development by knocking down proteins in flies expressing either EZHIP or H3 K27M suggests that their phenotypic differences are due to differences in the strength of PRC2 inhibition rather than interactions with different chromatin modifiers.

H3 K27M modifiers are robust across multiple tissue types

To determine the tissue specificity of the mechanisms of suppression and enhancement, we tested whether knockdown of the identified enhancers and suppressors could modify H3 K27M-mediated defects in an additional tissue. We expressed H3 K27M in the eye and identified disruption of the normally well-patterned photoreceptor units of the eye (Supplemental Figure 3.4B, Figure 3.3F). RNAi knockdown of suppressors identified in the wing similarly rescued wild-type eye development, and RNAi knockdown of enhancers caused further disruption of the photoreceptors (Figure 3.3F, Supplemental Figure 3.4C). As in the wing, some suppressors impaired eye development when expressed alone but were suppressed by H3 K27M (Supplemental Figure 3.4D). We conclude that H3 K27M phenotypes are mediated by similar chromatin modifiers in multiple tissues.

The enhancement and suppression of eye and wing H3 K27M phenotypes suggested a shared mechanistic basis, possibly at the level of gene expression. To directly compare gene expression, we performed RNA-seq in wing and eye-antennal discs. Using the system we developed for ubiquitous and inducible expression, we expressed H3 K27M or H3 K27R for 72 h before harvesting discs (Supplemental Figure 3.1A). Compared to H3 K27R control, H3 K27M upregulated 137 genes in the eye-antennal disc and downregulated 41 genes (Supplemental Figure 3.5A, B). The set of upregulated genes we identified were shared with those previously identified using a different transgenic system, demonstrating our ability to reproducibly identify H3 K27M-target genes (Supplemental Figure 3.5C).³²

49 genes were upregulated by H3 K27M in both wing and eye-antennal discs (Figure 3.3G). When we analyzed all 148 genes upregulated in H3 K27M wing discs as compared to controls, we identified similar average levels of increased gene expression in H3 K27M eye discs as compared to controls (Figure 3.3H & I). Reciprocally, when we did a similar analysis with the 137 upregulated genes in H3 K27M eye-antennal discs as compared to controls, we showed that these genes were also increased in average expression levels in H3 K27M wing discs as compared to H3 K27R controls (Supplemental Figure 3.5D, E). Far fewer genes were downregulated by H3 K27M in both tissues. Moreover, very few of these downregulated genes were shared between tissues (Supplemental Figure 3.5F). Overall, these data show that H3 K27M similarly disrupts gene expression in multiple tissues and support a model in which enhancers and suppressors modify H3 K27M

phenotypes by regulating a shared gene-regulatory network in multiple biological contexts.

Suppressors counteract H3 K27M transcriptional changes

We next sought to understand whether H3 K27M phenotypic suppression was mediated at the transcriptional level. We performed RNA-seq on wing discs expressing H3 K27M or H3 K27R with knockdown of each of four strong suppressors: *Asx*, *ash1*, *trx*, and *Nup153*. Consistent with earlier RNA-seq experiments, we used our temperature-inducible system to express the transgenes for 72 h. All four suppressors altered expression of hundreds of genes in H3 K27M wing discs. Suppressor RNAi preferentially downregulated genes in H3 K27M discs, consistent with their roles as transcriptional activators (Supplemental Figure 3.6A-D). Genes downregulated in discs co-expressing H3 K27M and suppressor RNAi compared to H3 K27M-alone discs were expressed at similar levels in discs co-expressing H3 K27R and suppressor RNAi, confirming their independent effects on gene regulation (Supplemental Figure 3.6E-H).

Because the proteins encoded by the strong suppressors positively regulate transcription, we reasoned that their knockdown may have reversed the derepression caused by H3 K27M, thereby restoring wild-type wing development. To test this, we examined the number of H3 K27M-upregulated genes with increased, decreased, or unchanged expression when co-expressing suppressor RNAi. In discs in which H3 K27M was combined with knockdown of the suppressor, the total RNA levels of 22-55% of the 148 genes with increased expression in H3 K27M alone were decreased. By comparison, only

3-13% of this gene set showed increased RNA levels (Figure 3.4A). When we assessed the average expression level of all 148 H3 K27M-upregulated genes, we showed that *Asx*, *ash1*, and *trx* RNAi partially or completely restored the average expression of these genes to levels similar to the H3 K27R control (Figure 3.4B, Supplemental Figure 3.7A). These data suggest that strong suppressors may facilitate increased expression of a subset of genes when H3 K27M is present.

Asx, ash1, and trx RNAi had broadly similar effects on gene expression. Indeed, 1269 genes were downregulated by all three suppressors in H3 K27M wing discs (Figure 3.4C, Supplemental Figure 3.7B). This gene set included 45 of the 148 H3 K27M-upregulated genes, further supporting the notion that these suppressors are directly required for the increased expression of these genes in the presence of H3 K27M (Supplemental Figure 3.7C). Asx, ash1, and trx RNAi also downregulated overlapping gene sets when expressed with H3 K27R, suggesting these proteins may share a set of target genes (Supplemental Figure 3.7D).

In contrast to *Asx*, *ash1*, and *trx* RNAi, *Nup153* RNAi did not alter the average expression H3 K27M-upregulated genes despite its ability to strongly suppress the phenotype caused by H3 K27M expression. Of the 1269 genes downregulated by *Asx*, *ash1*, and *trx* RNAi in H3 K27M wing discs, only 31 were also downregulated by *Nup153* RNAi (Figure 4.4C & D, Supplemental Figure 3.7E). Despite this limited overlap, nearly half of the genes downregulated by all four suppressors (42%) were genes that were increased in expression by H3 K27M Figure 3.4E). Of note, *Nup153* itself is downregulated by all four

suppressors, suggesting Nup153 may be important for driving the gene expression changes that result from H3 K27M (Figure 3.4D, F).

Discussion

Here, we generated developmental models of H3 K27M and EZHIP that recapitulate key biochemical features of the oncoproteins. We leveraged these models to systematically identify conserved modifiers of oncoprotein phenotypes. To our knowledge, we have performed the broadest screen to date for enhancers and suppressors of H3 K27M developmental phenotypes, and the only such screen for EZHIP. We found that targeting similar chromatin modifiers rescued both H3 K27M and EZHIP impairments, arguing that their phenotypes are mediated by similar factors. Critically, we found that suppressors rescued wild-type wing development without reversing PRC2 inhibition. Strong suppressors promote gene expression, supporting a model in which these proteins exacerbate the transcriptional changes driven by H3 K27M. Indeed, suppressor knockdown restored expression levels of H3 K27M-upregulated genes to those seen in healthy tissues. Altogether, we have identified novel modifiers of oncoprotein phenotypes, and described the means by which they reverse the developmental defects imposed by these oncoproteins.

It remains an open question whether the biochemical features of H3 K27M and EZHIP have phenotypic consequences. Here, we performed a rigorous, side-by-side comparison of EZHIP and H3 K27M phenotypes. We found that the severity of H3 K27M and EZHIP phenotypes increased alongside oncoprotein expression. These phenotypic data mirror

the competitive mode of PRC2 inhibition by H3 K27M and EZHIP.¹³ *In vitro*, EZHIP inhibits PRC2 more potently than H3 K27M. It is unknown whether this difference is biologically relevant. Using multiple transgene expression patterns, we find that EZHIP more severely impairs development than H3 K27M. Though we cannot be certain that these phenotypic differences are due to the respective potencies with which H3 K27M and EZHIP inhibit PRC2, this is the most likely explanation. Over 100 genes were upregulated upon H3 K27M expression in wing imaginal discs, coinciding with a loss of H3K27me3. Altogether, we find that the biochemical similarities and differences between H3 K27M and EZHIP are recapitulated by their tissue phenotypes. We therefore established the *Drosophila* wing as a powerful model with which to examine the mechanisms by which these oncoproteins disrupt normal development.

H3 K27M impairs hindbrain development by rewiring chromatin structure and gene regulation. During development, PRC2 interacts with myriad chromatin-regulatory proteins to maintain cell-type specific gene expression patterns. Thus, a host of chromatin-modifying proteins likely mediate the epigenetic and transcriptional changes found in DMG. The contributions of these chromatin modifiers to DMG pathogenesis are difficult to ascertain in tissue culture, where most studies of H3 K27M have been performed. We leveraged our developmental model of H3 K27M to systematically screen for enhancers and suppressors of the H3 K27M in the *Drosophila* wing. The phenotypic range of our screen exceeds what can be captured in cell-culture models, which typically use cell death to identify genetic interactions.^{35–39}

Enhancers and suppressors contribute to oncoprotein phenotypes in opposing ways. Knockdown of enhancers increased the severity of wing defects. These proteins are therefore bulwarks against further tissue impairment by H3 K27M. Polycomb proteins were highly enriched among enhancers and represented 3 of 6 strong enhancers we identified. Polycomb proteins have been identified as oncoprotein enhancers in previous *Drosophila* screens, though the mechanisms for enhancement were not explored. Residual Polycomb protein activity is important for DMG and PFA viability, as knockout of PRC1 or PRC2 activity is lethal in tissue culture. S5,40,41 Our findings indicate that residual Polycomb-protein activity is broadly required for the viability of H3 K27M-expressing tissues. Most of the enhancers we identified have not been published in prior work. It is possible that these proteins are particularly important buffers of H3 K27M in developing tissues, and would consequently be obscured in simplified tissue-culture models.

In contrast to enhancers, suppressors promote the detrimental effects of H3 K27M. Three of the five strong suppressors we identified deposit marks of active chromatin: Trx (H3K4me1/me2), Ash1 (H3K36me2), and Set2 (H3K36me3). A fourth, Asx, forms part of the PR-DUB complex that removes the repressive H2AK118ub (H2AK119ub in humans). Previous screens in *Drosophila* identified Ash1 as a suppressor of an H3 K27M phenotype.³² Set2 was not identified as a suppressor in that screen. However, Set2 was targeted with a germline-specific RNAi construct and was likely not knocked down efficiently. Our screen identified four H3K36 methyltransferases as suppressors: Ash1, Set2, NSD, and CG4565. These findings suggest that H3K36me2/me3 or their reader proteins thereof mediate the H3 K27M phenotype, rather than individual H3K36

methyltransferases being essential. In DMG tissue culture, knockdown of NSD1/2 or H3K36me2 reader proteins induced cell death. ³⁸ Given the variety of histone modifiers that emerged as suppressors in our screen, it is unlikely that H3K36me2/me3 is uniquely important to H3 K27M phenotypes in mammals. Rather, H3 K27M and EZHIP phenotypes may depend on transcriptional activators that catalyze a host of histone modifications. We found that suppressors did not restore normal levels of H3K27me3. These data argue that PRC2 inhibition by H3 K27M is necessary, but not sufficient to impair fly development. By depositing active histone modifications or removing repressive marks, suppressors may facilitate the gene-expression changes underlying oncoprotein phenotypes. The similar means by which EZHIP and H3 K27M inhibit PRC2 suggests they may share enhancers and suppressors. ^{13,14,30} We performed, to our knowledge, the first modifier screen of EZHIP tissue phenotypes. H3 K27M and EZHIP share many of the same suppressors, including Trx, Ash1, and CG4565, all writers of active histone modifications.

H3 K27M and EZHIP are specifically oncogenic in the developing human hindbrain. 42,43 It is possible that oncoprotein pathogenicity is mediated by the hindbrain-specific activities of certain chromatin modifiers. It was similarly possible that the enhancers and suppressors we identified were specifically important to wing oncoprotein phenotypes. To address this, we performed a limited screen in the *Drosophila* eye. We found that enhancers and suppressors robustly modify an H3 K27M eye phenotype. Our RNA-seq experiments demonstrate that H3 K27M causes similar transcriptional changes in wing and eye-antennal discs. Combined, our results suggest that the enhancers and suppressors we identified are essential mediators of oncoprotein phenotypes in diverse

biological contexts. These findings may deepen our understanding of the mechanisms by which H3 K27M and EZHIP hinder developing human tissues, as well.

The functions of our strong suppressors support a model in which oncoprotein phenotypes are driven by an imbalance between the repressive H3K27me3 and transcriptional activators (Figure 4G). In this model, PRC2 inhibition poises genes for derepression. Their aberrant expression would depend on the actions of transcriptional activators (suppressors). Suppressor knockdown would restore the critical generegulatory balance, allowing normal development to proceed. Such a model would explain why PRC2-inhibition is necessary but not sufficient to drive H3 K27M phenotypes. Compellingly, *Asx*, *trx*, and *ash1* RNAi partially or completely reversed the transcriptional changes imparted by H3 K27M. Knockdown of these three suppressors downregulated largely overlapping genes, implying that they suppress H3 K27M by similar mechanisms. Without the activating functions of these suppressors, H3 K27M may be unable to drive pathologic transcriptional changes.

Knockdown of Nup153, a fourth strong suppressor, robustly suppressed H3 K27M and EZHIP phenotypes. Nup153 is a nucleoporin protein that extensively binds euchromatin in.^{44,45} In mammalian tissue culture, Nup153 has been found to have mixed repressive and activating functions, including facilitating PRC1-mediated silencing.^{46,47} As a known transcriptional activator in *Drosophila*, Nup153 knockdown may rescue wing development by similar means to the other suppressors we tested. However, *Nup153* RNAi had largely distinct transcriptional effects. Despite having little overlap with other suppressors,

Nup153 itself was one of 31 genes downregulated by all four suppressor RNAi lines. Thus, Nup153 knockdown may be an essential feature of oncoprotein suppression in developing *Drosophila* tissues.

There is evidence that gene-regulatory imbalances drive other forms of cancer. 48–51 Many cancers are driven by mutations in transcriptional activators, including suppressors that emerged in our screen. The gene-expression programs in these cancers are mediated by the loss of transcriptional-activator activity and subsequent gene repression by PRC2. PRC2 activity is essential in these tumors. In parallel fashion, the suppressors we identify here appear to have fundamental roles in driving the transcriptional programs caused by H3 K27M and EZHIP. Future experiments examining the chromatin states underlying oncoprotein suppression may reveal additional strategies with which to counteract the deadly effects of these oncoproteins.

Materials and Methods

Fly strains/husbandry

All stocks were grown on molasses food at 25°C unless otherwise noted. N-terminally FLAG-tagged *EZHIP*, *H3.3 K27M* or *H3.3 K27R* were cloned into pUASt-attB (DGRC #1419) using PCR, restriction digest and ligation. Transgenes were integrated into the *M{3xP3-RFP.attP}ZH-86Fb* locus on chromosome three (Bloomington *Drosophila* Stock Center (BDSC) #24749), or into the *PBac{yellow[+]-attP-9A}VK14* locus on chromosome two (BDSC #9733) using PhiC31 integrase-mediated recombination with fluorescence marker removed (Best Gene, Chino Hills, CA).

Immunostaining

For imaginal wing disc immunostaining, flies carrying EZHIP, H3 K27M, H3 K27R, or Harvard Transgenic RNAi project (TRiP) lines were crossed to *nub-Gal4* (II); *UAS-Dcr-2* (X) (BDSC#25754) for wing-specific transgene expression. Wing imaginal discs were harvested from crawling third-instar larvae for immunostaining. Lines used to generate immunostaining in paper: *trx* RNAi (BDSC#31092), and H3 K27M. For eye-antennal disc immunostaining and enhancer/suppressor screening in the eye, a recombinant *ey-Gal4,GMR-Gal4* (II) line was used to drive transgene expression (gift from the Lab of Dr. Nansi-Jo Colley). H3 K27M was co-expressed with RNAi lines to perform enhancer/suppressor eye screen.

Wing and eye-antennal imaginal discs were dissected from crawling third-instar larvae into ice-cold 1X PBS. Discs were fixed for 30 minutes at room temperature in a 4% formaldehyde-1X PBS solution, then permeabilized with 1X PBS + 0.1% Triton X-100 (PBST). After permeabilization, discs were blocked with PBST + 1% BSA (PAT) for ten minutes at room temperature and incubated in PAT overnight at 4°C with the following primary antibodies: rabbit anti-H3K27me3 (1:1600) (Cell Signaling Technology #9733S), and mouse M2 anti-FLAG (Sigma #F1804). The following day, discs were washed in PBST and blocked with PBST + 2% normal goat serum for ten minutes prior to addition of secondary antibodies. Discs were incubated with secondary antibodies (1:2000) in PBST + 2% normal goat serum for four hours at room temperature. For FLAG staining, goat anti-mouse 488 DyLight conjugated secondary antibody was used (Fisher Scientific

#35502) was used. For H3K27me3, goat anti-rabbit conjugated Alexa Fluor 594 (Fisher Scientific #A-11001) secondary antibody was used. DAPI (ThermoFisher #D1306) was added to secondary antibody solution (1:2000) for 5 minutes before final washes and mounting. Discs were imaged at 10X using a Nikon Ti2-E epifluorescent microscope. Final images were processed using imageJ v1.52.

Adult wing and eye imaging

Adult fly were imaged while anesthetized. For wing imaging, flies were placed in 70% ethanol at -20°C for at least 15 minutes, but up to six weeks. Once removed from ethanol, wings were dissected from flies in 1x PBS solution and mounted in 70% glycerol. All images were acquired with an OMAX 18MP USB 3.0 C-Mount camera placed in the eyepiece of a dissecting microscope at 4X magnification. Camera operated with ToupLite imaging software on laptops. The following RNAi lines were used to generate adult fly wing images in this manuscript: *E*(*z*) RNAi (BDSC #31617), *trx* RNAi (BDSC #31092), *CycC* RNAi (BDSC #33753), and *Usp7* RNAi (BDSC #34708). The following RNAi lines were used to generate adult eye images: *E*(*z*) RNAi (BDSC #31617), *trx* RNAi (BDSC #31092), and *ash1* RNAi (BDSC #33705).

Enhancer/suppressor screen

Fly lines were generated for enhancer/suppressor screen using recombination of *nub-Gal4 (II)*; *UAS-Dcr-2 (X)* (BDSC #25754) with H3 K27M, H3 K27R, or EZHIP. Recombination was confirmed using PCR molecular screening, wing phenotyping, and immunostaining. Every RNAi line was crossed to the following fly lines to generate RNAi

and screen scores: *nub-Gal4* (*II*); *UAS-Dcr-2* (*X*), and the recombinant *nub-Gal4,H3 K27M(II)/CyO*; *UAS-Dcr-2* (*X*), respectively. RNAi and screen scores were generated by two independent researchers who were blinded to the identity of the RNAi target genes. Only RNAi lines classified as enhancers by both researchers were included in the final analysis. Every enhancer and suppressor was crossed to to *nub-Gal4,H3 K27R/CyO* (*II*); *UAS-Dcr-2* (*X*) to control for nonspecific effects of histone transgene overexpression. All suppressors were additionally crossed to *nub-Gal4*, *EZHIP/CyO* (*II*); *UAS-Dcr-2* (*X*). All recombinant lines were viable and fertile.

RNA-seq and CUT&RUN transgene expression

We generated a fly line to ubiquitously express H3 K27M, H3 K27R, and TRiP RNAi lines in a temperature-sensitive manner. Briefly, we used recombination of *Act5C-Gal4 (II)* (BDSC #25374) and *alphaTub84B-Gal80ts (II)* (BDSC #7019). Recombination was confirmed using PCR and immunostaining. *Act5C-Gal4*, *alphaTub84B-Gal80ts (II)* was crossed to fly lines carrying H3 K27M and H3 K27R in cages. Animals were reared at 25°C, a temperature at which Gal80 represses Gal4. Plates with molasses and yeast paste were exchanged at three hour intervals to stage discs at time of dissection. Embryos were aged on plates for 24 hours and picked into vials as first-instar larvae. Larvae were reared until 44 hours after egg laying (AEL), then shifted to 32°C to inactivate Gal80 and express transgenes for 72 hours.

RNA-sequencing

Imaginal wing and eye-antennal discs were harvested from crawling third-instar larvae. Larvae were staged to within 116 and 119 hours after egg laying. For each replicate, ten discs were dissected into ice cold 1X PBS solution. Three biological replicates were dissected for each genotype. After dissection, discs were incubated in Trizol (Invitrogen #15596026) for 5 minutes to dissolve tissue, then frozen at -20°C. RNA was precipitated using standard Trizol RNA isolation procedure and libraries were prepared using the TruSeq RNA sample prep kit v2 (Ilumina RS-122-2002). 75-base-pair reads were obtained using an Illumina NextSeq500 High-Throughput Sequencer. Sequencing was performed at the Northwestern University Sequencing (NUSeq) Core Facility. Suppressor RNAi lines used for RNA-seq included: *trx* RNAi (BDSC #31092), *ash1* RNAi (BDSC #33705), *Asx* RNAi (BDSC #31192), and *Nup153* RNAi (BDSC #32837).

Discs harvested for RNA-seq had the following genotypes:

- Act5C-Gal4, alphaTub84B-Gal80ts/H3 K27M
- Act5C-Gal4, alphaTub84B-Gal80ts/H3 K27M; Asx/trx/ash1/Nup153 RNAi/+
- Act5C-Gal4, alphaTub84B-Gal80ts/H3 K27R
- Act5C-Gal4, alphaTub84B-Gal80ts/H3 K27R; Asx/trx/ash1/Nup153 RNAi/+

RNA-seq analysis

RNA-seq data was aligned to the dm6 *Drosophila melanogaster* genome using HISAT v2.1.0.⁵² Multi-mapping reads were excluded from further analysis. featureCounts v1.5.3 was used to generate a table with reads assigned to annotated dm6 genes using UCSC

annotation r6.45.⁵³ Read counts were used to determine differentially expressed genes using DESeq2 v1.14.1.⁵⁴ Genes with an adjusted p-value <0.05 and log₂ fold change >1.5 were considered differentially expressed. Genes with <50 reads across all samples were excluded from analysis. Differential expression for selected groups of misregulated genes determined based on log₂, RPKM-normalized reads. Volcano plots and violin plots generated in RStudio v1.4.1106 using ggplot2 v3.4.2. Heat maps generated using pheatmap v1.0.12. Venn Diagrams generated using DeepVenn (arXiv:2210.04597). Mean-average (MA) plots generated using ggpubr v0.5.0 or ggplot2 v3.4.2.

Cleavage under targets, release under nuclease (CUT&RUN)

Wing imaginal discs were harvested from crawling third-instar larvae between 116 and 119 AEL. Two biological replicates were used to assay H3K27me3 for each genotype, and one replicate was used in IgG control. For each replicate, twenty discs were dissected into ice-cold PBS. Approximately 50,000 cells are in a third-instar larval wing disc, amounting to one million cells for each replicate. Intact wing discs were used for the entire protocol. Samples were washed three times in Wash Buffer (20mM HEPES pH 7.5, 150mM NaCl, 0.5 mM spermidine (Sigma S0266-1G), and Pierce EDTA-free Protease Inhibitor (ThermoFisher PIA32955)) and incubated with activated concanavalin-A (ConA) paramagnetic beads (EpiCypher SKU: 21-1401) for ten minutes in PCR strip tubes. Samples were resuspended in cold Antibody Buffer (Wash Buffer + 0.05% digitonin (Sigma Millipore 300410250MG) and 2mM EDTA (Fisher S311500)). 2 uL of SNAP-CUTANA K-MetStat nucleosomes (EpiCypher SKU: 19-1002) diluted 1:100 in Wash Buffer were added to each sample for spike-in normalization. Antibody was added to

samples at a 1:50 concentration and incubated overnight at 4°C (Rabbit anti-H3K27me3 (Cell Signaling Technology #9733S) or rabbit IgG control (ThermoFisher #10500C)). The following day, discs were washed with Digitonin Buffer (Wash Buffer + 0.05% digitonin (Sigma Millipore 300410250MG)), then incubated with pAG-MNase (EpiCypher SKU: 15-1016) for ten minutes to allow protein A/G binding to antibody. 1 uL of cold 100 mM CaCl₂ was added to samples to activate pAG-MNase and incubated on nutator for 2 hours at 4°C. Reaction was quenched with Stop Buffer (340 mM NaCl, 20 mM EDTA, 4 mM EGTA, 50 µg/mL RNase A , 50 µg/mL Glycogen). Chromatin was eluted from samples at 37°C for ten minutes, then DNA was purified with the Qiagen MinElute Reaction Cleanup Kit (Qiagen #28204). Libraries were prepared using the NEBNext Ultra II DNA Library Prep Kit for Illumina (NEB E7645L), and sequenced on the Illumina NovaSeq6000 High-Throughput Sequencer at the University of Wisconsin Biotechnology Center (UWBC). Sequencing produced 150-base-pair paired-end reads.

Discs harvested for CUT&RUN had the following genotypes:

- Act5C-Gal4, alphaTub84B-Gal80ts/H3 K27M
- Act5C-Gal4, alphaTub84B-Gal80ts/H3 K27R

CUT&RUN & ChIP analysis

Read quality was assessed using FASTQC (v0.11.9).⁵⁵ Adapters and low-quality bases were removed using Trimmomatic (v0.39.29).⁵⁶ Reads were mapped to the dm6 genome assembly⁵⁷ using Bowtie2.⁵⁸ Unmapped, multiply aligning, mitochondrial, and scaffold reads were removed. Nonspecific CUT&RUN signal was subtracted from H3K27me3

samples using IgG control for each genotype. MACS2 was to identify broad H3K27me3 peaks after merging replicates for each genotype. Standard MACS2 parameters were used to call narrow peaks for published Ph ChIP data. Antibody specificity was assessed using percentage of on-target spike-in reads compared to total spike-in reads. Merged alignment files were normalized using a combination of RPKM and spike-in. Spike-in normalization based on percentage of reads mapping to all barcoded nucleosomes. Integrated Genomics Viewer (v2.12.3) was used for visualization of normalized bigWig files. AH3K27me3 bigWig files were generated using bamCompare function in deepTools (v3.4.1). RPKM, spike-in normalized read counts for H3 K27R samples were subtracted from normalized H3 K27M read counts. Heat maps were generated using deepTools (v3.4.1) with RPKM, spike-in normalized bigWig files. Analysis of H3K27me3 enrichment at wing disc based on differentially expressed gene sets using rtracklayer (v3.16). Genomic annotations were derived from UCSC annotated dm6 genome r6.45.

Ordering RNAi screening lines

FlyMine online software was used to query all *Drosophila* genes with chromatin-related functional annotations.⁶³ Among these, ten chromatin-related gene ontology (GO) terms were selected for further analysis (Supplemental Figure 2A). siRNA and miRNA-related genes were removed given the RNAi-based screening approach used. Genes were excluded if not expressed in a wing imaginal disc-derived cell line based on available RNA-seq data ML-DmD21 (DGRC Stock #86).³⁴ Conservation of genes between *Drosophila* and humans was queried with *Drosophila* Integrative Ortholog Prediction Tool

(DIOPT), an integrated tool that uses nine ortholog predictors.⁶⁴ Only genes deemed to be highly conserved according to DIOPT were included in our screen.

All RNAi lines included in our screen were generated by the Transgenic RNAi Project (TRiP) from the Harvard *Drosophila* RNAi Screening Center (DRSC).⁶⁵ TRiP stocks were generated over multiple generations and used different cloning strategies to generate dsRNA transgenes for each target gene. Vectors vary by dsRNA expression level, and production of long- or short-hairpin dsRNA, which have weaker or stronger average target gene knockdown, respectively. We considered TRiP stocks "strong" or "weak" depending on their expressed dsRNA hairpin length. We used the Updated Targets of RNAi Reagents (UP-TORR) tool to determine genes TRiP RNAi lines have been generated.⁶⁶ Thus, we ordered long- and short-hairpin RNAi lines for every gene in our screen, based on reagent availability. Reagent availability was determined using the DRSC/TRiP Functional Genomics Resources Lookup.⁶⁶ Only somatically-expressing RNAi vectors were included in our screen (dsRNA constructs cloned into VALIUM1, VALIUM10, or VALIUM20).

Acknowledgements

We acknowledge the Harvard Transgenic RNAi Project and the Bloomington *Drosophila* Stock Center for generating RNAi lines and providing fly lines. We also acknowledge the University of Wisconsin-Madison Biotechnology Center and the NUSeq Core Facility for sequencing. Experiments were supported by grants from the National Institutes of Health: F30 CA260987-01, and the UW-Madison Carbone Cancer Center 144-AAK3783.

Figure 3.1

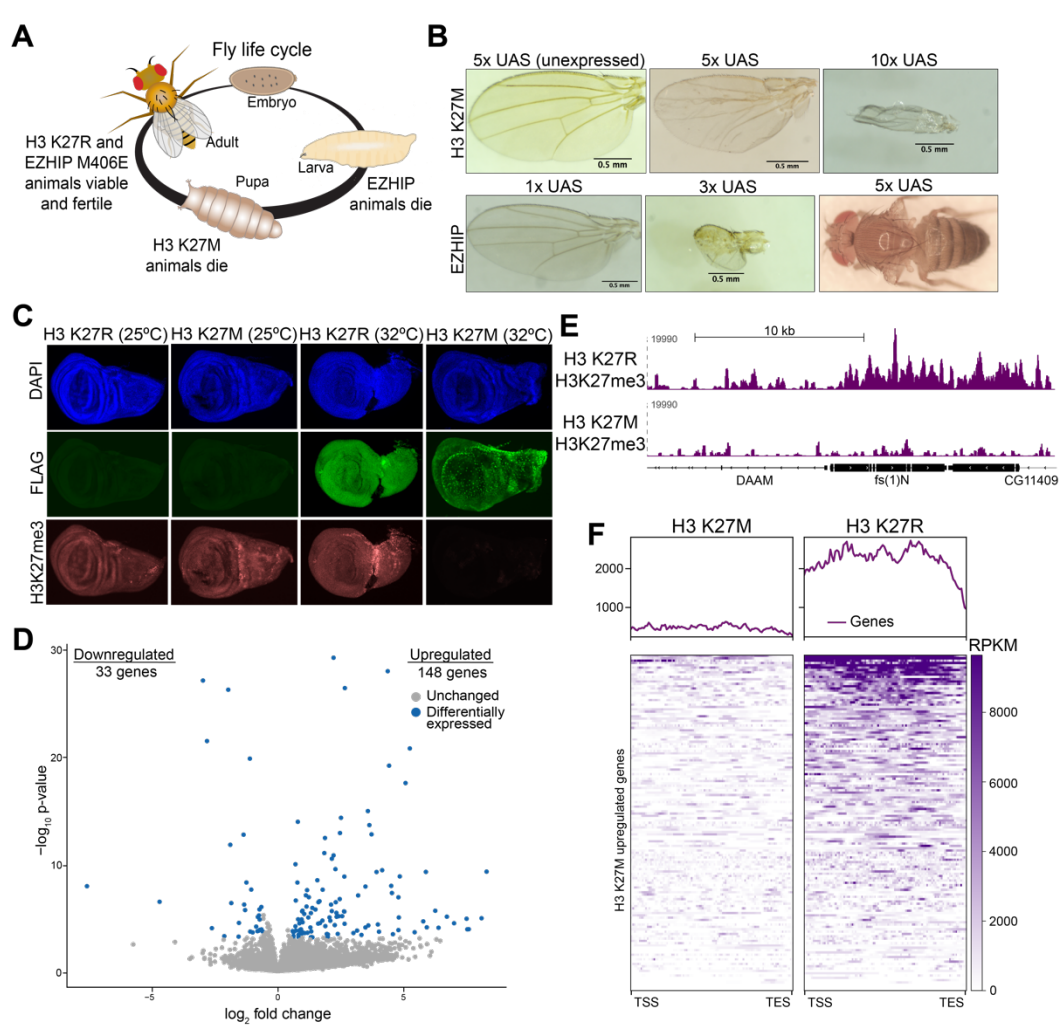


Figure 3.1 H3 K27M and EZHIP disrupt *Drosophila* development through inhibition of PRC2-mediated H3K27me3. A. Schematic showing the *Drosophila* life cycle. Fertilized embryos progress through larval and pupal stages before becoming mature adult flies. Developmental stage of EZHIP- or H3 K27M-induced lethality lethal are indicated. B. Adult fly wings in which H3 K27M or EZHIP expression is induced. The number of Gal4-binding sites (UAS) is correlated with the phenotypic severity. EZHIP expression causes more severe phenotypes than H3 K27M when driven by the same number of Gal4-binding sites. C. Immunostaining for FLAG (transgenes) and H3K27me3 (green and red, respectively). Transgenes are expressed under the control of actin-Gal4. At 25°C, Gal80 represses Gal4, and no transgene expression is observed. At 32°C, Gal80 is inactivated and Gal4-mediated transgene expression is activated. DAPI staining marks nuclei. **D.** Volcano plot indicating genes misregulated in wing discs expressing H3 K27M compared to H3 K27R control. Blue dots correspond to upregulated or downregulated genes (adjusted p-value < 0.05, fold change > 1.5). Gray dots correspond to genes with non-significant changes. E. Genome browser tracks of H3K27me3 CUT&RUN in wing discs expressing H3 K27M or H3 K27R over the gene fs(1)N). fs(1)N is upregulated in H3 K27M wing discs as compared to H3 K27R. F. Top: Average CUT&RUN signal intensity for H3K27me3 at 148 genes upregulated by H3 K27M compared to H3 K27R in wing discs. Bottom: Heat map of spike-in normalized RPKM counts. Genes sorted by mean H3K27me3 intensity from highest to lowest.

Figure 3.2

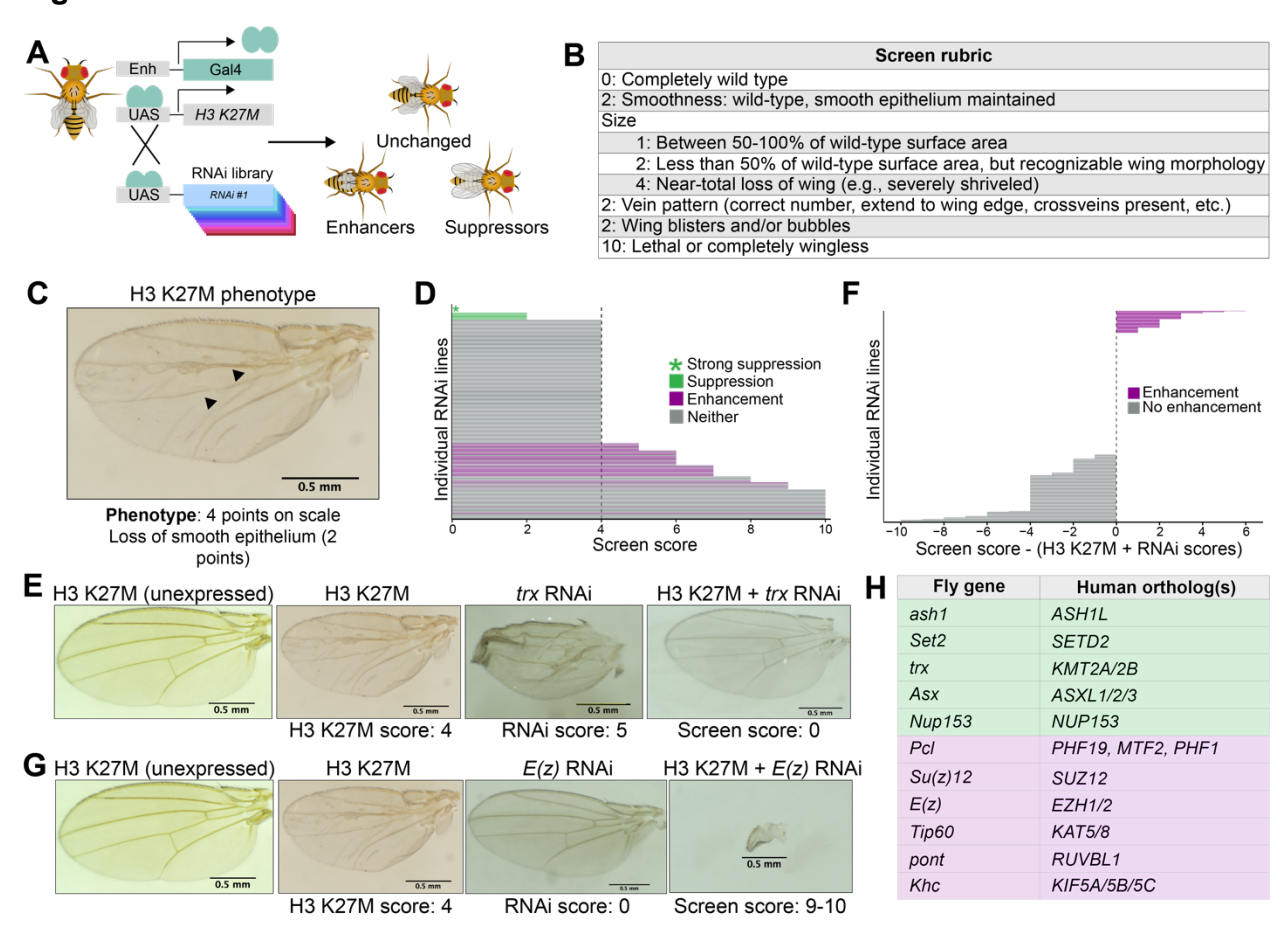


Figure 3.2. Conserved chromatin modifiers enhance or suppress phenotypes caused by H3 K27M in the wing. A. Genetic scheme used to perform unbiased screen. All RNAi lines were expressed alone and co-expressed with H3 K27M. B. Quantitative key used to score fly wings. All RNAi lines were assigned scores based on the total of points for each disrupted wing feature. C. Image of wild-type and H3 K27M wing phenotypes. H3 K27M-expressing wings have disrupted vein patterns and loss of smooth surface, but size is largely unaffected (4 points total). Arrowheads indicate where cross veins are missing. D. Screen score for all 630 RNAi lines. RNA lines with a screen score less than 4 were classified as suppressors (minimum 50% penetrance). Suppressors labeled in green. An asterisk indicates strong suppressors (score of 0). Enhancers labeled in purple. Lines that did not enhance or suppress labeled in gray. E. Examples of a strong suppressor. H3 K27M and suppressor phenotypes often mutually suppressed. F. Approach used to define H3 K27M enhancers. Screen scores exceeding the sum of H3 K27M and RNAi score were classified as enhancers and are labeled in purple. Gray lines did not enhance phenotype. G. Example of a strong enhancer. Combined phenotype exhibited synergy between H3 K27M and RNAi. H. Table of all strong suppressors (green) and enhancers (purple) and their human orthologs.

Figure 3.3

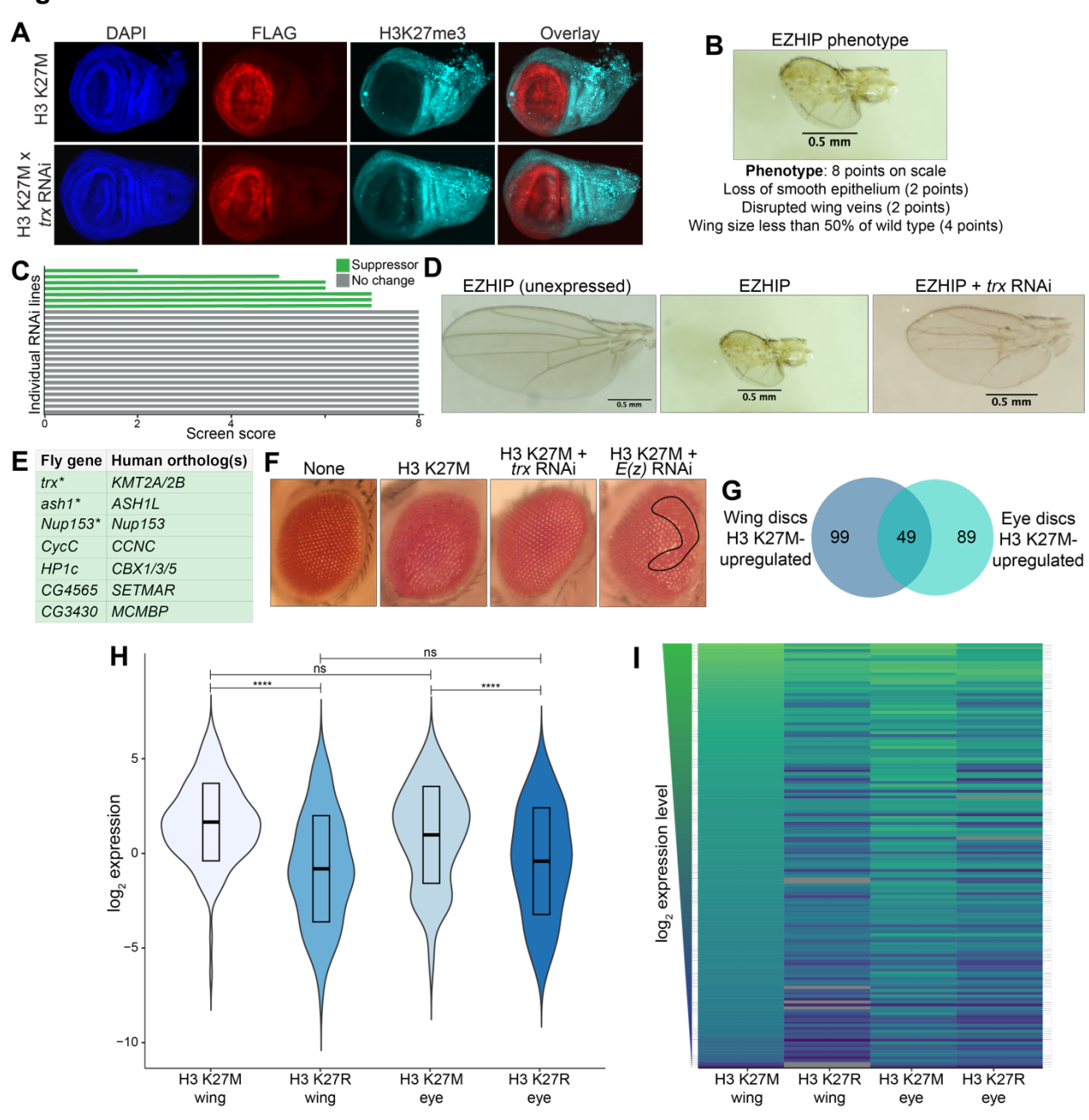


Figure 3.3. Similar chromatin modifiers and transcriptional changes underlie oncoprotein phenotypes in multiple tissues. A. H3K27me3 and H3 K27M (FLAG) immunostaining of wing imaginal discs from third-instar larvae. Transgenes expressed by nubbin-Gal4 driver. Transgene expression is in red. H3K27me3 is in cyan. **B.** Wing phenotype of *nubbin-Gal4* driven EZHIP expression. Points assigned using quantitative scale (8 points total). C. Score for all RNAi lines screened in conjunction with EZHIP expression. All H3 K27M suppressors were tested. Scores less than 8 points were classified as EZHIP suppressors and are labeled in green. RNAi lines labeled in gray did not modify the wing phenotype. **D.** Suppressed wing phenotype caused by RNAi of trx. Suppressors did not completely restore wild-type development in combination with EZHIP expression. E. Table of EZHIP suppressors and their human orthologs. Asterisks indicate strong H3 K27M suppressors. F. Examples of H3 K27M eye enhancers and suppressors. H3 K27M disorganizes photoreceptors on surface of eye. H3 K27M wing suppressors and enhancers similarly modify the H3 K27M eye phenotype. Transgenes expressed with eyeless, GMR-Gal4. Region outlined in black indicates loss of photoreceptors. G. Overlap among genes upregulated by H3 K27M in wing and eye discs. H. Violin plot showing average expression (RPKM, log2) of the 148 genes upregulated by H3 K27M in wing discs compared to H3 K27R. Expression of these genes also shown for eye discs. ns = not significant (adjusted p-value > 0.05). ****adjusted p-value < 0.0001. I. Heat map showing log₂ expression of genes upregulated by H3 K27M in wing discs. Genes ordered by average expression in H3 K27M wing discs.

Figure 3.4

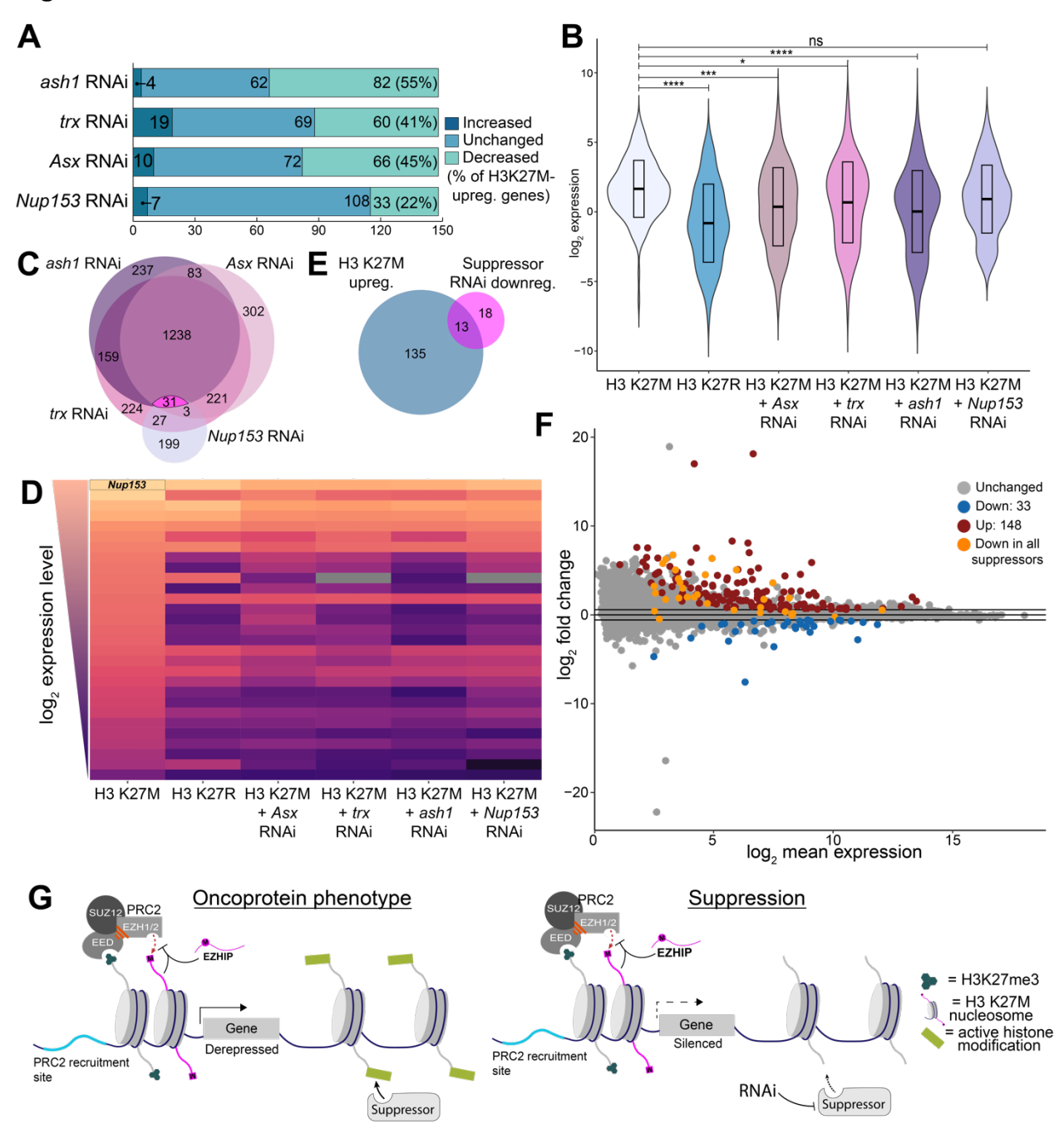
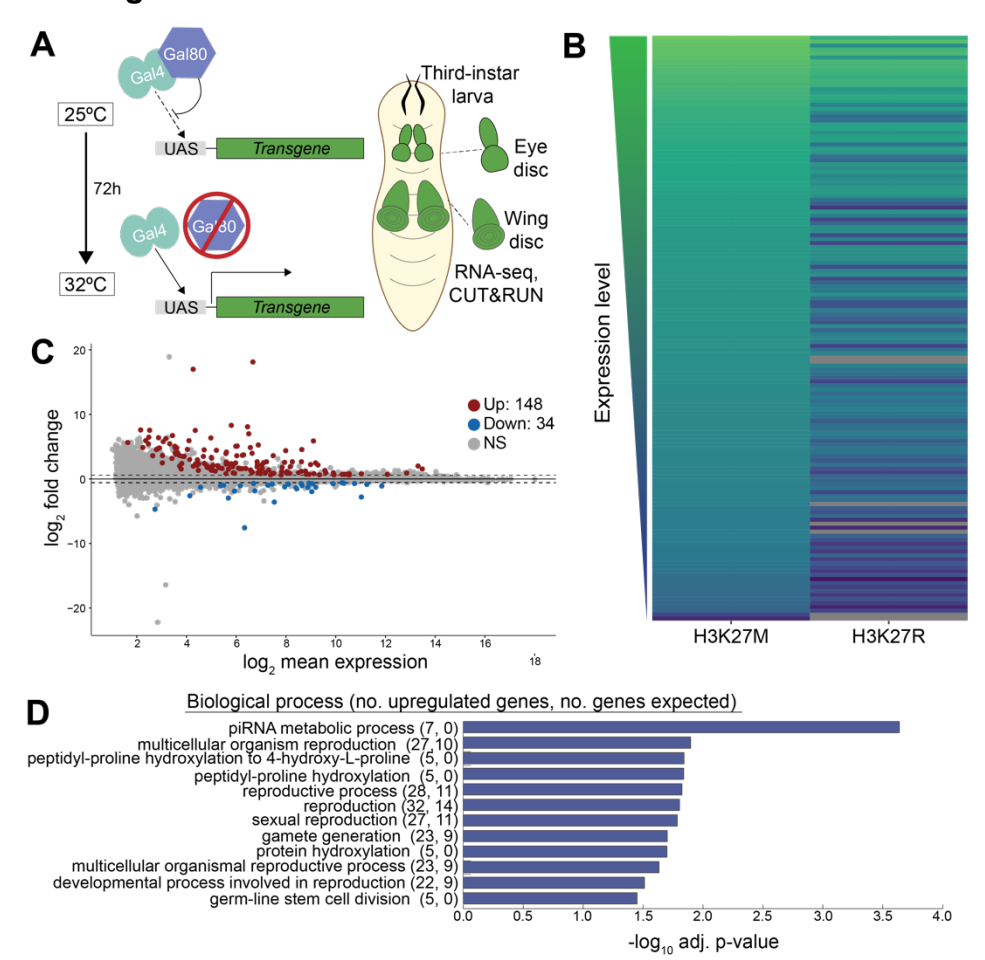


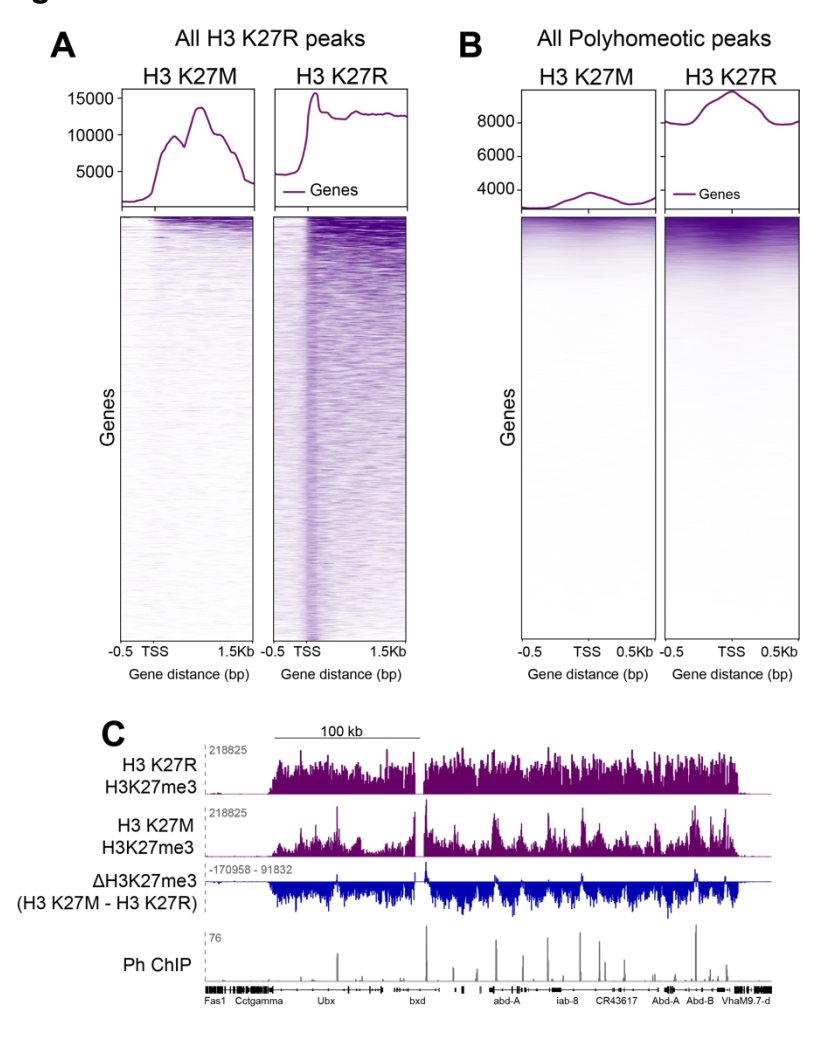
Figure 3.4. Suppressors counteract H3 K27M-mediated transcriptional changes.

A. Number of genes upregulated, downregulated, or unchanged in wing discs expressing H3 K27M with the indicated suppressor as compared to H3 K27M alone. B. Average expression (log₂ of RPKM) of the 148 genes upregulated by H3 K27M. Expression levels in H3 K27R control and upon co-expression of H3 K27M and suppressor RNAi. ns = not significant (adjusted p-value > 0.05). *adjusted p-value < 0.05. ***adjusted p-value < 0.001. ****adjusted p-value < 0.0001. C. Overlap among genes downregulated by wing discs expressing H3 K27M with ash1, trx, Nup153, or Asx RNAi compared to H3 K27M alone. **D.** Heat map showing expression (log₂ of RPKM) of the 31 genes downregulated by all four suppressors. Nup153 is labeled. E. Overlap between genes downregulated by all four suppressor RNAi lines and genes upregulated by H3 K27M. F. MA plot highlighting differentially expressed genes in H3 K27M wing discs compared to H3 K27R. Dark red dots indicate upregulated genes (adjusted p-value < 0.05, fold change > 1.5). Bright red dots indicate genes downregulated by all four suppressors. Blue dots indicate downregulated genes. Gray dots indicate genes with unchanged expression. G. Model of oncohistone chromatin states. Left: EZHIP and H3 K27M inhibit PRC2 spreading, reducing H3K27me3 at most genomic regions. Loss of H3K27me3 coincides with increased active histone modifications, deposited by suppressor proteins. Suppressor proteins promote gene derepression and oncohistone phenotypes. Right: Despite continued PRC2 inhibition, knockdown of suppressor proteins restores wild-type gene expression patterns and allows for healthy development to proceed.

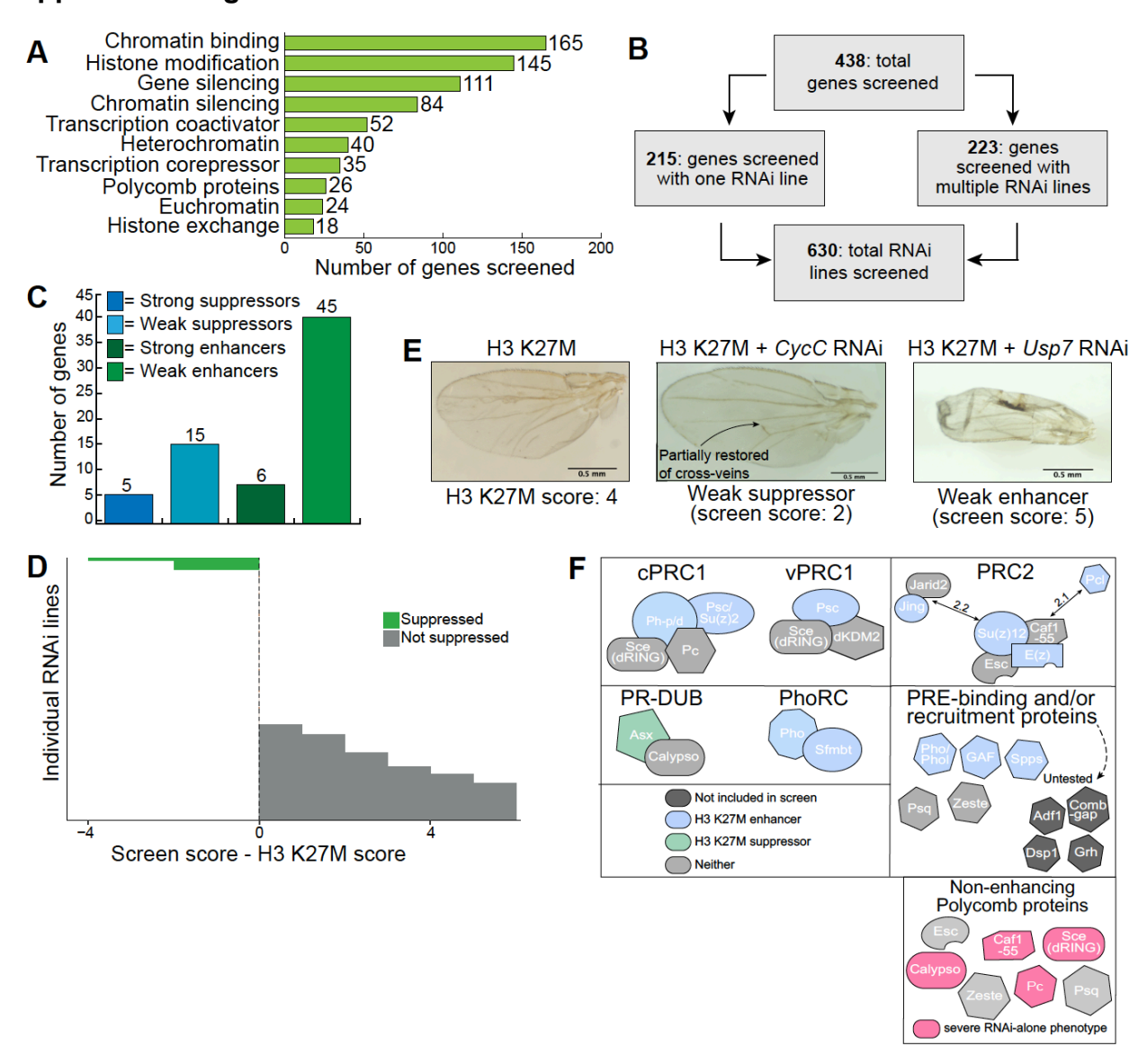


Supplemental Figure 3.1. H3 K27M promotes expression of germline-related genes.

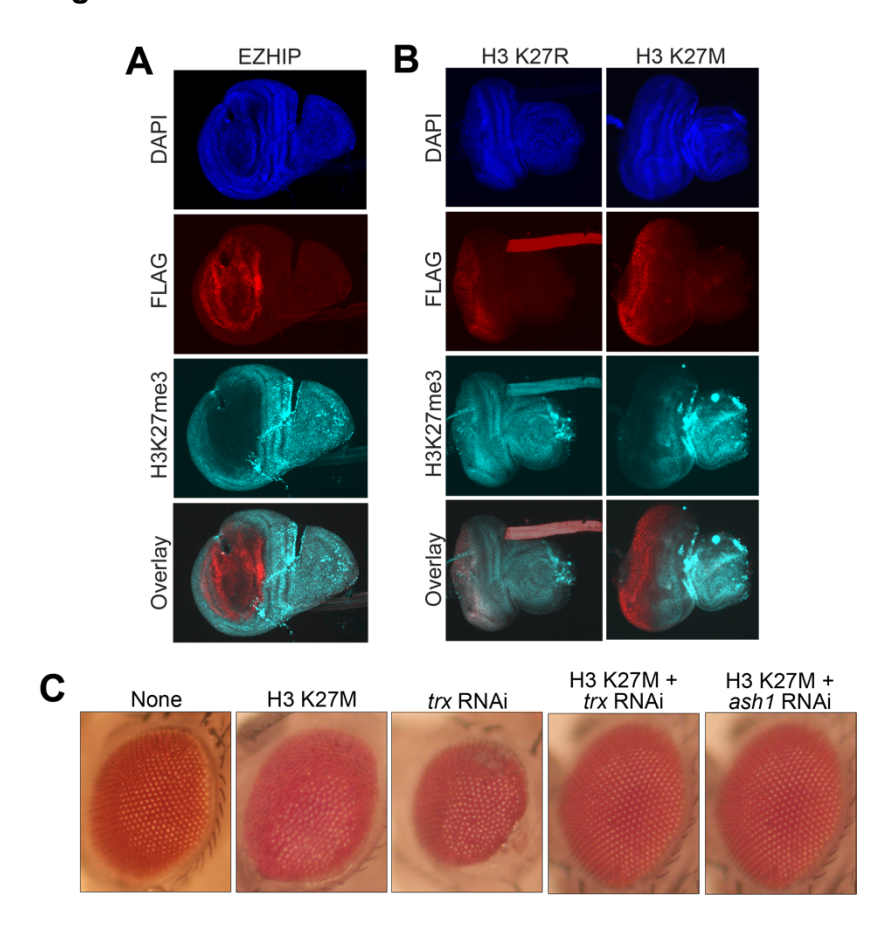
A. Schematic of transgene expression system used for RNA-seq and CUT&RUN. Transgenes expression under control of ubiquitously expressed *actin-Gal4* driver. *tubulin-Gal80ts* is a ubiquitously expressed, temperature-sensitive Gal4 inhibitor. At 25°C, Gal80ts is active and represses Gal4-mediated transgene expression. At 32°C, Gal80ts is inactivated, permitting transgene expression. 72 hours after shifting developing animals to 32°C, imaginal discs were harvested from third-instar larvae and used for RNA-seq or CUT&RUN. **B.** MA plot highlighting differentially expressed genes in H3 K27M wing discs compared to H3 K27R. Red dots indicate genes upregulated by H3 K27M. Blue dots indicate genes downregulated by H3 K27M (adjusted p-value < 0.05, fold change > 1.5). Gray dots indicate genes with unchanged expression levels. **C.** Expression (log₂ RPKM) of the 148 genes upregulated in wing discs expressing H3 K27M compared to H3 K27R (adjusted p-value < 0.05; fold change > 1.5). **D.** Gene ontology (GO) analysis for genes upregulated by H3 K27M in wing discs. Number of genes upregulated by H3 K27M listed first in parentheticals, followed by expected number of upregulated genes.



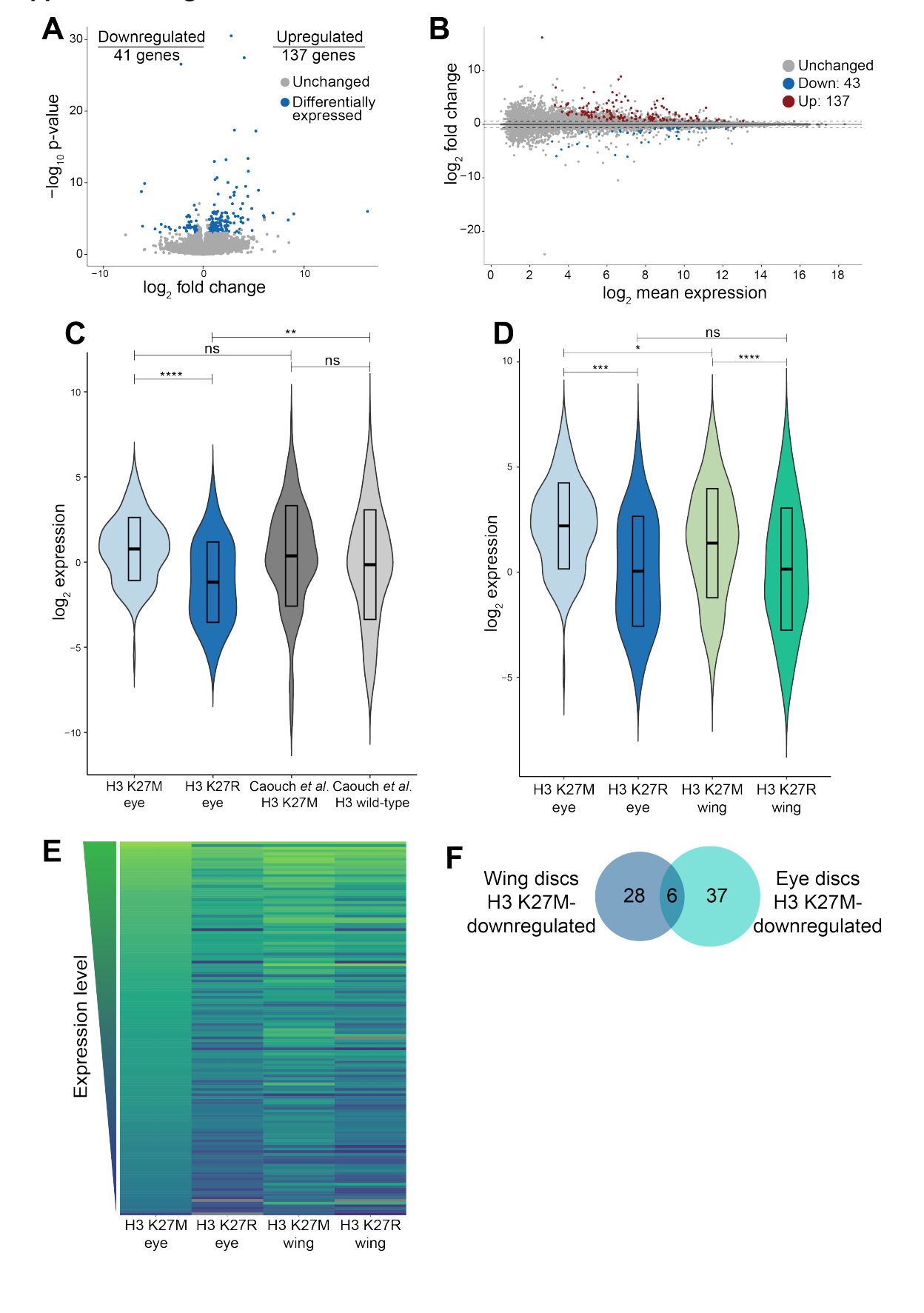
Supplemental Figure 3.2. H3 K27M expression results I a near-complete loss of H3K27me3. A. H3K27me3 CUT&RUN in wing discs expressing H3 K27M or H3 K27R. Metaplots of H3K27me3 enrichment (normalized for both RPKM and spike-in controls) at all H3K27me3 peaks identified in wing discs expressing H3 K27R (top). Normalized H3K27me3 enrichment at genes overlapping H3K27me3 peaks in H3K27R wing discs, sorted by highest to lowest signal intensity (bottom). B. H3K27me3 CUT&RUN in wing discs expressing H3 K27M or H3 K27R. Top: Metaplots of H3K27me3 enrichment (normalized for both RPKM and spike-in controls) at Polyhomeotic (Ph) peaks in wing discs.⁶⁰ Polyhomeotic peaks indicate PRC2-recruitment sites. Bottom: Normalized H3K27me3 enrichment at every Ph peak in wing discs, sorted by highest to lowest H3K27me3 enrichment. C. Genome browser track of normalized H3K27me3 enrichment at Ubx and Abd-A/Abd-B, which are subject to Polycomb-mediated repression in the wing disc (top). Difference in normalized H3K27me3 enrichment between wing discs expressing H3 K27M and H3 K27R. Regions with positive signal indicate increased H3K27me3 in H3 K27M wing discs as compared to H3 K27R (middle). Ph enrichment in wing discs, based on published ChIP-seg (bottom).60 Regions with positive signal in ΔH3K27me3 overlap Ph peaks.



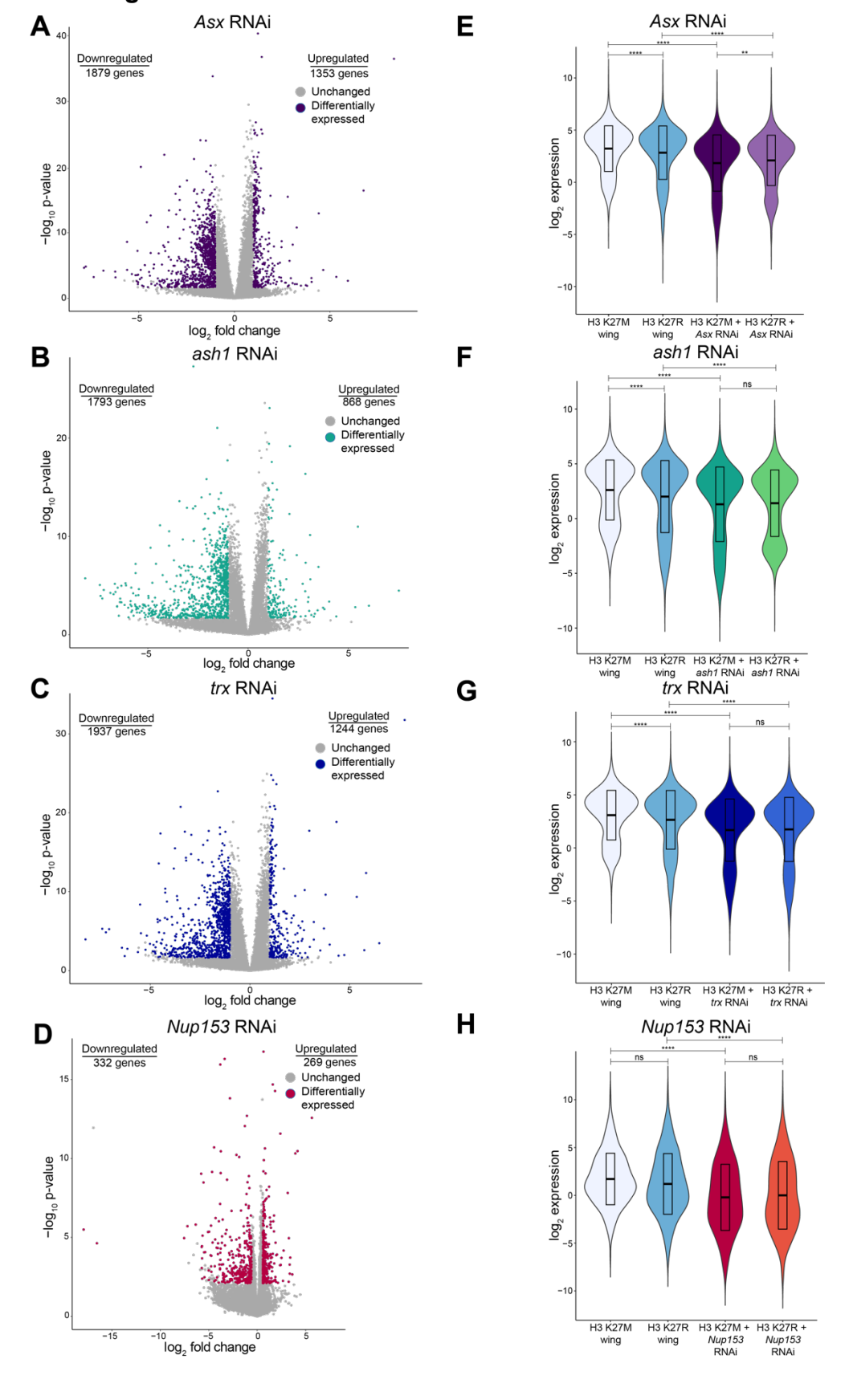
Supplemental Figure 3.3. Knockdown of conserved chromatin modifiers identifies enhancers and suppressors of H3 K27M phenotypes. A. Bar chart quantifying number of genes included in each chromatin-related gene ontology (GO) category chosen for screen. Number of genes in each category listed next to each bar. Many genes were included in more than one of these GO category. B. Schematic of the scale of the RNAi screen. C. Number of enhancers and suppressors identified in screen. Enhancers and suppressors were divided into weak and strong subtypes. **D.** Difference between screen score and H3 K27M-alone score for all 630 RNAi lines. A negative value (screen score -H3 K27M score < 0) was scored as suppression. A score of -4 was given to flies in which wild-type wing development was restored and were considered strong suppressors. E. Examples of a weak suppressor (Cyc) or weak enhancer (Usp7). F. Summary of Polycomb proteins included in screen. Polycomb proteins were the most enriched functional group among our suppressors. Blue indicates enhancement of the H3 K27M phenotype. Green indicates suppression. Light gray indicates the lack of enhancement or suppression. RNAi knockdown of a subset of Polycomb proteins, indicated in pink, caused such strong phenotypes that it was not possible to identify synergy with H3 K27M by the scoring system used.



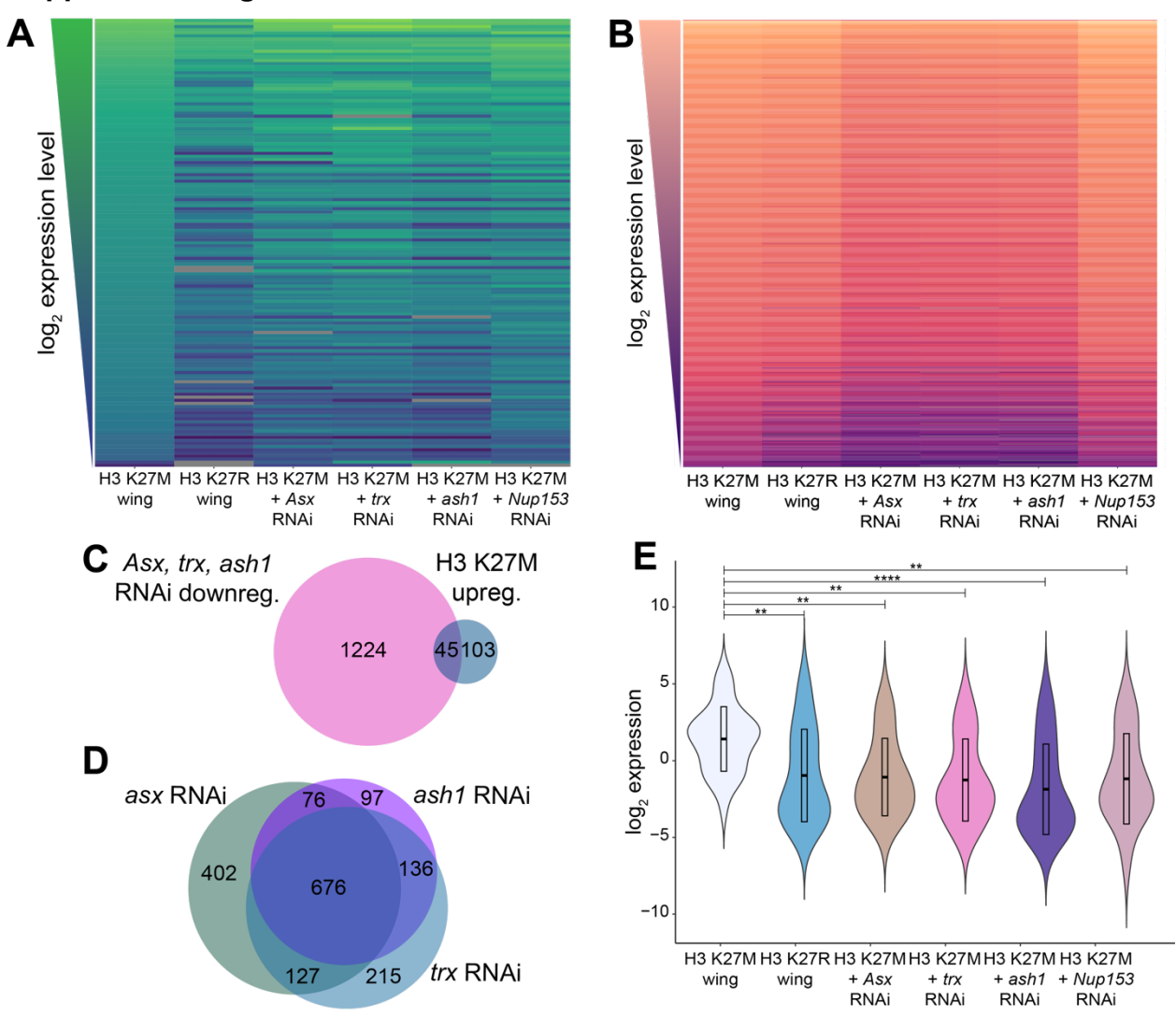
Supplemental Figure 3.4. H3 K27M and EZHIP phenotypes are suppressed in multiple tissues independent of PRC2 inhibition. A. Immunostaining for FLAG (transgene) and H3K27me3 in wing imaginal discs dissected from third-instar larvae. EZHIP was expressed under control of *nubbin-Gal4*. DAPI marks the nuclei. B. Immunostaining for FLAG (transgene) and H3K27me3 in eye-antennal imaginal discs dissected from third-instar larvae. Transgenes expressed under control of *eyeless*, *GMR-Gal4*. DAPI marks the nuclei. C. Examples of suppression H3 K27M-mediated eye defects. H3 K27M disorganizes photoreceptors on surface of eye. Co-expression of H3 K27M with *ash1* RNAi rescues wild-type eye development. *trx* RNAi disrupts normal eye development when expressed alone. Co-expression of H3 K27M and *trx* RNAi produces wild-type eyes.



Supplemental Figure 3.5. H3 K27M induces similar transcriptional changes in developing wings and eyes. A. Volcano plot of gene expression in eye-antennal discs expressing H3 K27M as compared to H3 K27R-expressing controls. Blue dots indicate differentially expressed genes (adjusted p-value < 0.05, fold change > 1.5). Gray dots indicate genes with non-significant changes. B. MA plot of genes in eye-antennal discs expressing H3 K27M as compared to H3 K27R-expressing controls. Red dots indicate genes upregulated by H3 K27M. Blue dots indicate genes downregulated by H3 K27M (adjusted p-value < 0.05, fold change > 1.5). Gray dots indicate genes whose expression was not significantly changed. **C.** Violin plot comparing average expression (RPKM, log2) of 137 genes upregulated by H3 K27M in eye-antennal discs as compared to H3 K27R. Expression of these genes in RNA-seq experiments from eye-antennal discs expressing H3 K27M or wild-type H3 using the eyeless-Gal4 driver, which expresses transgenes a restricted region of the disc (see Supplemental Figure 4B for representative expression pattern). ns = not significant (adjusted p-value > 0.05). ** adjusted p-value < 0.01. **** adjusted p-value < 0.0001. **D.** Violin plot comparing average expression (RPKM, log₂) of 137 genes upregulated by H3 K27M in eye-antennal discs compared to H3 K27R. Expression level of these genes also shown for H3 K27M and H3 K27R wing discs. ns = not significant (adjusted p-value > 0.05). *adjusted p-value < 0.05. *** adjusted p-value < 0.001. **** adjusted p-value < 0.0001. E. Heat map of log2 individual expression of 137 genes upregulated by H3 K27M in eye-antennal discs as compared to H3 K27R controls. Expression of these genes in H3 K27M and H3 K27R wing discs also shown. F. Venn diagram of the overlap between genes downregulated in wing discs and eye-antennal discs expressing H3 K27M as compared to H3 K27R controls.



Supplemental Figure 3.6. Suppressor RNAi lines alter thousands of genes independently of H3 K27M. A-D: Volcano plots showing gene expression in wing discs expressing H3 K27M and suppressor RNAi as compared to H3 K27M alone. Blue dots indicate differentially expressed genes (adjusted p-value < 0.05, fold change > 1.5). Gray dots indicate genes with non-significant changes. E-H: Violin plots showing average expression (log₂ of RPKM) of genes downregulated in wing discs expressing H3 K27M and suppressor RNAi as compared to H3 K27M alone. Expression of these genes shown in H3 K27M and H3 K27R with and without RNAi of the listed suppressor. ns = not significant (adjusted p-value > 0.05).** adjusted p-value < 0.01. **** adjusted p-value < 0.0001.



Supplemental Figure 3.7. Nup153 is a potential mediator of oncoprotein suppression. A. Heat map showing expression (log₂ of RPKM) of 148 genes upregulated by H3 K27M in wing discs as compared to H3 K27R. Expression is shown for H3 K27M. H3 K27R and H3 K27M co-expressed with Asx, trx, ash1, or Nup153 RNAi. B. Heat map showing expression (log₂ of RPKM) of 1269 genes downregulated on Asx, trx, and ash1 RNAi compared to H3 K27M, H3 K27R, or H3 K27M + Nup153 RNAi wing discs. C. Venn diagram showing overlap between 148 genes upregulated by H3 K27M, and 1269 genes downregulated by Asx, trx, and ash1 RNAi when co-expressed with H3 K27M compared to H3 K27M alone. **D.** Venn diagram showing overlaps between genes downregulated by Asx, trx, and ash1 RNAi when co-expressed with H3 K27R as compared to H3 K27R alone. E. Violin plot showing average expression (RPKM, log₂) of 31 genes downregulated by knockdown of all four suppressors when co-expressed with H3 K27M compared to H3 K27M alone. Expression levels of these genes shown for H3 K27M and H3 K27R wing discs. ns not significant (adjusted p-value > 0.05). ** adjusted p-value < 0.01. **** adjusted p-value < 0.0001.

Strong suppressors

Weak suppressors
Strong enhancers
Weak enhancers

Supplemental Table 3.1

BDSC ID	Target gene	Human ortholog(s)
36130, 31050, 33705	ash1	ASH1L
31092	trx	KMT2A/2B
33705	Set2	SETD2
31192	Asx	ASXL1/2/3
32873, 30504	Nup153	Nup153
42502	Br140	BRPF1/3
34520	brahma	SMARCA2/A4
28679	sna	SNAI1/2/3
31631	CG4565	SETMAR
31613	Sirt2	Sirt1/2/3
33904	Eaf6	Meaf6
55884	Cdc7	Cdc7
34033	NSD	NSD1/2/3
33365	chif	DBF4, DBF4B
33753		CCNC
44645	Úsp47	USP47
33962	HP1c	CBX1/3/5, MPHOSPH8
34784		TARBP2
34662		MED1
77419		MCMBP
33945	Pcl	PHF19, MTF2, PHF1
31191	Su(z)12	SUZ12
31617	E(z)	EZH1/2
28563	Tip60	KAT5, KAT8
50972	pont	RUVBL1
25898	Khc	KIF5A/5B/5C
38261, 31161	Psc	BMI1, PCGF proteins
31626	msl-1	MSL1
31481	gpp	DOT1L
32469	wda	TAF5L
31618	Esc	EED
63018	ph-d	PHC1/2/3
31190	ph-p	PHC1/2/3
31609	pho 	YY1, YY2
35750	jing	AEBP2
64924	ash2	ASH2L
28905 31093	Ada3	TADA3
27027	Sirt7 chm	SIRT7 KAT7
34708	Usp7	USP7
32926	Wdr82	WDR82
57721	Kdm4b	KDM4A/4B/4C/4D/4E
33704	Set1	SETD1A/1B
44481	ctrip	TRIP12
33696, 41698	Ndf	GLYR1
42819	Rbbp5	RBBP5
25994	Lpt	KMT2C/2D, LOC107985798
57293	JIL-1	RPS6KA4/A5
58264	KDM3	KDM3A/3B
34665, 58248	Chd1	CHD1/2
67277	NC2-alpha	DRAP1
28695	Pax	PXN, TGFB1I1, LPXN

58342	CG32564	POU2AF1
28888	mnb	DYRK1A/1B
32840	polybromo	PBRM1
40940	Trl	BTBD18
62185	Spps	SP1/3/4
62477	puf	USP34
67992	fl(2)d	WTAP
33093	Cp190	ZBTB47
51427	bin3	MEPCE
38241	pum	PUM1/2
42566, 31660	Clk	CLOCK, NPAS2, PER1/2/3
28572	MED26	MED26
33677, 33678	MED9	MED9
33710	MED19	MED19
61979	Cap-D3	NCAPD3
38285	osa	ARID1A/1B
34697	MED4	MED4
31627	msl-2	MSL2
32419	Sbf	SBF1/2

Supplemental Table 3.1. List of all H3 K27M enhancers and suppressors. First column: Bloomington *Drosophila* Stock Center (BDSC) identification numbers for RNAi lines in table. Second column: *Drosophila* target genes for each RNAi line in screen. Third column: Names of human orthologs for each enhancer and suppressor.

Supplemental Table 3.2.

BDSC ID	Target gene	RNAi score	H3 K27R score
42511	Set2	0	0
33706	Set2	2	2
31092	Trx	5	5
36130	Ash1	4	4
9330	GFP	0	0
31617	E(z)	0	0
33705	Ash1	6	6
31631	CG4565	0	0
28679	sna	0	0
31626	msl-1	0	0
31481	gpp	0	0
32469	wda	2	2
31093	Sirt7	0	0
31161	Psc	0	6
38261	Psc	2	7
31609	pho	0	0
35750	jing	0	0
31192	Asx	0	0
42502	Br140	Ö	0
31613	Sirt2	Ö	0
32891	Jarid2	0	0
34520	brm	0	0
33945	Pcl	5	5
39012	msl-1	Ö	0
31125	wda	0	0
27024	jing	1	1
31191	Su(z)12	2	2
33904	Eaf6	0	0
34708	Usp7	0	0
32926	Wdr82	0	0
57293	JIL-1	0	0
31190	ph-p	Ö	Ő
63018	ph-d	0	0
34665	Chd1	0	Ö
58248	Chd1	0	0
33696	Ndf	0	0
41698	Ndf Ndf	0	0
28563	Tip60	3	3
31618	esc	0	0
33704	Set1	0	0
34033	NSD	0	0
42819	Rbbp5	0	0
25994		0	0
64924	Lpt ash2	0	0
		0	0
33365 57721	Chif/Hysl1 Kdm4B	0	0
28905	Ada3	0	0
50972		0	0
	pont Tri	0	
40940	Trl Trl		0
67265	Trl	3 0	3
27027 44645	chm	0	0
44645	Usp47	U	U

62185	Spps	0	0
62477	puf	0	0
67992	fl(2)d	0	0
44481	ctrip	0	0
33903	Cp190	0	0
33962	HP1c	0	0
34784	r2d2	0	0
25898	Khc	0	0
51427	bin3	0	0
67277	NC2alpha	0	0
57443	CG13287	0	0
42614	Pax	0	0
28695	Pax	0	0
58342	CG32564	0	0
28888	mnb	0	0
32840	polybromo	0	0
33753	CycC	0	0
77170	Lpin	0	0
28572	MED26	0	0
33677	MED9	0	0
33678	MED9	0	0
33710	MED19	0	0
34662	MED1	0	0
38241	pum	0	0
32837	Nup153	0	0
30504	Nup153	0	0
42566	Clk	0	0
31660	Clk	0	0
77419	CG3430	0	0
61979	Cap-D3	0	0
26756	Śmox	0	0
38285	osa	0	0
34697	MED4	0	0
31627	msl-2	0	0
32419	Sbf	0	0

Supplemental Table 3.2. Enhancers and suppressors do not exhibit nonspecific interactions with overexpressed histone transgenes. First column: Bloomington Drosophila Stock Center (BSDC) identification number for each RNAi line. Second column: Target gene for each RNAi line. Third column: Score assigned to each RNAi line when expressed alone in wing. Fourth column: Score assigned to each RNAi line when expressed with *H3 K27R* in wing.

Supplemental Table 3.3

BDSC	Target	RNAi			
ID	gene	score		EZHIP score	
31092	trx		5		2
33753	CycC		0		5
33705	ash1		6		6
33962	Hp1c		0		7
31631	CG4565		0		7
30504	Nup153		0		7
32837	Nup153		0		8
34520	brahma		0		8
28679	sna		0		8
33706	Set2		2		8
31192	Asx		0		8
42502	Br140		0		8
31613	Sirt2		0		8
77419	CG3430		0		6
34662	MED1		0		8
34784	r2d2		0		8
44645	Usp47		0		8
55884	Cdc7		0		8
34033	NSD		0		8
51016	chif		0		8
33904	Eaf6		0		8
33365	Chif/Hyls1		0		8
33706	Set2		2		8

Supplemental Table 3.3. EZHIP and H3 K27M are suppressed by similar chromatin-related proteins. First column: Bloomington Drosophila Stock Center (BSDC) identification number for each RNAi line. Second column: Target gene for each RNAi line. Genes labeled in green were classified as EZHIP suppressors. Third column: Score assigned to each RNAi line when expressed alone in wing. Fourth column: Score assigned to each RNAi line when expressed with EZHIP in wing.

References

- (1) Schwartzentruber, J.; Korshunov, A.; Liu, X.-Y.; Jones, D. T. W.; Pfaff, E.; Jacob, K.; Sturm, D.; Fontebasso, A. M.; Quang, D.-A. K.; Tönjes, M.; Hovestadt, V.; Albrecht, S.; Kool, M.; Nantel, A.; Konermann, C.; Lindroth, A.; Jäger, N.; Rausch, T.; Ryzhova, M.; Korbel, J. O.; Hielscher, T.; Hauser, P.; Garami, M.; Klekner, A.; Bognar, L.; Ebinger, M.; Schuhmann, M. U.; Scheurlen, W.; Pekrun, A.; Frühwald, M. C.; Roggendorf, W.; Kramm, C.; Dürken, M.; Atkinson, J.; Lepage, P.; Montpetit, A.; Zakrzewska, M.; Zakrzewski, K.; Liberski, P. P.; Dong, Z.; Siegel, P.; Kulozik, A. E.; Zapatka, M.; Guha, A.; Malkin, D.; Felsberg, J.; Reifenberger, G.; von Deimling, A.; Ichimura, K.; Collins, V. P.; Witt, H.; Milde, T.; Witt, O.; Zhang, C.; Castelo-Branco, P.; Lichter, P.; Faury, D.; Tabori, U.; Plass, C.; Majewski, J.; Pfister, S. M.; Jabado, N. Driver Mutations in Histone H3.3 and Chromatin Remodelling Genes in Paediatric Glioblastoma. *Nature* 2012, *482* (7384), 226–231. https://doi.org/10.1038/nature10833.
- (2) Wu, G.; Broniscer, A.; McEachron, T. A.; Lu, C.; Paugh, B. S.; Becksfort, J.; Qu, C.; Ding, L.; Huether, R.; Parker, M.; Zhang, J.; Gajjar, A.; Dyer, M. A.; Mullighan, C. G.; Gilbertson, R. J.; Mardis, E. R.; Wilson, R. K.; Downing, J. R.; Ellison, D. W.; Zhang, J.; Baker, S. J.; St. Jude Children's Research Hospital–Washington University Pediatric Cancer Genome Project. Somatic Histone H3 Alterations in Pediatric Diffuse Intrinsic Pontine Gliomas and Non-Brainstem Glioblastomas. *Nat. Genet.* 2012, 44 (3), 251–253. https://doi.org/10.1038/ng.1102.
- (3) Lewis, P. W.; Müller, M. M.; Koletsky, M. S.; Cordero, F.; Lin, S.; Banaszynski, L. A.; Garcia, B. A.; Muir, T. W.; Becher, O. J.; Allis, C. D. Inhibition of PRC2 Activity by a

- Gain-of-Function H3 Mutation Found in Pediatric Glioblastoma. *Science* **2013**, *340* (6134), 857–861. https://doi.org/10.1126/science.1232245.
- (4) Chan, K.-M.; Fang, D.; Gan, H.; Hashizume, R.; Yu, C.; Schroeder, M.; Gupta, N.; Mueller, S.; James, C. D.; Jenkins, R.; Sarkaria, J.; Zhang, Z. The Histone H3.3K27M Mutation in Pediatric Glioma Reprograms H3K27 Methylation and Gene Expression. *Genes Dev.* 2013, 27 (9), 985–990. https://doi.org/10.1101/gad.217778.113.
- (5) Bender, S.; Tang, Y.; Lindroth, A. M.; Hovestadt, V.; Jones, D. T. W.; Kool, M.; Zapatka, M.; Northcott, P. A.; Sturm, D.; Wang, W.; Radlwimmer, B.; Højfeldt, J. W.; Truffaux, N.; Castel, D.; Schubert, S.; Ryzhova, M.; Şeker-Cin, H.; Gronych, J.; Johann, P. D.; Stark, S.; Meyer, J.; Milde, T.; Schuhmann, M.; Ebinger, M.; Monoranu, C.-M.; Ponnuswami, A.; Chen, S.; Jones, C.; Witt, O.; Collins, V. P.; von Deimling, A.; Jabado, N.; Puget, S.; Grill, J.; Helin, K.; Korshunov, A.; Lichter, P.; Monje, M.; Plass, C.; Cho, Y.-J.; Pfister, S. M. Reduced H3K27me3 and DNA Hypomethylation Are Major Drivers of Gene Expression in K27M Mutant Pediatric High-Grade Gliomas. *Cancer Cell* 2013, 24 (5), 660–672. https://doi.org/10.1016/j.ccr.2013.10.006.
- (6) Bayliss, J.; Mukherjee, P.; Lu, C.; Jain, S. U.; Chung, C.; Martinez, D.; Sabari, B.; Margol, A. S.; Panwalkar, P.; Parolia, A.; Pekmezci, M.; McEachin, R. C.; Cieslik, M.; Tamrazi, B.; Garcia, B. A.; Rocca, G. L.; Santi, M.; Lewis, P. W.; Hawkins, C.; Melnick, A.; Allis, C. D.; Thompson, C. B.; Chinnaiyan, A. M.; Judkins, A. R.; Venneti, S. Lowered H3K27me3 and DNA Hypomethylation Define Poorly Prognostic Pediatric Posterior Fossa Ependymomas. *Science Translational*

- Medicine **2016**, 8 (366), 366ra161-366ra161. https://doi.org/10.1126/scitranslmed.aah6904.
- (7) Pajtler, K. W.; Witt, H.; Sill, M.; Jones, D. T. W.; Hovestadt, V.; Kratochwil, F.; Wani, K.; Tatevossian, R.; Punchihewa, C.; Johann, P.; Reimand, J.; Warnatz, H.-J.; Ryzhova, M.; Mack, S.; Ramaswamy, V.; Capper, D.; Schweizer, L.; Sieber, L.; Wittmann, A.; Huang, Z.; van Sluis, P.; Volckmann, R.; Koster, J.; Versteeg, R.; Fults, D.; Toledano, H.; Avigad, S.; Hoffman, L. M.; Donson, A. M.; Foreman, N.; Hewer, E.; Zitterbart, K.; Gilbert, M.; Armstrong, T. S.; Gupta, N.; Allen, J. C.; Karajannis, M. A.; Zagzag, D.; Hasselblatt, M.; Kulozik, A. E.; Witt, O.; Collins, V. P.; von Hoff, K.; Rutkowski, S.; Pietsch, T.; Bader, G.; Yaspo, M.-L.; von Deimling, A.; Lichter, P.; Taylor, M. D.; Gilbertson, R.; Ellison, D. W.; Aldape, K.; Korshunov, A.; Kool, M.; Pfister, S. M. Molecular Classification of Ependymal Tumors across All CNS Compartments, Histopathological Grades, and Age Groups. *Cancer Cell* 2015, 27 (5), 728–743. https://doi.org/10.1016/j.ccell.2015.04.002.
- (8) Pajtler, K. W.; Wen, J.; Sill, M.; Lin, T.; Orisme, W.; Tang, B.; Hübner, J.-M.; Ramaswamy, V.; Jia, S.; Dalton, J. D.; Haupfear, K.; Rogers, H. A.; Punchihewa, C.; Lee, R.; Easton, J.; Wu, G.; Ritzmann, T. A.; Chapman, R.; Chavez, L.; Boop, F. A.; Klimo, P.; Sabin, N. D.; Ogg, R.; Mack, S. C.; Freibaum, B. D.; Kim, H. J.; Witt, H.; Jones, D. T. W.; Vo, B.; Gajjar, A.; Pounds, S.; Onar-Thomas, A.; Roussel, M. F.; Zhang, J.; Taylor, J. P.; Merchant, T. E.; Grundy, R.; Tatevossian, R. G.; Taylor, M. D.; Pfister, S. M.; Korshunov, A.; Kool, M.; Ellison, D. W. Molecular Heterogeneity and CXorf67 Alterations in Posterior Fossa Group A (PFA) Ependymomas. *Acta Neuropathol* 2018, *136* (2), 211–226. https://doi.org/10.1007/s00401-018-1877-0.

- (9) Gessi, M.; Capper, D.; Sahm, F.; Huang, K.; von Deimling, A.; Tippelt, S.; Fleischhack, G.; Scherbaum, D.; Alfer, J.; Juhnke, B.-O.; von Hoff, K.; Rutkowski, S.; Warmuth-Metz, M.; Chavez, L.; Pfister, S. M.; Pietsch, T.; Jones, D. T. W.; Sturm, D. Evidence of H3 K27M Mutations in Posterior Fossa Ependymomas. *Acta Neuropathol* 2016, 132 (4), 635–637. https://doi.org/10.1007/s00401-016-1608-3.
- (10) Filbin, M. G.; Tirosh, I.; Hovestadt, V.; Shaw, M. L.; Escalante, L. E.; Mathewson, N. D.; Neftel, C.; Frank, N.; Pelton, K.; Hebert, C. M.; Haberler, C.; Yizhak, K.; Gojo, J.; Egervari, K.; Mount, C.; Galen, P. van; Bonal, D. M.; Nguyen, Q.-D.; Beck, A.; Sinai, C.; Czech, T.; Dorfer, C.; Goumnerova, L.; Lavarino, C.; Carcaboso, A. M.; Mora, J.; Mylvaganam, R.; Luo, C. C.; Peyrl, A.; Popović, M.; Azizi, A.; Batchelor, T. T.; Frosch, M. P.; Martinez-Lage, M.; Kieran, M. W.; Bandopadhayay, P.; Beroukhim, R.; Fritsch, G.; Getz, G.; Rozenblatt-Rosen, O.; Wucherpfennig, K. W.; Louis, D. N.; Monje, M.; Slavc, I.; Ligon, K. L.; Golub, T. R.; Regev, A.; Bernstein, B. E.; Suvà, M. L. Developmental and Oncogenic Programs in H3K27M Gliomas Dissected by Single-Cell RNA-Seq. Science 2018, 360 (6386), 331–335. https://doi.org/10.1126/science.aao4750.
- (11) Mackay, A.; Burford, A.; Carvalho, D.; Izquierdo, E.; Fazal-Salom, J.; Taylor, K. R.; Bjerke, L.; Clarke, M.; Vinci, M.; Nandhabalan, M.; Temelso, S.; Popov, S.; Molinari, V.; Raman, P.; Waanders, A. J.; Han, H. J.; Gupta, S.; Marshall, L.; Zacharoulis, S.; Vaidya, S.; Mandeville, H. C.; Bridges, L. R.; Martin, A. J.; Al-Sarraj, S.; Chandler, C.; Ng, H.-K.; Li, X.; Mu, K.; Trabelsi, S.; Brahim, D. H.-B.; Kisljakov, A. N.; Konovalov, D. M.; Moore, A. S.; Carcaboso, A. M.; Sunol, M.; de Torres, C.; Cruz, O.; Mora, J.; Shats, L. I.; Stavale, J. N.; Bidinotto, L. T.; Reis, R. M.; Entz-Werle, N.;

- Farrell, M.; Cryan, J.; Crimmins, D.; Caird, J.; Pears, J.; Monje, M.; Debily, M.-A.; Castel, D.; Grill, J.; Hawkins, C.; Nikbakht, H.; Jabado, N.; Baker, S. J.; Pfister, S. M.; Jones, D. T. W.; Fouladi, M.; von Bueren, A. O.; Baudis, M.; Resnick, A.; Jones, C. Integrated Molecular Meta-Analysis of 1,000 Pediatric High-Grade and Diffuse Intrinsic Pontine Glioma. *Cancer Cell* **2017**, *32* (4), 520-537.e5. https://doi.org/10.1016/j.ccell.2017.08.017.
- (12) Vinci, M.; Burford, A.; Molinari, V.; Kessler, K.; Popov, S.; Clarke, M.; Taylor, K. R.; Pemberton, H. N.; Lord, C. J.; Gutteridge, A.; Forshew, T.; Carvalho, D.; Marshall, L. V.; Qin, E. Y.; Ingram, W. J.; Moore, A. S.; Ng, H.-K.; Trabelsi, S.; H'mida-Ben Brahim, D.; Entz-Werle, N.; Zacharoulis, S.; Vaidya, S.; Mandeville, H. C.; Bridges, L. R.; Martin, A. J.; Al-Sarraj, S.; Chandler, C.; Sunol, M.; Mora, J.; de Torres, C.; Cruz, O.; Carcaboso, A. M.; Monje, M.; Mackay, A.; Jones, C. Functional Diversity and Cooperativity between Subclonal Populations of Pediatric Glioblastoma and Diffuse Intrinsic Pontine Glioma Cells. *Nat Med* 2018, *24* (8), 1204–1215. https://doi.org/10.1038/s41591-018-0086-7.
- (13) Jain, S. U.; Do, T. J.; Lund, P. J.; Rashoff, A. Q.; Diehl, K. L.; Cieslik, M.; Bajic, A.; Juretic, N.; Deshmukh, S.; Venneti, S.; Muir, T. W.; Garcia, B. A.; Jabado, N.; Lewis, P. W. PFA Ependymoma-Associated Protein EZHIP Inhibits PRC2 Activity through a H3 K27M-like Mechanism. *Nature Communications* 2019, 10 (1), 2146. https://doi.org/10.1038/s41467-019-09981-6.
- (14) Piunti, A.; Smith, E. R.; Morgan, M. A. J.; Ugarenko, M.; Khaltyan, N.; Helmin, K. A.; Ryan, C. A.; Murray, D. C.; Rickels, R. A.; Yilmaz, B. D.; Rendleman, E. J.; Savas, J. N.; Singer, B. D.; Bulun, S. E.; Shilatifard, A. CATACOMB: An Endogenous

- Inducible Gene That Antagonizes H3K27 Methylation Activity of Polycomb Repressive Complex 2 via an H3K27M-like Mechanism. *Science Advances* **2019**, *5* (7), eaax2887. https://doi.org/10.1126/sciadv.aax2887.
- (15) Hübner, J.-M.; Müller, T.; Papageorgiou, D. N.; Mauermann, M.; Krijgsveld, J.; Russell, R. B.; Ellison, D. W.; Pfister, S. M.; Pajtler, K. W.; Kool, M. EZHIP/CXorf67 Mimics K27M Mutated Oncohistones and Functions as an Intrinsic Inhibitor of PRC2 Function in Aggressive Posterior Fossa Ependymoma. *Neuro Oncol* 2019, 21 (7), 878–889. https://doi.org/10.1093/neuonc/noz058.
- (16) Ragazzini, R.; Pérez-Palacios, R.; Baymaz, I. H.; Diop, S.; Ancelin, K.; Zielinski, D.; Michaud, A.; Givelet, M.; Borsos, M.; Aflaki, S.; Legoix, P.; Jansen, P. W. T. C.; Servant, N.; Torres-Padilla, M.-E.; Bourc'his, D.; Fouchet, P.; Vermeulen, M.; Margueron, R. EZHIP Constrains Polycomb Repressive Complex 2 Activity in Germ Cells. *Nature Communications* 2019, *10* (1), 3858. https://doi.org/10.1038/s41467-019-11800-x.
- (17) Margueron, R.; Justin, N.; Ohno, K.; Sharpe, M. L.; Son, J.; Drury Iii, W. J.; Voigt, P.; Martin, S. R.; Taylor, W. R.; De Marco, V.; Pirrotta, V.; Reinberg, D.; Gamblin, S. J. Role of the Polycomb Protein EED in the Propagation of Repressive Histone Marks. *Nature* 2009, 461 (7265), 762–767. https://doi.org/10.1038/nature08398.
- (18) Hansen, K. H.; Bracken, A. P.; Pasini, D.; Dietrich, N.; Gehani, S. S.; Monrad, A.; Rappsilber, J.; Lerdrup, M.; Helin, K. A Model for Transmission of the H3K27me3 Epigenetic Mark. *Nature Cell Biology* **2008**, *10* (11), 1291–1300. https://doi.org/10.1038/ncb1787.

- (19) Jiao, L.; Liu, X. Structural Basis of Histone H3K27 Trimethylation by an Active Polycomb Repressive Complex 2. Science 2015, 350 (6258), aac4383. https://doi.org/10.1126/science.aac4383.
- (20) Diehl, K. L.; Ge, E. J.; Weinberg, D. N.; Jani, K. S.; Allis, C. D.; Muir, T. W. PRC2 Engages a Bivalent H3K27M-H3K27me3 Dinucleosome Inhibitor. *Proceedings of the National Academy of Sciences* 2019, *116* (44), 22152–22157. https://doi.org/10.1073/pnas.1911775116.
- (21) Stafford, J. M.; Lee, C.-H.; Voigt, P.; Descostes, N.; Saldaña-Meyer, R.; Yu, J.-R.; Leroy, G.; Oksuz, O.; Chapman, J. R.; Suarez, F.; Modrek, A. S.; Bayin, N. S.; Placantonakis, D. G.; Karajannis, M. A.; Snuderl, M.; Ueberheide, B.; Reinberg, D. Multiple Modes of PRC2 Inhibition Elicit Global Chromatin Alterations in H3K27M Pediatric Glioma. *Science Advances* 2018, *4* (10), eaau5935. https://doi.org/10.1126/sciadv.aau5935.
- (22) Justin, N.; Zhang, Y.; Tarricone, C.; Martin, S. R.; Chen, S.; Underwood, E.; De Marco, V.; Haire, L. F.; Walker, P. A.; Reinberg, D.; Wilson, J. R.; Gamblin, S. J. Structural Basis of Oncogenic Histone H3K27M Inhibition of Human Polycomb Repressive Complex 2. *Nature Communications* 2016, 7 (1), 11316. https://doi.org/10.1038/ncomms11316.
- (23) Harutyunyan, A. S.; Krug, B.; Chen, H.; Papillon-Cavanagh, S.; Zeinieh, M.; De Jay, N.; Deshmukh, S.; Chen, C. C. L.; Belle, J.; Mikael, L. G.; Marchione, D. M.; Li, R.; Nikbakht, H.; Hu, B.; Cagnone, G.; Cheung, W. A.; Mohammadnia, A.; Bechet, D.; Faury, D.; McConechy, M. K.; Pathania, M.; Jain, S. U.; Ellezam, B.; Weil, A. G.; Montpetit, A.; Salomoni, P.; Pastinen, T.; Lu, C.; Lewis, P. W.; Garcia, B. A.;

- Kleinman, C. L.; Jabado, N.; Majewski, J. H3K27M Induces Defective Chromatin Spread of PRC2-Mediated Repressive H3K27me2/Me3 and Is Essential for Glioma Tumorigenesis. *Nature Communications* **2019**, *10* (1), 1262. https://doi.org/10.1038/s41467-019-09140-x.
- (24) Brien, G. L.; Bressan, R. B.; Monger, C.; Gannon, D.; Lagan, E.; Doherty, A. M.; Healy, E.; Neikes, H.; Fitzpatrick, D. J.; Deevy, O. Simultaneous Disruption of PRC2 and Enhancer Function Underlies Histone H3. 3-K27M Oncogenic Activity in Human Hindbrain Neural Stem Cells. *Nature Genetics* 2021, 53 (8), 1221–1232.
- (25) Nagaraja, S.; Quezada, M. A.; Gillespie, S. M.; Arzt, M.; Lennon, J. J.; Woo, P. J.; Hovestadt, V.; Kambhampati, M.; Filbin, M. G.; Suva, M. L.; Nazarian, J.; Monje, M. Histone Variant and Cell Context Determine H3K27M Reprogramming of the Enhancer Landscape and Oncogenic State. *Molecular Cell* 2019, 76 (6), 965-980.e12. https://doi.org/10.1016/j.molcel.2019.08.030.
- (26) Larson, J. D.; Kasper, L. H.; Paugh, B. S.; Jin, H.; Wu, G.; Kwon, C.-H.; Fan, Y.; Shaw, T. I.; Silveira, A. B.; Qu, C.; Xu, R.; Zhu, X.; Zhang, J.; Russell, H. R.; Peters, J. L.; Finkelstein, D.; Xu, B.; Lin, T.; Tinkle, C. L.; Patay, Z.; Onar-Thomas, A.; Pounds, S. B.; McKinnon, P. J.; Ellison, D. W.; Zhang, J.; Baker, S. J. Histone H3.3 K27M Accelerates Spontaneous Brainstem Glioma and Drives Restricted Changes in Bivalent Gene Expression. *Cancer Cell* 2019, 35 (1), 140-155.e7. https://doi.org/10.1016/j.ccell.2018.11.015.
- (27) Reiter, L. T.; Potocki, L.; Chien, S.; Gribskov, M.; Bier, E. A Systematic Analysis of Human Disease-Associated Gene Sequences In Drosophila Melanogaster. Genome Res. 2001, 11 (6), 1114–1125. https://doi.org/10.1101/gr.169101.

- (28) Rubin, G. M.; Lewis, E. B. A Brief History of Drosophila's Contributions to Genome Research. Science 2000, 287 (5461), 2216–2218. https://doi.org/10.1126/science.287.5461.2216.
- (29) Lewis, E. B. A Gene Complex Controlling Segmentation in Drosophila. *Nature* **1978**, 276 (5688), 565–570. https://doi.org/10.1038/276565a0.
- (30) Jain, S. U.; Rashoff, A. Q.; Krabbenhoft, S. D.; Hoelper, D.; Do, T. J.; Gibson, T. J.; Lundgren, S. M.; Bondra, E. R.; Deshmukh, S.; Harutyunyan, A. S.; Juretic, N.; Jabado, N.; Harrison, M. M.; Lewis, P. W. H3 K27M and EZHIP Impede H3K27-Methylation Spreading by Inhibiting Allosterically Stimulated PRC2. *Molecular Cell* 2020, 80 (4), 726-735.e7. https://doi.org/10.1016/j.molcel.2020.09.028.
- (31) Berlandi, J.; Chaouch, A.; De Jay, N.; Tegeder, I.; Thiel, K.; Shirinian, M.; Kleinman, C. L.; Jeibmann, A.; Lasko, P.; Jabado, N.; Hasselblatt, M. Identification of Genes Functionally Involved in the Detrimental Effects of Mutant Histone H3.3-K27M in Drosophila Melanogaster. *Neuro Oncol* 2019, 21 (5), 628–639. https://doi.org/10.1093/neuonc/noz021.
- (32) Chaouch, A.; Berlandi, J.; Chen, C. C. L.; Frey, F.; Badini, S.; Harutyunyan, A. S.; Chen, X.; Krug, B.; Hébert, S.; Jeibmann, A.; Lu, C.; Kleinman, C. L.; Hasselblatt, M.; Lasko, P.; Shirinian, M.; Jabado, N. Histone H3.3 K27M and K36M Mutations de-Repress Transposable Elements through Perturbation of Antagonistic Chromatin Marks. *Molecular Cell* 2021, *81* (23), 4876-4890.e7. https://doi.org/10.1016/j.molcel.2021.10.008.

- (33) McGuire, S. E.; Le, P. T.; Osborn, A. J.; Matsumoto, K.; Davis, R. L. Spatiotemporal Rescue of Memory Dysfunction in Drosophila. *Science* **2003**, *302* (5651), 1765–1768. https://doi.org/10.1126/science.1089035.
- (34) Stoiber, M.; Celniker, S.; Cherbas, L.; Brown, B.; Cherbas, P. Diverse Hormone Response Networks in 41 Independent Drosophila Cell Lines. G3 Genes|Genomes|Genetics 2016, 6 (3), 683–694. https://doi.org/10.1534/g3.115.023366.
- (35) Kumar, S. S.; Sengupta, S.; Lee, K.; Hura, N.; Fuller, C.; DeWire, M.; Stevenson, C. B.; Fouladi, M.; Drissi, R. BMI-1 Is a Potential Therapeutic Target in Diffuse Intrinsic Pontine Glioma. *Oncotarget* 2017, 8 (38), 62962–62975. https://doi.org/10.18632/oncotarget.18002.
- (36) Mo, Y.; Duan, S.; Zhang, X.; Hua, X.; Zhou, H.; Wei, H.-J.; Watanabe, J.;
 McQuillan, N.; Su, Z.; Gu, W.; Wu, C.-C.; Vakoc, C. R.; Hashizume, R.; Chang, K.;
 Zhang, Z. Epigenome Programming by H3.3K27M Mutation Creates a
 Dependence of Pediatric Glioma on SMARCA4. *Cancer Discovery* 2022, *12* (12),
 2906–2929. https://doi.org/10.1158/2159-8290.CD-21-1492.
- (37) Panditharatna, E.; Marques, J. G.; Wang, T.; Trissal, M. C.; Liu, I.; Jiang, L.; Beck, A.; Groves, A.; Dharia, N. V.; Li, D.; Hoffman, S. E.; Kugener, G.; Shaw, M. L.; Mire, H. M.; Hack, O. A.; Dempster, J. M.; Lareau, C.; Dai, L.; Sigua, L. H.; Quezada, M. A.; Stanton, A.-C. J.; Wyatt, M.; Kalani, Z.; Goodale, A.; Vazquez, F.; Piccioni, F.; Doench, J. G.; Root, D. E.; Anastas, J. N.; Jones, K. L.; Conway, A. S.; Stopka, S.; Regan, M. S.; Liang, Y.; Seo, H.-S.; Song, K.; Bashyal, P.; Jerome, W. P.; Mathewson, N. D.; Dhe-Paganon, S.; Suvà, M. L.; Carcaboso, A. M.; Lavarino, C.;

- Mora, J.; Nguyen, Q.-D.; Ligon, K. L.; Shi, Y.; Agnihotri, S.; Agar, N. Y. R.; Stegmaier, K.; Stiles, C. D.; Monje, M.; Golub, T. R.; Qi, J.; Filbin, M. G. BAF Complex Maintains Glioma Stem Cells in Pediatric H3K27M Glioma. *Cancer Discovery* **2022**, *12* (12), 2880–2905. https://doi.org/10.1158/2159-8290.CD-21-1491.
- (38) Yu, J.-R.; LeRoy, G.; Bready, D.; Frenster, J. D.; Saldaña-Meyer, R.; Jin, Y.;
 Descostes, N.; Stafford, J. M.; Placantonakis, D. G.; Reinberg, D. The H3K36me2
 Writer-Reader Dependency in H3K27M-DIPG. Science Advances 2021, 7 (29),
 eabg7444. https://doi.org/10.1126/sciadv.abg7444.
- (39) Zhang, L.; Nesvick, C. L.; Day, C. A.; Choi, J.; Lu, V. M.; Peterson, T.; Power, E. A.; Anderson, J. B.; Hamdan, F. H.; Decker, P. A.; Simons, R.; Welby, J. P.; Siada, R.; Ge, J.; Kaptzan, T.; Johnsen, S. A.; Hinchcliffe, E. H.; Daniels, D. J. STAT3 Is a Biologically Relevant Therapeutic Target in H3K27M-Mutant Diffuse Midline Glioma. *Neuro-Oncology* 2022, 24 (10), 1700–1711. https://doi.org/10.1093/neuonc/noac093.
- (40) Michealraj, K. A.; Kumar, S. A.; Kim, L. J. Y.; Cavalli, F. M. G.; Przelicki, D.; Wojcik, J. B.; Delaidelli, A.; Bajic, A.; Saulnier, O.; MacLeod, G.; Vellanki, R. N.; Vladoiu, M. C.; Guilhamon, P.; Ong, W.; Lee, J. J. Y.; Jiang, Y.; Holgado, B. L.; Rasnitsyn, A.; Malik, A. A.; Tsai, R.; Richman, C. M.; Juraschka, K.; Haapasalo, J.; Wang, E. Y.; De Antonellis, P.; Suzuki, H.; Farooq, H.; Balin, P.; Kharas, K.; Van Ommeren, R.; Sirbu, O.; Rastan, A.; Krumholtz, S. L.; Ly, M.; Ahmadi, M.; Deblois, G.; Srikanthan, D.; Luu, B.; Loukides, J.; Wu, X.; Garzia, L.; Ramaswamy, V.; Kanshin, E.; Sánchez-Osuna, M.; El-Hamamy, I.; Coutinho, F. J.; Prinos, P.; Singh, S.; Donovan,

- L. K.; Daniels, C.; Schramek, D.; Tyers, M.; Weiss, S.; Stein, L. D.; Lupien, M.; Wouters, B. G.; Garcia, B. A.; Arrowsmith, C. H.; Sorensen, P. H.; Angers, S.; Jabado, N.; Dirks, P. B.; Mack, S. C.; Agnihotri, S.; Rich, J. N.; Taylor, M. D. Metabolic Regulation of the Epigenome Drives Lethal Infantile Ependymoma. *Cell* **2020**, *181* (6), 1329-1345.e24. https://doi.org/10.1016/j.cell.2020.04.047.
- (41) Mohammad, F.; Weissmann, S.; Leblanc, B.; Pandey, D. P.; Højfeldt, J. W.; Comet, I.; Zheng, C.; Johansen, J. V.; Rapin, N.; Porse, B. T.; Tvardovskiy, A.; Jensen, O. N.; Olaciregui, N. G.; Lavarino, C.; Suñol, M.; de Torres, C.; Mora, J.; Carcaboso, A. M.; Helin, K. EZH2 Is a Potential Therapeutic Target for H3K27M-Mutant Pediatric Gliomas. *Nature Medicine* 2017, 23 (4), 483–492. https://doi.org/10.1038/nm.4293.
- (42) Mendez, F. M.; Núñez, F. J.; Garcia-Fabiani, M. B.; Haase, S.; Carney, S.; Gauss, J. C.; Becher, O. J.; Lowenstein, P. R.; Castro, M. G. Epigenetic Reprogramming and Chromatin Accessibility in Pediatric Diffuse Intrinsic Pontine Gliomas: A Neural Developmental Disease. *Neuro Oncol* 2020, 22 (2), 195–206. https://doi.org/10.1093/neuonc/noz218.
- (43) Monje, M.; Mitra, S. S.; Freret, M. E.; Raveh, T. B.; Kim, J.; Masek, M.; Attema, J. L.; Li, G.; Haddix, T.; Edwards, M. S. B.; Fisher, P. G.; Weissman, I. L.; Rowitch, D. H.; Vogel, H.; Wong, A. J.; Beachy, P. A. Hedgehog-Responsive Candidate Cell of Origin for Diffuse Intrinsic Pontine Glioma. *Proceedings of the National Academy of Sciences* 2011, 108 (11), 4453–4458. https://doi.org/10.1073/pnas.1101657108.
- (44) Mendjan, S.; Taipale, M.; Kind, J.; Holz, H.; Gebhardt, P.; Schelder, M.; Vermeulen, M.; Buscaino, A.; Duncan, K.; Mueller, J.; Wilm, M.; Stunnenberg, H. G.;

- Saumweber, H.; Akhtar, A. Nuclear Pore Components Are Involved in the Transcriptional Regulation of Dosage Compensation in Drosophila. *Molecular Cell* **2006**, *21* (6), 811–823. https://doi.org/10.1016/j.molcel.2006.02.007.
- (45) Vaquerizas, J. M.; Suyama, R.; Kind, J.; Miura, K.; Luscombe, N. M.; Akhtar, A. Nuclear Pore Proteins Nup153 and Megator Define Transcriptionally Active Regions in the Drosophila Genome. *PLOS Genetics* **2010**, *6* (2), e1000846. https://doi.org/10.1371/journal.pgen.1000846.
- (46) Jacinto, F. V.; Benner, C.; Hetzer, M. W. The Nucleoporin Nup153 Regulates Embryonic Stem Cell Pluripotency through Gene Silencing. *Genes Dev.* 2015, 29 (12), 1224–1238. https://doi.org/10.1101/gad.260919.115.
- (47) Toda, T.; Hsu, J. Y.; Linker, S. B.; Hu, L.; Schafer, S. T.; Mertens, J.; Jacinto, F. V.; Hetzer, M. W.; Gage, F. H. Nup153 Interacts with Sox2 to Enable Bimodal Gene Regulation and Maintenance of Neural Progenitor Cells. *Cell Stem Cell* 2017, 21 (5), 618-634.e7. https://doi.org/10.1016/j.stem.2017.08.012.
- (48) Biegel, J. A.; Zhou, J.-Y.; Rorke, L. B.; Stenstrom, C.; Wainwright, L. M.; Fogelgren,
 B. Germ-Line and Acquired Mutations of INI1 in Atypical Teratoid and Rhabdoid
 Tumors1. Cancer Research 1999, 59 (1), 74–79.
- (49) Drosos, Y.; Myers, J. A.; Xu, B.; Mathias, K. M.; Beane, E. C.; Radko-Juettner, S.; Mobley, R. J.; Larsen, M. E.; Piccioni, F.; Ma, X.; Low, J.; Hansen, B. S.; Peters, S. T.; Bhanu, N. V.; Dhanda, S. K.; Chen, T.; Upadhyaya, S. A.; Pruett-Miller, S. M.; Root, D. E.; Garcia, B. A.; Partridge, J. F.; Roberts, C. W. M. NSD1 Mediates Antagonism between SWI/SNF and Polycomb Complexes and Is Required for

- Transcriptional Activation upon EZH2 Inhibition. *Molecular Cell* **2022**, *82* (13), 2472-2489.e8. https://doi.org/10.1016/j.molcel.2022.04.015.
- (50) Wang, L.; Zhao, Z.; Ozark, P. A.; Fantini, D.; Marshall, S. A.; Rendleman, E. J.; Cozzolino, K. A.; Louis, N.; He, X.; Morgan, M. A.; Takahashi, Y.; Collings, C. K.; Smith, E. R.; Ntziachristos, P.; Savas, J. N.; Zou, L.; Hashizume, R.; Meeks, J. J.; Shilatifard, A. Resetting the Epigenetic Balance of Polycomb and COMPASS Function at Enhancers for Cancer Therapy. *Nat Med* 2018, 24 (6), 758–769. https://doi.org/10.1038/s41591-018-0034-6.
- (51) Wang, X.; Wang, S.; Troisi, E. C.; Howard, T. P.; Haswell, J. R.; Wolf, B. K.; Hawk, W. H.; Ramos, P.; Oberlick, E. M.; Tzvetkov, E. P.; Ross, A.; Vazquez, F.; Hahn, W. C.; Park, P. J.; Roberts, C. W. M. BRD9 Defines a SWI/SNF Sub-Complex and Constitutes a Specific Vulnerability in Malignant Rhabdoid Tumors. *Nat Commun* 2019, 10 (1), 1881. https://doi.org/10.1038/s41467-019-09891-7.
- (52) Kim, D.; Langmead, B.; Salzberg, S. L. HISAT: A Fast Spliced Aligner with Low Memory Requirements. *Nat Methods* 2015, 12 (4), 357–360. https://doi.org/10.1038/nmeth.3317.
- (53) Liao, Y.; Smyth, G. K.; Shi, W. FeatureCounts: An Efficient General Purpose Program for Assigning Sequence Reads to Genomic Features. *Bioinformatics* 2014, 30 (7), 923–930. https://doi.org/10.1093/bioinformatics/btt656.
- (54) Love, M. I.; Huber, W.; Anders, S. Moderated Estimation of Fold Change and Dispersion for RNA-Seq Data with DESeq2. *Genome Biology* 2014, 15 (12), 550. https://doi.org/10.1186/s13059-014-0550-8.

- (55) Babraham Bioinformatics FastQC A Quality Control tool for High Throughput Sequence Data. https://www.bioinformatics.babraham.ac.uk/projects/fastqc/ (accessed 2023-04-19).
- (56) Bolger, A. M.; Lohse, M.; Usadel, B. Trimmomatic: A Flexible Trimmer for Illumina Sequence Data. *Bioinformatics* 2014, 30 (15), 2114–2120. https://doi.org/10.1093/bioinformatics/btu170.
- (57) dos Santos, G.; Schroeder, A. J.; Goodman, J. L.; Strelets, V. B.; Crosby, M. A.; Thurmond, J.; Emmert, D. B.; Gelbart, W. M.; the FlyBase Consortium. FlyBase: Introduction of the Drosophila Melanogaster Release 6 Reference Genome Assembly and Large-Scale Migration of Genome Annotations. *Nucleic Acids Research* 2015, 43 (D1), D690–D697. https://doi.org/10.1093/nar/gku1099.
- (58) Langmead, B.; Salzberg, S. L. Fast Gapped-Read Alignment with Bowtie 2. *Nat Methods* **2012**, *9* (4), 357–359. https://doi.org/10.1038/nmeth.1923.
- (59) Model-based Analysis of ChIP-Seq (MACS) | Genome Biology | Full Text. https://genomebiology.biomedcentral.com/articles/10.1186/gb-2008-9-9-r137 (accessed 2023-04-19).
- (60) Loubiere, V.; Delest, A.; Thomas, A.; Bonev, B.; Schuettengruber, B.; Sati, S.; Martinez, A.-M.; Cavalli, G. Coordinate Redeployment of PRC1 Proteins Suppresses Tumor Formation during Drosophila Development. *Nature Genetics* 2016, 48 (11), 1436–1442. https://doi.org/10.1038/ng.3671.
- (61) Thorvaldsdóttir, H.; Robinson, J. T.; Mesirov, J. P. Integrative Genomics Viewer (IGV): High-Performance Genomics Data Visualization and Exploration. *Briefings in Bioinformatics* 2013, 14 (2), 178–192. https://doi.org/10.1093/bib/bbs017.

- (62) Ramírez, F.; Ryan, D. P.; Grüning, B.; Bhardwaj, V.; Kilpert, F.; Richter, A. S.; Heyne, S.; Dündar, F.; Manke, T. DeepTools2: A next Generation Web Server for Deep-Sequencing Data Analysis. *Nucleic Acids Research* 2016, 44 (W1), W160–W165. https://doi.org/10.1093/nar/gkw257.
- (63) Lyne, R.; Smith, R.; Rutherford, K.; Wakeling, M.; Varley, A.; Guillier, F.; Janssens, H.; Ji, W.; Mclaren, P.; North, P.; Rana, D.; Riley, T.; Sullivan, J.; Watkins, X.; Woodbridge, M.; Lilley, K.; Russell, S.; Ashburner, M.; Mizuguchi, K.; Micklem, G. FlyMine: An Integrated Database for Drosophila and Anopheles Genomics.
 Genome Biol 2007, 8 (7), R129. https://doi.org/10.1186/gb-2007-8-7-r129.
- (64) Hu, Y.; Flockhart, I.; Vinayagam, A.; Bergwitz, C.; Berger, B.; Perrimon, N.; Mohr, S. E. An Integrative Approach to Ortholog Prediction for Disease-Focused and Other Functional Studies. *BMC Bioinformatics* 2011, 12 (1), 357. https://doi.org/10.1186/1471-2105-12-357.
- (65) Perkins, L. A.; Holderbaum, L.; Tao, R.; Hu, Y.; Sopko, R.; McCall, K.; Yang-Zhou, D.; Flockhart, I.; Binari, R.; Shim, H.-S.; Miller, A.; Housden, A.; Foos, M.; Randkelv, S.; Kelley, C.; Namgyal, P.; Villalta, C.; Liu, L.-P.; Jiang, X.; Huan-Huan, Q.; Wang, X.; Fujiyama, A.; Toyoda, A.; Ayers, K.; Blum, A.; Czech, B.; Neumuller, R.; Yan, D.; Cavallaro, A.; Hibbard, K.; Hall, D.; Cooley, L.; Hannon, G. J.; Lehmann, R.; Parks, A.; Mohr, S. E.; Ueda, R.; Kondo, S.; Ni, J.-Q.; Perrimon, N. The Transgenic RNAi Project at Harvard Medical School: Resources and Validation. *Genetics* 2015, 201 (3), 843–852. https://doi.org/10.1534/genetics.115.180208.

(66) Hu, Y.; Roesel, C.; Flockhart, I.; Perkins, L.; Perrimon, N.; Mohr, S. E. UP-TORR: Online Tool for Accurate and Up-to-Date Annotation of RNAi Reagents. *Genetics* 2013, 195 (1), 37–45. https://doi.org/10.1534/genetics.113.151340.

Conclusions and Future Directions

Summary

H3 K27M and EZHIP are potent inhibitors of Polycomb repressive complex 2 (PRC2), a histone methyltransferase that deposits the repressive histone H3 lysine 27 (H3K27me3). PRC2 inhibition by these oncoproteins drives diffuse midline glioma (DMG), and posterior fossa ependymoma type A (PFA). These tumors have severely reduced H3K27me3, leading to aberrant gene activation. Despite this overall loss, H3K27me3 is retained at sites of PRC2 recruitment. Prior to this work (Chapter 2), it was unclear how H3 K27M and EZHIP drove the selective loss of H3K27me3 from broad regions. In mammalian and *Drosophila* tissue-culture models, we showed that EZHIP specifically inhibits the allosterically active (spreading) form of PRC2. H3K27me3 at PRC2-recruitment sites does not require allosteric activation of the complex, sparing these regions from loss of H3K27me3. Overall, this work provided a mechanism for the H3K27me3 enrichment patterns found in DMG and PFA.

Gene expression changes in DMG and PFA tumors correlate with the loss of H3K27me3 and concomitant gains in active histone modifications. The importance of additional chromatin-modifying proteins, including those that deposit these active marks, has not been rigorously tested in a developing model organism. Here, we leveraged models of H3 K27M and EZHIP to screen for chromatin-related enhancers and suppressors of oncoprotein phenotypes in *Drosophila* (Chapter 3). Rather than restoring PRC2 function, suppressor knockdown reversed the transcriptional changes imparted by H3 K27M. Altogether, this work identified critical mediators of oncoprotein phenotypes and put forward mechanisms by which oncoproteins can be neutralized in developing tissues.

Conserved chromatin modifiers are essential components of oncoprotein developmental defects

During hindbrain development, PRC2 represses self-renewal genes and promotes differentiation.¹ By inhibiting PRC2, H3 K27M and EZHIP rewire the transcriptional programs that coordinate healthy development. These gene-expression changes are thought to induce a differentiation block in hindbrain tissues.^{2–5} PRC2-mediated gene silencing is reinforced or opposed by other chromatin-modifying proteins.⁶ These chromatin modifiers may facilitate the transcriptional and chromatin-state alterations found in DMG and PFA. However, the contributions of these proteins to oncogenesis are difficult to discern in tissue-culture models with restricted phenotypic ranges. To recapitulate the complexity of tissue development, it is critical to examine the effects of H3 K27M and EZHIP in developing model organisms. We leveraged *Drosophila* tissue models of H3 K27M and EZHIP to perform a comprehensive screen for enhancers and suppressors of the H3 K27M wing phenotype. Knockdown of over 50 genes modified the phenotype, demonstrating that H3 K27M developmental defects are mediated by many chromatin-related factors.

H3 K27M and EZHIP have striking biochemical similarities.^{7,8} We tested these oncoproteins side-by-side and found that EZHIP causes more extreme wing phenotypes than H3 K27M, and was suppressed by 6 of the 20 H3 K27M wing suppressors. The remaining 14 genes were largely weak H3 K27M suppressors. Whereas we readily identified weak suppressors of H3 K27M using our quantitative scoring rubric, detecting such changes in the extreme phenotype proved difficult. Compared to H3 K27M, EZHIP

dramatically impaired development of all tissues in which it was expressed. These data are likely to do EZHIP being a more potent inhibitor of PRC2 than H3 K27M, though we cannot conclude this with certainty. A potentially critical form of EZHIP regulation mediating *Drosophila* phenotypes is phosphorylation of serine residues in its C-terminus, near the 12-residue peptide that mediates PRC2 inhibition. Truman Do of the Lewis Lab has generated evidence that phosphorylation of EZHIP is required for PRC2 inhibition (unpublished). The kinase(s) that mediate EZHIP phosphorylation in humans are unknown. Given these data, we generated transgenic *Drosophila* lines expressing a mutant form of EZHIP, in which all serine residues were mutated to alanine. Phosphomutant EZHIP caused no phenotypes and did not affect fly. We also screened conserved kinases for suppression of the wild-type EZHIP wing phenotype but not identify suppressors.

There is evidence that EZHIP alters additional pathways that could explain the phenotypic differences between EZHIP and H3 K27M in *Drosophila*. EZHIP physically interacts with PALB2, a component of the homologous recombination (HR) DNA-repair pathway.⁹ The EZHIP-PALB2 interaction disrupts formation of the HR DNA-repair complex. Therapeutically, this sensitizes EZHIP-expressing cells to DNA damage repair inhibitors. The relevance of these data in a developmental context could be determined in *Drosophila*, since HR DNA-repair machinery is highly conserved. We could assess whether EZHIP-expressing wing discs incur more DNA damage than their H3 K27M counterparts by staining discs for γ-H2AX. Moreover, we could screen DNA-repair genes for their ability to enhance or suppress EZHIP and H3 K27M wing phenotypes.

Outside of DNA repair, studies of PFA tumors have identified metabolic conditions that may be required for disease pathogenesis. ¹⁰ Patient-derived PFA tumor cells can only be cultured *in vitro* under hypoxic conditions. Oxygen concentration anticorrelates with H3K27me3 in PFA tissue culture. This may be explained by hypoxia-mediated restriction of S-adenosylmethionine (SAM), the substrate used by PRC2 to catalyze H3K27me3. ¹⁰ Though we could not grow *Drosophila* under extreme hypoxic conditions, we could assess the relative importance of different metabolic pathways to oncoprotein phenotypes by targeting them genetically in EZHIP- and H3 K27M-expressing tissues.

A fine balance: determining the mechanisms of H3 K27M suppression

Our screen revealed suppressors whose knockdown restores wild-type development in H3 K27M-expressing tissues. Accordingly, suppressor proteins promote the deleterious effects of H3 K27M in these tissues. We tested whether suppression of the H3 K27M wing phenotype had a transcriptional basis by conducting RNA-seq experiments in wing discs. *Asx, trx,* and *ash1* RNAi partially or completely restored the expression of H3 K27M-upregulated genes towards that of H3 K27R discs. These transcriptional changes may underlie rescue of normal development. Trx, Ash1, and Set2 strong suppressors all deposit marks of active chromatin. Upon H3 K27M-mediated inhibition of PRC2, these modifications may become enriched at genes where H3K27me3 is lost. To test whether H3 K27M-upregulated genes are direct targets of these suppressors, we could perform CUT&RUN in wing discs against H3K4me1/me2 (Trx), H3K36me2 (Ash1), and H3K36me3 (Set2). An enrichment of these marks at H3 K27M-upregulated genes would

solidify a model in which H3 K27M triggers a gene-regulatory imbalance at key developmental genes. Indeed, an altered gene-regulatory balance between transcriptional activators and repressors has been implicated as a cause of multiple chromatin-related cancers.^{11–15} However, suppressors could promote oncoprotein phenotypes independently from the histone modifications they deposit.

Trx has long been recognized for its role in antagonizing Polycomb-mediated repression. As a transcriptional activator, Trx likely mediates H3 K27M and EZHIP phenotypes by facilitating gene derepression where H3K27me3 is lost. The catalytic-independent activity of Trx is known. Altered levels of H3K4me1/me2 in wing discs may therefore not explain the mechanism by which Trx mediates H3 K27M wing defects. To distinguish the importance of Trx catalytic and noncatalytic functions, we could cross flies with a catalytically inactive *trx* allele to H3 K27M-expressing flies. If a *trx*-mutant fly line rescued H3 K27M phenotypes, it would support the notion that H3K4me1/me2 are mediators of H3 K27M transcriptional changes.

Though H3 K27M suppressors are generally involved in transcriptional activation, we found that knockdown of Asx, a Polycomb protein, also suppressed H3 K27M. Asx is a member of the Polycomb repressive deubiquitinase (PR-DUB) complex. To our knowledge, this is the first time that PR-DUB has been identified as a mediator of H3 K27M phenotypes. PR-DUB removes excessive H2AK118ub from intergenic regions, which concentrates PRC1 and PRC2 at target genes. 18–20 Excess H2AK118ub accumulation in intergenic regions redistributes PRC1 and PRC2 away from their target

genes, causing gene derepression. PR-DUB has mostly been studied for its role in Polycomb-mediated repression. However, H2AK118ub removal promotes transcriptional activation at non-Polycomb targets.¹⁷ Thus, PR-DUB has dual repressive and activating roles in gene regulation.

PR-DUB promotes Polycomb-mediated repression under normal circumstances but could exacerbate Polycomb-protein dysfunction in the context of H3 K27M. As described earlier, inhibition of allosterically active PRC2 by H3 K27M drives the loss of H3K27me3 from spreading regions. However, H3K27me3 is retained at PRC2 recruitment sites. Studies in mammalian tissue culture have found that PRC1 binding increases at regions that retain H3K27me3, but is reduced at sites that lose H3K27me3. PR-DUB-mediated removal of H2AK118ub may compound this effect, further concentrating PRC1 at sites with residual H3K27me3. Upon knockdown of Asx, increased global H2AK118ub could recruit PRC1 and PRC2 to derepressed genes, restoring repressive activity at sites where H3K27me3 had been lost. These hypotheses could be tested by performing CUT&RUN against H2AK118ub, PRC1, and PRC2 subunits in wing discs expressing H3 K27M with and without *Asx* RNAi.

Last lines of defense: determining mechanisms of oncoprotein enhancement

Knockdown of enhancers further impairs wing development. Thus, these proteins limit the severity of H3 K27M developmental defects. Prominent among the enhancers we identified were Polycomb proteins. In tissue-culture models of DMG, genetic and chemical targeting of PRC1 and PRC2 produce lethality.^{21,22} Tumors therefore cannot tolerate

further loss of Polycomb protein function, which parallels our findings in the *Drosophila* wing. Other studies in *Drosophila* have described H3 K27M-enhancement as well, though the mechanism of enhancement was not assessed.^{23,24} Outside of Polycomb proteins, many enhancers of the H3 K27M wing phenotype have not been identified in tissue-culture models of DMG.

Our suppressor RNA-seq data support a model in which H3 K27M triggers an imbalance between the repressive H3K27me3 and transcriptional activators. It is possible that enhancers serve as buffers against more severe transcriptional changes, which we could test with additional RNA-seq experiments. If this hypothesis is correct, we would expect to find a more dramatic upregulation of genes disrupted by H3 K27M in wing discs. This is the most likely explanation for enhancement of the H3 K27M phenotype upon Polycomb-protein knockdown. Alternatively, enhancers may regulate separate sets of genes. For example, H3 K27M-upregulated genes were enriched for piRNA and germline-related functions. Some enhancers may repress additional piRNA and germline-related genes. In this scenario, enhancer-knockdown and H3 K27M expression would synergize to produce more drastic wing phenotypes.

One potential example of alternative mechanisms for enhancement is the Tip60 complex. Two Tip60 complex members were identified as a strong enhancers. Similarly to PR-DUB, Tip60 has been associated with dual repressive and activating roles in gene regulation, which is at least partially independent of Tip60 acetyltransferase activity. Tip60 acetylates H4K16, which positively regulates gene expression. Interestingly, Tip60

also facilitates PRC1 and PRC2 repression, though the precise mechanisms for this are unclear.²⁸ If Tip60 repressive activity underlies its role as an enhancer, its knockdown may abolish wing development by mechanisms that parallel Polycomb-protein knockdown. If Tip60 H4K16 acetyltransferase activity buffers H3 K27M defects, it likely does so by regulating a separate set of genes that maintain wing development. As with Polycomb enhancers, these alternatives could be distinguished by RNA-seq.

H3 K27M enhancers and suppressors in mammalian tissue culture

H3 K27M and EZHIP are thought to impair differentiation of human hindbrain tissues. ^{2–5} Targeting DMG and PFA susceptibilities may trigger distinct outcomes, including cell death or relief of the differentiation blockade. To explore these strategies, it is important to study H3 K27M and EZHIP in model systems with a broad range of phenotypic outcomes. Our enhancer/suppressor screen demonstrates that H3 K27M-expressing wings can be restored to wild-type development, or abolished altogether. H3 K27M suppressors may be particularly difficult to identify in tissue culture, as *in vitro* models have no obvious phenotype with which to identify developmental rescue.

Several approaches could be taken to test the importance of enhancers and suppressors in mammalian tissue culture. Ideally, enhancers and suppressors could be knocked down in DMG cell lines. If these proteins are important to DMG viability, we would expect to find proliferative defects, or, less likely, advantages. Instead of being essential for DMG cell viability, enhancers and suppressors may mediate the early steps of tumorigenesis. In an effort to identify the cell of origin for DMG, a previous study differentiated pluripotent stem

cells along an oligodendroglial lineage and compared the chromatin and transcriptional state of these cells to DMG.²⁹ One could perform similar experiments in pluripotent stem cells, by expressing H3 K27M and assessing impairment of differentiation beyond a certain point in the differentiation trajectory. Knockdown of suppressors and enhancers during differentiation may trigger earlier or later blockades, revealing critical roles for these proteins in oncogenic transformation.

References

- (1) Tsuboi, M.; Kishi, Y.; Yokozeki, W.; Koseki, H.; Hirabayashi, Y.; Gotoh, Y.
 Ubiquitination-Independent Repression of PRC1 Targets during Neuronal Fate
 Restriction in the Developing Mouse Neocortex. *Developmental Cell* 2018, 47 (6), 758-772.e5. https://doi.org/10.1016/j.devcel.2018.11.018.
- (2) Filbin, M. G.; Tirosh, I.; Hovestadt, V.; Shaw, M. L.; Escalante, L. E.; Mathewson, N. D.; Neftel, C.; Frank, N.; Pelton, K.; Hebert, C. M.; Haberler, C.; Yizhak, K.; Gojo, J.; Egervari, K.; Mount, C.; Galen, P. van; Bonal, D. M.; Nguyen, Q.-D.; Beck, A.; Sinai, C.; Czech, T.; Dorfer, C.; Goumnerova, L.; Lavarino, C.; Carcaboso, A. M.; Mora, J.; Mylvaganam, R.; Luo, C. C.; Peyrl, A.; Popović, M.; Azizi, A.; Batchelor, T. T.; Frosch, M. P.; Martinez-Lage, M.; Kieran, M. W.; Bandopadhayay, P.; Beroukhim, R.; Fritsch, G.; Getz, G.; Rozenblatt-Rosen, O.; Wucherpfennig, K. W.; Louis, D. N.; Monje, M.; Slavc, I.; Ligon, K. L.; Golub, T. R.; Regev, A.; Bernstein, B. E.; Suvà, M. L. Developmental and Oncogenic Programs in H3K27M Gliomas Dissected by Single-Cell RNA-Seq. *Science* 2018, 360 (6386), 331–335. https://doi.org/10.1126/science.aao4750.
- (3) Lange, C.; Huttner, W. B.; Calegari, F. Cdk4/CyclinD1 Overexpression in Neural Stem Cells Shortens G1, Delays Neurogenesis, and Promotes the Generation and Expansion of Basal Progenitors. Cell Stem Cell 2009, 5 (3), 320–331. https://doi.org/10.1016/j.stem.2009.05.026.
- (4) Mendez, F. M.; Núñez, F. J.; Garcia-Fabiani, M. B.; Haase, S.; Carney, S.; Gauss, J. C.; Becher, O. J.; Lowenstein, P. R.; Castro, M. G. Epigenetic Reprogramming and Chromatin Accessibility in Pediatric Diffuse Intrinsic Pontine Gliomas: A Neural

- Developmental Disease. *Neuro Oncol* **2020**, *22* (2), 195–206. https://doi.org/10.1093/neuonc/noz218.
- (5) Monje, M.; Mitra, S. S.; Freret, M. E.; Raveh, T. B.; Kim, J.; Masek, M.; Attema, J. L.; Li, G.; Haddix, T.; Edwards, M. S. B.; Fisher, P. G.; Weissman, I. L.; Rowitch, D. H.; Vogel, H.; Wong, A. J.; Beachy, P. A. Hedgehog-Responsive Candidate Cell of Origin for Diffuse Intrinsic Pontine Glioma. *Proceedings of the National Academy of Sciences* 2011, 108 (11), 4453–4458. https://doi.org/10.1073/pnas.1101657108.
- (6) Kuroda, M. I.; Kang, H.; De, S.; Kassis, J. A. Dynamic Competition of Polycomb and Trithorax in Transcriptional Programming. *Annual Review of Biochemistry* 2020, 89 (1), 235–253. https://doi.org/10.1146/annurev-biochem-120219-103641.
- (7) Jain, S. U.; Do, T. J.; Lund, P. J.; Rashoff, A. Q.; Diehl, K. L.; Cieslik, M.; Bajic, A.; Juretic, N.; Deshmukh, S.; Venneti, S.; Muir, T. W.; Garcia, B. A.; Jabado, N.; Lewis, P. W. PFA Ependymoma-Associated Protein EZHIP Inhibits PRC2 Activity through a H3 K27M-like Mechanism. *Nature Communications* 2019, 10 (1), 2146. https://doi.org/10.1038/s41467-019-09981-6.
- (8) Jain, S. U.; Rashoff, A. Q.; Krabbenhoft, S. D.; Hoelper, D.; Do, T. J.; Gibson, T. J.; Lundgren, S. M.; Bondra, E. R.; Deshmukh, S.; Harutyunyan, A. S.; Juretic, N.; Jabado, N.; Harrison, M. M.; Lewis, P. W. H3 K27M and EZHIP Impede H3K27-Methylation Spreading by Inhibiting Allosterically Stimulated PRC2. *Molecular Cell* 2020, 80 (4), 726-735.e7. https://doi.org/10.1016/j.molcel.2020.09.028.
- (9) Han, J.; Yu, M.; Bai, Y.; Yu, J.; Jin, F.; Li, C.; Zeng, R.; Peng, J.; Li, A.; Song, X.; Li, H.; Wu, D.; Li, L. Elevated CXorf67 Expression in PFA Ependymomas Suppresses

- DNA Repair and Sensitizes to PARP Inhibitors. *Cancer Cell* **2020**, *38* (6), 844-856.e7. https://doi.org/10.1016/j.ccell.2020.10.009.
- (10) Michealraj, K. A.; Kumar, S. A.; Kim, L. J. Y.; Cavalli, F. M. G.; Przelicki, D.; Wojcik, J. B.; Delaidelli, A.; Bajic, A.; Saulnier, O.; MacLeod, G.; Vellanki, R. N.; Vladoiu, M. C.; Guilhamon, P.; Ong, W.; Lee, J. J. Y.; Jiang, Y.; Holgado, B. L.; Rasnitsyn, A.; Malik, A. A.; Tsai, R.; Richman, C. M.; Juraschka, K.; Haapasalo, J.; Wang, E. Y.; De Antonellis, P.; Suzuki, H.; Farooq, H.; Balin, P.; Kharas, K.; Van Ommeren, R.; Sirbu, O.; Rastan, A.; Krumholtz, S. L.; Ly, M.; Ahmadi, M.; Deblois, G.; Srikanthan, D.; Luu, B.; Loukides, J.; Wu, X.; Garzia, L.; Ramaswamy, V.; Kanshin, E.; Sánchez-Osuna, M.; El-Hamamy, I.; Coutinho, F. J.; Prinos, P.; Singh, S.; Donovan, L. K.; Daniels, C.; Schramek, D.; Tyers, M.; Weiss, S.; Stein, L. D.; Lupien, M.; Wouters, B. G.; Garcia, B. A.; Arrowsmith, C. H.; Sorensen, P. H.; Angers, S.; Jabado, N.; Dirks, P. B.; Mack, S. C.; Agnihotri, S.; Rich, J. N.; Taylor, M. D. Metabolic Regulation of the Epigenome Drives Lethal Infantile Ependymoma. *Cell* 2020, *181* (6), 1329-1345.e24. https://doi.org/10.1016/j.cell.2020.04.047.
- (11) Biegel, J. A.; Zhou, J.-Y.; Rorke, L. B.; Stenstrom, C.; Wainwright, L. M.; Fogelgren,
 B. Germ-Line and Acquired Mutations of INI1 in Atypical Teratoid and Rhabdoid
 Tumors1. Cancer Research 1999, 59 (1), 74–79.
- (12) Drosos, Y.; Myers, J. A.; Xu, B.; Mathias, K. M.; Beane, E. C.; Radko-Juettner, S.; Mobley, R. J.; Larsen, M. E.; Piccioni, F.; Ma, X.; Low, J.; Hansen, B. S.; Peters, S. T.; Bhanu, N. V.; Dhanda, S. K.; Chen, T.; Upadhyaya, S. A.; Pruett-Miller, S. M.; Root, D. E.; Garcia, B. A.; Partridge, J. F.; Roberts, C. W. M. NSD1 Mediates Antagonism between SWI/SNF and Polycomb Complexes and Is Required for

- Transcriptional Activation upon EZH2 Inhibition. *Molecular Cell* **2022**, *82* (13), 2472-2489.e8. https://doi.org/10.1016/j.molcel.2022.04.015.
- (13) Versteege, I.; Sévenet, N.; Lange, J.; Rousseau-Merck, M.-F.; Ambros, P.; Handgretinger, R.; Aurias, A.; Delattre, O. Truncating Mutations of HSNF5/INI1 in Aggressive Paediatric Cancer. *Nature* **1998**, *394* (6689), 203–206. https://doi.org/10.1038/28212.
- (14) Wang, L.; Zhao, Z.; Ozark, P. A.; Fantini, D.; Marshall, S. A.; Rendleman, E. J.; Cozzolino, K. A.; Louis, N.; He, X.; Morgan, M. A.; Takahashi, Y.; Collings, C. K.; Smith, E. R.; Ntziachristos, P.; Savas, J. N.; Zou, L.; Hashizume, R.; Meeks, J. J.; Shilatifard, A. Resetting the Epigenetic Balance of Polycomb and COMPASS Function at Enhancers for Cancer Therapy. *Nat Med* 2018, 24 (6), 758–769. https://doi.org/10.1038/s41591-018-0034-6.
- (15) Wang, X.; Wang, S.; Troisi, E. C.; Howard, T. P.; Haswell, J. R.; Wolf, B. K.; Hawk, W. H.; Ramos, P.; Oberlick, E. M.; Tzvetkov, E. P.; Ross, A.; Vazquez, F.; Hahn, W. C.; Park, P. J.; Roberts, C. W. M. BRD9 Defines a SWI/SNF Sub-Complex and Constitutes a Specific Vulnerability in Malignant Rhabdoid Tumors. *Nat Commun* 2019, *10* (1), 1881. https://doi.org/10.1038/s41467-019-09891-7.
- (16) Ingham, P. W. Differential Expression of Bithorax Complex Genes in the Absence of the Extra Sex Combs and Trithorax Genes. *Nature* **1983**, *306* (5943), 591–593. https://doi.org/10.1038/306591a0.
- (17) Mishra, B. P.; Zaffuto, K. M.; Artinger, E. L.; Org, T.; Mikkola, H. K. A.; Cheng, C.; Djabali, M.; Ernst, P. The Histone Methyltransferase Activity of MLL1 Is

- Dispensable for Hematopoiesis and Leukemogenesis. *Cell Reports* **2014**, *7* (4), 1239–1247. https://doi.org/10.1016/j.celrep.2014.04.015.
- (18) Bonnet, J.; Boichenko, I.; Kalb, R.; Jeune, M. L.; Maltseva, S.; Pieropan, M.; Finkl, K.; Fierz, B.; Müller, J. PR-DUB Preserves Polycomb Repression by Preventing Excessive Accumulation of H2Aub1, an Antagonist of Chromatin Compaction.
 Genes Dev. 2022, 36 (19–20), 1046–1061. https://doi.org/10.1101/gad.350014.122.
- (19) Conway, E.; Rossi, F.; Fernandez-Perez, D.; Ponzo, E.; Ferrari, K. J.; Zanotti, M.; Manganaro, D.; Rodighiero, S.; Tamburri, S.; Pasini, D. BAP1 Enhances Polycomb Repression by Counteracting Widespread H2AK119ub1 Deposition and Chromatin Condensation. *Molecular Cell* 2021, 81 (17), 3526-3541.e8. https://doi.org/10.1016/j.molcel.2021.06.020.
- (20) Fursova, N. A.; Turberfield, A. H.; Blackledge, N. P.; Findlater, E. L.; Lastuvkova, A.; Huseyin, M. K.; Dobrinić, P.; Klose, R. J. BAP1 Constrains Pervasive H2AK119ub1 to Control the Transcriptional Potential of the Genome. *Genes Dev.* 2021, 35 (9–10), 749–770. https://doi.org/10.1101/gad.347005.120.
- (21) Mohammad, F.; Weissmann, S.; Leblanc, B.; Pandey, D. P.; Højfeldt, J. W.; Comet, I.; Zheng, C.; Johansen, J. V.; Rapin, N.; Porse, B. T.; Tvardovskiy, A.; Jensen, O. N.; Olaciregui, N. G.; Lavarino, C.; Suñol, M.; de Torres, C.; Mora, J.; Carcaboso, A. M.; Helin, K. EZH2 Is a Potential Therapeutic Target for H3K27M-Mutant Pediatric Gliomas. *Nature Medicine* 2017, 23 (4), 483–492. https://doi.org/10.1038/nm.4293.
- (22) Kumar, S. S.; Sengupta, S.; Lee, K.; Hura, N.; Fuller, C.; DeWire, M.; Stevenson, C. B.; Fouladi, M.; Drissi, R. BMI-1 Is a Potential Therapeutic Target in Diffuse Intrinsic

- Pontine Glioma. *Oncotarget* **2017**, *8* (38), 62962–62975. https://doi.org/10.18632/oncotarget.18002.
- (23) Berlandi, J.; Chaouch, A.; De Jay, N.; Tegeder, I.; Thiel, K.; Shirinian, M.; Kleinman, C. L.; Jeibmann, A.; Lasko, P.; Jabado, N.; Hasselblatt, M. Identification of Genes Functionally Involved in the Detrimental Effects of Mutant Histone H3.3-K27M in Drosophila Melanogaster. *Neuro Oncol* 2019, 21 (5), 628–639. https://doi.org/10.1093/neuonc/noz021.
- (24) Chaouch, A.; Berlandi, J.; Chen, C. C. L.; Frey, F.; Badini, S.; Harutyunyan, A. S.; Chen, X.; Krug, B.; Hébert, S.; Jeibmann, A.; Lu, C.; Kleinman, C. L.; Hasselblatt, M.; Lasko, P.; Shirinian, M.; Jabado, N. Histone H3.3 K27M and K36M Mutations de-Repress Transposable Elements through Perturbation of Antagonistic Chromatin Marks. *Molecular Cell* 2021, *81* (23), 4876-4890.e7. https://doi.org/10.1016/j.molcel.2021.10.008.
- (25) Acharya, D.; Hainer, S. J.; Yoon, Y.; Wang, F.; Bach, I.; Rivera-Pérez, J. A.; Fazzio, T. G. KAT-Independent Gene Regulation by Tip60 Promotes ESC Self-Renewal but Not Pluripotency. *Cell Reports* 2017, *19* (4), 671–679. https://doi.org/10.1016/j.celrep.2017.04.001.
- (26) Galarneau, L.; Nourani, A.; Boudreault, A. A.; Zhang, Y.; Héliot, L.; Allard, S.; Savard, J.; Lane, W. S.; Stillman, D. J.; Côté, J. Multiple Links between the NuA4 Histone Acetyltransferase Complex and Epigenetic Control of Transcription.
 Molecular Cell 2000, 5 (6), 927–937. https://doi.org/10.1016/S1097-2765(00)80258-0.

- (27) Sapountzi, V.; Logan, I. R.; Robson, C. N. Cellular Functions of TIP60. The International Journal of Biochemistry & Cell Biology 2006, 38 (9), 1496–1509. https://doi.org/10.1016/j.biocel.2006.03.003.
- (28) Qi, D.; Jin, H.; Lilja, T.; Mannervik, M. Drosophila Reptin and Other TIP60 Complex Components Promote Generation of Silent Chromatin. *Genetics* **2006**, *174* (1), 241–251. https://doi.org/10.1534/genetics.106.059980.
- (29) Nagaraja, S.; Quezada, M. A.; Gillespie, S. M.; Arzt, M.; Lennon, J. J.; Woo, P. J.; Hovestadt, V.; Kambhampati, M.; Filbin, M. G.; Suva, M. L.; Nazarian, J.; Monje, M. Histone Variant and Cell Context Determine H3K27M Reprogramming of the Enhancer Landscape and Oncogenic State. *Molecular Cell* 2019, 76 (6), 965-980.e12. https://doi.org/10.1016/j.molcel.2019.08.030.